Development and verification of ShorelineS on longshore sediment transport and spit formation

A CASE STUDY OF LOBITO, ANGOLA

C. Mudde

Deltares
Enabling Delta Life

TU Delft

Development and verification of ShorelineS on longshore sediment transport and spit formation

A case study of Lobito, Angola

By

Casper Mudde

Department of Hydraulic Engineering
Section: Coastal Engineering

in partial fulfilment of the requirements for the degree of

Master of Science
in Civil Engineering

at the Delft University of Technology
to be defended publicly on 21 November 2019, at 11:00 AM.

Thesis committee:	Prof.dr.ir S.G.J. Aarninkhof	TU Delft
	Dr. Ir. M.A. de Schipper	TU Delft
	Ir. W.P. de Boer	TU Delft / Deltares
	Dr. Ir. B.J.A. Huisman	Deltares

Preface

This report is written as final fulfilment for the completion of my M.Sc. study at the Delft University of Technology, Faculty of Civil Engineering and Geosciences at the Section of Coastal Engineering. This research was performed in at Deltares, I'm grateful that I had the opportunity to cooperate with this great company. I would like to take this opportunity to highlight some important people whom without this thesis would not be possible.

Firstly, I would like to thank all the enthusiastic and helpful people at Deltares and at the TU Delft which contributed by giving practical and technical advice during the past months. In particular, I would like to thank my committee: Stefan Aarninkhof, Matthieu de Shipper, Bas Huisman and Wiebe de Boer. Their knowledge and input helped me to find the right direction during this journey. Despite the busy and important agendas, you provided me with valuable feedback during the collective progress meetings and individual moments of contact. Your dedication and passion for our work field inspires me.

A special thanks to my daily supervisor at Deltares, Bas Huisman, whom always believed in my abilities. His endless enthusiasm and positive attitude really gave me energy to keep going at moments I was insecure. The weekly meetings were really valuable for me both academic as well on personal level.

I also would like to thank all my fellow (graduation) students (and now friends), here at Deltares and during my study at the TU Delft. They made the last three years a great and a less lonely experience, thanks to them I can look back with great joy at my years as a student.

Lastly, and most importantly, I want to thank my friends and family for their support during my study and this graduation journey. My mother for giving me the opportunity to study and my girlfriend who motivated me and distracted me during our free time when I was, sometimes too, focused on my thesis. She helped me to find the right balance between my graduation- and personal life; you're the best!

I would like to dedicate this thesis to my father, who is no longer among us. He introduced me as a child into the world and wonders of technology. His passion inspired me to find my way into the field of civil engineering. Dad, I owe it to you.

Casper Mudde
Delft, November 2019

Summary

In the field of coastal engineering computational models are a commonly used tool by the coastal engineer. Computational models can, for example, be used to gain insight into dynamics of a coastal system, to gain insight/hindcast the historical development or can be used as engineering tool to assess the efficiency and consequences of a proposed measure on the coastal system. Different types of computational models exist ranging from coastal area models, which can be used to model the hydrodynamics and morphodynamic in detail, but requires a great computational effort, to coastline models, which can be used to efficiently model the overall coastline evolution. However, the applicability of those coastline models, such as UNIBEST-CL+, is restricted as they can usually only be applied for relatively simple (straight) coastlines where the coastal evolution is limited and can be related to its initial formation and position. This creates a gap where existing models are either too complex and time-expensive to use for engineering application at larger scales or are to too simple and too schematic. In ShorelineS (Shoreline Simulation), a new coastline model, the coastline is schematized as a polyline which can freely move around in the model space. This allows for flexibility in the model, in which coastal sections can split, merge and can undergo drastic changes with respect to its initial position. Together with the use of numerical routines to prevent instabilities, ShorelineS promises to overcome this gap.

In this thesis the capabilities of this new model was assessed. The focus is on a unique potential modelling feature of this coastline model namely, the modelling of spit formation. Spit formation is a coastal feature where, under the influence of high angle waves, a landform extends from the coastline. It is thereby a typical use case of this new model as the modelling of spits requires ShorelineS' flexibility and long-term efficiency. The objective of the research in this thesis is threefold: 1) to gain insight into physical processes related to spit formation 2) to validate Longshore Sediment Transport (LST) rates in ShorelineS and 3) to validate migration and shape of spit formation in ShorelineS. The naturally formed spit of Lobito has been used as a case study in this thesis.

The aim of the first objective is to have a better understanding of the possible mechanisms related to the formation of the observed shape of the spit formation. From the analysis of existing natural spits around the world a conceptual model on the spit shape has been presented. In this conceptual model thee typical spit shapes were defined based on the morphological appearance. This conceptual model provides a first broadening insight into the possible spit shapes and relevant processes. Further, more detailed, analysis on spit formation processes was done by means of a XBeach modelling study. In this modelling study the influence of different environmental aspects (wave conditions, wave climates and tide) and geometric aspects of a spit (spit head shape and width) have been assessed. This was done by an analysis of the resulting distribution of the LST along the head of a spit for different model scenarios, in which the previously mentioned aspects were isolated. It was found that especially the bimodality of the wave climate (i.e., a wave climate where apart from a predominance average high angle wave orientation a wave component originating from a secondary, opposite, direction is present) is an important process controlling the resulting spit shape. In unidirectional wave climates the shape (and width) of the spit is determined by the reach of the LST over the head of the spit. This reach is depending on the combined effect of wave refraction and wave height reduction over the head. In a bimodal wave climate, the waves from the secondary orientation tend to redistribute the sediment over the head of the spit. This leads to a sediment supply for parts of the spit (i.e., over the tip) which cannot be reached by the LST due to the predominant high angle wave, resulting in a wider, recurved tip.

For the Lobito spit over 90% of the wave climate is originated from a small band of wave angles ($\varphi_w = 244°$ to $248°$). Under this forcing, and by imposing the natural spit shape, the LST over the head decayed linearly. This in is line for the distribution as characterized for an equilibrium spit (i.e., shape matching the natural forcing, resulting in a migration with a constant shape and width) as described by Petersen et al. (2008). When other spit geometries (i.e., symmetric, wider or smaller) were imposed in the Lobito model scenario 'unnatural' LST-distributions around the head were found. The latter can be used to judge whether a certain imposed spit geometry matches the natural forcing (or not).

In coastline models, and so in ShorelineS, the coastline evolution is driven by gradients in the LST. A correct representation of the LST therefore forms the basis of a coastline model. This was the aim of the second research objective. The LST in ShorelineS is computed using so called 'LST-Bulk formulae'. Those empirical formulae determine the net wave-induced LST along the coast (Q_s) based on the (breaking) wave conditions ($H_{s,br}$ and $\varphi_{w,br}$). The use of LST-bulk formulae, instead of more advanced semi-processed based transport formulae, is required to preserve the long-term efficiency of the model. The breaking wave conditions in ShorelineS are derived from an offshore defined wave climate, as the nearshore wave transformation, thus breaking wave parameters, change under influence of morphological change. It was found that for this wave transformation calculation the reorientation of the nearshore depth contours, with respect to the offshore fixed orientation, has a large influence on those breaking wave parameters for reorienting coastlines. In the original ShorelineS

model all depth contours were assumed (schematized) to be coastline parallel, therefore all depth contours (up to the location of the imposed wave climate) would rotate accordingly under coastal evolution. This assumption results in an incorrect wave transformation when the coastline deviates with respect to the offshore depth contours, directly resulting in an incorrect estimation of the LST through the LST-bulk formulae. The latter is especially of importance for coastline orientation which deviate significantly with respect to the offshore fixed depth contours. The schematization of the depth contours was improved in ShorelineS by the implementation of the so called 'Dynamic Boundary' which fixes the orientation of the offshore depth contours up to a certain depth (the depth of the dynamic boundary) but allows the reorientation of the active zone (i.e., the zone between the dynamic boundary and the coastline) which is more in line with the observed coastline evolution in reality. It was shown, by means of a model-to-model comparison of ShorelineS with UNIBEST-LT and wave (climate) data from a SWAN model, that with the implementation of the dynamic boundary in ShorelineS the wave transformation, thus LST-calculation, was made more accurate and robust (independent of the location at which the wave climate is imposed in the model).

For the third research goal the capabilities of modelling spit formations with ShorelineS was evaluated. Three different modelling aspects regarding spit formation were defined, namely the modelling of the spit migration direction, the spit width/shape and migration rate. The migration direction of the spit can be related to the coastline angle for which the sediment transport maximizes, the so called 'critical angle'. In the original model routine the critical angle was fixed to the theoretical angle of $\sim 45°$ (relative angle between coastline normal and incoming wave direction) as suggested by Ashton et al. (2006b). However, continuing on the previous finding on the modelling of LST, it was found that the angle of maximum transport is also influenced by the nearshore wave transformation and the effect of the reorientation of the depth contours. An updated routine was suggested and implemented in ShorelineS, which determines the critical angle is based on the actual local maximum transport for each timestep and grid point depending on the actual wave- condition and transformation. Using model scenarios by hindcasting the Lobito spit, it was shown that both the dynamic boundary condition and the use of a variable critical angle were required to be able to correctly hindcast/predict the spit orientation for the Lobito case study using ShorelineS. Without those improvements the resulted spit was oriented $37°$ more seaward with respect to the observed orientation, thus resulting in a completely wrong long-term prediction.

Regarding the modelling of the shape and width of spit formation it was found that with the current simplified quasi-uniform wave model (refraction) and shielding routine in ShorelineS it is not possible to correctly model the linear decay of the LST distribution over the head of a spit as found in the XBeach modelling study (first objective). The distribution of is therefore manually controlled LST as part of the so called 'upwind-routine' in ShorelineS once the coastline reaches the critical angle. In the original ShorelineS model, and original model routine, the sediment decay over this part was defined rather arbitrary without a physical meaning. In fact; the width and shape, and thereby migration rate, were directly influenced by the user defined grid resolution. An improved version of the upwind correction has been suggested and implemented as a proof-of-concept. In this proof-of-concept the LST over the head of the spit decreases linearly once the critical angle is exceeded based on a user defined spit width parameter. This forces the sediment distribution over the head of the spit corresponding to the 'equilibrium spit shape' as described by Petersen et al. (2008) and as found in the XBeach modelling study. With this updated model routine, the spit shape and migration in ShorelineS is made more robust and independent of the of the grid resolution.

This research, and the suggested improvements, contribute to the overall understanding of the capabilities of ShorelineS. By this a first important step in (better) incorporating the physical representation of spit formation processes in the ShorelineS coastline model was made. The work regarding the further development of this relatively new ShorelineS coastline model is not yet done. Based on the findings of this thesis, next steps for future research are amongst others the further investigation into the influence of the bathymetry (increasing depth) on the spit formation rate and the further research into predicting the expected spit width for a given environment.

Table of content

Appendices

Appendix A: Existing spit inventory

Appendix B: XBeach modelling results for different spit geometries

Appendix C: Data sheets LST-comparison ShorelineS versus UNIBEST-LT

Appendix D: Sensitivity analysis LST-formulae (UNIBEST)

List of Symbols

Symbol	Description	Unit
ρ_w	Density of water	kg/m^3
ρ_s	Density of solid	kg/m^3
Q_s	Longshore sediment transport rate	kg/m^3
c	Wave velocity	m/s
c_g	Wave group velocity	m/s
n	Ratio wave group velocity over wave velocity	$-$
k	Calibration coefficient CERC-formula	$-$
k_2	Calibration coefficient CERC-formula by Ashton et al. (2001) including wave refraction	$-$
γ	Breaker index	$-$
H_s	Significant wave height	m
h	Water depth	m
S_{yx}	Alongshore component of the radiation stress, driving the alongshore current	N/m
p	Porosity	$-$
φ_w	Wave angle (wave normal w.r.t. north) (Figure 2-3)	°
φ_c	Coastline orientation (coastline normal w.r.t. north) (Figure 2-3)	°
φ_{loc}	Local wave angle (relative to coastline normal) (Figure 2-3)	°
φ_{eq}	Equilibrium coastline orientation at which $Q_s = 0$	°
$\Delta\varphi_{eq}$	Phase shift; Difference in computed coastline equilibrium orientation by ShorelineS and expected coastline orientation	°
ΔA	Relative amplitude factor/error; describes magnitude difference in computed longshore sediment transport magnitude by ShorelineS versus expected quantity.	$-$
β	Bottom slope	°
T_p	Peak period	s
D_{50}	Median grain diameter	m
K_{swell}	Swell factor in (van Rijn, 2014) transport formula	$-$
D_c	Active profile height	m
W_c	Critical / minimal barrier width (Leatherman, 1979)	m
c_1	UNIBEST parameter describing the magnitude of the fitted S, φ-curve	$-$
c_2	UNIBEST parameter describing the curviness of the fitted S, φ-curve	$-$

Commonly used subscripts

x_0	At offshore location
x_{br}	At the breaker line
x_{db}	At the dynamic boundary

List of Figures

List of Tables

1 Introduction

1.1 Background

Many coasts around the world experience erosion and/or accretion as a result of, for example, sea level rise, river damming, coastal structures and natural long-term coastline variations. Coastal protection works have therefore been applied at many coasts to protect valuable infrastructure and residential areas. The philosophy on coastal defence has changed over the last decades (Delta Programme, 2013; Hanley et al., 2014). In the second half of the 20th century the main solution to counteract coastal erosion was the construction of hard measures such as sea walls, groyne schemes or (offshore) breakwaters which resulted in impacts on the coastal/natural system such as reduction of sediment supply in down-drift areas and degradation of/change in the biodiversity (Rangel-Buitrago et al., 2018). New forms of coastal management strategies introduced a different approach. As, for example, in recent Dutch projects such as the Sand Engine and the reinforcement of the Hondsbossche and Pettemer sea defence. For those projects sandy soft solutions were used to not only improve the coastal safety but also a great attention was paid for the effect on the natural system.

Nowadays coastal models are a commonly used tool by coastal engineers to understand the driving processes and effects of human interventions and changing natural conditions on the coastal system. These sandy (soft) solutions do require coastal models to predict the (long term) effectiveness of such projects. A large range of different models exists. The choice of a model depends amongst others on the spatial and temporal scale at which the dominant hydrodynamic or morphological processes act, the required detail of the output information and the available computer power. Coastal profile models, such as XBeach 2DV, can be used to analyse the difference between the summer and winter profile while complex coastal area models can for used to assess, for example, the effect of complex flow patterns due to waves and tidal currents on the coastal morphology. Coastal area models, such as Delft3D, can be used to model those projects in high detail, however they require a lot of expertise and computation power which makes such models less suitable to perform long term calculations. Less complex (single-line) coastline models, such as UNIBEST-CL+, can be used to perform long term simulations but existing coastline models are limited to simulate more or less straight diffusive (stable) coastlines. This creates a gap where existing models are either too complex and time-expensive to use for engineering application at larger scales or are to too simple and too schematic (Roelvink et al., 2018) .

To overcome this gap between available models a new model called ShorelineS (Shoreline Simulation) (Roelvink et al., 2018) was developed based on a new approach as described by Hurst et al. (2015). In ShorelineS the coastline stretches are defined as strings of grid points which can freely move around which allows for splitting and merging of coastal sections (i.e., islands). With the implemented upwind correction as described by Ashton et al. (2006a) the model is suitable for long term simulations on geometric complex (e.g., curved) coastlines in unstable beach regimes, which was not yet feasible in the existing coastline models. At the same time the modelling still requires less expertise and computation time compared to coastal area models.

Principle tests have been performed to show the potential and flexibility of the model (Roelvink et al., 2018). In Figure 1-1 one of those tests is shown based on an overview of different coastal shapes along a fictional coastline described by van Rijn (1998). This test shows that ShorelineS can indeed represent drastic coastline changes, but since it is only a fictional principle test the results cannot be validated.

To asses the applicability of this new model, and its potential as a new computational tool for coastal projects, further validation is required on real life use case situations.

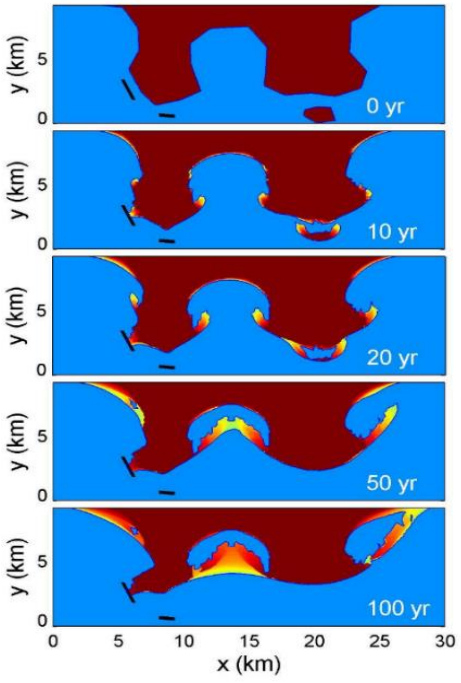

Figure 1-1 – ShorelineS model applied on van Rijn overview of coastal shapes (Roelvink et al., 2018) *Red indicates oldest depositions and yellow the most recent.*

1.2 Objectives and research question

In this thesis the capabilities of this new model was assessed. The focus is on a unique potential modelling feature of this coastline model namely, the modelling of spit formation. Spit formation is a coastal feature where, under the influence of high angle waves, a landform extends from the coastline. It is thereby a typical use case of this new model as the modelling of spits requires ShorelineS' flexibility and long-term efficiency.For this the model is applied on a study area at Lobito (Angola) (Figure 1-2). Three research objectives are defined:

Figure 1-2 – Lobito spit (Google LLC., 2019)

1) **Objective 1: Gain insight into physical processes related to spit formation**
   In order to be able to assess the ShorelineS model on spit formation insight is required into which general processes are relevant for spit formation and how those (combined) processes contribute to the final formation in nature. This knowledge can be used to understand the observed natural spit shape (in this case the Lobito shape) but also to improve the numerical model routines, reflecting those processes, as used in ShorelineS.
2) **Objective 2: Validate Longshore Sediment Transport rates in ShorelineS**
   The performance of the LST module in ShorelineS and the currently implemented LST-formulas is evaluated in this of part of the study. A correct representation of the longshore sediment transport rates forms the basis of a coastline model. This is therefore an essential step before the model could be applied on actual real-life study (spit) cases.
3) **Objective 3: Validate migration and shape of spit formation in ShorelineS**
   The potential ability of ShorelineS to model spit formation due to high angle wave exposure is a unique feature compared to existing shoreline models. The ability of ShorelineS to correctly predict spit formation and how to incorporate the relevant processes (objective 1) into the model routines is evaluated in this part of the thesis.

The defined research objectives applied on the study area have led to the formulation of the following research question:

> *What are the capabilities of the ShorelineS coastline model, applied on the Lobito Spit case to accurately model/predict the longshore sediment transport and spit formation? And how can this be improved?*

1.3 Approach

The core of this thesis, the assessment of the predictive skill of ShorelineS, is examined using model tests on the case study of the Lobito spit located in Angola (Figure 1-2). This case study was selected since the Lobito spit was developed naturally under the influence of high angle wave exposure. Furthermore, validation data an models are available from a recent coastline evolution study of this spit by Deltares (2015), which can be used to validate the ShorelineS model. In general the following general approach was followed:

1. Gain insight into the current knowledge and relevant processes (literature study)
2. Gain insight into the model schematisation of those processes (Model analysis)
3. Test current performance of the ShorelineS model (Base case)
4. Identify missing processes/improvements based on literature and/or model results
5. Propose and, if possible, implement improvements for the ShorelineS model
6. Test performance of the improvements

Step 1 and 2 are related to the first objective, to gain insight into the relevant processes. The steps 3-6 were looped through for each (aspect) of the second and third research objective.

Gain insight into processes related to spit formation

To get a broad insight into the relevant processes related to Spit formation an inventory of existing natural spits was done. Supported by the literature study on spit formation processes insight into typical spit shapes was gained. The influence of different potential processes was assessed by means of a modelling study in XBeach for different model scenarios (i.e., variation in environmental conditions and imposed spit geometry).

Regarding this first objective the following sub research questions are defined:

- What processes are responsible for the direction and shape of spit growth?
- How is the final spit formation (shape) related to the local environmental circumstances?

Longshore Sediment Transport

The validation of the longshore sediment transport rates was done by means of a quantitative assessment of the by ShorelineS modelled transport rates along the spit of the case study of Lobito. The performance of ShorelineS was quantified by means of a comparison to data originating from the Deltares (2015) project for which a calibrated UNIBEST-CL+ model was used to usefully model (hindcast) the observed coastline changes at Lobito. The calibrated transport curves (S, φ-curves) from this UNIBEST model were quantitatively compared (i.e., transport magnitude and overall shape for different coastal orientations) to results of the ShorelineS model.

Regarding the longshore sediment transport the following sub research questions are defined:

- What processes determine the alongshore transport rates?
- How can those processes be represented in ShorelineS?
- What is the performance of the different LST-formulations LST-module in ShorelineS compared to the UNIBEST-model?

Spit formation

For the assessment of the spit formation in ShorelineS three characteristic aspects of a spit were defined (Figure 1-3); 1) the migration-direction of the spit form, 2) the width of the spit formation and 3) the migration rate of the spit.

Regarding those aspects two research(sub) questions are defined:

- How can the different processes and aspects be represented in ShorelineS?
- What is the performance of ShorelineS on modelling spit formation?

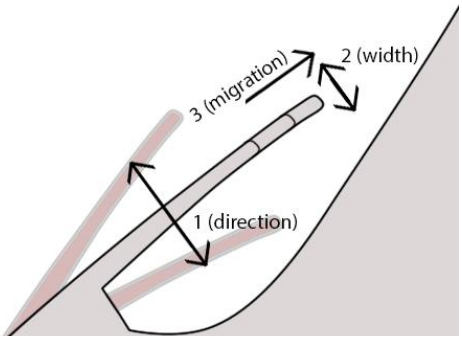

Figure 1-3 - Aspects on spit formation: 1) direction, 2 width, 3) migration rate

The performance of predicting the different modelling aspects was assessed by a hindcast of the initial Lobito spit evolution using ShorelineS and a comparison to the known current/historical orientation. Based on this, and the knowledge gained in the study into the possible physical processes (objective 1), missing processes/ possible improvements could be identified and implemented in ShorelineS.

A more extensive description of the applied methods for each part is provided in the corresponding chapter(s).

1.4 Outline

Chapter 2 gives a summary of the literature study which has been carried out to gain knowledge of the topics which are be addressed in this thesis. Chapter 3 provides a description of the study area of Lobito describing the historical spit evolution and relevant environmental conditions. Chapter 4 elaborates on the first research objective; to gain insight into the spit formation processes. In this chapter an inventory and analyse of existing natural formed spits is presented together with a more detailed analysis on possible processes using XBeach. Chapter 5 focusses on the modelling (and validation) of longshore sediment transport in ShorelineS. In Chapter 6 the modelling performance of ShorelineS on spit formation is further investigated. For this the modelling of different aspects of a spit (Figure 1-3) was evaluated by hindcasting of the Lobito spit together with an analysis of the model routines representing spit formation processes. This thesis concludes with Chapter 7, in which the overall key findings (conclusions) are summarized as well as recommendations for future research.

2 Literature review

This chapter provides a summary on the theoretical background which is used in this thesis. It starts, in Section 2.1, with a description of spits and the theory on spit formation. In Section 2.2 a description on the calculation of longshore sediment transport is provided, focussing on the description of different LST-bulk formulae. The basic principles of computational modelling for coastal engineering and a description on the commonly used coastline model UNIBEST-CL+ is given in Section 2.3. In Section 2.4 describes the current state and basic functionality of the ShorelineS model.

2.1 Spit formation

A spit is a landform which extends seaward from the coastline with one free end while the other end is still connected to the coastline. In this section the different types and aspects regarding (the formation of) spits is discussed.

2.1.1 Type of spits

Ashton et al. (2006b) made a classification of spits (Figure 2-1). This classification is derived from numerical model tests which relates the occurrence of a flying spit related to the wave forcing. Parameter A represents the portion of waves from one direction and parameter U the portion of high angle waves in the local the wave climate. This shows that flying spits are likely to arise for environments with a very uniform high angle wave climate. For situations where a more varying wave climate is present (besides the dominant high angle-wave) the flying spit will be flattered out and thus have a less pronounced (rhythmic) shapes such as sand waves (smooth) or cuspate bumps (pointed).

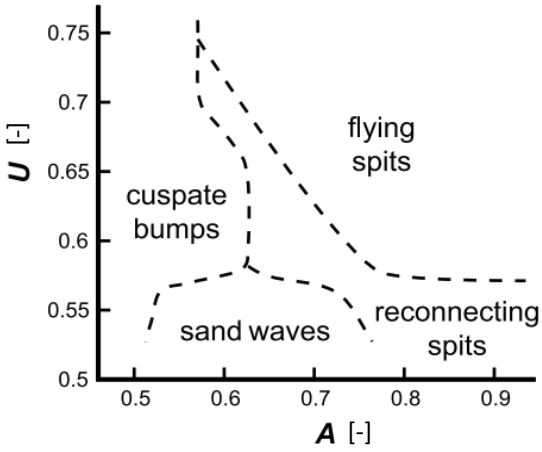

Figure 2-1 – Plot with shoreline shapes with variation of wave climate variables A and U.(Ashton et al., 2006)

Another classification of spit types was made by Ollerhead (1993) (Figure 2-2). This classification of barrier systems is based on the number of free ends and the barrier (and coastline) geometry. For a spit (one free end) three general types were distinguished:

1. **Flying (or landward expanding) spits**
   Unstable coastal feature originating from alongshore transport by high-angle waves. Typically leaving the coastline at an angle.
2. **Continuation spit**
   Pointed tongue extending into the sea at abrupt interruptions of the coastline. Typically, parallel to the coastline.
3. **Constrained bay-mouth spit**
   Similar to a continuation spit but located in between a bay.

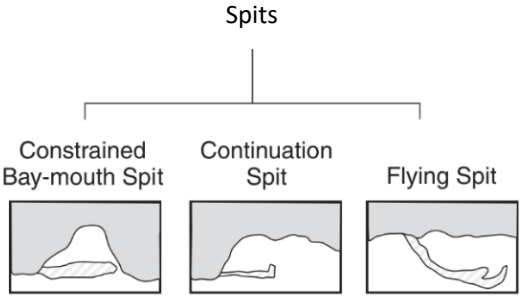

Figure 2-2 –Type of spits as defined by Ollerhead (1993). Image adopted from Davidson-Arnott (2009)

The mechanisms as described by Ashton et al. (2006a) are based on ideal cases for which the shape is mainly controlled by the local wave action only. It should be remarked that apart from this classification in nature the overall appearance and especially the head of the spit can differ quite substantially. Lindhorst et al. (2010) showed for example that the shape and formation of the spit of Sylt Island can be closely related to the steep bathymetry (ridge) and presence of a tidal inlet with strong tidal currents which forced this particular spit to recurve.

2.1.2 Formation of spit

Flying spit

Alongshore sediment transport (Q_s) can generally be described with a CERC-like sinusoidal function (Section 2.2) of the wave angle (φ_w) relative to the shoreline orientation (φ_c) (Figure 2-3, left):

$$Q_s \sim {H_s}^{2,5} \sin 2(\varphi_{loc}) \qquad 2.1$$

The rate of change in alongshore sediment transport $\partial Q_s/\partial x$ along a coastline results in deposition ($\partial Q_s/\partial x < 0$) or erosion ($\partial Q_s/\partial x > 0$) of material.

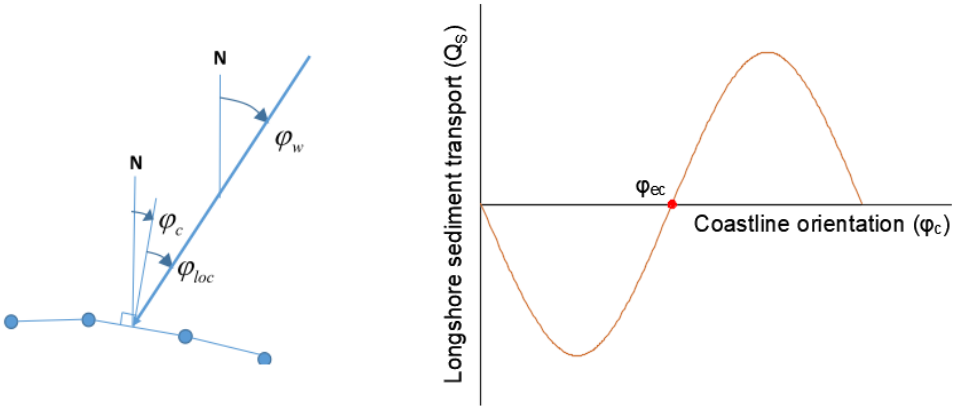

Figure 2-3- Left: Definition of wave- (φ_w), coast- (φ_c) and relative- (φ_{loc}) angles as used in this thesis and the ShorelineS-model (Roelvink et al., 2018) Right: Typical S, φ-curve

The LST-relation is often visualised using a S, φ-curve[1] (Figure 2-3, right). This curve shows the change the LST-rate for different coastal orientations. The so called "Equilibrium coastline orientation" (φ_{eq}) denotes the orientation for which the transport is zero. The S, φ-curve can be used to get insight into the rate of change in LST for a given coastline. For so called 'low-angle waves' $\varphi_{loc} < \sim 45°$ small perturbation on a straight shoreline will be smoothed out (stable). For angles $\varphi_{loc} > \sim 45°$ the opposite will happen; erosion around the flanks and sedimentation on the top of the perturbation (i.e., a seaward growth / unstable) (Figure 2-4).

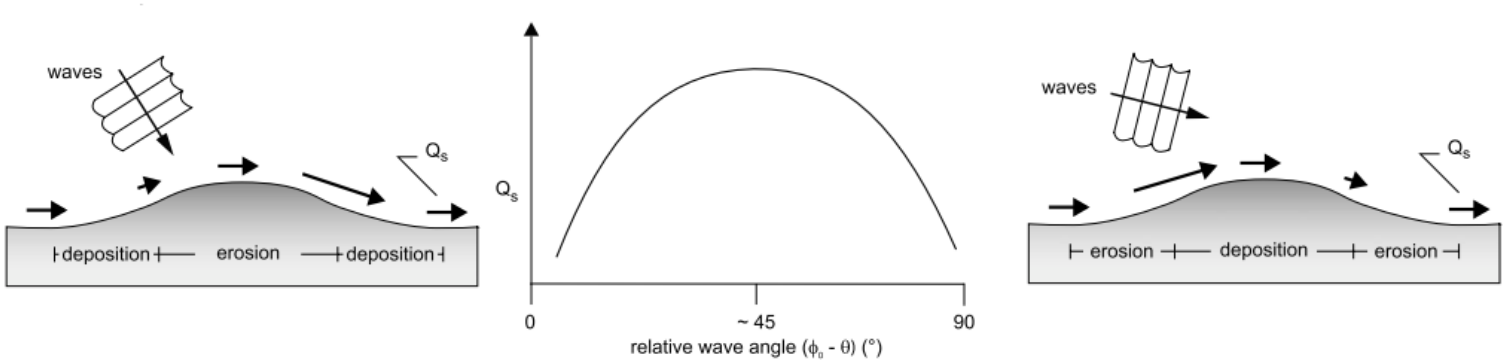

Figure 2-4 – Effect of incoming wave on coastline permutation for low angle waves (left) and high angle waves (right) (Szmytkiewicz e al., 2000) *Note the relative wave angle ($\phi_0 - \theta$) is referred to φ_{loc} in this thesis.*

[1] S, φ-curves can both be visualized as function of a changing wave angle (φ_w) for a fixed coastline orientation (φ_c) or the other way around: for a fixed wave angle and a changing coastline orientation. In literature both ways are used. In this thesis the coastline orientation is used as variable (thus a fixed wave angle).

Ashton et al. (2006a) describes that this in seaward direction growth is not infinite since it is limited by the angle for which the alongshore sediment transport is maximum at $\varphi_{loc} \approx 45°$ defined as the critical angle ($\varphi_{loc,crit}$) (Figure 2-5). Once the flank of the spit approaches this angle it will therefore not steepen further. Eroded material originating from the up-drift side of the spit will migrate over the flank towards the tip/end of the spit. This effectively results in an extension or growth of the spit under the angle of maximum sediment transport.

This extending spit will eventually create a sheltered zone which is shadowed from the direct wave approach under angle φ_w. This describes the initial formation of a flying spit.

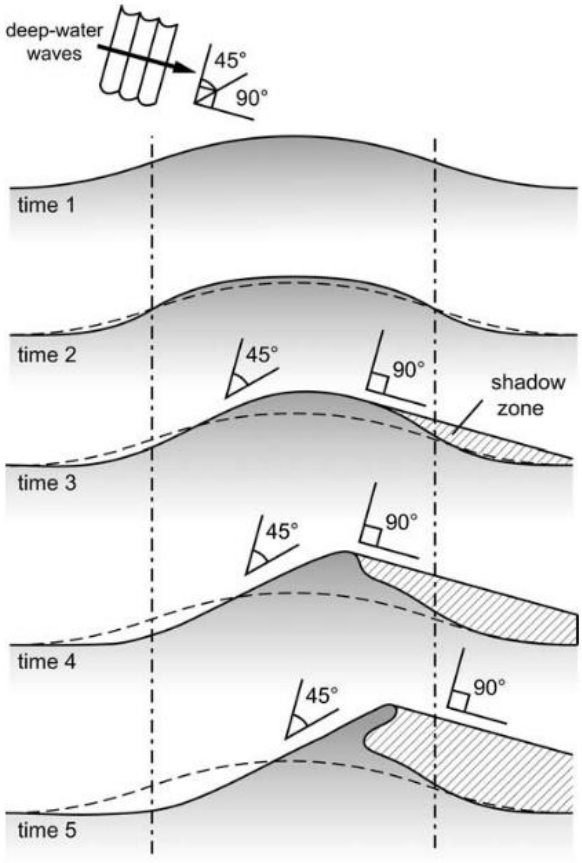

Figure 2-5 – Unstable spit formation under high angle waves (Andrew D. Ashton and Murray 2006a

Continuation spit

Spits can also form around abrupt interruptions of a coastline such as a headland, the end of an island, a harbour entrance, estuary etc. (See classification of Ollerhead 1993, Figure 2-2). For this type of spit a dominant sediment transport direction along the coast is still required to keep the spit intact, however in contrast to the flying spits, a continuation spit can also form in a dominant low-angle wave climate. Since the spit is basically an extension of the coastline updrift the shape follows this direction. The spit gradually builds out due to the deposition of coastal material at the tip of the spit.

A continuation spit can be divided in two general morphological components as described by (Ashton et al., 2016): (Figure 2-6).

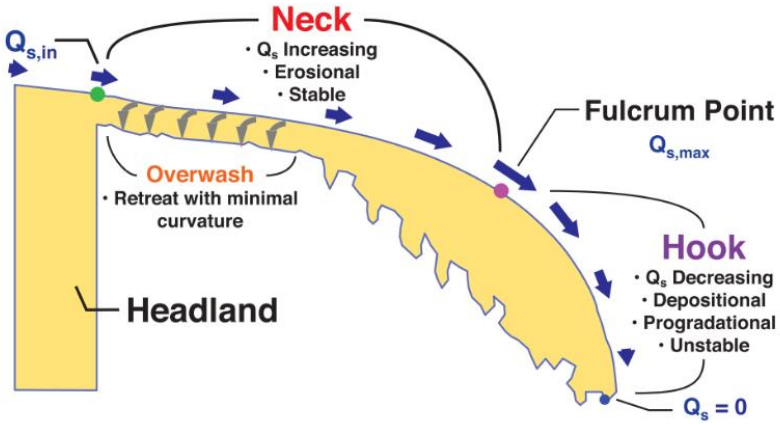

Figure 2-6 – Definition of morphological components of continuation spit by (Ashton et al., 2016)

- **Neck**
  The neck is the part of the spit which follows the orientation of the coastline it extends from. For low-angle waves this part is still subject to erosion (assuming an eroding headline) resulting in a gradual retreat and a minimal curvature of the neck. The width of the neck is sustained due to overwash (Section 2.1.3). Due to this curvature the relative angle of the incoming wave with respect to orientation of the neck is increasing, resulting in an increasing sediment transport rate (Q_s) over the neck and thus an increasing curvature (erosion). At some point in reaches the angle of maximum sediment transport ($Q_{s,max}$) at which $\varphi_{loc,crit} \approx 45°$. This point is defined as the Fulcrum point
- **Hook**
  The hook (or recurved head) of a spit experiences a high-angle incoming wave since it is located beyond the fulcrum point (as defined). Therefor the behaviour and orientation of the hook is driven by the same mechanisms as the flying spit. From this point the relative between the wave angle and coastline orientation increases further thus on the sediment transport decreases (thus deposition at the hook) from $Q_{s,max}$ at the fulcrum point to $Q_s = 0$ at the tip of the spit. (see next section, Figure 2-7)

2.1.3 Migration and width of spit

A spit is not a fixed landform, over time it can extend (grow, increase of overall length) or migrate (move, no significant change in overall length). The migration of the spit can be in two directions; parallel to the coastline and towards the coast (landwards).

Petersen et al. (2008) described in more detail the width extension (growth) of a spit at the head/hook of a spit. Based on the following simple mass balance (Eq. 2.2) the relation of the migration (growth) rate of a spit (v) with the sediment supply at the tip ($Q_{l,max}$), the width of the spit (W) and the local depth (h) can be expressed.

$$Q_{l,max} = vWh(1-p) \qquad 2.2$$

The 'equilibrium' shape of a spit is defined by Petersen et al. (2008) as the combination of shape and width under a constant forcing for which the shape grows with a fixed shape and width. In case of an equilibrium spit head the alongshore sediment transport along the head is characterised by two properties. 1) The sediment transport should be zero at the end (tip) of the width of the spit as there cannot pass sediment over the tip (this would broaden the spit). 2) The alongshore sediment transport should decay linearly along the width of the spit, a linear decay implies a constant gradient thus a uniform sedimentation along the spit. The latter is a requirement to ensure the fixed shape (thus no change) of the head of the spit.

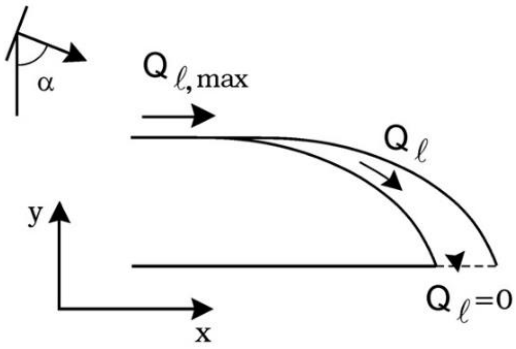

Figure 2-7 – Sediment transport decrease over tip of the spit (Petersen et al., 2008)

The processes as discussed or mentioned in existing literature and, in addition, with some hypothesized processes gives a rough idea in the possible mechanisms controlling the width and shape of a spit (Figure 2-8).

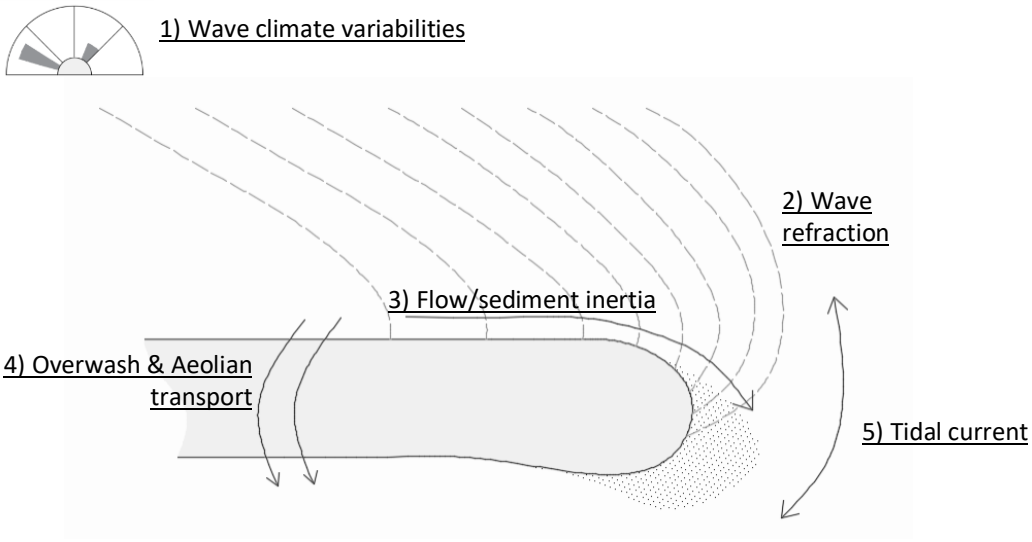

Figure 2-8 -Inventory of possible processes influencing the width of the spit

1) Wave climate variabilities
Spits are formed in an environment with a predominance high angle wave climate. The overall migration direction of the spit can be related to this wave angle (Section 2.1.2). In addition to the dominance wave direction (wind) waves originating form a less high angle or opposite angle can be present as a constant secondary wave forcing or a seasonal variability in the wave climate. Those wave directions can be of importance as they are able to transport sediment along the spit towards 'sheltered' parts of the spits' head which are not exposed by the waves from the dominant high angle direction (see also point 2: wave refraction) (Serizawa et al., 2019).

2) Wave refraction
Along the neck of the spit the wave refraction can be assumed quasi-uniform as the curvature of the coastline is limited, however at the head of the spit the curvature increases which can result in non-uniform effects as wave focussing at the tip and/or diffraction (Petersen et al., 2008).

3) Flow/sediment inertia
As along the head of a spit the coastline gets more sheltered, the wave energy (thus flow) will decrease. The concentration of suspended sediment will not directly adjust to the hydrodynamic forcing but experiences a certain time lag $(T \propto h/\, w_s)$ which can result in deposition (a supply) of sediment within the sheltered zones.

4) Over wash / Aeolian transport
In addition to wave forcing leading to sediment transport, sand can also be transported by over land by overwash and aeolian process. Those processes are therefore an important supplier of sand for locations where the wave energy and tidal currents are limited. Leatherman (1979) describes the relation of the spit migration (and width) due to the overwash process. As the flank or the neck of a spit erodes the width of the spit, formed by the initially deposited material, reduces. The width of a thinned spit is maintained by front-to-back transport of material over the spit by wave-overtopping (mainly) or aeolian (wind-induced) transport.

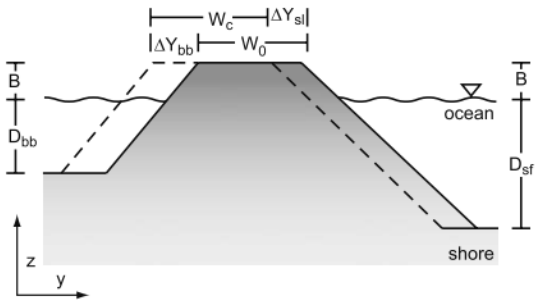

Figure 2-9 – Overwash process (Szmytkiewicz et al., 2000)

This mechanism ensures a minimal/critical barrier width (W_c) but also introduce a method to describe the alongshore and landward migration of spits. In a case that the water depth behind the spit is smaller than the water depth at the exposed side of the spit $(D_{bb} < D_{sf}$, Figure 2-9) overwash can also widen a spit.

5) Tidal Current
A tide can lead to an alongshore flow leading to sediment transport and/or redistribution along the head of a spit.

2.2 Longshore sediment transport

Sediment is set into motion when the shear stress at a particle exceeds a certain threshold. Longshore sediment transport (LST) is the movement of sediment particles along (parallel to) the coastline. When this transport increases at a certain location the coastline can erode at this location, this can be used to calculate the LST, and gradients of it along the coast, which is one of the drivers for coastline changes.

To calculate and model the LST-rates in principle two methods can be distinguished: (Mil-Homens, 2016)

- **Process based models:** In those models all physics which have an influence on the LST are aimed to be modelled. This require formulations and information of complex interactions of processes (e.g., (breaking) waves, tidal currents, entrainment & suspension etc.) to derive flow velocity and/or the shear stress at the bed. Processed based model can be used to get insight into detailed spatial distribution of the sediment transport but require high computational effort.
- **Bulk longshore sediment transport formulations:** Those models do not include all processes but give an estimation of the longshore sediment rate. Bulk LST-formulae are based on simplified expressions representing the physical processes calibrated with empirical derived coefficients from field data and physical model tests. As the names suggests bulk LST-formulae do not give the distribution of the sediment over the cross-shore profile but provide a cross-shore integrated transport.

Process based models might give detailed information of the LST and the distribution of it, however they usually require detailed data as input (measured parameters or parameters calculated with the help of computational extensive hydrodynamic models) to produce reliable results. Bulk LST-formulae, in contrast to this, usually require only some general relatively easy to measure wave data as input and are less computation extensive. This makes a good calibrated LST bulk-formula very suitable to preform long term calculations.

In bulk-LST formulae the LST-rates are usually related to net longshore currents which move the sediment along the coast. Those currents can have different origins i.e., tide, wind and waves. For waves the oscillating wave motion will stir up the sediment but will not result in a net transport.

The most general form an LST-bulk formula is: $LT = K\,P$; where LT is the longshore transport rate, K a calibration coefficient and P the longshore wave power. The longshore wave power can be related to the wave induced longshore current driven by a gradient in the radiation stress ($\partial S_{yx}/\partial x$)which was described by Longuet-Higgins (1970):

$$S_{yx} = n \cos\varphi_{\,loc} \sin\varphi_{loc}\; E \qquad 2.3$$

Where $n = c_g/c$ the ratio between the group wave velocity (c_g) and the wave velocity (c) , φ_{loc} the relative angle between the wave crest and the coastline and E the wave energy $E = 1/8\;\rho_w\;g\;H^2$. The gradient in radiation stress is only nonzero (assuming along shore uniform depth contours) for obliquely incident waves within nearshore. This can also be observed in eq. 2.3: the "$\cos\varphi_{loc}\sin\varphi_{loc}$" term will change at the nearshore due to refraction, the variation in the ratio $n = c_g/c$ can be described by the dispersion relation and change from $n = 1/2$ to $n = 1$ when waves travel from deep to shallow water according to linear wave theory. The wave energy E changes due to variations in wave height (H) such as wave- shoaling, -refraction and -breaking.

The most commonly used and newly improved bulk LST-formulae are:

- CERC developed by USACE (1984a)
- Kamphuis (1992)
- Improved Kamphuis by Mil-homens et al. (2013)
- van Rijn (2014)

The LST-rates can be expressed in different units (e.g., dry mass per second $[kg/s]$, volume per year $[m^3/yr]$) in the next sections all formulae are expressed in volume per second $[m^3/s]$ (thus accounting for relative density and pores) which can be used to determine volumetric cross-shore profile change.

CERC

The CERC (Coastal Engineering Research Center) formula is one of the oldest LST-formulae developed by of the ASCE (American Society of Civil Engineers) during the 1940's. The full CERC formula as described in USACE (1984b) is:

$$Q_s = k\frac{\rho_w g^{0.5}}{16\sqrt{\gamma}(\rho_s-\rho_w)(1-p)}H_{s,br}^{2.5}\sin(2\varphi_{loc,br}) \qquad 2.4$$

In which k is a calibration coefficient, ρ_s and ρ_w the density of the sediment and water, p the porosity,γ the breaking parameter and $H_{s,br}$ the significant breaking wave height. Although the original CERC formula was derived from sandy beach field data rather intuitively, it can be explained from a physical perspective. In eq. 2.4 the dependency of the of the local wave angle and wave height as formulated in eq. 2.3 can be recognized.

The coefficient k is obtained by calibration using datasets. USACE (1984b) prescribes a value of $k = 0.39$. Different attempts are done to relate this coefficient to physical processes by, for example, inducing a dependency of the bed slope (β) or grain size (D_{50}) (Mil-Homens, 2016).

The CERC formula, and LST-Bulk formulae in general, requires the breaking wave conditions as input parameter. Those quantities however might vary along a, for example, undulating coastline due to variations in refraction and can thus not assumed to be a constant value. A variation of the original CERC formula (eq. 2.4) was therefore suggested by Ashton et al. (2001) which uses deep water wave conditions:

$$Q_s = k_2 \, H_0^{12/5} \, T^{1/5} \cos^{6/5}(\varphi_{loc,0}) \sin(\varphi_{loc,0}) \qquad 2.5$$

The factor $k_2 = \left(\sqrt{g\gamma}/2\pi\right)^{1/5}$ accounts for the prediction of the refraction assuming shore parallel depth contours and depth limited breaking. An advantage of this formula over the original CERC formula is that the constant offshore wave conditions can be used as input parameter.

Kamphuis

Kamphuis (1992) derived a Bulk LST-formula based on extensive physical model tests. The coefficients of the formula were determined and calibrated using field data sets. In contrast to the CERC formula, Kamphuis analysed and included the dependency of the bed slope (β). According to the studied field data an increasing sediment transport was noticed for increasing bed slopes. Besides small variations due to varying grain size (D_{50}) was included. Resulting in the following formula:

$$Q_s = \frac{1}{(\rho_s - \rho_w)(1-p)} 2.27 T_p^{1,5} \tan\beta^{0.75} D_{50}^{-0.25} H_{s,br}^2 \sin^{0.6}(2\varphi_{loc,br}) \qquad 2.6$$

This formula is more sensitive to the wave period (T_p) and includes a term for the bed slope (β) and grain size (D_{50}). The dependency of the relative wave angle was included in the same way as for the CERC formula, however its influence was found to be less pronounced resulting in the exponent of 0.6 over the wave power term.

Re-evaluation by Mil-Homens

Mil-homens et al. (2013) revaluated the CERC and Kamphuis LST-formulae. For this additional data sets were used to recalibrate and improve the coefficients and/or exponents. It was concluded that the predictive skill of the original Kamphuis (1992) formula was improved the most. Resulting in the following updated formula:

$$Q_s = \frac{1}{(\rho_s - \rho_w)(1-p)} 0.149 H_{s,br}^{2.75} T_p^{0.89} \tan\beta^{0.86} D_{50}^{-0.69} \sin^{0.5}(2\varphi_{loc,br}) \qquad 2.7$$

Van Rijn 2014

Van Rijn (2014) proposed a “simple general expression for longshore transport of sand, gravel and shingle”. For this a detailed process based cross-shore profile model (CROSMOR) was used to analyse the influence of particle size, wave period and cross-shore profile on LST:

$$Q_s = \frac{1}{(\rho_s - \rho_w)(1-p)} 0.0006 \, K_{swell} \, \rho_s \, \tan\beta^{0.4} \, D_{50}^{-0.6} \, H_{s,br}^{2.5} \, V_{total} \qquad 2.8$$

In addition to existing LST-formulae as discussed before in this LST-formula also accounts for:

- A swell factor K_{swell}. Regular swell waves resulted in higher (factor 1.5) LST compared to wind waves with similar height. To take this into account a swell correction factor K_{swell} was included in the new formula. This correction value K_{swell} ranges from 1 (no swell) to 1.5 (swell only) depending on the percentage of low-period swell of the total wave record.

- Additional alongshore currents (tide, wind) other than wave induced alongshore currents. The total velocity is calculated with $V_{total} = V_{wave} + 0.01p_1V_1 + 0.01\ p_2V_2$ where V_1 and V_2 are the positive and negative combined (tide + wind) currents along the coast and the representative percentage of time p_1, p_2. For a fully symmetric flow $p_1 = p_2 = 50\%$ the effect is zero.

  The alongshore current is defined as $V_{wave} = 0.3\left(gH_{s,br}\right)^{0.5} \sin(2\varphi_{loc,br})$ which is expressed in a similar form and width a similar dependency as the wave power component as the CERC and Kamphuis formula.

The formula was tested and validated using a wide range of field- and physical model test data. Its performance has also been compared to the earlier described LST-formulae from which it was concluded that the new formulation performed better. (van Rijn, 2014).

2.3 Computational modelling

A computer can perform a large quantity of calculations within a short period of time. This can be used to map a part of the real world into an abstract number space. By translating 'real world' physical laws into (simplified) mathematical algorithms, a computer can do a simulation of this mapped part (Figure 2-10).

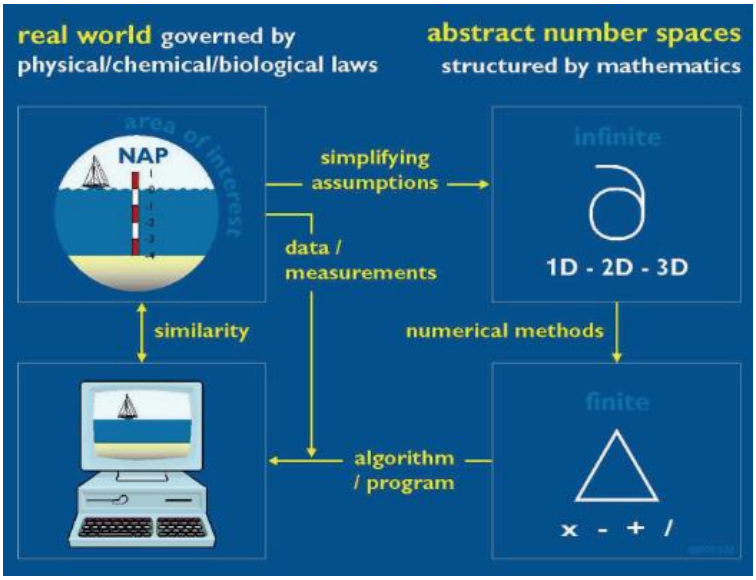

Figure 2-10 – Translation of real world problem in computational program (Zijlema, 2015)

This principle is widely applied within the field of coastal engineering to predict and analyse the effect of human interventions and/or climate change on a coastal system. The computational power of a computer is not infinite therefore, depending on the temporal and spatial scale of the to be simulated situation, a suitable simulation model approach should be chosen (Cowell et al., 1995) (Figure 2-11).

In general simulation models for coastal engineering can be subdivided into three types: (Roelvink et al., 2011)

1. Cross-shore profile models
2. Coastline models
3. Coastal area models

Each model type in general, but also each specific modelling application (software package) itself, has its own limitations based on the applied simplifications and assumptions. Before setting up a model it should be known which hydro- and morphodynamic processes are of importance and thus should be included in the model.

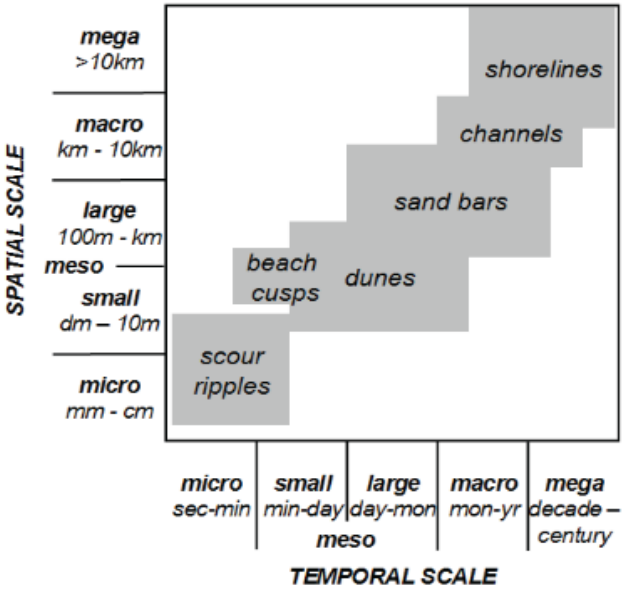

Figure 2-11 – Spatial and temporal scales of typical coastal morphological features. (Cowell et al., 1995 adopted from Winter, 2011)

Independent of the type of the model a coastal model is build up around a basic morphodynamic model loop (Figure 2-12). This loop is looped through each timestep (Δt) of the simulation. Each simulated loop represents a period of time of morphodynamical evolution of the 'real world'.

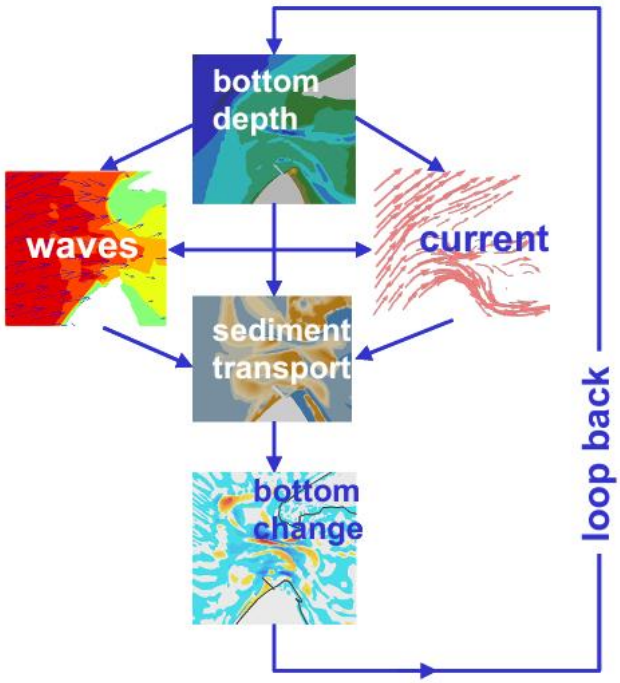

Figure 2-12 –General morphological loop of coastal model. (Roelvink et al., 2011)

Step 1: (initial) Bottom depth
The loop starts with an initial or updated bottom depth (bathymetry). The initial bathymetry can be derived from actual field data (maps, depth surveys) or can be assumed using equilibrium relations for beach profiles such as the Dean-profile.

The to be used bathymetry in a model depends among others on the available data, required level of detail of the simulation and model type.

In the bathymetry also representative bed composition information such as sediment distribution and roughness should be included.

Step 2: Calculate hydrodynamics
In the second step the hydrodynamics are calculated using the bathymetry, bed composition and the user defined boundary conditions (wave climate, tides, meteorological data etc.).

Step 3: Calculate sediment transport
Based on the hydrodynamics the sediment transport at each location within the model can be calculated.

Step 4: Calculate bottom change
In the last step the bottom change (Δz_b) gets calculated. In general; when more sediment comes in then goes out at a certain location the bed increases by Δz_b. This can be used to update the (initial) bathymetry by adding/subtracting bed level change: $z_{b,1} = z_{b,0}\ ^{+}/_{-}\ \Delta z_b$

After this loop the model loops back to step 1 and starts over the simulation using the updated bathymetry. In the following sections a description of the different type of models is given.

2.3.1 Computational model types

In this section a general description is given on different model types (i.e., coastal area-, coastline- and cross-shore profile models).

Coastal Area Models

Where Coastal profile models focusses on cross shore dynamics and coastline models on longshore sediment transport, Coastal area models, such as Delft 3D and XBeach, can be applied in cases where those cannot be separated, for example when modelling complex bathymetric changes around tidal inlets (e.g., migrating channels and shoals) (Roelvink et al., 2011).

A distinction can be made in 2DH (Horizontal) and 3D model coastal area models. In 2DH models the depth average flow is computed which is then used to calculate the sediment transport, thus following the direction of the depth average flow. In a 3D model velocity profiles are computed, this allows for the inclusion of processes which effect the distribution of the velocity profile (i.e., undertow/return flow, density flows, wave asymmetry).

The computation of the (depth average) flow field for each timestep increases the computation time significantly, this makes coastal area models less suitable to preform long term coastal simulations.

Coastline models

The main purpose of a coastline model is to investigate the (long term) evolution of the coastline. In most coastline models the cross-shore profiles are of a fixed shape referred as one-line (or single-line) models, thus do not include cross-shore process. This simplification is valid under the assumption that (fast) cross shore processes will reshape/force a profile into an equilibrium profile, whereas coastline models are usually used to assess longer term coastline variations.

Under this assumption a shift of the shoreline (dy) implies an equidistant shift of the cross-shore profile over the same distance (dy) over the entire active profile (D_C) (Figure 2-13).

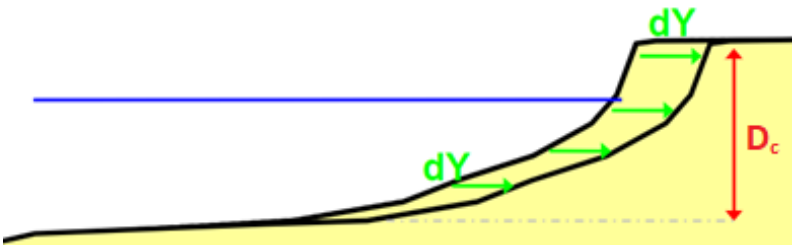

Figure 2-13 – Shift (dy) of cross shore profile over active profile height (D_c) (Huisman, 2012)

The shift of the coastline is related to the gradients in the along shore sediment transport (Q_s) along the shore. From conservation of mass it follows that:

$$\frac{\partial y}{\partial t} = -\frac{1}{D_c}\frac{\partial Q_s}{\partial x} \qquad 2.9$$

In a coastline model the coastline is divided into coupled transects or gridcells/points. For each gridcell and each timestep the alongshore sediment transport is calculated, when the along shore sediment transport rate increases over a grid cell this requires the coastline to retreat according to this basic equation.

In addition to one-line models multiple line models (n-line) models do exist in which the cross-shore profile can be subdivided into layers. This allows for sediment exchange within the cross-shore profile based on the deviation and steepness with respect to an known equilibrium profile (Huisman, 2014). Multiple line models can be used to analyse coastline changes with more detail including simple relationships for cross shore sediment interaction.

In contrast to coastal area models, where sediment transport is computed based on local flow velocities based on hydrodynamic calculations, coastline models generally uses (bulk) LST-formulae (Section 2.2). This reduces the computation time for coastline models which makes it suitable for long term calculations. The ShorelineS model, which will be used in this thesis, is a coastline model-type and is further described in section 2.4. In section 2.3.3 the existing coastline model UNIBEST-CL+ is described.

Cross-shore profile models

A cross-shore model focusses on the modelling of sediment transport due to cross-shore processes such as wave skewness/asymmetry, undertow, long wave setup. It can be used to analyse the change in the cross-shore profile such as bar/offshore nourishment migration, seasonal winter/summer profile changes and (storm) erosion.

Cross-shore profile models, such as XBeach 2DV have proven predictive capabilities especially for storm events on the time scale of storms and seasons. (van Rijn et al., 2003). Regrading spit formations

2.3.2 Wave transformation

In this thesis the focus is on modelling using a coastline model (ShorelineS). In those models the wave induced longshore sediment transport is calculated using LST-bulk formulae (Section 2.2). The LST-bulk formulae require input information on the nearshore wave characteristics (second step of the general morphological loop, Figure 2-12), namely the breaking wave conditions $H_{s,br}$ and φ_{br}.

Measurements of breaking parameters are usually limited, besides the wave field can spatially vary along a coastline as the wave breaking is influenced on the local nearshore characteristics (e.g., local slope, water depth etc). Even if such

measurements are available, morphological change (coastline evolution) in the model will also influence the breaking wave parameters over time. This underlines the need for the computation of the breaking wave parameters as part of the model routine for coastline models.

In coastline models the breaking wave parameters are usually derived from a more offshore (i.e., at deeper water) defined wave climate which are not influenced by the coastline. From this fixed offshore point, a wave transformation is required to determine the breaking wave parameters. This wave transformation can be considered as a separate module of the coastline model and different methods (and models) can be used for this purpose. Complex wave models, such as SWAN (Booij et al., 1999), are very suitable to perform this nearshore wave transformation but require computational power and detailed information of the nearshore and offshore bathymetry. As the wave transformation it is part of the morphological model loop the computational efficiency of the wave transformation calculation directly influences the overall computational efficiency of the coastline model. To preserve the overall long-term efficiency of a coastline model, the required computational effort for the wave transformation should be in balance with the rest of the model. This requires schematization of the nearshore wave propagation. In most traditional coastline models, and the current version of ShorelineS (Section 2.4), the nearshore wave transformation is limited to simplified calculations of the wave- shoaling and refraction (i.e., Snells law).

Wave refraction is influenced by the coastal bathymetry (Holthuijsen, 2010). This requires information/schematization of the bathymetry (the depth contours) in the coastline model. The depth contours in coastline models, as in ShorelineS (Section 2.4), are commonly assumed all coastline parallel. Evolution or rotation of the coastline therefore result in a rotation of the full cross-shore profile (i.e., all depth contours) when sand is added or lost. Another way to schematise the bathymetry under the influence of coastal evolution is by the concept of the 'dynamic boundary' (Figure 2-14) as, for example, used in UNIBEST. The dynamic boundary is based on the fact that sediment transport due to wave interaction is limited to the nearshore (active) part of the profile only. The dynamic boundary subdivides the cross-shore profile into two parts; a dynamic and a static part. In the dynamic part, in between the dynamic boundary and coastline, the depth contours will always be parallel to the coastline, rotation of the coastline result will result in an equal rotation of the depth contours in this part. In the static part the depth contours are fixed in at a certain initial or known orientation.

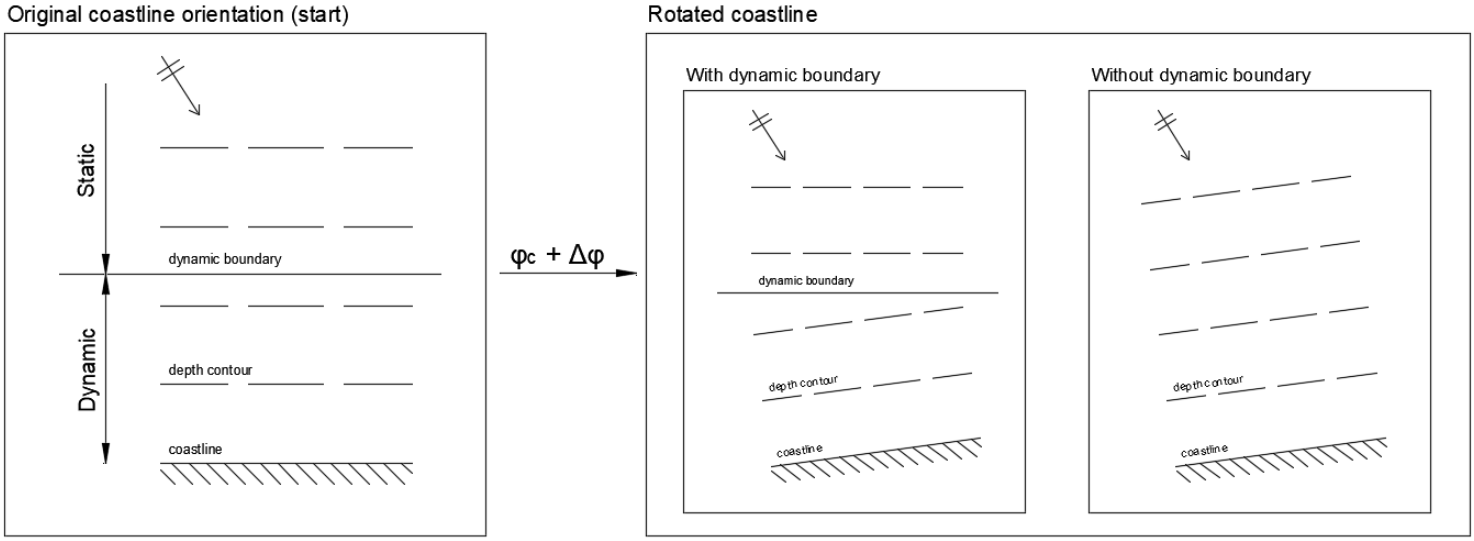

Figure 2-14 – Schematic visualisation of the principle of a coastline model with and without a dynamic boundary.

2.3.3 UNIBEST-CL+

UNIBEST-CL+ (Uniform Beach Sediment Transport) is a coastline model developed by Deltares. This section gives a summary of the basic functionality of UNIBEST-CL+ which will be used for this thesis. UNIBEST-CL+ consists of two sub modules basically a combination of a cross-shore model and a coastline model:

- **UNIBEST-LT (Cross-shore model)**
  This module calculates the tide and wave induced longshore current and resulting sediment transport. Using this the alongshore sediment transport curves (S, φ-curves, Figure 2-3) are determined. This module assumes a uniform alongshore coastline.

- **UNIBEST-CL (Coastline model)**
  The results of the UNIBEST-LT module are used as input for the UNIBEST-CL module. This module calculates the coastline changes due to gradients in the alongshore sediment transport rates.

Basic model definition

In UNIBEST-CL the coastline is schematised by a curved line fitted through user defined "Basic points" (which describe the coastline position) and "Basic y-points" (which describe the coastline orientation). Along this line grid points can be assigned at which the longshore transport will be determined (Figure 2-15). This implies that coastline changes in UNIBEST-CL are always related to a reference line.

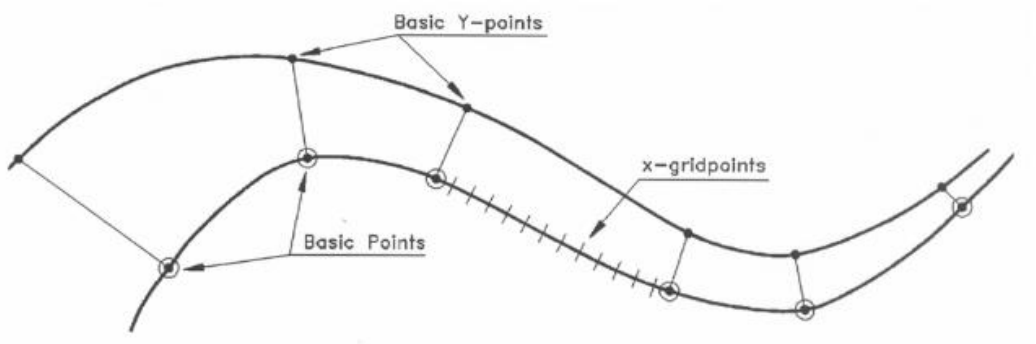

Figure 2-15 – Coastline definition in UNIBEST-CL (Deltares, 2011)

The longshore transport rates are derived from user defined Transport Rays. A Transport Ray includes a function which describes the longshore transport as sinusoidal function of the coastal orientation similar to the LST bulk formulae (Section 2.2):

$$Q_s = c_1(\varphi_c - \varphi_{eq})e^{-\left(c_2(\varphi_c-\varphi_{eq})\right)^2} \qquad 2.10$$

The fit parameters c_1 and c_2 are fitted for a specific combination of a cross-shore profile and wave climate and are thus only valid for that specific location.

Transport Rays can be generated using the UNIBEST-LT module in the following way:

- The user defines a cross-shore profile (shape + sediment characteristics) and provides wave-tide data.
- A nearshore wave transformation can either be done using the build in built-in random wave propagation and decay (ENDEC model Battjes et al., 1985) or nearshore transformed wave data calculated with an external model can be imported (e.g., SWAN).
- To calculate the alongshore sediment rates serval formulae, both semi-processed based and bulk formulae, are available.
- UNIBEST-LT also provides the cross-shore distribution of the sediment transport. For bulk formulae a cross shore distribution is assumed related (distributed) to the flow velocities over the active profile.
- The alongshore sediment rates are calculated for a series of coastline rotations (with respect to the initial coastline orientation)
- The calculated total alongshore transports rates (integrated over the cross-shore profile) are fitted on a simple transport function (Eq. 2.10), which is a function of the coast angle only $Q_s = f(\phi_c)$.

In the UNIBEST-CL module the gradients in the longshore sediment transport, thus coastline change, are based on the local coastline orientation and the transport rays. The use of Transport Rays within the CL module makes the model much more computation effective as for the simulation of the actual coastline evolution, it is not necessary to recalculate the entire wave transformation field and resulting transport rates every timestep (as required as input for the more complex processed formulae).

Structures

In UNIBEST three type of structures can be assigned along the coastline: groynes, offshore breakwaters and revetments. As described above, the alongshore transport rays are derived based on an undisturbed alongshore uniform coastline leading to a global transport.

The global transport is not valid in the sheltered areas created by structures (i.e., groynes and offshore breakwaters). At those areas local transport functions can be assigned which overwrites the global transport. The local transport functions are user defined functions describing the, usually limited or reduced, transport rates (Figure 2-16).

For active groynes a bypass function is implemented into UNIBEST. The bypassing mechanism 'blocks' a certain percentage of the alongshore sediment transport based on the known cross-shore sediment distribution and the extension of the groyne.

Revetments (or non-erodible coastal stretches) fixes the coastline over a certain stretch or form a threshold for erosion while sediment can still bypass a revetment. The sediment transport at the down drift site of a revetment will be fixed to the same value as the transport at the updrift side.

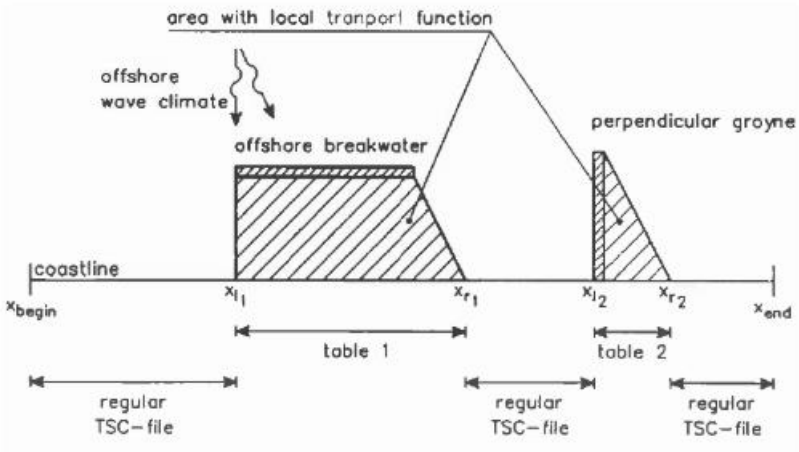

Figure 2-16- Areas with local transport functions in UNIBEST-CL (Deltares, 2011)

2.4 ShorelineS

ShorelineS (Shoreline Simulation) is a new single-line coastline model in development by J.A. Roelvink (Deltares/Unesco-IHE/TU Delft) and B.J.A. Huisman (Deltares/TU Delft). In the section below a short description is given of the basic structure and features of ShorelineS based on the revision 24 (Dated 04-02-2019) model MATLAB source code.

In ShorelineS the coastline is schematized as a polyline with strings and gridpoints (x_i, y_i), where i is the gridpoint index. Evolution of the gridpoints result in a coastal evolution, as the attached strings change accordingly. The gradient in longshore sediment transport rate (Q_s) over the string in between two grid points (x_{i-1}, y_{i-1}) and (x_i, y_i) is used to determine the displacement of the grind point for each timestep (Δt with timestep index j) by solving a typical mass conservation equation (eq. 2.9):

$$\Delta n_i^j = -\frac{1}{D_c}\frac{2(Q_{s,i}^j - Q_{s,i-1}^j)}{L_i}\Delta t \qquad 2.11$$

In which $L_i = \sqrt{(x_{i+1} - x_{i-1})^2 + (y_{i+1} - y_{i-1})^2}$ is the segment length between the two adjacent gridpoints to calculate the gradient in sediment transport $(\partial Q_s / \partial s)$. D_c is defined as the active height (Figure 2-13) over which the coastal profile migrates. The displacement $(\Delta x, \Delta y)$ of each gridpoint can be easily derived from the normal displacement Δn.

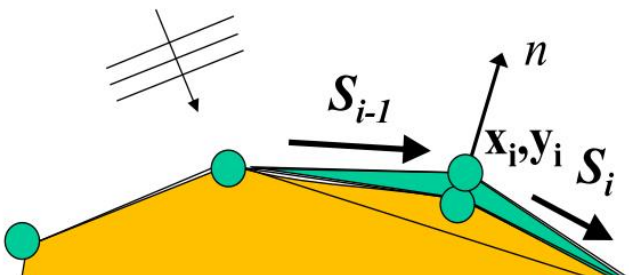

Figure 2-17 – Coastline definition in ShorelineS (Roelvink et al., 2018)

In contrast to current commonly used coastline models such as UNIBEST, which uses a single (initial) coastline reference line (Figure 2-15) with this coastline schematisation in ShorelineS the polyline (coastline) can split and merge and individual strings can stretch and shrink freely independent of an initial/reference position. This allows for a flexibility of the coastline and individually defined coastal sections in the model.

The longshore transport rate (Q_s) in ShorelineS is determined using LST-bulk formulae. Currently six bulk LST-formulae are available in ShorelineS (Table 2-1):

Short	Description	EQ
CERC3	Full CERC formula	2.4
CERC2	Modified CERC formulae by (Szmytkiewicz et al., 2000) based on offshore wave conditions, including refraction	2.5
CERC1	Simplified CERC formula, similar to eq. 2.4, but using H_0 and $\varphi_{loc,0}$ instead of $H_{s,br}$ and $\varphi_{loc,br}$	-
KAMP	Original (Kamphuis, 1991) formula	2.6
MILH	Re-evaluated Kamphuis formula by (Mil-Homens et al., 2013)	2.7
VR14	A Simple General Expression For Longshore Transport Of Sand, Gravel And Shingle by (van Rijn, 2014)	2.8

Table 2-1 – Available LST-formulae in ShorelineS

2.4.1 Morphodynamic loop

In this section the morphodynamic loop of ShorelineS is walked through. Per step a short description of the executed task is given, some steps (functions) of ShorelineS are treated more extensive in the remainder of this section. A coastline can exist of more coastline sections. Each coastline section is looped over individually for each timestep Δt.

it	**Time Loop**
1	Draw wave condition *An offshore wave condition is drawn form a wave time series or wave climate file.*

i_{mc}	**Loop over coast sections**
1	**Compute alongshore s-grid** *Converts specified shoreline (x,y)-file into grid line (*Figure 2-17*) with grid spacing based on input parameter ds*
2	**Calculate nearshore wavefield** *See below for more description of this function.*
3	**Check if section is cyclic or not** *'Island' type of coastline where the 'start' of a coastal section is connected to the 'end'. A non-cyclic coastline section requires boundary conditions.*
4	**Compute coast angles and local wave angles**. *The coast angle (φ_c) and wave angle (φ_w) are computed w.r.t. coast normal. The local angle (φ_{loc}) is defined as the angle between φ_c and φ_w, (Figure 2-3).*
5	**Check which points in shadow zone of other coast sections or structures** *See below for more description of this function.*
6	**Compute sediment transport rates** *Calculates Q_s using selected LST-formula*
7	**Calculate wave diffraction** *Currently under development, not activated yet in this release.*
8	**Perform upwind correction to local wave angles** *See below for more description of this function.*

9	**Set sediment transport to zero for large angles $\varphi_{loc} > 90°$** A wave will not reach the coastline for angles larger than $90°$
10	**Set transports zero where a structure cuts through the coastline** *See below for more description of this function.*
11	**Check which points lie in nourishment polygon** *A nourishment area can be assigned, this step checks if a certain grid point lies within the assigned nourishment area.*
12	**Checks and apply boundary conditions for non-cyclic coastline sections** *See below for more description of this function.*
13	**Check and apply local sink/source terms** *Local sink and source terms for sediment can be specified at a certain location. In this step the terms are added/subtracted to/from the calculated Q_s.*
14	**Compute coastline changes normal to local direction** *Calculate Δn (eq.* 2.11*) and, if present, nourishment rates are added effectively increasing the coastal change Δn.*
15	**Compute changes to x- and y-positions** *The normal coastline change Δn gets decomposed in x and y direction and added to the 'old' coastline position (x, y) to determine the new coastline position.*
16	**Apply schematized overwash process when spit or barrier is too narrow** *See below for more description of this function.*
17	**Insert coastline into the coastlines collection** *It places the updated coastline section, which it extracted during the beginning of this loop, back in the entire coastline string.*
18	**Merge coastline sections that intersect** *See below for more description of this function.*
	End of loop over coastline sections
End of time loop	

Table 2-2 – Morphological loop of ShorelineS

Nearshore wave field

To preserve the computational efficiency of the model, the wave transformation in ShorelineS is currently includes the wave shoaling and wave refraction, assuming coastline parallel depth contours (Section 2.3.2). The wave transformation is required to derive the breaking wave conditions, as some of the LST-formulations (Table 2-1) require breaking wave conditions to predict the LST.

Hard structures and wave shadowing

Hard structures can be added as polylines, hard structures have two main effects on the shoreline evolution:

1. **A structure can block longshore transport**
   This is implemented by setting the longshore transport to zero $Q_s = 0$ at locations where hard structures intersect with the coastline
2. **A structure can shelter the coastline from waves for certain wave angles**
   The shadowed zone is determined by extending the angle of the wave along the tip of a structure or coastline. This creates a projection (shadowed zone) on the adjacent coastline (Figure 2-18). In the shadow zone the longshore sediment transport is set to zero.
   Currently the wave sheltering and sediment blocking by hard structures is under development to implement more advanced bypassing.

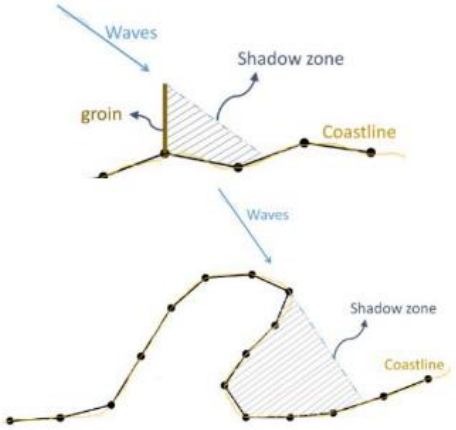

Figure 2-18 – Wave sheltering due to structures (top) or coastal geometry (bottom)(Roelvink et al., 2018)

Upwind correction (spit formation)

The formation of spits due to high-angle wave exposure is controlled with a so called upwind-correction as described by Ashton et al. (2006a) (Section 2.1.2). This correction is applied for the cases where over a section of the coast one part experiences low angle waves and the adjacent part experiences high angle waves, or vice versa (i.e.,: φ_{loc} changes from $\varphi_{loc} < \varphi_{crit}$ at one point to $\varphi_{loc} > \varphi_{crit}$ at the next gridpoint). In both cases the sediment transport will set to maximum ($Q_{s,max}$) which prevents coastline instabilities and fixes the spit's orientation to the critical angle.

In practical modelling this implies that without this correction sediment will build up in front of the top of a spit leading to instabilities over time (Figure 2-19, top), when this correction is applied the sand is 'transferred' over the top into the next point. This way the upwind correction allows for a smooth spit development (Figure 2-19, bottom).The effects of the enforcement of the maximum sediment transport on the model evolution is small, as the gradients in Q_s are small when approaching the maximum transport.

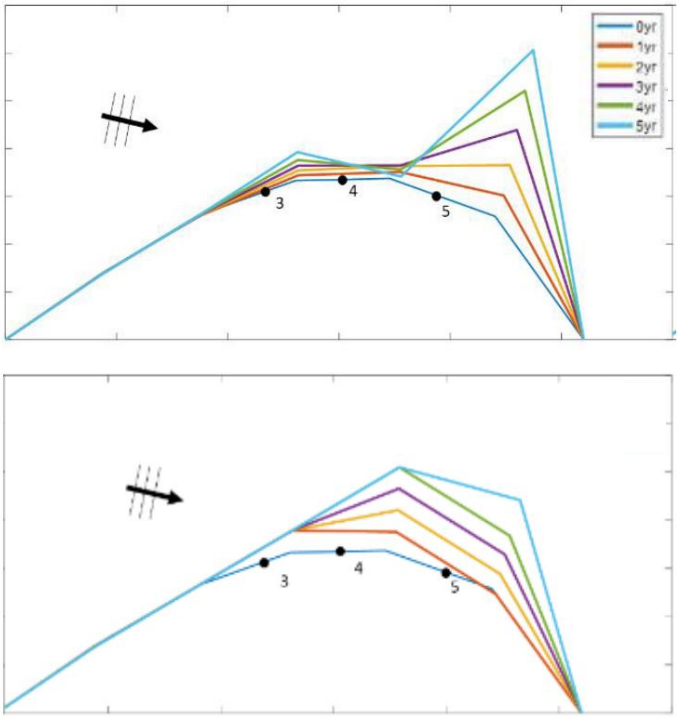

Figure 2-19 - Coastline evolution without (top) and with upwind correction (bottom) The model without upwind correction shows a growth instability (Roelvink et al., 2018)

Boundary conditions

For a non-cyclic coastline, the coastline will be cut off at the boundaries of the model. Therefore, boundary conditions for the sediment transport should be imposed at the beginning and end of the coastline which represent the influence of the 'outside world' in the model. Currently the following types of boundary conditions can be imposed in ShorelineS:

1. **Neumann boundary (Default setting)**
   Sets the sediment transport $Q_{s,1}$ at the first point (or last $Q_{s,i}$) point equal to the transport $Q_{s,2}$ second (or second-last $Q_{s,i-1}$) point. This way there will be no sediment change at the boundaries of the model implying a free in and outflow of sediment along the coast.
2. **Constant orientation**
   Sets the sediment transport at the start or end boundary to a fixed value for the entire simulation based on the initial transport related to the initial coastline orientation. This fixes the orientation of the coastline according to its initial condition.
3. **Dirichlet (function)**
   Sets the sediment transport at the start or end boundary according to a predefined (known) incoming sediment discharge, implying a constant incoming (or outgoing) sediment rate.
4. **Dirichlet (wall)**
   Sets the sediment transport at the start or end boundary to zero efficiently implying a 'fixed' wall where no sediment can transport through.

Overwash process

The width of the spit is controlled by an implemented overwash process as described by Leatherman (1979), (Section 2.1.3). ShorelineS checks the spit width (measured along the incident wave direction) for every timestep, if the width of the spit/barrier is smaller than a user defined predefined minimal or critical width W_c (due to landward erosion) it extends the gridpoint at the landward side so that the minimum width is maintained (Figure 2-20).

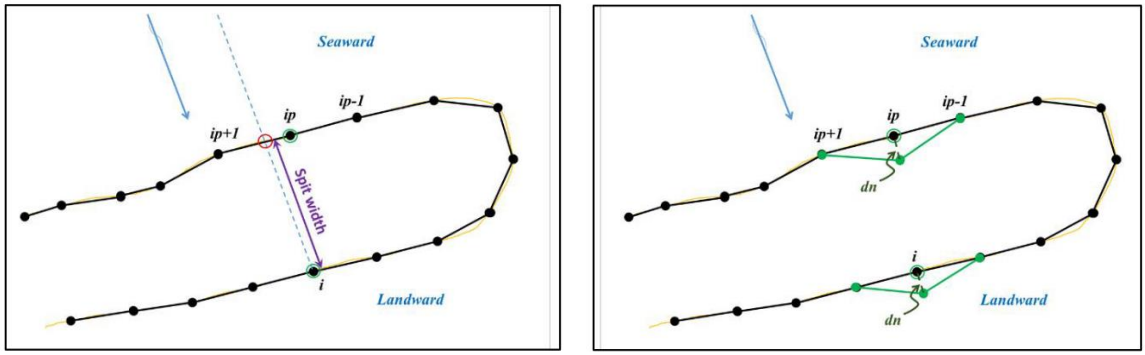

Figure 2-20 – Overwash schematization in ShorelineS maintaining minimum width (Roelvink, Huisman, and Elghandour 2018)

Splitting and merging

ShorelineS allows for coastline sections to split from or merge with each other. When a coastline section intersects with another (earlier separate) coastline section, ShorelineS merges the two separate strings into one new connected single coastline section.

3 Study case: Lobito, Angola

The Lobito spit will be used as a case study for this thesis, in this chapter general information is this case study is described. Section 3.1 provides information on the local environmental conditions In Section 3.2 the historical and recent spit development is described.

Lobito is a town located in Angola at the South-central Africa coast of the Atlantic Ocean (Figure 3-1). The coastline of this area is characterised by the presence of a 5km (approx.) long sand spit which forms the bay of Lobito. Nowadays the naturally sheltered bay is used for (still expanding) port activities. The sand spit itself is now considered as the most attractive area of the city on which luxurious beach clubs, restaurants, hotels and residences are present.

Figure 3-1 – Location of Lobito (Google LLC., 2019)

3.1 Environmental conditions

The groyne field at the spit of Lobito is already been evaluated by Deltares (2015) for the purpose of getting better insight into the past observed behaviour and the effect on the coastline due to possible changes (improvements) on this groyne field. As part of this research data concerning the local environmental conditions was gathered. For the next sections most of the information, unless stated differently, is adopted from this research.

Tide

At Lobito a semi-diurnal tide is present (Figure 3-2), the average tidal range fluctuates between $1.2m$ (spring tide) and $0.6m$ (neap tide).

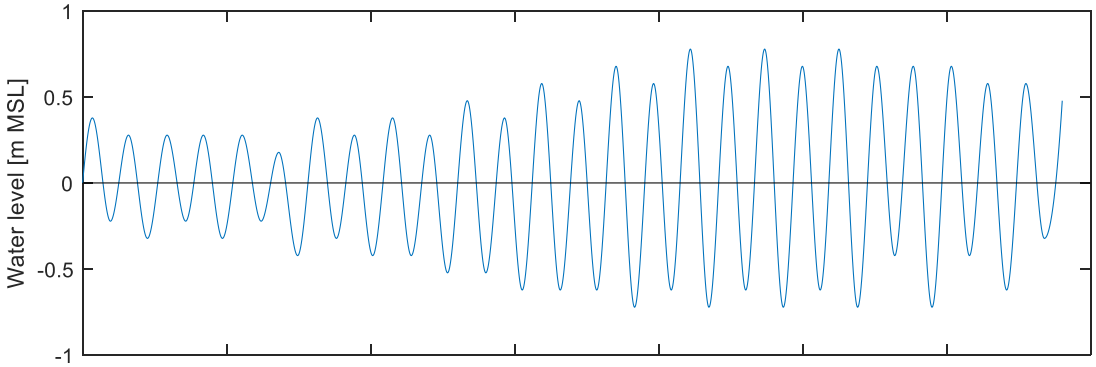

Figure 3-2 – 14 day tidal time series at Lobito port (24-07-2019 – 06-08-2019) (The UK hydrographic office Admiralty EasyTide, 2019)

Waves

The offshore wave climate at the coast of Angola is characterised by South-Westerly swell waves with a wave period of 8 to 15 seconds and a yearly maximum significant wave height (H_s) up to 2 meters (Figure 3-3).

The year-average nearshore wave conditions near of the Lobito Spit are determined using a SWAN model. With this model the offshore wave and wind data was transformed to the nearshore zone. A year-averaged wave climate was created which consist of 42 wave conditions (Figure 3-4 (left)).

In the wave field for the most dominant wave condition is shown in Figure 3-4 (right), from this is it clear to see that waves approach the coastline under a very high angle where as they reach the nearshore a reduction in wave height (wave breaking) as well as wave refraction towards the coast is visible.

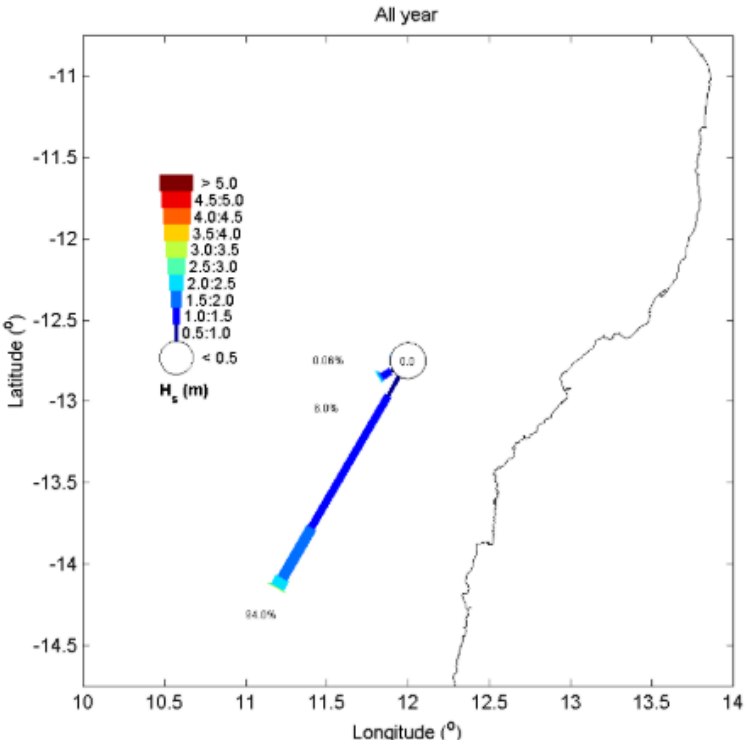

Figure 3-3 – Offshore wave climate at Lobito (Deltares, 2015)

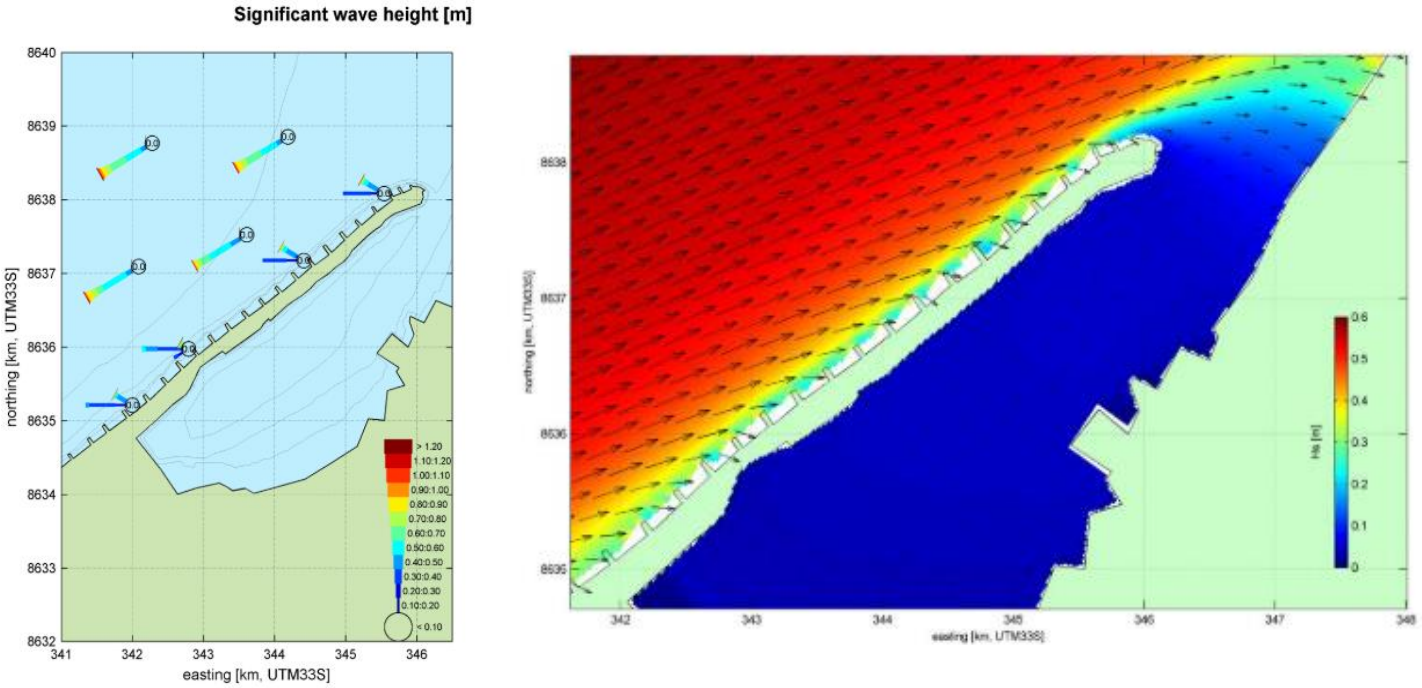

Figure 3-4 – Yearly near shore wave climate calculated with SWAN (left) Wavefield for most dominant wave condition (right (Deltares, 2015)

Bathymetry

A detailed measurement (survey) of the bathymetry in the nearshore is available, in combination with other sources (Nautical maps, GEBCO) a larger bathymetry was created (Figure 3-5).

It can be observed that the slope of the nearshore is very steep (1:15 to 1:20) up to a water depth of approximately 4 meters.

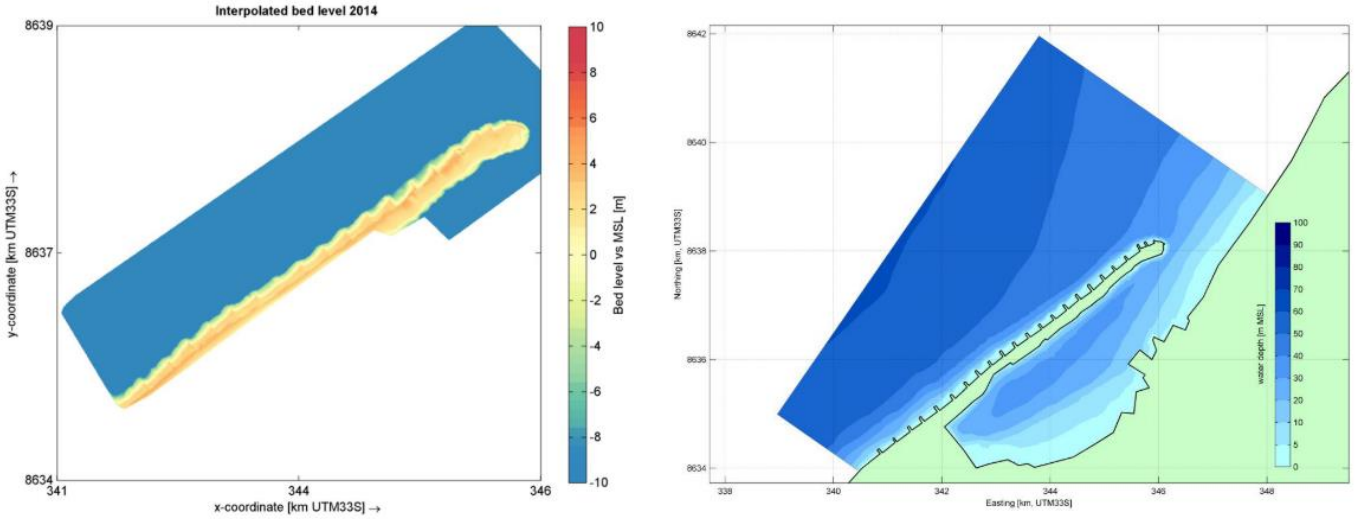

Figure 3-5 – Bathymetry of Lobito spit (Deltares, 2015)

Sediment

The main source of sediment for this coastal system originates from the Catumbela river mouth delta (see next section). This river mouth, located approximately 14km updrift (south west) from the sand spit, provides and created sand bodies along the coastline. (Dinis et al., 2016).

Based on the observed shoreline changes over the last years (2004-2014), a rough estimation of the alongshore sediment transport was made in Deltares (2015): in the coastline in between the most southerly constructed groyne and the 7th groyne (counted from the tip of the spit) has moved seawards over a distance of 90 meters during the last 50 years as result from the filling of the groyne sections. This requires a net accumulation within this cell in the order of $50.000\ to\ 80.000\ m^3/yr$. Over this period no/neglectable accretion down drift of the 7th groyne is observed and is therefore estimated at $0\ to\ 20.000\ m^3/yr$ resulting in a net incoming alongshore transport at the southern boundary of 50.000 to $100.000\ m^3/yr$ (Figure 3-6).

Figure 3-6 – Longshore sediment transport volumes at Lobito (Deltares 2015)

3.2 Historical spit development

The historical evolution of the coastline is analysed by Dinis et al. (2018). The geometry of the delta can be linked to the alternating north- and southward migration of the Catumbela river mouth which over time created a seaward extending delta (Figure 3-7).

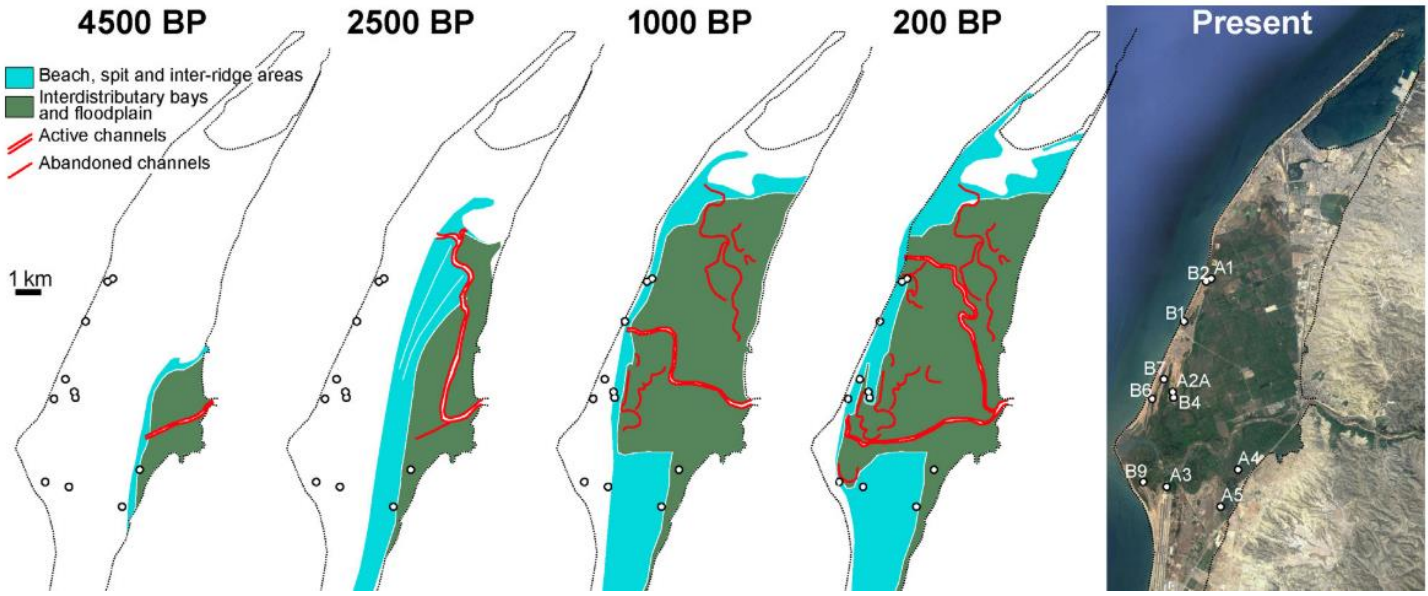

Figure 3-7 – Historical formation of Catumbela Delta (Dinis et al., 2018)

Due to the development and orientation of the delta the waves approach the coastline at the south (updrift) flank of the delta almost shore normal, while at the north (down drift) flank the waves approach the coast locally at a very high angle thus promoting unstable shoreline development. This had led to the formation of the characteristic spit at Lobito.

Information of the historical formation and migration of the Lobito Spit is scarce. According to Castanho et al. (1973) the spit extended rapidly northward with a migration speed of about $18 - 20\ {}^{m}/_{year}$ during the 19th and early 20th centuries (Figure 3-8). The migration of the spit was stopped by the construction of a groyne field.

In 1963 the construction of a groyne field was initiated. The two main reasons for the construction of the groyne field were: (Castanho, 1973; Kristensen et al., 2017)

1. The spit migration could lead to closure of the natural formed lagoon. This closure is undesirable since the lagoon is being used for port activities. The development of the groynes halted the spit migration by blocking the alongshore sediment transport.
2. The spit forms a natural protection for the harbour and densely populated city. Widening of the relatively small spit was desirable to lower the risk of breaching during a storm event. By catching the sediment within the groyne field, the spit would be widened.

In total 28 groynes were constructed with an average length of $100m$ and with an average spacing of $300m$. The construction of

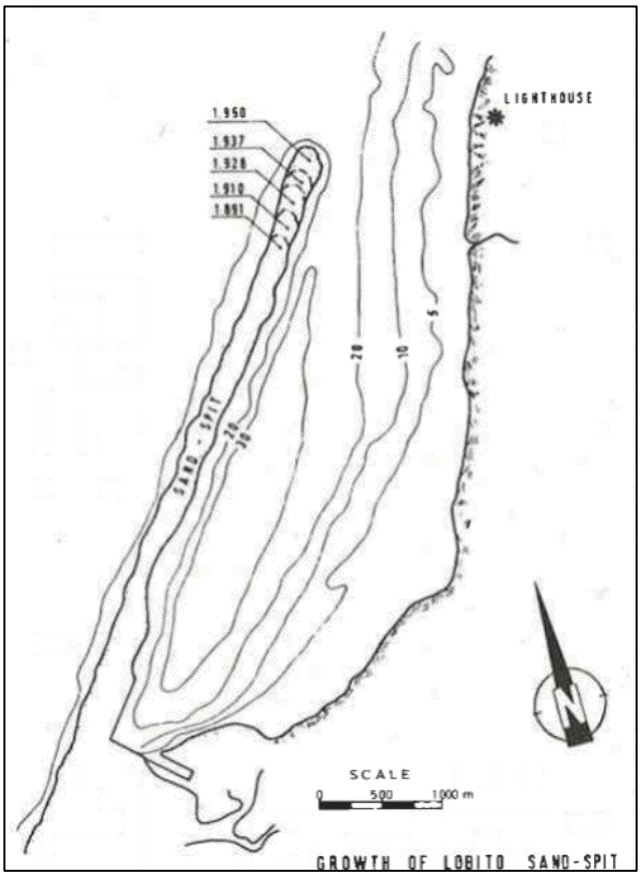

Figure 3-8 – Growth of Lobito spit 1890-1950 Castanho et al. (1973)

the groynes started in 1963 at the tip of the spit. The first 16 groynes were constructed one by one over a period of 8 years, Figure 3-9 (left) shows an aerial photo of the spit after the construction of the first 5 groynes. From this picture the working method becomes clear: first a groyne was constructed, after construction the sediment was blocked by the groyne thus the shoreline accreted, once the shoreline fully accreted towards the tip of the groyne the next groyne was be constructed at the point where the accreted shoreline crosses the initial shoreline.

This way the sediment transport is blocked stopping the spit migration and the spit is widened by the seaward shifted shoreline. After the construction of the groynes a typical sawtooth shaped coastline was visible (Figure 3-9. (right)).

Figure 3-9 – Coastline development after construction of first 5 groynes (left) Sawtooth coastline after construction of 16 groynes. (Deltares, 2015)

After the construction of the groynes the alongshore sediment stared filling up the area within two groynes even further starting at the most southerly located groynes. The sediment will fill up a groyne section until sediment can bypass the down drift groyne, after this the next groyne section will start to fill up. From 2004 on higher resolution images are available in Google Earth on which the sequential filling of the groyne field from north to south can be distinguished. (Figure 3-10).

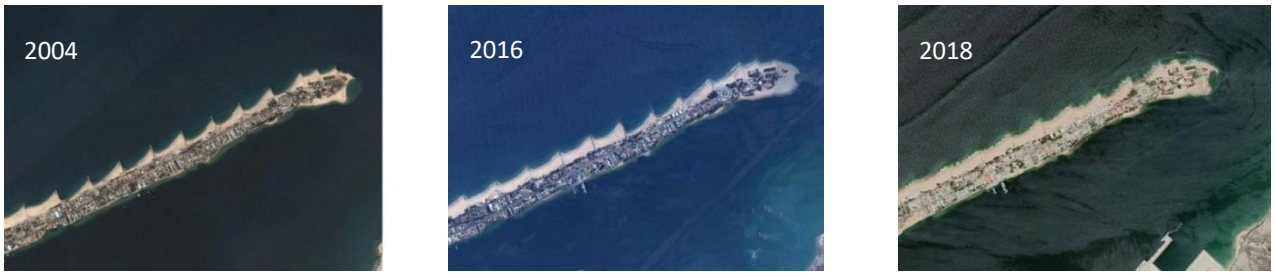

Figure 3-10 -Gradually filling up of groyne sections during 2004-2018

In 2011 a nourishment was done ($589.000 m^3$) at tip of the spit and in between the first 4 groyne sections to counteract the local erosion within the groyne schemes and effectively speeding up the filling of those sections.

The actions and resulting effect on the shoreline are summarized in Table 3-1.

Year	Action	Effect on coastline
1963 - 1971	Construction of 16 groynes at spit. One by one (north to south)	Sediment gets trapped behind groyne, shoreline accretes towards tip. (sawtooth shaped coastline) Spit migration stops
1984/1985	Construction of 12 groynes south from spit	Widening of beach updrift of spit
80's - now	-	Alongshore sediment sequential fills up and bypass groyne sections. (south to north) resulting in a less pronounced sawtooth shape coastline. Coastline (incl. under waterline depth contours) shift seawards.
2011	Sand nourishment at tip of the spit and first 4 groyne sections.	Extension of tip at the lagoon side, early filled up groyne sections at the tip of the spit.

Table 3-1 – Summary of historical interventions at Lobito and effect on the coastline

4 Spit formation processes

From the literature study (Section 2.1) insight was gained into the different possible mechanisms influencing and controlling the spit formation. In this chapter the spit formation processes are further explored.

In Section 4.1 an inventory and analysis is made of existing natural spits. This analysis focusses on the appearance of different spits, the historical formation and the local environmental conditions. The result of this step is a conceptual model which can be used to classify different spit shapes.

In Section 4.2 a detailed 2DH model (XBeach) was used to gain better insight into the hydrodynamics and /initial sediment transport patterns along the head of the spit for different environmental and geometric aspects. The influence of amongst others wave climate, tide and shape of the spit on the transport capacity along the spit analysed. This provides a more detailed insight into the physical processes controlling the shape and width of a spit.

The chapter ends (Section 4.3) with a discussion on the results of each step and an overall discussion followed by a summary of the conclusions

4.1 Conceptual model spit shapes

To get better insight into the spit shape (width) an inventory was made of 14 spits in nature, spread over 11 locations around the world (Figure 4-1). For each spit a brief analysis was carried out based on site specific (geological) studies and open data sources such as tidal charts (Meteo365.com Ltd., 2019) and (historical) Google Earth satellite imagery focusing on the following aspects:

1. Shape and dimensions of the spit
2. Local environmental conditions such as wave conditions and tidal range
3. Historical and current evolution of the spit / the sediment budget.

In Appendix A a brief analysis per spit can be found, the main dimensions and conditions are summarised in Table 4-1.

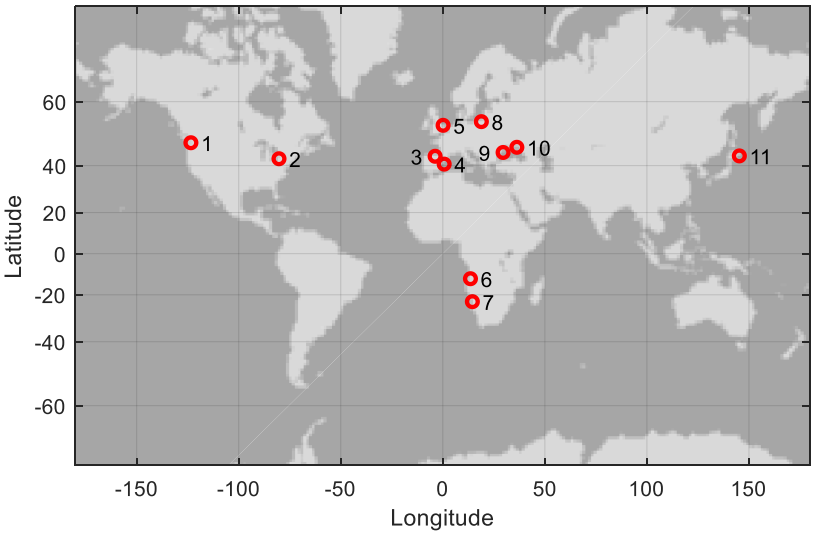

Figure 4-1 – World map showing locations of the analyzed spits

#	Name	Location	Tidal range [m]	Length [km]	W_{neck} [m]	W_{head} [m]	Literature
1	Ediz Hook	USA	3.27	5.5	40	250	(Campbell et al., 2019; Schwartz et al., 1987; Wegmann et al., 2012)
2	Long point	USA	0	37	1000-1500	1500-2000	(Davidson-Arnott et al., 1994, 2003; Stewart et al., 1988)
3	El Puntal	Spain	4.8	2.7	100	180	(Losada et al., 1991; Medellín et al., 2008)
4	Punta de la Banya	Spain	0.21	18.3	110	1000-2000	(Jiménez et al., 2004; Ribeiro et al., 2012; Rodríguez-Santalla, 2004)
5	Spurn Head	UK	6.4	5.5	75	380	(Ciavola, 1997)
6	Lobito	Angola	1.7	5.2	300	320	n/a[1]
7a	Walvisbaai	Nambia	1.9	22	800	1500-2000	(Bosman et al., 2008; Elfrink, Berry Prestedge Gordon, 2003; Serizawa et al., 2019)
7b				51 (1)[2]	350 (280)[2]	2500 (1000)[2]	

8	Hel Penninsula	Poland	0.03	34	190	2700	(Furmanczyk et al., 1995; Hanson, n.d.; Różyński, 2010; Szmytkiewicz et al., 1999)
9	Danube Delta	Romania	0.1	18	200	600-800	(Dan, 2013; Vespremeanu-Stroe et al., 2015)
10a	Azov	Ukraine	0.02	28	80	1800	(Kosyan et al., 2019; Rusu et al., 2018; Uda et al., 2014)
10b				27	60	1000-2000	
10c				44	160	3000-5000	
11	Notsukezaki Spit	Japan	1.3	22	50	1000	(Hayashi et al., 2011)

Table 4-1 - Summary of analysed spits. [1]The Lobito spit is used as case study for this thesis and treated extensively in chapter 3. [2]The second spit at the Walvisbaai (donated as 7b) consists of two parts with the upper (spit) at the head of overall spit. The values in the brackets indicate the dimensions of this upper part of the spit.

Based on the literature study on possible processes controlling the shape of the spit (Section 2.1.3, Figure 2-8) and analysed natural spits (Appendix A) a conceptual model was defined. This conceptual model describes the three commonly type spit head shapes, which can be observed in nature. The classification is primarily based the appearance of the spit, supported by a hypothesis on the relevant to the local environmental characteristics leading to a specific spit type.

Type A – Straight

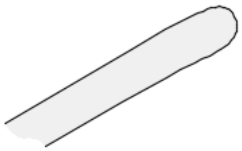

Figure 4-2 - Typical shape of the A-type spit

The type A spit is characterised by the lack of a clear distinguishable head compared to other analysed spits/spit types. The width of the tip of the spit is for this type similar to the width of the neck of the spit.

This type of spit was found in environments where waves are coming from solitary one direction (i.e., uni-directed wave climate). For example in swell-wave environments or locations where waves from other directions are blocked by the coastal geometry.

The effect of the tide (or the lack of it) seems of less importance for this type of spit with respect to the other spit types. It is hypothesised that for this spit type the width and shape is mainly controlled by the reach (refraction) of the dominant uniform wave direction along the head.

Type B – Smoothed round head

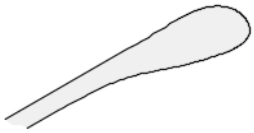

Figure 4-3 -Typical shape of the B--type spit

This type of spit is characterised by relatively narrow straight neck with respect to the neck, which (gradually) widens towards the tip (head). The head is shaped as a smoothed landmass (such as an island) which is orientated in line or slightly recurved land inwards with respect to the spit's neck.

This type of spit was be found in environments with a relatively large tidal range and a wave climate with, in addition to a predominance high angle wave orientation, a secondary wave component (i.e., bimodal wave climate). It was hypothesised that the formation of the neck and the overall orientation is controlled by the predominance high angle waves. The supply of sediment over the head is controlled by the secondary wave component which, in contrast to the predominance wave direction, is able to reach (refract around) further around the head of a spit. The main difference in environmental characteristics for this type compared to the type C spit is the presence of a significant tide, which can be related to the smoothing of the spits' coastline and smoothed head shape.

Type C – Shoots

Figure 4-4 - Typical shape of the C-type spit

This type is of spit is characterised by the head which consist of a composition of long narrow 'shoots'. In contrast to the type A- and B-spit the head is not a smoothed and evenly distributed land mass but consists of ridges (the 'shoots') alternated by low land areas, channels or enclosed water bodies. For some of the analysed spits classified as type C overwash fans were found along the backside of the neck.

This spit shape was found in environments in which in addition to a predominance wave orientation a secondary wave component is present (the bimodality in the wave climate, similar to the type B spit). It was hypothesised that the lack of

a significant tidal range in those particular environments prevents the smoothing of the head and coastline. This results in the presence of the characteristic 'shoots' and overwash fans. In cases where a clear seasonal or yearly variation in wave direction is present (i.e., most months of the year high angle waves, except for some months) the individual 'shoots' at the head are best distinguished by clear lines of vegetation, sand and waterbodies and thereby reflect the seasonal variability as 'annual rings', as shown by Serizawa et al. (2019).

In Figure 4-5 the classification of the analysed spits (Appendix A) using the conceptual model is shown. The Lobito spit is according to this classification a type A spit. It should be noticed that in reality the classification is not a strictly bounded grouping but rather a spectrum with where a certain spit can be a combination of two types (i.e., as observed for the Walvisbaai spits (no. 7)).

The conceptual model is primarily based on the observed (morphological) appearance of the spit formation. Although the types are supported by characteristics and combination of the wave climate (bimodality) and tide it should be noted that location specific circumstances such as the local bathymetry, (wave) interaction with structures/ coastline geometry and or historical human induced costal works can also have an influence on the final spit shape.

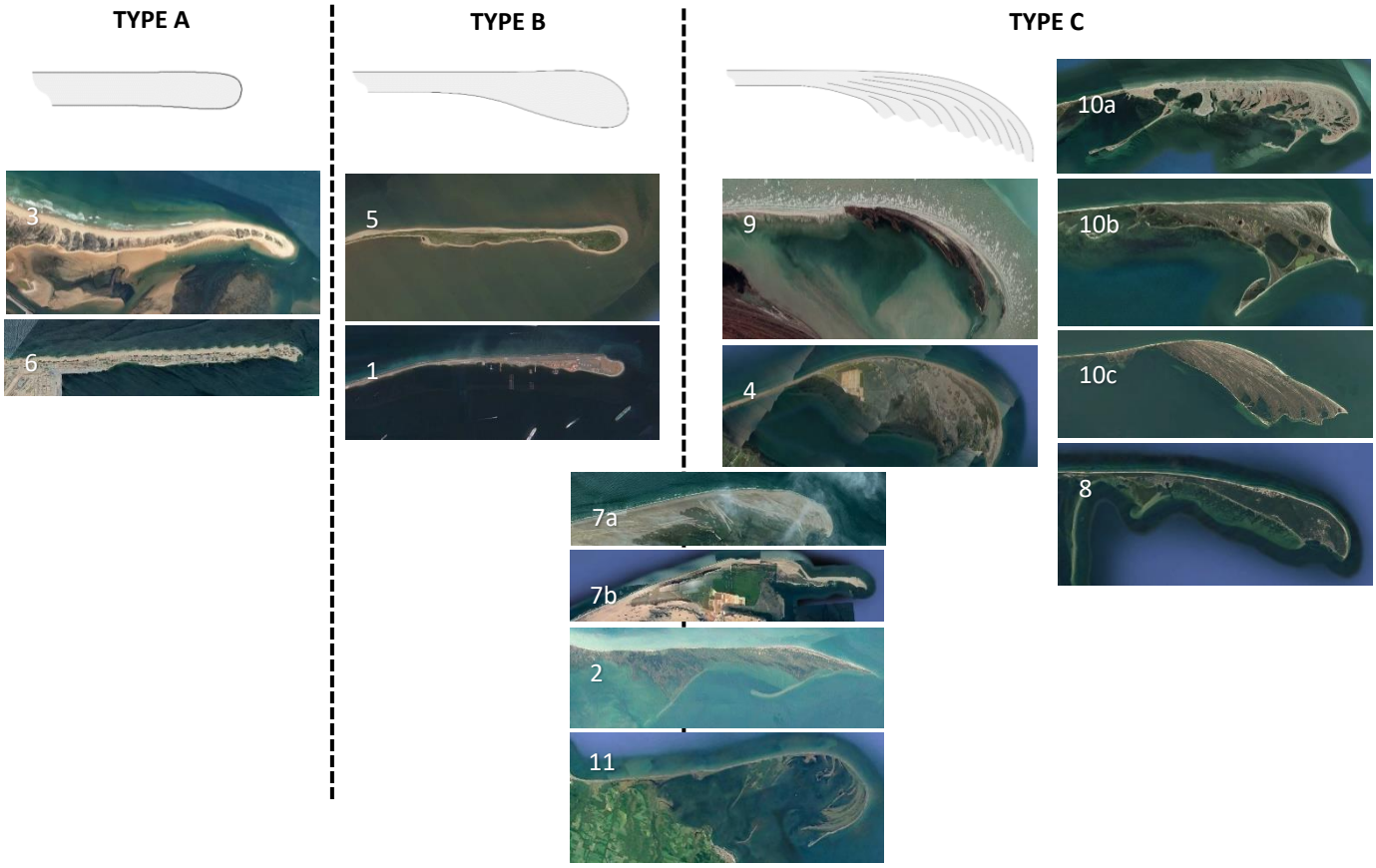

Figure 4-5 – Classification of the analyzed spits based on the conceptual model

4.2 Detailed modelling of spit formation

In this section a XBeach modelling study was done to get detailed insight into the sediment transport patterns along a spit for different possible forcing mechanisms.

4.2.1 Methods

To investigate the influence/contribution of different processes to the shape and width of a spit, a detailed computational model was applied on the Lobito Spit case study (Chapter 3). From this the hydrodynamics (e.g., wave field and currents along the spit's head) and the resulting transport patterns for different modelling cases provide, amongst others, insight into the resulting distribution of sediment along the head of the spit. The latter is especially of interest as the gradient in longshore sediment is the main driver for coastal evolution in the ShorelineS coastline model. This knowledge valuable as it can be used to better understand and incorporate the relevant processes in the ShorelineS model routines. There will be no morphological update used in the model as the interest is on the 'initial' transport for a given, imposed, fixed coastline/spit shape.

The modelling study will not only be used to gain insight into the relevant processes for the Lobito case, but also in a broader context: to gain insight into how different processes (as discussed in the literature study Section 2.1.3) contribute to the spit formation. For the latter 'what-if' scenarios were applied on the Lobito reference case. The analysis focuses on the following possible forcing mechanisms:

1. **Wave climate**
   The influence on the hydrodynamics and transport capacity along the spit due to the different (extreme) components of the wave climate. A 'what if' scenario using a wave from a secondary (opposite) direction is applied to gain insight into the effect of the bimodality of a wave climate on the spit formation.
2. **Tide**
   Influence of the tide and resulting tide-induced currents and transport along the head of a spit.
3. **Shape and width of the spit**
   In addition to the current shape of the Lobito spit, a 'what-if' analysis was done using different hypothetical spit shapes and varying a width.

4.2.2 Model set-up

General model settings

For the detailed model simulation of the Lobito Spit case study the open-source numerical model XBeach was used. This model includes hydrodynamic processes such as the wave transformation (Wave breaking, - refraction and -shoaling) for short waves, wave set-up, long-wave transformation and unsteady currents as well as morphodynamic processes. XBeach has options for both hydrostatic- (Stationary and instationary/surfbeat) and non-hydrostatic-modelling (wave-resolving). For this modelling purpose the hydrostatic Surfbeat 2DH area mode was used, which includes short wave motion and variations of the wave height on scale of the wave group, thus not resolving each individual wave as the non-hydrostatic mode. The latter is reducing the required computational effort significantly for the Surfbeat mode compared to the non-hydrostatic model.

All calculations are based on the initial bathymetry i.e.: the wave field and sedimentation transport patterns are all based on the initial bathymetry with no morphological update in the model. A summary of the general XBeach model parameters is stated in Table 4-2.

Model settings	
Mode	Surfbeat (Short wave, Long wave, flow)
Model time	1hr for model runs without tide / 24hr for modelrun with tide
CLF	0.7
Left boundary	Neumann (no gradient in surface elevation and velocity)
Right boundary	Neumann (no gradient in surface elevation and velocity)
Offshore boundary	Waterlevel (static/tide) + waves
Land boundary	Land (closed)

Sediment transport settings	
Transport model	Van Thiel-van Rijn
D_{50}	5mm
Porosity	0.4
Bed friction	Manning (XBeach standard)

Table 4-2 – General model settings and parameters of the XBeach model

Wave climate

At the offshore boundary a wave climate is applied. For an average wave condition the model runtime is in the order of 3.5 – 4 hours to hydrodynamics an initial sediment transport pattern. To reduce the computational time the full wave climate consisting of 42 wave scenarios (Section 3.1) was reduced. This was done by grouping the wave climate into 8 bins: 4 fixed directional bins and 2 wave height bins resulting in 8 representative wave conditions (Table 4-3, Figure 4-6). The weight (relative duration) of each representative wave condition is based on the duration of the original wave conditions per wave bin in combination with a proxy for the sediment transport per wave condition ($S \propto H_s^2$).

In addition to the reduced wave climate, also a single representative wave condition was used to investigate the influence of the individual/extreme conditions versus the average condition. This single representative wave condition was derived by using UNIBEST where the average longshore transport for a straight coastline from the full wave climate was represented by a single condition. (Further described in Chapter 5, Section 5.1.3).

To assess the effect of the wave climate bimodality a wave condition from opposite direction with respect to the average/high angle direction is used as for a hypothetical 'What-if' scenario.

Descr.	Hs [m]	Tp [s]	Dir [°]	Dur
RWC1	0.58	9.35	245.07	0.76
RWC2	0.80	9.97	246.68	0.17
RWC3	1.00	11.09	249.82	0.06
RWC4	0.72	9.32	248.86	0.012
RWC5	1.20	11.67	254.80	4E-4
RWC6	1.35	11.67	263.10	1E-4
RWC7	0.88	9.46	259.60	1E-4
RWC8	1.49	14.39	253.62	1E-4
AVER	0.68	9.46	246.70	1
OPPO	0.5	6.00	27.00	n/a

Table 4-3 - Wave conditions used in the XBeach model runs. RWC=Reduced wave condition, AVER=Single representative wave condition, OPPO=wave scenario originating from direction opposite to dominance direction.

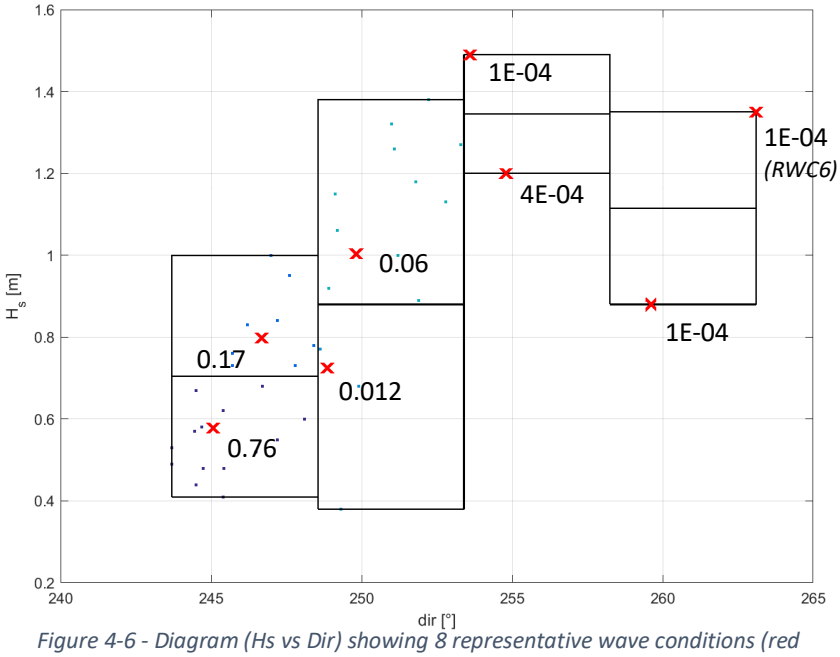

Figure 4-6 - Diagram (Hs vs Dir) showing 8 representative wave conditions (red crosses) and duration resulting from 8 fixed bins. 42 original wave conditions are indicated by the dots

Tide

For the model case in which a tide was applied a 24-hour 'average' signal consisting of two HW and two LW was used from the 14-days tidal cycle as measured at the Lobito Port (Figure 4-7). The tide is applied as time varying water level signal boundary condition at the offshore boundary.

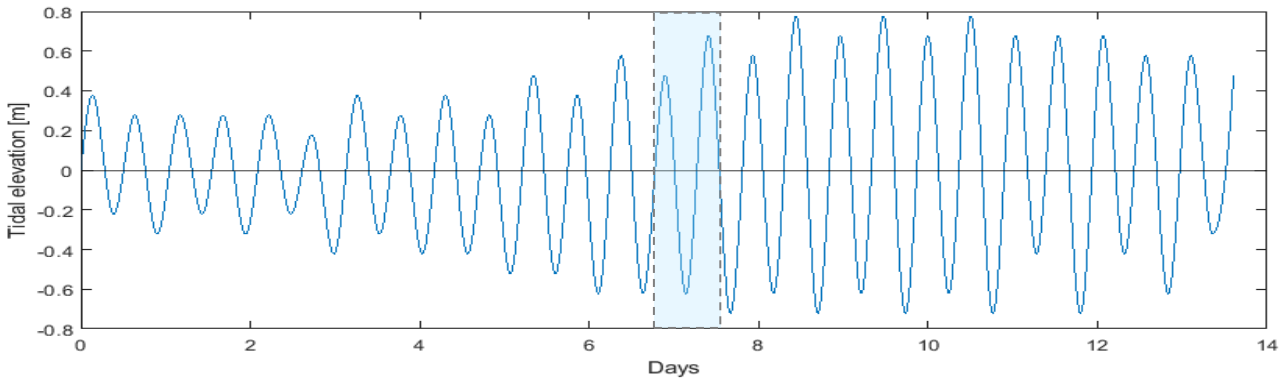

Figure 4-7 - 14-day tidal signal at Lobito port, 24hr time signal used in model run highlighted in blue (The UK hydrographic office Admiralty EasyTide, 2019)

Spit shapes

For the analysis of the first two points of interest (influence of wave/tidal forcing) a base shape spit was derived. This shape is based on the current shape of the Lobito spit's head using recent (record 06-2019) Google Earth satellite imagery and the available bathymetry. The groynes and in between sand pockets are smoothed/averaged out to generate a smooth coastline along the spit as expected and found in nature (Figure 4-8).

For the third point of interest, the more general what-if analysis using different shapes, in addition to the current shape four hypothetical shapes were derived. The following spit shapes were used (Table 4-4):

- **Round shape**
  Rounded off symmetrical spit head, the radius of the circular shape equals the half the width of the spit.
- **Elongated shape 1:2**
  This symmetrical shape is more elongated / elliptical compared to the round shape. The ratio of the width versus the length equals 1:2
- **Elongated shape 1:3**
  Similar to previous shape but now with a width versus length ratio of 1:3
- **Blunt shape**
  Asymmetrical blunt shape, in essence a half-elongated shape (ratio 1:3) over the entire width of the spit with the back (lee side of the spit) cut off.

Figure 4-8 – Averaged/ smoothed out coastline used to generate spit bathymetry shown in red

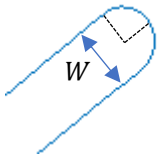	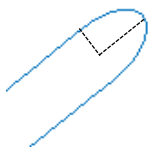	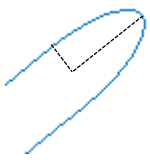	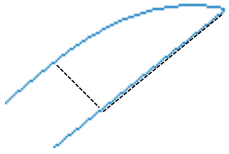
Round	**Elongated (1:2)**	**Elongated (1:3)**	**Blunt**

Table 4-4 – Hypothetical shapes used in the 'what-if'-analysis

For all shapes (including the current shape) the width of the shape has been variated by scaling it from a fixed point. This fixed point is located at the start of the head shape, the scaling is done land inward, this way the coastline of the spit is the same for all different shapes at the seaward position (no updrift changes). All shapes are scaled in two directions as a ratio to the base width (W_{base}), keeping the shape proportions the same for each case (Figure 4-9).

The scaling ratio and spit width are included in Table 4-5

	Spit width (W_{spit}) [m]			
Shape	$a)\ 0.75W_{bas}$	$b)\ W_{base}$	$c)\ 1.25W_{bas}$	$d)\ 1.5W_{base}$
Current	240	180	300	360
Shape var.	160	120	160	240

Table 4-5 – Scaling ratio and corresponding width for different modelled spit shapes

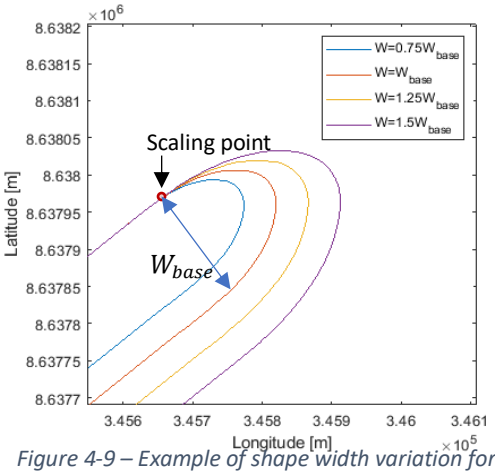

Figure 4-9 – Example of shape width variation for elongated (1:2) shape

Bathymetry

The available bathymetry of the Lobito spit dates from when the groynes were already constructed thus, including the sawtooth filled groyne pockets (Section 3.2) and other human intervention such as the construction of a breakwater and execution of a sand nourishment. This bathymetry does not reflect a natural spit, which is of interest for this modelling study. In order to be able to generate a smooth natural spit and to be able to change the shape and width of the spit without changing the surrounding bathymetry the following routine was applied (Figure 4-10): A smooth bathymetry was derived for the Lobito coastline without the spit (Figure 4-10, left), this bathymetry is used as underlying bathymetry, it reaches along the entire stretch of the spit (+2km) and up to the 50m depth contour at the offshore boundary. The bathymetry of the spit itself was generated based on the average coastline (MSL=0m) and the average cross shore profile uniformly applied along this coastline. The cross-shore profile is based on the average profile along the spit spit (slope 1:20 up to $4m$ depth, offshore slope 1:3.5 for $d > 4m$) (Section 3.1).

The two separate bathymetries of Lobito without the spit and the spit only are combined by finding the minimum depth per grid point (Figure 4-10, right) which basically place the spit on top of the underlying bathymetry. This procedure allows for a simple and straightforward generation of different bathymetries for different spit shapes/widths ('what-if' analysis) without influencing the surrounding bathymetry.

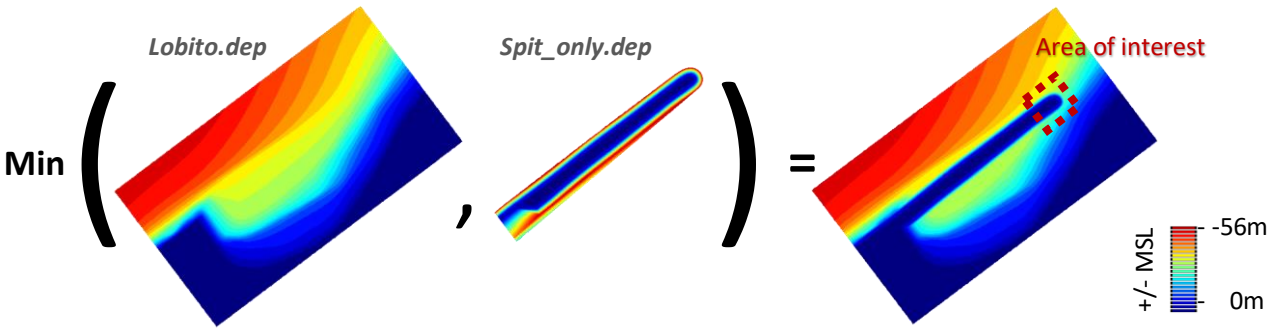

Figure 4-10 – Routine to generate smooth spit bathymetry for Lobito XBeach model runs.

Within the area of interest at the head of the spit (indicated in Figure 4-10) a locally refined grid size of $d_x = d_y = 5.6m$, to reduce computational time the grid cells outside the area of interest are larger ($d_x = d_y = 50m$).

4.2.3 Modelling scheme

All previously mentioned model variations are combined into 9 different cases (Table 4-6).

Case #	Case description	Wave climate (Table 4-3)	Spit shape	Tide	Sim time
1	Base case,	RWC	Current	No	1hr
2	Base case + single repr. wave	AVAR	Current	No	1hr
3	Base case + Opposite wave	OPPO	Current	No	1hr
4	Base case + tide	AVER	Current	Yes	24hr
5(a-d)	Width variations of current shape	AVER	Current (+Width variations a-d)	No	1hr
6(a-d)	Shape/width variation 1	AVER	Round	No	1hr
7(a-d)	Shape/width variation 2	AVER	Elongated (1:2)	No	1hr
8(a-d)	Shape/width variation 3	AVER	Elongated (1:3)	No	1hr
9(a-d)	Shape/width variation 4	AVER	Blunt	no	1hr

Table 4-6 – Modelling scheme summarizing the preformed model runs, the a-d suffix corresponds to the imposed width of the base (Table 4-4)

4.2.4 Model results

In this section the model results and observations for the different model cases are provided. All results are focussed round the head of the spit at the area of interest (Figure 4-10).

Base case

For the base case (case 1, Table 4-6) the average wave pattern for the wave climate (Figure 4-11, left) clearly shows the wave refraction towards and around the head of the spit. At tip of the spit wave rays are focussing on the head of the spit (1), more eastwards from the tip wave rays tend to diverge and are orientated both towards the spit as well deflect towards original coastline. This pattern can be linked to the observed mean wave height around the head of the spit (Figure 4-11, right). Here the wave spreading and, in addition to this, the wave shielding of the spit itself lead to an overall wave height- and thus wave energy reduction along the head of the spit.

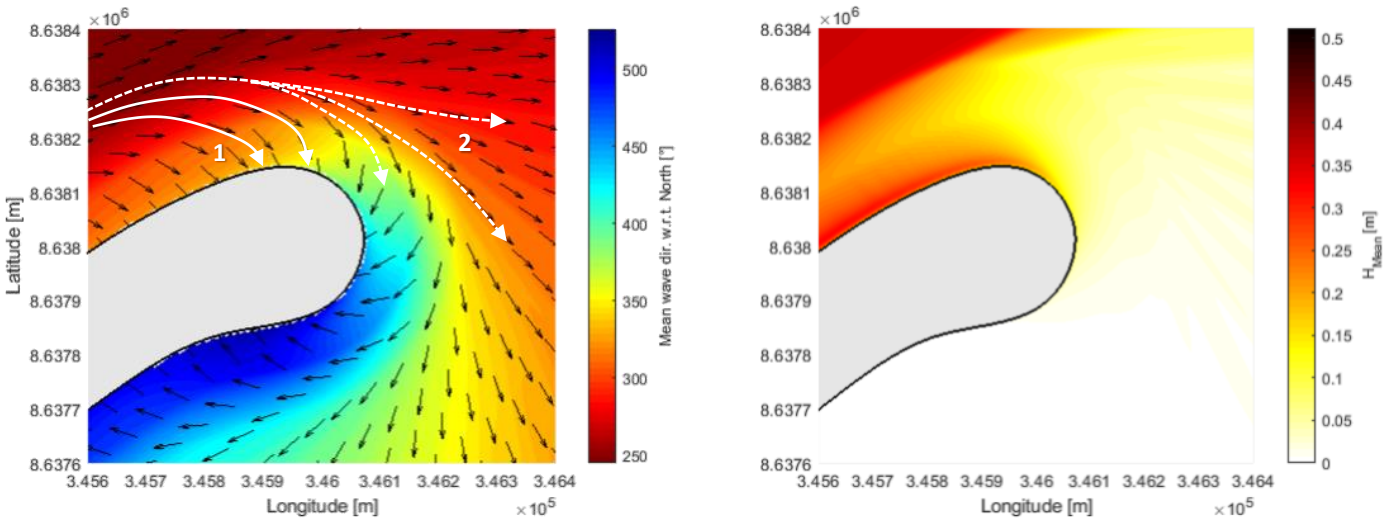

Figure 4-11- Left: Mean wave direction. Right: Mean wave height. Both averaged for the reduced (8 wave conditions)

In the surfzone the breaking waves generate an alongshore current (Figure 4-12, left). The alongshore current reduces as the wave energy reduces. The current drives the sediment transport, therefore the mean sediment transport pattern (Figure 4-12, right) is similar to the flow pattern.

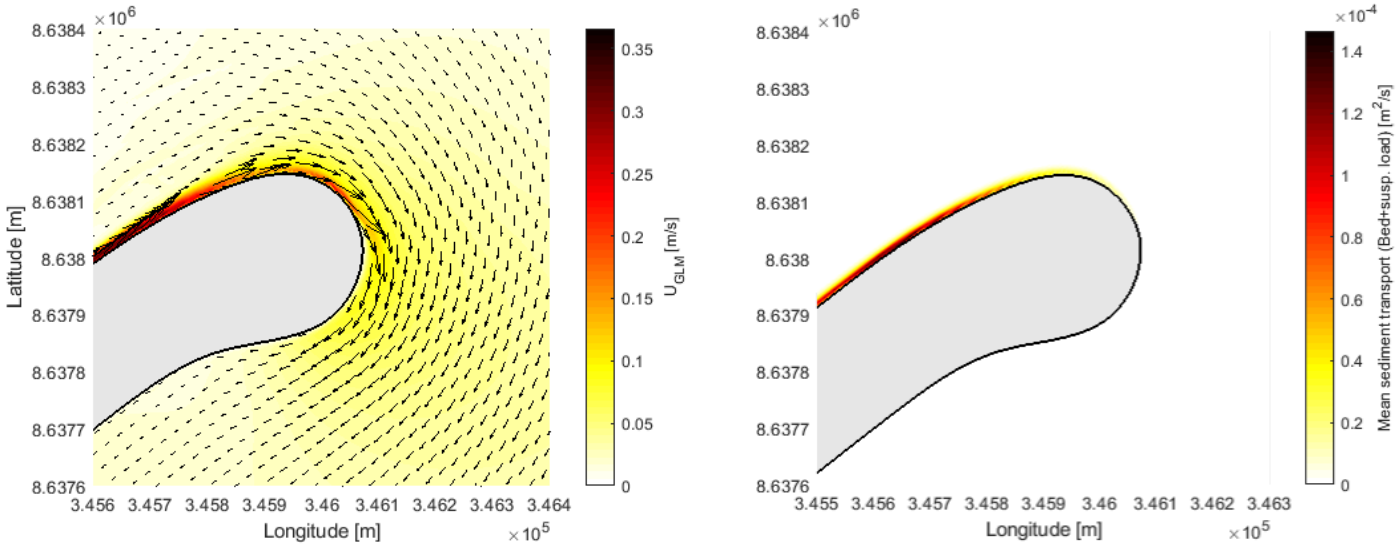

Figure 4-12 – Left: Mean flow velocity (GLM) Right: Resulting mean sediment transport. Both averaged for the reduced (8 wave conditions)

From the sediment transport pattern, the net (and gross) alongshore transport can be derived. This was done by integration of sediment transport along perpendicular cross sections along the spit (Figure 4-13).

The net alongshore transport is fairly constant updrift from head of the spit (the neck) with a magnitude $10 \cdot 10^{-4}\, m^3/s$ or $53 \cdot 10^3\, m^3/yr$ (including pores $p = 0.4$) which is in the same order of magnitude as the observed alongshore transport at the Lobito spit ($50 \cdot 10^3$ to $100 \cdot 10^3\, m^3/yr$, Section 3.1). Moving towards the head of the spit the sediment transport first increases after which it gradually, approximately linearly, decreases over the head of the spit. A linear decay results in a constant gradient in alongshore transport (Q_S), thus a uniform sedimentation along the spit. This implies that over time the spit will build out while the shape of the spit is retained (i.e., it is an equilibrium shape as described by Petersen et al. (2008)).

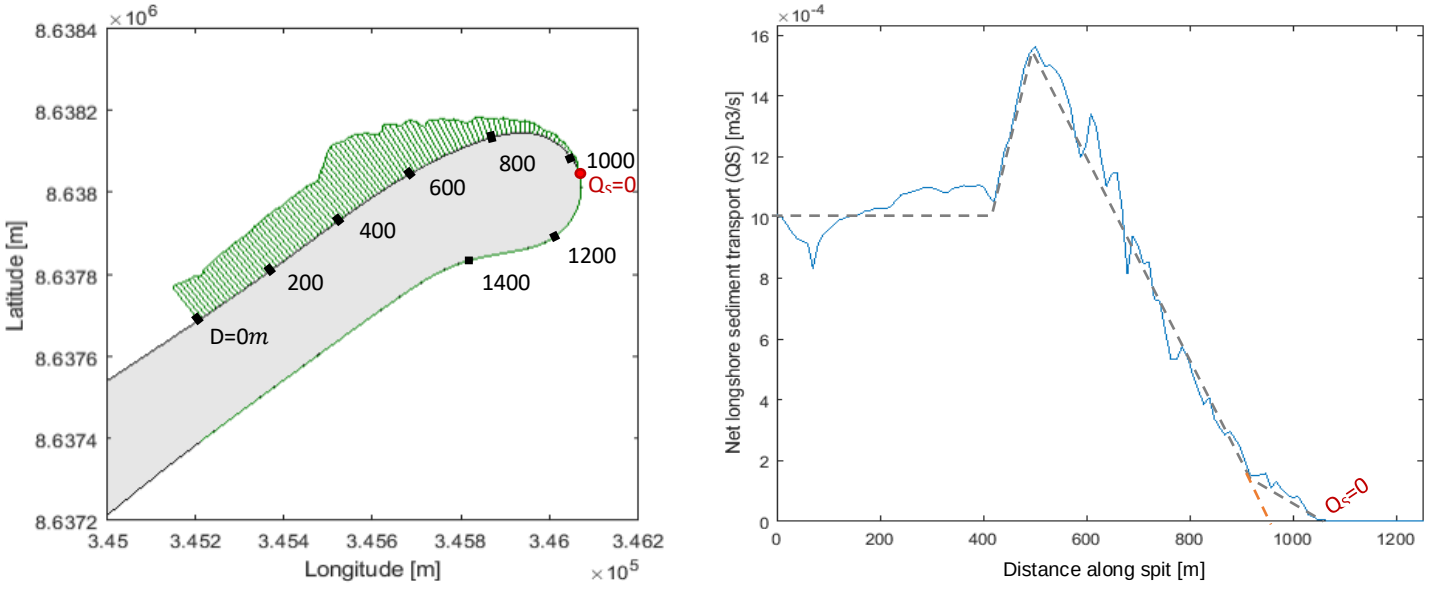

Figure 4-13 – Left: alongshore sediment transport plotted along the spit (qualitative) Right: Plot of quantitative net integrated alongshore transport along the distance of the spit.

The sediment transport, however, does not reach along the entire front side (or width) of the head spit. The transport reaches to $d \approx 970m$ (based on linear extension of the decay) up to $d \approx 1030m$ (actual $Q_s = 0$ point Figure 4-13, right). In terms of width of the spit this corresponds to respectively 170m (53%) up to 215m (67%) of the maximum width of the head of the spit ($W_{head,max} = 320m$). The remaining part of spit is not supplied with sediment by the wave action which would imply it would not be able to 'grow' over time together with the part over which the sediment transport reaches. For this particular shape (based on the current head of the spit) it should be noted that the maximum width ($W_{head,max}$) is larger than the width of the base/neck of the spit ($W_{base} = 240m$,Table 4-5) due to the extended bugle shape (in between $d = 1100 - 1400m$) which was formed by nourishments at the end of the spit (Figure 4-8).

Influence of wave climate

To analyse the variability of the sediment transport within the wave climate itself a comparison (Figure 4-14) was made between the result of the reduced wave climate (Base case, case 1), the contribution of the wave within the wave climate with the largest relative angle with respect to the spit (RWC6 of case 1, Table 4-3) and the result of case 2, which only consist of one representative wave condition. From this the following observations can be made. When comparing the result of the reduced wave climate versus the result of the single representative wave condition it stands out that the results match both in magnitude and the overall sediment distribution and decay along the spit. The sediment transport reaches for both cases approximately the same distance along the spit.

When comparing the results of the reduced wave climate versus the contribution of the wave condition with the largest relative wave angle (RWC6) larger differences can be observed. In addition to the higher relative angle, the wave height, thus wave energy, for this wave condition is also larger ($H_s = 1.35m$) than the average condition ($H_s \approx 0.7m$), this resulted in a factor 35 times higher overall transport magnitude than the average condition. The second observation which can be made for this wave condition (RWC6) is that the distance along the spit which the sediment transport reaches is higher than for the averaged condition, which implies that certain extreme conditions (i.e., wave condition(s) with a less obliquely incident wave angle as part of an overall very obliquely wave climate) can 'push' the sediment further around the tip of a spit compared to the average conditions. However, as already 93% of the reduced and/or full wave climate of Lobito (Table 4-3 resp. Table 5-3) consists of wave conditions with a wave direction in the range of $244° - 248°$, the contribution and thereby influence of those extreme events on the overall/yearly averaged sediment distribution over the head of the Lobito spit is very limited.

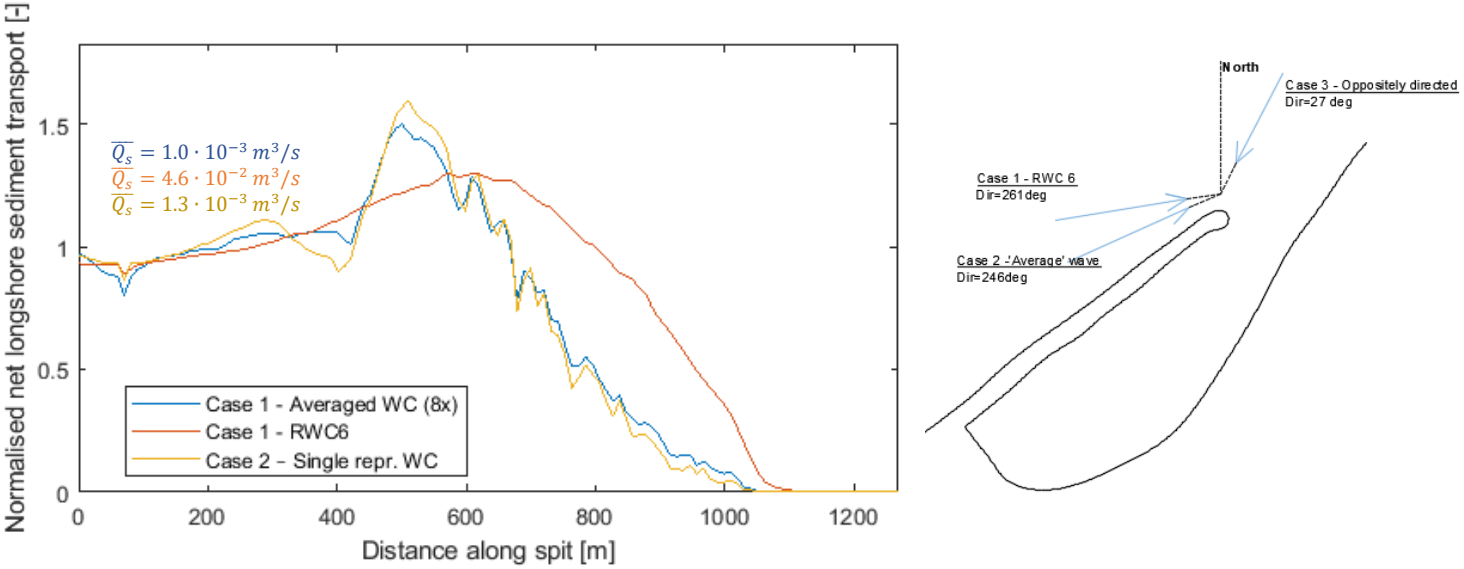

Figure 4-14 - Left: Normalized net longshore transport for averaged case, wave condition 8 and the single representative case. Transport normalized by the averaged updrift sediment transport (indicated by value). Right: Visual representation of the different considered wave directions with respect to the Lobito spit.

Influence of wave climate bimodality

The 'What-if'-scenario (case 3) in which a wave oriented from an opposite direction of the average wave condition was imposed to the Lobito case (Figure 4-14, right), provides better insight into how certain conditions and the bimodality of the wave climate can contribute to the development of the width of a spit. The results of this case show (Figure 4-15) how sediment can be (re-)distributed over the head of a spit. For all the wave conditions in the original wave climate for Lobito the direction of the alongshore transport along the spit is in one direction: from west to east. For this case a clear split in gross transport can be observed at the head of the spit. This leads to first a local increase of the sediment transport (erosion) followed direct decrease (sedimentation) over the tip and backside of the head of the spit. By this, waves oriented from a deviant direction with respect to the dominant or average wave direction form a mechanism which can push the sand along the head of the spit.

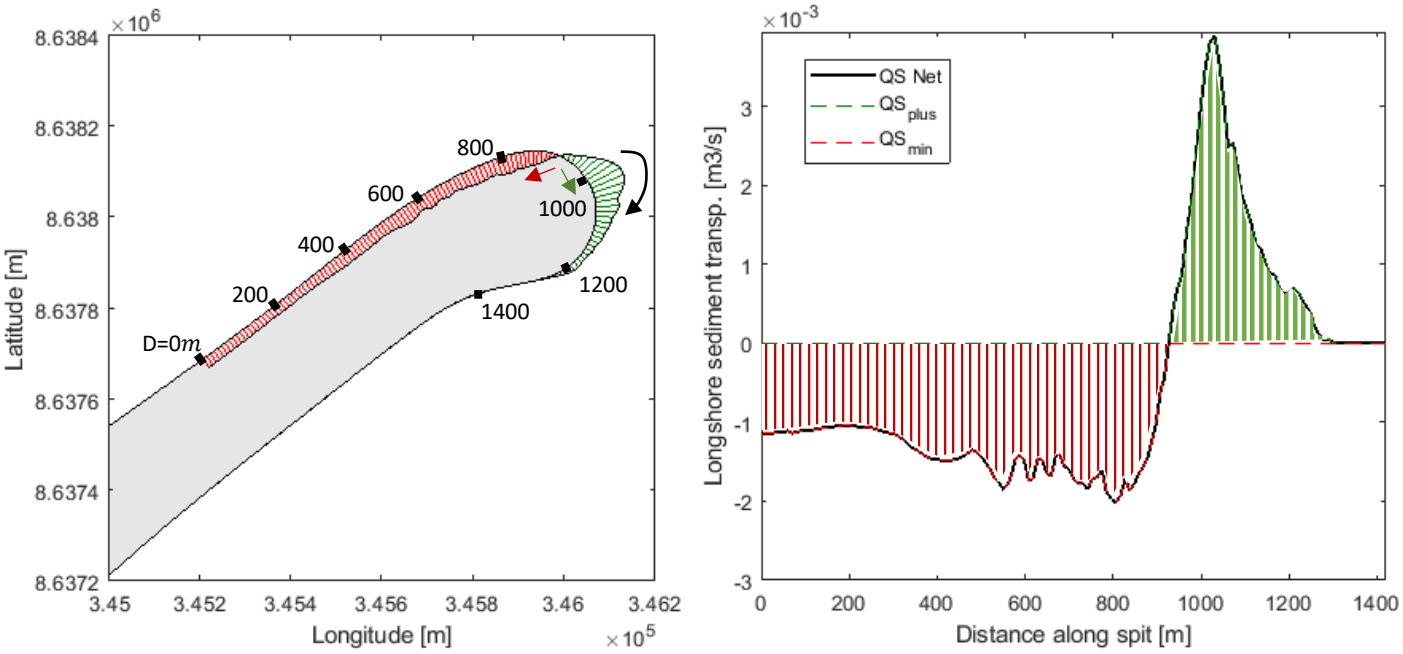

Figure 4-15 – Gross transport along the spit for case 3 (Wave from opposite direction)

The result of this 'what-if'-scenario was combined with the result of the reference case (case 1) to get insight into the potential influence of a bimodality of the wave climate on transport distribution along the spit. This was done by adding the opposite wave condition (case 3) to the wave (reduced) climate (Figure 4-6) with a duration of 7 days.

This resulted in an average alongshore transport distribution along the spit (Figure 4-16). It can be observed that the mean transport magnitude is slightly reduced along the neck of the spit and a part of the head of the spit since a part of the transport of the 'what-if' scenario is directed in the opposite direction (Figure 4-15). This plot also shows that the average transport reaches a larger distance along the spit (redistributed), compared to the reference case. This indicates that a larger part of the head of the spit for this combined case is supplied with sediment, thus is able to build out/migrate.

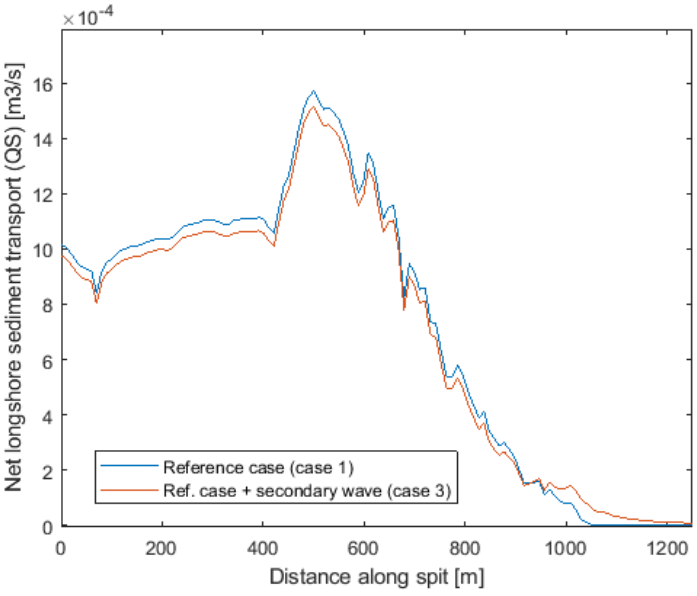

Figure 4-16 – Net averaged wave climate transport distribution along the head of the spit for the reference case versus the wave climate combined with a wave component from an opposite direction.

Influence of tide

In the previous discussed model runs the forcing was induced by waves only. In model case 4 a 24-hour water level signal, consisting of two tidal cycles, was applied to the model to analyse the influence on the sediment transport along the head of the spit due to the tide. The first cycle was used to spin up the numerical model.

The (averaged) flow field around the spit was considered at three characteristics to get insight into the effect of the tide (Figure 4-17):

1. **During flood**
   During flood the water level rises. The landmass of the spit partly encloses a part of the waterbody, leading to a water basin with a wet surface area of $\sim 8.5 km^2$ surrounded by the spit and the coastline of Lobito (e.g., Figure 3-1). During flood the rising water level will result to an inflow of water in this semi-enclosed water basin through the opening of the basin, which is located in between the head of the spit and the mainland of Lobito. The tide and the flow through this opening will result in an overall flow pattern directed inwards (Figure 4-17, bottom left).
2. **During ebb**
   During ebb an opposite pattern can be observed (Figure 4-17, bottom center): the water level falls leading to an overall outflow of the water from the semi-enclose water basin. This leads to a flow in the opposite direction with respect to the flow as observed during flood. It should be noticed that the flow direction close to the coastline, caused by the high obliquely incident wave action, is still directed along the spit. This results in a flow field where within the breaker zone the flow is directed from west to east and more offshore from east to west.
3. **During slack**
   Around slack tide, where the flow/water level reverses from falling to rising or vice versa, there no clear in nor outflow pattern can be distinguished.

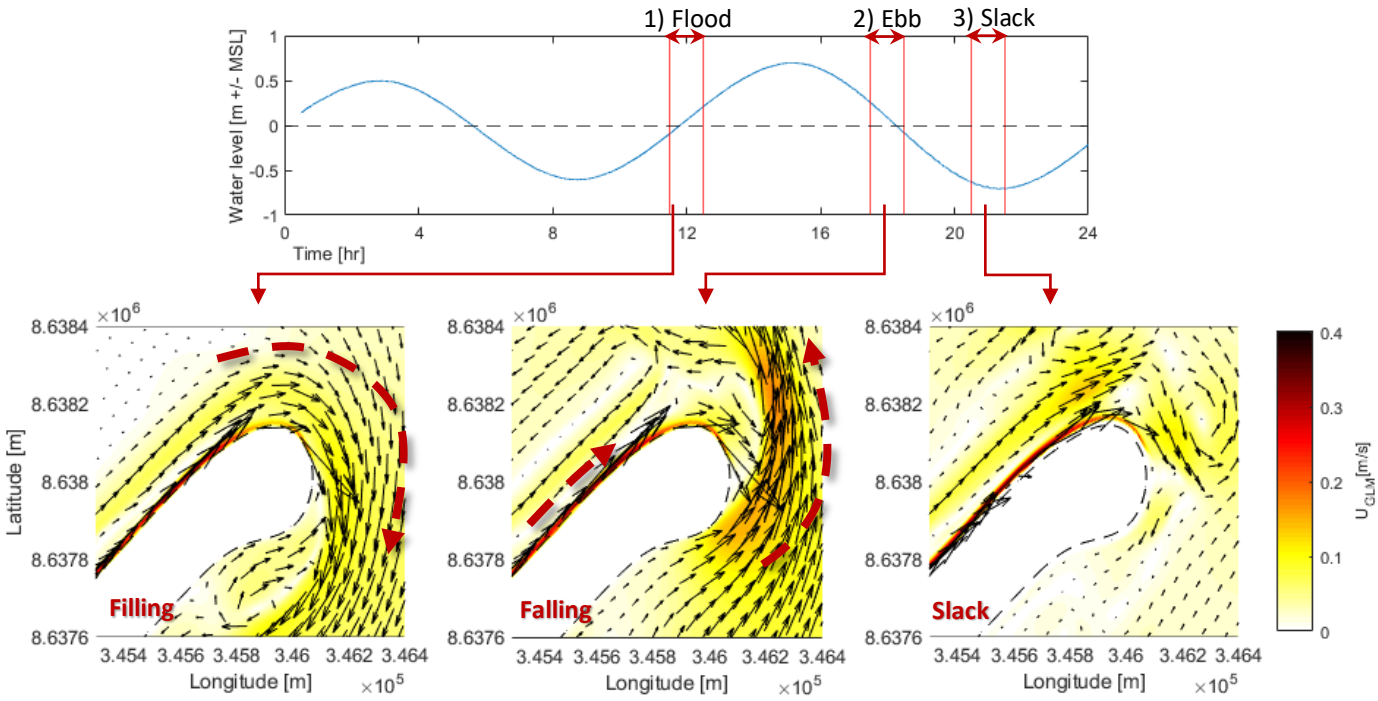

Figure 4-17 – Flow velocity field around the head of the Lobito spit for three characteristics moments during the tidal cycle

When looking at the resulting alongshore sediment transport along the head of the spit no significant increase nor decrease in both the magnitude as well as the distance the transport reaches can be observed when comparing the three characteristic moments of the tide (Figure 4-18, left). The alongshore transport during the tide has a comparable magnitude and distribution as the model run without the tide (reference, case 2).

The fact that, although an increase in flow velocity due the tidal (currents) can be observed, no significant change in sediment transport pattern in the model run was found, can be related to the location of the increased flow. A transect at the tip of the spit provides insight into the distribution of the alongshore flow velocity for the characteristic moments over the cross-shore profile (Figure 4-18, right). Close to the waterline, within the surfzone, a peak in the flow velocity can be observed. This peak is also present in the reference model run (case 2) without the tide, which indicates that this peak is related to the wave induced alongshore current. The peak in alongshore flow velocity is in the same order of magnitude in the tidal model run during flood and ebb. During slack-tide the peak is of slightly less magnitude and shifted due to the lower water level at this time. Moving more offshore larger differences with respect to the reference case without the tide can be observed. During flood the average flow velocity increases over this part, resulting in the inflow as discussed earlier. During ebb the outflow in opposite direction can be observed at a distance $> 150m$, which is beyond the point where the cross-shore profile steepens with a local depth around 20-25m. This implies that the tidal flow is focussed at the deeper parts of the profile compared to the surfzone while the alongshore sediment transport (Figure 4-12) is located where the wave induced alongshore current dominate.

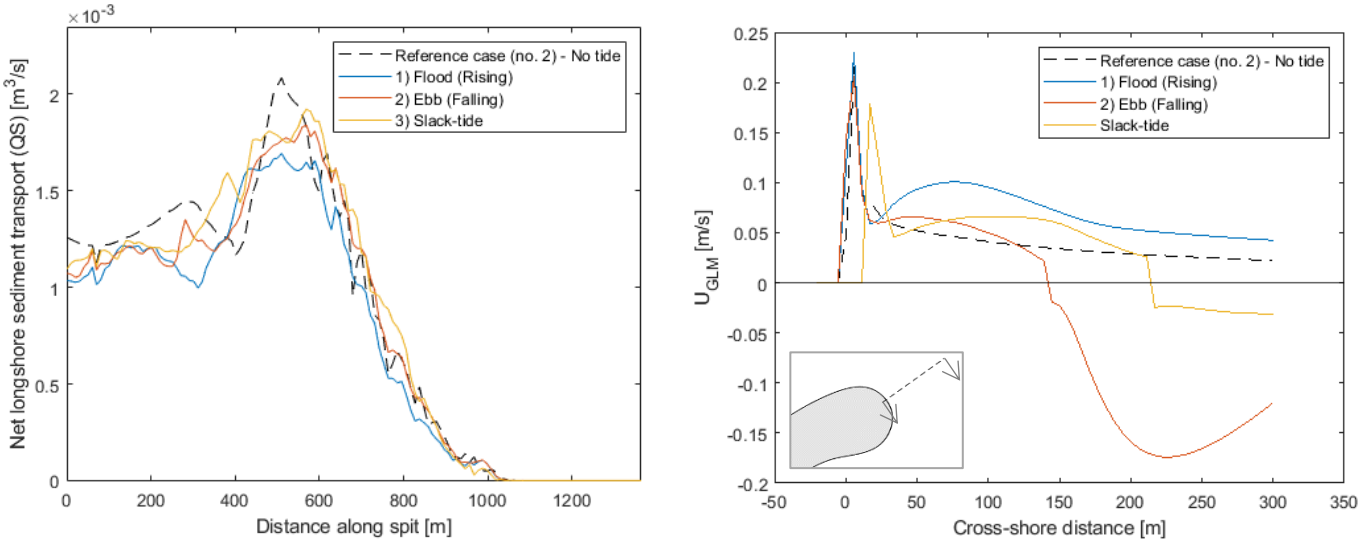

Figure 4-18 - Left: Plot with sediment destitution along spit for different characteristic moments over the tide and the reference case (case 2) Right: Cross shore distribution of flow velocities over a transect at the head of the spit, Positive directed = net inflow Negative values = net outflow

Influence of spit shape

At the head of a spit two characteristic length scales can be distinguished (Figure 4-19): 1) the alongshore distance along the head of the spit and 2) the width of the landmass of the spit, defined at the neck of the spit. To be able to analyse and compare the alongshore sediment distribution for different shapes and width of the spit, the alongshore sediment transport in can be plotted versus the relative width of the spit. That is: the alongshore distance (d) at a certain point relative to the total alongshore distance over the entire width (starting at the 'scaling point', Figure 4-9). By this the relative width equals 0 at $d = 0$ and $W = 0$, and 1 at $W = W_{spit}$ which makes it possible to compare the distribution for different shapes with different widths.

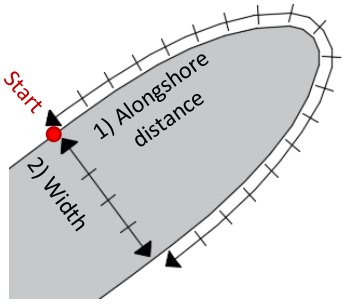

Figure 4-19 – Two characteristic length scales at the head of the spit

When comparing the distribution of the sediment transport for different shape cases with a width equal to the base width (Table 4-5, b) $W = W_{base}$) the following observations can be made (Figure 4-20). For current shape and the blunt shape (asymmetrical cases) the transport gradually decreases over the distance along the spit approximated linearly. This is in line with the earlier observed transport distributions of the base case (Case 1,2 and 4). For the other, symmetrical, shapes (Elongated ratio 1:2 and 1:3 and the rounded shape) a sudden peak (increase in transport) followed by a drop in the transport rate can be observed. In contrast to the Elongated 1:2 (Case 7b) and round shape (Case 6b), for the Elongated 1:3 shape (Case 8b) the first part of the transport distribution up to the peak ($d \approx 800m$) is still decreasing gradually decreasing.

When looking at the location of the peak in the transport relative to the width of the spit it can be observed that the position of the peak matches for all cases and is located around $W_{peak} \approx 0.5W_{spit}$. This position corresponds, for the symmetrical shapes, to the tip of the head of the spit, after which the coastline curves back.

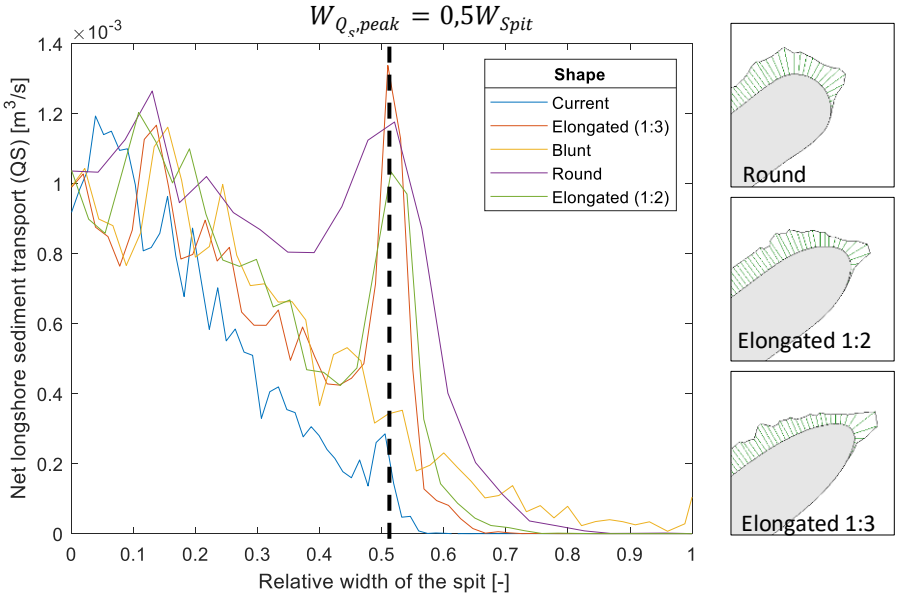

Figure 4-20 - Left: Net transport for different shapes versus relative width of the spit, Right: Visual representation of sediment transport along the three symmetrical shapes

The peak and sudden drop in the (initial) sediment transport distribution is not expected to occur along a natural coastline or a spit with an equilibrium width and shape (i.e., shape which is fixed in time but migrates as the spit 'grows'). It is thereby an indicator that the imposed shape and width of the spit as used in a certain XBeach model run does not match the forcing in the model. The rapid increase followed by decrease in transport will theoretically lead to local erosion and sedimentation further along the spit, that is, basically extending the initial width of the tip.

The wave-forcing and the resulting sediment pattern for the base case, as discussed in the previous sections, already showed that the transport capacity due to the high-incident wave forcing at Lobito spit is not able to push the sediment around the tip. In addition to this, for the symmetrical shapes the sudden drop in transport can also be related to the observed wave field around the head of the spit. The wave height, thus wave energy, quickly drops around the tip similar to the sudden drop in sediment transport. This concept is supported by the model runs in which the width of the base of the spit was variated (e.g., Figure 4-21, for elongated 1:3 Case 8a-d, appendix B for all shape cases).

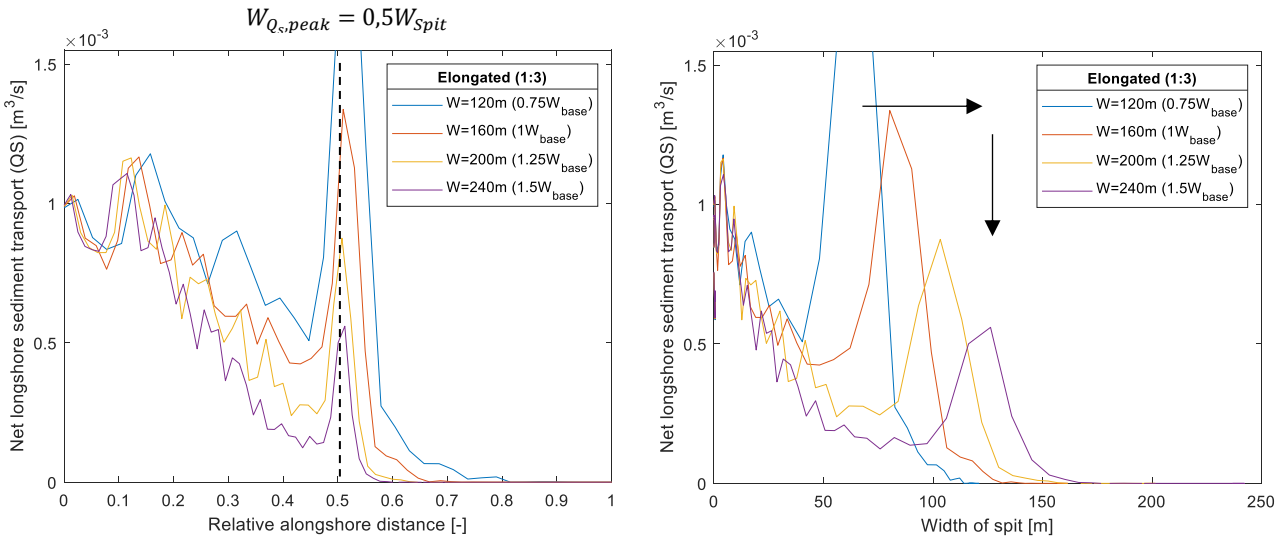

Figure 4-21 – Distribution of net alongshore sediment transport for elongated (Ratio = 1:3) shape with a different width. Left Relative distance, Right: actual alongshore distance

This shows that as the in the model imposed spit gets wider (or smaller) the peak and sudden drop in sediment transport shifts accordingly and is consistently located at the tip of spit at the half of the full width ($W_{peak} = 0.5\ W_{spit}$). As the spit gets wider the magnitude of the transport decreases in a more linear way and the peak gets smaller. This is an indicator that the overall spit is in a more equilibrium shape/width. For all symmetrical shape cases it can be observed that there is hardly any sediment transport behind the tip. This implies that for the Lobito case certain symmetrical case is unlikely to arise as there is no transport mechanism which can supply sediment to the backside.

For the asymmetrical shape (blunt case, Case 9a-d) the following observations can be made when varying the width (Figure 4-22). As the width gets smaller (e.g., Case 8a, $W = 0.75W_{base}$) the peak in sediment transport appears at the tip, similar as which was observed for the symmetrical shapes. As the spit gets wider (e.g., Case 8d, $W = 1.5W_{base}$) it can be observed that this peak reduces while over the last part of the width ($W \gtrsim 160m$) no sediment is supplied.

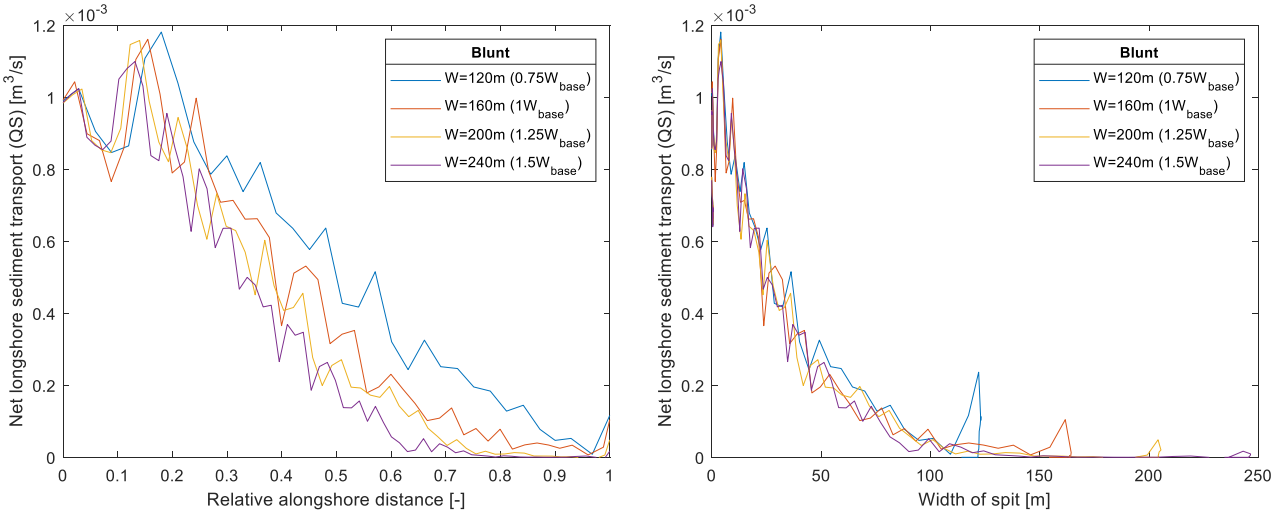

Figure 4-22 - Distribution of net alongshore sediment transport for blunt shape with a different width.

4.3 Discussion and conclusions

In this chapter the processes and mechanisms influencing the formation of a spit are further explored. In Section 4.3.1 limitations and a reflection on the presented results of the conceptual model and the XBeach modelling study is presented. In Section 4.3.2 the overall conclusions this chapter are summarised.

4.3.1 Discussion

Conceptual model for spit width

The conceptual model is the result of an analysis of a limited data and a limited number of spits. The classification is primarily based on the observed (morphological) appearance of the spit formation supported by the characteristics of the local wave climate (bimodality) and tide. Other local specific circumstances such as the bathymetry, (wave) interaction with structures/ coastline geometry, historical human induced costal works or long-term change variations etc. might also influence the final spit shape but considered in detail in this classification. The goal of the conceptual model, however, is to provide a broad view and classification of different natural spit formations. This conceptual model can for this purpose be used to get a first classification of existing or newly forming spits based on a limited number of parameters.

As part of the literature study two existing spit/coastline classifications, by Ollerhead (1993) and Ashton et al. (2006b), were already discussed (Section 2.1.1). The 'classification of barrier systems with one free end' (i.e., spits) by Ollerhead (1993) is primarily based on the original coastline geometry/location where spits arise (e.g., a continuation spit extending from a headland or a flying spit leaving the coastline). The classification done by Ashton et al. (2006b) describes the coastline shape based on two parameters: 1) (A) the portion of waves from one direction and 2) (U) the portion of high angle waves. This (coastline) classification is more based if spits will arise at all.

The presented conceptual is more focussed on when a spit has formed in a coastal system what it can looks like, and thus zooms in on the actual appearance of the spit itself (compared to the other two classifications). The environmental aspect of the bimodality of the wave climate was used for this conceptual model, which is also been used by Ashton et al. (2006b).

However, in this model no distinction in the spit shape is made (i.e., 60%-100% bimodality with sufficient a high angle orientation leads to a flying spit) nor influence of the seasonal variability is taken into account.

Detailed modelling of spit formation

The Lobito spit has been used as a reference case in the detailed modelling study in XBeach. The interest in this study is in the processes related to natural spits. The Lobito (spit) bathymetry, which was affected by human induced (e.g., construction of the groyne scheme), was therefore adjusted to resemble a natural spit formation. This includes the smoothing of the (average) coastline and the use of an average cross-shore profile along the entire spit (Section 4.2.2). The schematized spit used in the model might locally differ from the original, natural, spit of Lobito for which no detailed bathymetrical information is available. However, for the purpose of this study, to get insight into the influence of different processes on the transport distribution the interest is not on the actual quantitative results for the Lobito spit but rather in the overall transport distribution patterns along the spit and relative influence of the different considered model cases. The net alongshore transport for the reference case resulted in transport quantities which are in the same order of magnitude as observed in front of the interventions at Lobito, which indicates that the schematisation is a realistic representation of the natural spit.

The assessment and interpretation of initial LST-distribution from the XBeach model studies have been used to discuss the morphological state of the Lobito spit and spit shape variations. For natural coastlines in general an overall smooth gradient in the longshore transport capacity is expected. In the results of the different XBeach model runs two 'unnatural' peaks were observed: 1) for shape variations a sudden peak and subsequent drop in transport capacity at the tip ($W = 0.5W_{spit}$) was observed. (Figure 4-23, top) and 2) a local increase at the start of the head of a spit (Figure 4-23, bottom). It is important to notice that all patterns are initial patterns, based on a schematized bathymetry as discussed before. An implication of this is that the assumed natural cross shore profile and initial, smoothed out, spit coastline might necessarily not match the natural forces along the entire imposed spit. Initial variations (peaks) in the initial longshore sediment transport can therefore be often relate to initial local erosion and sedimentation patterns to initially 'adjust' the bathymetry to better match the forcing and might smooth out over time.

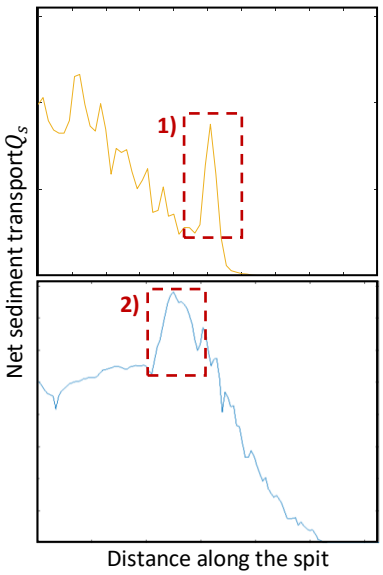

Figure 4-23 - The observed peaks in LST distribution for different XBeach modelling scenarios Top: At the half width for a asymmetric shape Bottom: At beginning of spit head for the current spit shape case

The sudden peak and drop which arises at the tip of the spit (Figure 4-23, top), are very likely to be related to the mismatch between the natural forcing and the imposed spit shape. The focussing of waves on the tip and the sudden drop (shielding) of waves behind the tip resulted in the observed peak and drop in transport, this could also be observed in the velocity field around the spit head for certain shape cases.

It is likely that the increase over the start of the head of a spit (Figure 4-23, bottom) is (partly) related to the initial imposed bathymetry. However, it can be argued that this local increase might also have a physical/natural background: near the head the flow diverges (i.e., free outflow) which potentially reduces the set up along the last part of the neck and beginning of the head of the spit. This set up difference might result in a set-up driven flow which locally increases the flow velocity thus sediment transport. More detailed modelling or measurements are required to support or reject this hypothesis.

For the interest of this model study it is important to mention that the analysis and subsequent conclusions are based on the overall (qualitative) transport pattern compared for different cases.

For Lobito the tide did not significantly influence the alongshore sediment transport (magnitude and distribution). This does not imply that the tide does not influence the shape and/or width of the spit per definition: It's likely that the influence of the tide depends on parameters such as the tidal range, the cross-shore profile and the enclosed basin wet area.

Determination of equilibrium spit width

For the Lobito case the current shape provided a good indication of the expected spit width and shape. This information might not be known at prior for other locations where no spit is present yet. The alongshore sediment distribution provides insight to judge whether the shape and width of the applied spit in the model matches the natural forcing: An approximately linearly decay of the wave climate averaged sediment transport to zero over the entire spit width indicates that the shape and width agrees with the natural forcing (i.e., a so called 'equilibrium spit shape' as described by Petersen et al. (2008))

By this, the analysis using an advanced coastal area model (e.g., as been done in Section 4.2), can be used as a framework to iteratively derive an indication of the spit width and shape which agrees with the natural forcing. Such iterative study can be performed as follows (Figure 4-24):

- The first iteration starts with an arbitrary initial shape in the model, as an example the symmetric elongated with a width of 120m shape (Case 8b) from the of the Lobito case study was used.
- From this QS distribution the peak at the large peak at $W = 0.5W_{spit}$ can be observed which indicates, as discussed earlier, that for this model run the applied spit width is not sufficient to reduce the sediment transport to zero over the available width/distance and also indicates that there is no mechanism which supplies sediment around the tip of the symmetric shape.
- For the second iteration therefore, a wider spit should be imposed in the model. From this resulting LST-distribution it can be observed that the peak is still present but reduced in magnitude. This indicates that the wider shape is more in agreement with the natural forcing compared to the first iteration. However; there is still no transport behind the tip.

This procedure (i.e., adjustment of spit shape and width for next iteration based on the expert judgement on the LST-distribution) should continue until transport distribution the approaches the linear decay over the entire width. This way the natural spit shape based on the local natural forcing can be found. For the Lobito spit case this results in an asymmetric (blunt) shape spit with a width in the order of 160-200m which matches the width and shape as observed in nature.

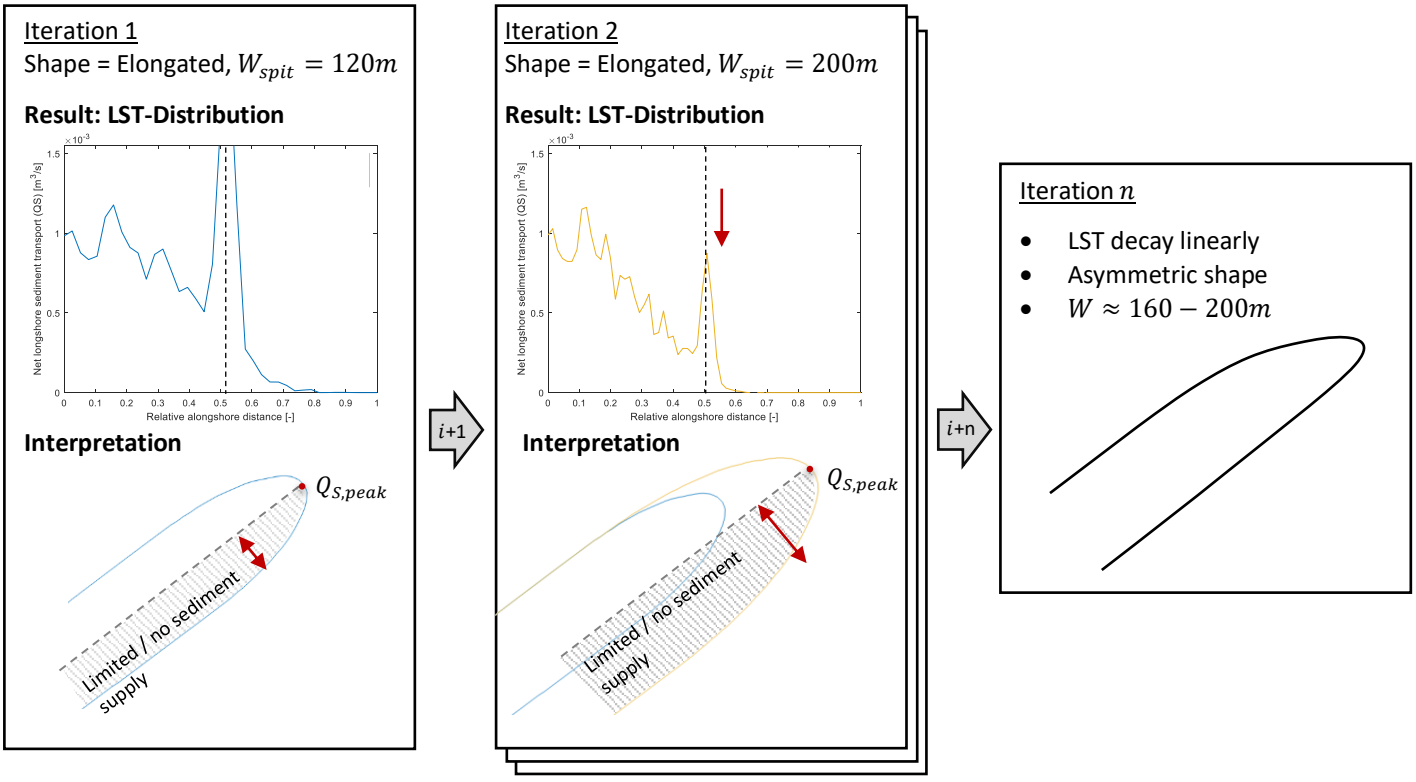

Figure 4-24 – Schematization of iterative framework to derive indication of the equilibrium spit width

4.3.2 Conclusions

Based on the analysis of the spits a conceptual model was derived. In this conceptual model three spit types were defined. The classification is primarily based the appearance of the spit, supported by a hypothesis on the relevant to the local environmental characteristics leading to a specific spit type. Namely: the spreading of the local wave climate and the presence (or lack) of the tide. In general, it can be observed that the tide, if present, promotes the 'smoothing' of (the head) of the spit whereas the (seasonal) variability in the wave climate can result in the typical shoots around the head of the spit.

In the conceptual model three characteristic spit types are distinguished:

- **Type A**: This type is characterised by a very straight formation, there is no clear distinction between the head and the neck of the spit. This type of spit was found in environments in which the wave climate is very uni-directed. The influence of the tide on the appears be of less importance for the final shape of the spit. The Lobito spit can be classified as a type A spit.
- **Type B**: This type is characterised by a smoothed rounded of head which has a considerable lager width than the neck it is attached to. This type was found in environments where both a tide is present in combination with the presence of a (seasonal) secondary wave component (i.e., bimodal wave climate).
- **Type C**: This type is characterised by a head which, in contrast to the type B, consist of shoots and ridges at the head. This type was found in environments where a (seasonal) bimodal wave climate was present but where the tidal range is neglectable. The absence of the tide prevents the smoothing of the head of the spit, resulting in the typical shoots.

The goal of the detailed model analysis was twofold: 1) in a broad context to gain different processes (as discussed in the literature study) contribute to the spit formation and 2) applied to the Lobito spit case which processes are of relevance for the spit formation at Lobito.

XBeach simulations for the reference (Lobito) case, with a reduced wave climate (8 conditions) and no tide, were used to get insight into hydrodynamics and transport distribution around the head of a spit. This showed that the wave energy decreases over the head of a spit as the waves get shielded and waves are deflected (refracting towards) both the spit and the adjacent original coastline. As result both the alongshore current and thereby the alongshore transport also decreases along the spit. The alongshore transport decays approximately linearly over the head of the spit, a constant decay implies a constant sedimentation and thereby a uniform migration of the head of the spit. (i.e., a so called 'equilibrium spit shape' as described by Petersen et al. (2008))

Different model cases were performed to gain insight into the influence on the transport distribution along the head of a spit by the wave climate, tide and shape/width of the spit.

- **Influence of wave climate**
  The transport distribution caused by waves with a less obliquely indecent wave angle with respect to the spit are able to push the sediment further along the head compared to the average condition. Certain waves should thereby not be neglected at prior when investigating the spit width.
  The wave climate at Lobito is very high angle dominated with 93% of the waves with an offshore wave orientation within $244°$ - $248°$. For this reason, the magnitude and transport distribution over the head of the spit for the wave climate (8 conditions) versus the single representative wave ($\varphi_w = 246°$) showed a good match. However, this might not be the case for another, more directional spread, wave climates.
- **Influence of wave climate bimodality**
  The potential contribution of bimodality of the wave climate and the influence of the width of a spit was analysed by 'what-if'-model scenario, in which a wave from secondary direction (i.e., opposite with respect to the average direction) was applied to the model. This showed that those waves are able to push the sediment around the tip, similar to the less obliquely incident waves from the wave climate as mentioned earlier. A fundamental difference between those two mechanisms is that those secondary waves rather redistribute the sediment over the head of a spit, this does not directly contribute to the migration of the spit. A clear split in the gross sediment transport can be observed around the head of the spit. This in contrast to the influence of the less obliquely incident wave from the wave climate, from which the sediment supply is directed in one direction along the entire neck and head of the spit. For the Lobito case there is no indication for the presence of such secondary wave condition.
- **Influence of tide**
  The influence of the tide was analysed by applying a 24hr tide signal to the XBeach model. The hydrodynamic results showed the of filling and emptying of the by the spit enclosed water basin. This leads to a clear inflow and outflow pattern in the flow velocity field around the opening (near the head of the spit) of this water basin. In the resulting

alongshore sediment transport, however, there was no significant change both in magnitude and the distance of which the alongshore sediment distribution reached over the head of the spit for the different characteristic moments (flood, ebb and slack-tide) compared to the reference case without the tide. From this it can be concluded that the tide does not significantly influence the width and shape of the spit of the Lobito spit. The cross-shore distribution of the flow velocity explains why although an in- and decrease in flow velocity was observed, this did not result in an in- or decrease in the alongshore transport: the tidal currents are located in deeper parts of the cross-shore profile, in the surfzone the wave induced are dominating for all cases.

- **Influence of shape**
  The influence of the shape was analysed by applying, in addition to the current shape, four hypothetical spit shapes to the model the symmetric round and elongated shapes with a width to length ratio of 1:2 and 1:3 and an asymmetric blunt shape. For all symmetrical shape cases it can be observed that there is hardly any sediment transport behind the tip under the influence of the average high angle wave condition for the Lobito case. There is no transport mechanism (such as the secondary wave and/or tidal influence) which can transport sediment around the tip. As the sediment cannot reach the coastline behind the tip, a peak followed by a sudden drop in the sediment transport can be observed at the tip, which is for the symmetrical shapes located at the half of the entire spit width. This is sudden drop is a proxy which indicates that shape is not in an equilibrium shape (See discussion, Section 4.3.1) as there is no transport to the backside of the symmetrical shape of the spit, this part would have not supply of sediment. This indicates that for the Lobito case certain symmetrical case is unlikely to arise.
- **Influence of width**
  The influence of the width of the spit was analysed by scaling the current and four hypothetical shapes. By this the proportions of the shapes were fixed while the overall shapes could be remained. For all symmetrical shape cases it can be observed that, under the influence of a single high angle wave, there is hardly any sediment transport behind the tip independent of the width. The peak and drop in sediment transport are fixed at $W = 0.5W_{spit}$ which is in line with the previous finding.
  For the Lobito spit, by imposing the expected asymmetrical shape (previous point, current and/or blunt shape), the following can be concluded: When the imposed spit width is too small the sediment decay cannot take place over restricted alongshore distance over the spit, and a peak at the end of the head of the spit could be observed. When the imposed spit was imposed too wide over a part of the head of the spit no sediment was supplied. Both observations confirm that there is a width which matches the natural forcing. From this it can be concluded that the equilibrium width of the spit should have a width of 160-200m with an asymmetrical/blunt shape, this corresponds to the actual spit (not taking into account the added beach between the groyne field). This finding, together with the previous finding on the influence of the shape, can be used as second proxy to estimate the spit width of the equilibrium shape which matches the natural forcing (See discussion, Section 4.3.1).

5 Longshore sediment transport in ShorelineS

The longshore sediment transport is investigated in this chapter with a comparison of computed LST in ShorelineS to an existing (calibrated) model case for the LST along the spit of Lobito, Angola.

Section 5.1 introduces the main topics of interest which are investigated in this in this chapter and describes the methods (model set up) used to do so. The analysis of the results of those cases described in section 5.2. In Section 5.3 a validation case for the Sandmotor is presented to test the validity of the results on a different scenario. The chapter ends with a discussion and conclusions in Section 5.4 on the presented results and analysis.

5.1 Methods

The performance of ShorelineS to predict LST a comparison was investigated by means of a comparison with the existing coastline model UNIBEST-CL+ (Section 2.3.3). For this the output of the calibrated UNIBEST-LT model for the Lobito was used as a baseline prediction as It is complex to measure the LST along a coastline itself. Actual LST-measurements therefore do hardly exist (Cooper et al., 2007). Usually the LST-quantities are derived from changes in bathymetry and/or observed Shoreline evolution. This was also been done for Lobito (Figure 3-6). However, this only provides the transport rates for one specific (initial) coastal orientation. By taking into account the whole S, φ-curve (and not only the transport for a specific (initial) coastline orientation) valuable insight is obtained into the change in LST for reorientation of the coast over a large range of possible orientations. This is used to gain better insight in the performance of predicting the LST in ShorelineS under morphological evolution of the coastline.

The transport curves (S, φ-cuvres), as generated by UNIBEST-LT, were used to quantitively compare the results of the two different models. The S, φ-cuvres of UNIBEST-LT provide a good source of comparison since they are computed using a straight uniform coastline, the calculated LST-quantities are therefore not influenced by the actual coastline geometry and/or structures. As result the calculated LST- quantities along a certain coastline is only related to the applied wave condition(s), cross shore profile properties, nearshore wave transformation and sediment transport formulation.

The UNIBEST-LT model scenario were reproduced in ShorelineS (i.e., using the same boundary conditions and input parameters). This made possible to assess the performance of the ShorelineS model. The main goal of this chapter is to assess the current performance of the LST module of ShorelineS, for this two main topics are of interest:

1. **The nearshore wave transformation**
   The nearshore transformed wave parameters are important to calculate the LST-quantity for a coastline using an LST-bulk formula (Section 2.3.2). A correct nearshore wave transformation forms thereby the basis of a coastline model. The wave parameters directly influence among others the magnitude and direction of the LST-transport for different orientations of a coastline.

2. **The LST-computation by different LST-formulae**
   LST-bulk formulae calculate the LST-quantity based on the (transformed) wave conditions and sediment conditions. Thus, not only the performance of the wave transformation but also the correct implementation and performance of the LST-formulae itself is of importance in order to correctly estimate the LST-rates. For this topic, a comparison is made of the results on different LST-formulae in ShorelineS are compared with both calibrated results for Lobito as well to the results of the same model scenario in UNIBEST using the same(uncalibrated) LST-bulk formula.

In addition to the Lobito case study the ShorelineS model was also applied on a different case, namely the Sandmotor at Kijkduin, The Netherlands. The model scenario (i.e., wave climate conditions, sediment characteristics and coastal geometry) are different for this case. The goal of this second modelling case is to verify the general applicability of results and conclusions from the Lobito case.

5.1.1 UNIBEST Model (Reference model)

UNIBEST-CL+ has been developed, improved and successfully applied on a large variety of coastal project throughout the years. The existing UNIBEST model for the Lobito spit coastline (Deltares, 2015) has been used to successfully hindcast and model the recent local coastal evolution at this location (Section 3.2; i.e., filling of groyne schemes).

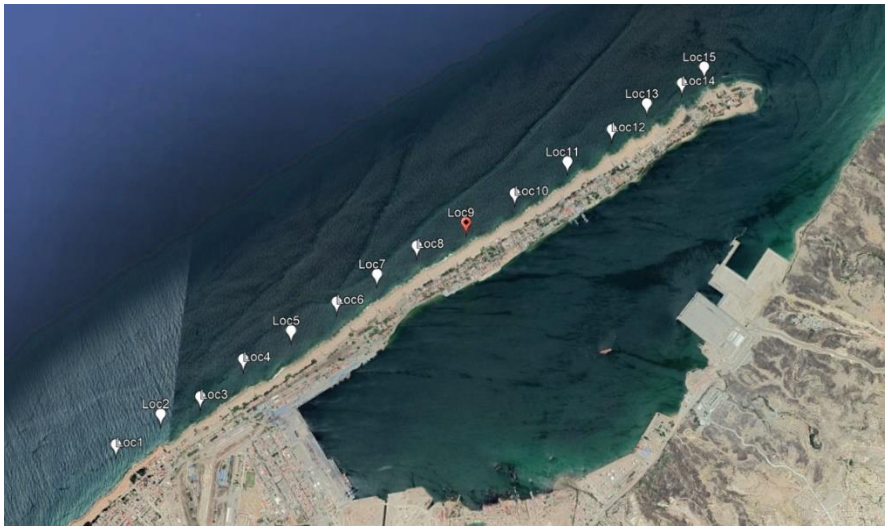

Figure 5-1 – Cross sections defined in Deltares (2015) UNIBEST model

In this model 15 locations along the coastline and spit are defined (Figure 5-1). For those locations the local transport rates have been computed using the UNIBEST-LT module using a local wave climate. A SWAN wave computation was used to transform the offshore yearly wave climate a local wave climate for each location to a water depth of 20m, approximately 200m from the coastline.

UNIBEST-LT requires a cross-shore profile as input for the calculation, for this the one single representative cross shore profile used for all locations derived from the bathymetry measurements: a nearshore with an average slope of 1:20 up to a depth of about 4m. Bellow this depth the slope becomes steeper with an average slope of 1:7. It should be noted that although UNIBEST-LT uses this representative nearshore profile, the complexity of the foreshore bathymetry is implicitly included in the UNIBEST as it uses nearshore wave conditions from 20 SWAN computations.

For all locations the yearly LST-rates were calculated using the semi processed based Bijker (1971, 1967) transport formula. The calibration for this model was done on the basis of the observed shoreline change for the period 2004-2014 with a net transport of $50.000 - 80.000\ m^3/yr$ (section 3.1). Validation was done by the hindcasting of the coastal evolution (filling of the groyne schemes) over the last years. The S, φ-curves along the spit (Figure 5-2) were used as calibrated reference data to compare the ShorelineS model with. The equilibrium angle (φ_{eq}) for which $Q_s = 0$ of $\varphi_{eq} = 275° - 280°$ for all locations, with a maximum transport at $\varphi = 315 - 320°$.

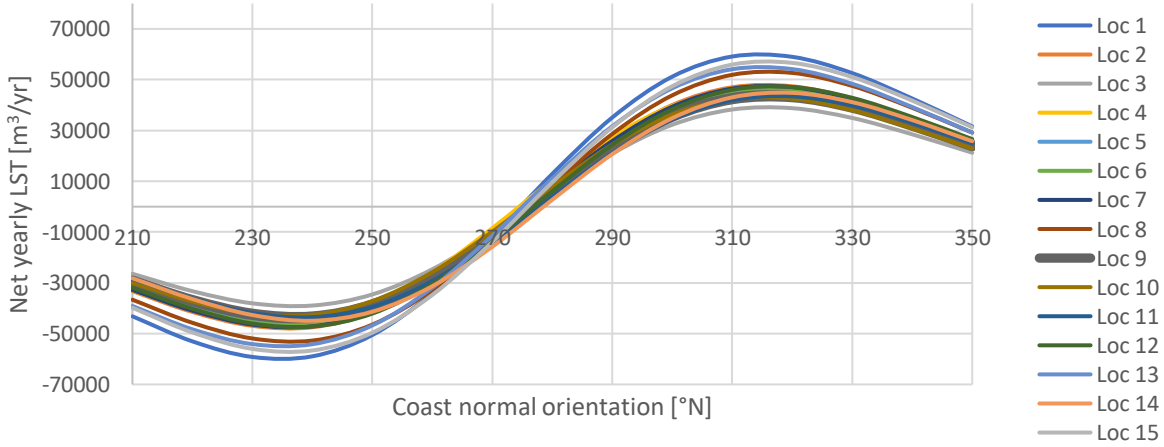

Figure 5-2 – Resulting S, φ-curves from UNIBEST-LT simulations for 15 locations along the Lobito sand spit.

5.1.2 Implementation of the dynamic boundary in ShorelineS

One of the main assumptions underlying a classical (single line) coastline models is the assumption of the fixed shape on the cross-shore profile. Traditional coastline models, as well as the current version of ShorelineS (section 2.4), rotate the full cross-shore profile (all depth contours) under coastal evolution. This assumption might over-simplify the effect of a coastline rotation on the coastal profile because sediment transport due to wave interaction is limited to the nearshore (active) part of the profile only, therefore it is not expected that depth contours outside the active part get reoriented.

To account for this effect the concept (Section 2.3.2) of the dynamic boundary has been implemented in ShorelineS as follows: The wave transformation including effects of the dynamic boundary can be subdivided into three separate steps (Figure 5-3): 1) a transformation from 'offshore' (depth at which the wave climate is specified) towards the location of the dynamic boundary, 2) the rotation at the dynamic boundary and 3) the wave transformation in the nearshore in from the dynamic boundary towards the breaker depth.

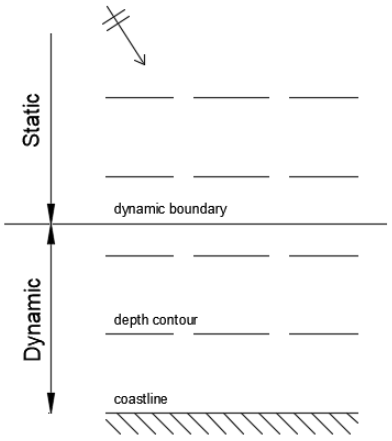

Figure 5-3 – Distinction of dynamic (active) and static part of the coast in concept of dynamic boundary

'Offshore' to dynamic boundary (Static part)

In the first step the 'offshore' applied wave condition $H_{s,0}$ is transformed towards the dynamic boundary to determine the wave height at the dynamic boundary $H_{s,db}$ due to shoaling and refraction. In general, the wave transformation can be formulated as:

$$H_{s,db} = K_s \, K_r \, H_{s,0} \tag{5.1}$$

The shoaling coefficient (K_s) and refraction coefficient (K_r) can be determined from using an energy flux balance over the wave ray (assuming no energy loss) by comparing the wave group speed offshore (subscript 0) and at the dynamic boundary (subscript db):

$$K_s = \left(\frac{n_0 \, c_0}{n_{db} \, c_{db}}\right)^{0.5} \tag{5.2}$$

And refraction coefficient:

$$K_r = \left(\frac{b_0}{b_{db}}\right)^{0.5} \tag{5.3}$$

Assuming parallel depth uniform contours, the wave angle for different locations on the profile can be determined using Snell's law:

$$\sin(\varphi_{loc,db,A}) = \frac{c_{db}}{c_0}\sin(\varphi_{loc,0}) \tag{5.4}$$

In which $\varphi_{loc,db,A}$ and $\varphi_{loc,0}$ are related to the orientation of the offshore / deep water depth contours φ_f.
The effective width over which energy is distributed (i.e.,: b_0, b_{db}) is related to the rotation of the waves which means that eq. 5.3 can be rewritten, using the rules of geometry, to:

$$K_r = \left(\frac{\cos(\varphi_{loc,0})}{\cos(\varphi_{loc,db})}\right)^{0.5} \tag{5.5}$$

Combination of eq. 5.2. and eq. 5.5 results in the following function describing the change in wave height due to wave shoaling and refraction:

$$H_{s,db} = \left(\frac{n_0 \, c_0}{n_{db} \, c_{db}}\right)^{0.5} \left(\frac{\cos(\varphi_{loc,0})}{\cos(\varphi_{loc,db,A})}\right)^{0.5} H_{s,0} \tag{5.6}$$

This expression describes the wave transformation due to wave shoaling and reflection towards the dynamic boundary. The wave speed (c) is calculated in ShorelineS using an explicit solution of the wave dispersion equation by Guo, 2002 as function of the wave period (T_p) and local water depth (h).

At the dynamic boundary

The dynamic boundary in ShorelineS is schematized as a single point (line) in space implying a sudden change in the orientation of the depth contours (Figure 5-4).

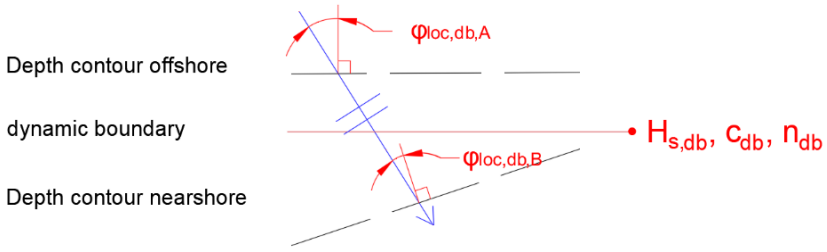

Figure 5-4 – Schematisation of dynamic boundary and used parameters in ShorelineS, note that location A and B are defined at the same location, thus at the same depth h_{db}.

Due to this schematization the only parameter changing at the dynamic boundary is the relative angle of the wave with respect to the coastline parallel depth contour nearshore. This new relative angle at the dynamic boundary ($\varphi_{loc,db,B}$) can be determined using the known relative angle $\varphi_{loc,db,A}$ prior to rotation and the relative rotation of the coast (and nearshore depth contours) with respect to the fixed offshore depth contours:

$$\varphi_{loc,db,B} = \varphi_{loc,db,A} + (\varphi_c - \varphi_f) \qquad 5.7$$

Dynamic boundary to breaker depth (Dynamic part)

The last step is to determine the breaking wave conditions at the breaker line ($n_{br}; c_{br}; \varphi_{loc,br}; H_{s,br}$). The wave transformation over the dynamic part can be determined similarly as for static part, assuming parallel depth contours, using eq. 5.6 but now applied on the dynamic part:

$$H_{s,br} = \left(\frac{n_{db}\, c_{db}}{n_{br}\, c_{br}}\right)^{0.5} \left(\frac{\cos(\varphi_{loc,db,B})}{\cos(\varphi_{loc,br})}\right)^{0.5} H_{s,db} \qquad 5.8$$

The relative angles are now related to the depth contours in the dynamic part of the profile (Figure 5-4).

The water depth (and location of) at the breaker line is unknown, therefore eq. 5.8 cannot be solved. To be able to solve this equation a number of assumptions are applied based on van Rijn (2011):

1. The ratio group to phase velocity at the breaker line n_{br} is assumed close to 1, $n_{br} \cong 0.95$ assuming shallow water conditions which holds for breaking waves.
2. The local relative wave angle at the breaker line $\varphi_{loc,br}$ is assumed close to 0°, $\cos(\varphi_{loc,br}) \cong 0.95$. Which is valid for almost fully shore normal refracted (breaking) waves.
3. c_{br} is approximated using the shallow water wave speed $c_{br} \approx \sqrt{h_{br}\, g}$
4. The wave height at the breaker line is approximated using the breaker index $\gamma = H_{s,br}/h_{br}$

Applying those assumptions to eq. 5.8 results in an explicit formulation for breaker depth estimation:

$$h_{br} = \left(\frac{H_{s,db}^2\, n_{db}\, c_{db}\, \cos(\varphi_{loc,db,B})}{0{,}95 \cdot 0{,}95\, \gamma^2\, \sqrt{g}}\right)^{0.4} \qquad 5.9$$

When directly calculating the water depth at the breaker line using the deep-water wave height $H_{s,0}$ in literature usually a 'calibration value' α is used which summarizes assumptions 1 and 2. Based on a deep water group phase ratio $n_0 = 0.5$ this value: $\alpha = n_{br} \cos(\varphi_{loc,br}) \frac{1}{n_0} = 1.8$, which is commonly used in literature. This factor has been included in the formulation as implemented in ShorelineS:

$$h_{br} = \left(\frac{H_{s,db}^2\, n_{db}\, c_{db}\, \cos(\varphi_{loc,db,B})}{\frac{0{,}5}{n_1}\, \alpha\, \gamma^2\, \sqrt{g}}\right)^{0.4} \qquad 5.10$$

The wave height at the breaker line $H_{s,br}$ can be determined using h_{br} and the breaker index γ. The relative wave angle at the breaker line $\varphi_{loc,br}$ can be determined using Snell's law (eq. 5.4) applied over the dynamic part using $\varphi_{loc,db,B}$.

5.1.3 Model set up

Output of the UNIBEST model is available at 15 locations along the coast, for this study it is chosen to focus on location 9 (indicated by the red marker in Figure 5-1).

To bet better insight into the behaviour of the ShorelineS model two variations are considered, leading to four model cases (Table 5-1).

1. **Variation in applied wave climate**
   For the best reproduction of the UNIBEST-LT model the same (nearshore, $d = 20m$) wave climate is used. To assess the performance and robustness of the wave transformation module and the influence on the resulting LST-quantities an offshore ($d = 56m$) wave climate is used.
2. **Inclusion of the dynamic boundary (DB)**
   It was hypothesized that the concept of a dynamic boundary lead to a better representation of refraction and thus better prediction of the LST-quantities. To test the effect all cases are considered without the inclusion of the dynamic boundary (denoted as "traditional approach") and with the inclusion of the dynamic boundary.

	Wave climate	
	Offshore	**Nearshore (UB)**
No DB	I	II
With DB	III	IV

Table 5-1 – Definition of model cases. (UB) indicates that for those cases the used wave climate is the same as used in the calibrated Unibest model

Performance rating

The results in terms of performance are rated in two ways, the main method used is visual comparison of the transport curves of UNIBEST verses the ones as produced by ShorelineS. In addition to visual judgement of overall shape of the S, φ-curves two indicators are used to support the visual observations, namely the absolute phase shift ($\Delta\varphi_{eq}$) of the point of zero transport or the equilibrium coastline orientation φ_{eq} and the relative amplitude factor $\Delta A = A_{ss}/A_{UB}$, which describes the difference in overall magnitude (Figure 5-5).

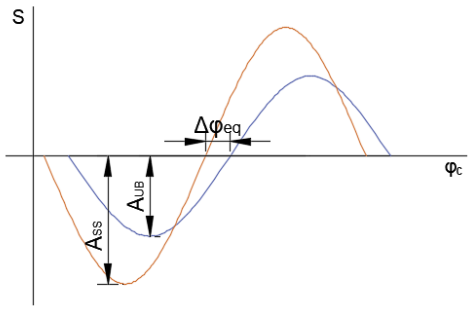

Figure 5-5 - Quantities used for rating the performance of ShorelineS compared to Unibest calibrated result

Generation of S, φ-curves using ShorelineS

In ShorelineS the LST-rate is calculated using an LST-bulk formula at every timestep for every location using the actual coastline orientation and wave condition. This approach is fundamentally different compared the way UNIBEST determines the LST-rate; in which the S, φ-curve is computed and stored for selected user defined scenarios. Due to this difference in approach there is no need to calculate and/or record the actual full S, φ-cuvres in ShorelineS.

A number of ShorelineS model runs were performed, every model run the coastline is rotated by $\Delta\varphi = 10°$. The starting point of the runs is a straight initial coastline (length 5km) and a fixed incoming wave. Since it is in ShorelineS technically easier to rotate the wave angle it was chosen to fix the coastline orientation and rotate the incoming wave angle (Figure 5-6). The result of both methods is the same; a change in the relative incoming wave angle φ_{loc} thus change in LST. Using the recorded calculated yearly LST-quantities for every rotation $\Delta\varphi$ the S, φ-curves can be constructed.

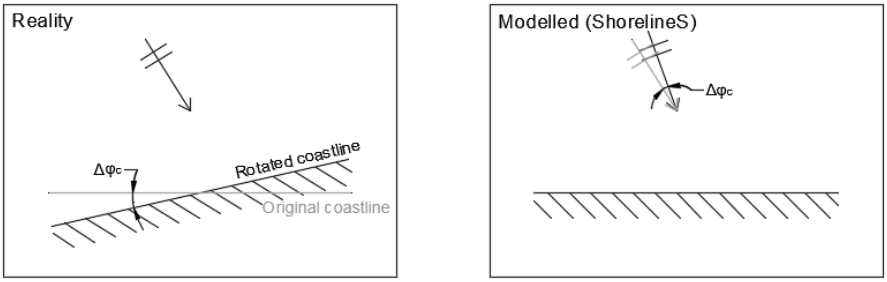

Figure 5-6 – Schematization of the operation of generating S, φ-curves in ShorelineS; rotation the incoming wave with $\Delta\varphi_c$ instead of the actual coastline. The effect is the same, a change in the relative orientation φ_{loc}

Wave climate

In the calibrated UNIBEST model an annual local nearshore wave climate at location 9 consisting of 42 conditions was used to generate the yearly net LST-rates. This local nearshore wave climate was derived using SWAN (Section 3.1). Including all the 42-wave conditions in ShorelineS is not required for the purpose of assessing the performance of the LST-module. For this reason, the wave climate was reduced to one representative wave condition for which the net transport rates (S, φ-curve) of the original calculation including all conditions matches the calculation using one representative wave condition (Figure 5-7). The representative wave condition is used as input for case II and IV. The S, φ-curve computed by UNIBEST using the representative wave condition will be used as reference transport curve (baseline) for assessment of the ShorelineS model, denoted as "UB calibrated".

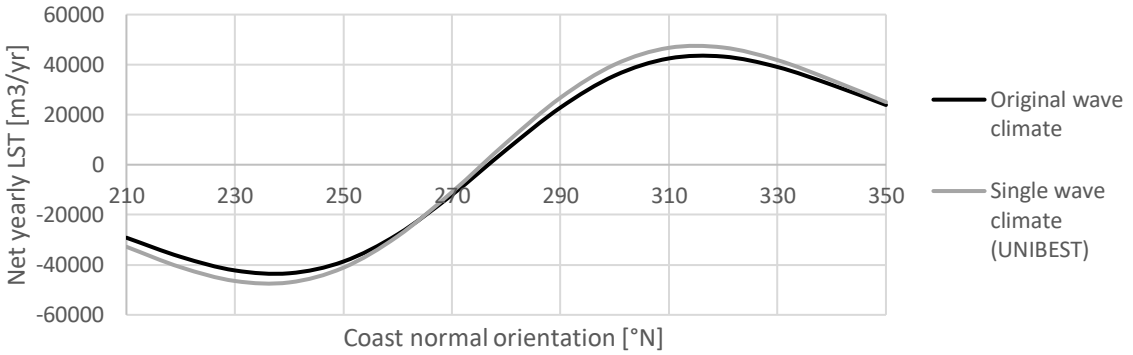

Figure 5-7 – Plot with S, φ-curves calculated with UNIBEST for full wave climate (42 wave conditions) and representative single wave condition used for modelling cases in ShorelineS.

The selected representative wave condition is one of the 42 original wave conditions, in theory this wave could be finetuned/adjusted until it matches the transport rates of the original conditions even better. However, using an actual wave condition which is part of the original wave conditions makes it possible to get insight into the wave transformation of this specific wave condition at different locations in the existing wave model. This is used to extract a representative wave at the offshore boundary of the SWAN wave model, at 2.5km away from the coast at a local depth of 56m (Figure 5-8). This wave condition will be used for case I and III, this single representative wave condition was also been used in the XBeach analysis in Chapter 4.

Table 5-3 (p. 57) includes the original wave climate, located 96 km offshore, the nearshore and newly derived offshore wave climate.

Input parameters

Table 5-2 provides a summary of all input parameters used for the model cases. As this is a model-to-model most sediment- and modelling- parameters are directly adopted from the calibrated UNIBEST-LT model to best reproduce the model scenario in ShorelineS. In ShorelineS the bathymetry or cross shore profile is not required as input, instead characteristic values as the nearshore slope ($\tan\beta$) and the water depth at the location of the wave climate (h_{deep}) and dynamic boundary ($h_{nearshore}$) are used in certain transport formulae and used to determine the nearshore wave transformation including effects of the dynamic profile (Section 5.1.2). Those characteristic values are derived from the cross-shore profile as used in the UNIBEST model.

Figure 5-8 – Location of nearshore wave climate (red maker), used for calibrated UNIBEST model and case II and IV in ShorelineS, and offshore wave climate, used for case I and III. Dashed lines indicate boundaries wave model.

		Case I	Case II	Case III	Case IV	Unibest	Unit
General	$H_{s,0}$	0.68	0.42	0.68	0.42	0.42	m
	T_p	9.456					s
	φ_w	246.7	265.4	246.7	265.4	265.4	°
	φ_c	325					°
	D_{50}	0.0005					m
	ρ_w	1250					kg/m^3
	ρ_s	2650					kg/m^3
	γ	0.8					$-$
	p	0.4					$-$
	Sediment formulation	CERC 1,2,3, Kamphuis, Mil-Homens, Van Rijn 2014				Bijker[2], Van Rijn 2004, CERC, Kamphuis	
	Dynamic boundary	No	No	Yes, using $h_{nearshore}$		Activated, defined at x=160m (d=14m)	
ShorelineS	$\tan\beta$	0.05 (1:20)					$-$
	h_{deep}	56	20	56	20		m
	$h_{nearshore}$[3]	56	20	14	14		m
	Coastline	5km straight coastline					

Table 5-2 – Input parameters for ShorelineS LST-cases

[2] Bijker is used in the original calibrated UNIBEST-LT model. Reruns of the model using Van Rijn 2004, CERC and Kamphuis transport formulations were carried out to compare the results of the same formula between UNIBEST and Shorelines.
[3] To 'deactivate' the dynamic boundary in the model the intermediate water depth of the dynamic boundary was set equal to the offshore water depth.

	Original climate				**Offshore**				**Nearshore (Loc9)**			
	x= 255009, y=8672446				x=342242, y= 8638617 ($h = 56m$)				x=343439, y=8636484 ($h = 20m$)			
	Figure 3-3				*Figure 5-8, flag*				*Figure 5-8, red marker*			
	H_0	T_p	φ_w	**Dur**	H_0	T_p	φ_w	**Dur**	H_0	T_p	φ_w	**Dur**
1	0.75	8.5	300	0.03	0.88	9.456	259.6	0.03	0.65	9.456	277.1	0.03
2	1.25	10.5	300	0.05	1.35	11.67	263.1	0.05	1.02	11.67	283.0	0.05
3	1.75	11	300	0.01	1.5	11.67	260.0194	0.01	1.1	11.67	281.5	0.01
4	1.75	12	197.5	0.04	0.49	11.67	243.7	0.04	0.27	11.67	263.7	0.04
5	2.25	14.5	197.5	0.02	0.78	14.39	248.4194	0.02	0.42	14.39	274.1	0.02
6	0.75	9.5	202.5	0.36	0.38	9.456	249.3076	0.36	0.26	9.456	270.3	0.36
7	1.25	10.5	202.5	3	0.48	10.5	244.751	3	0.29	10.5	264.4	3
8	1.75	11.5	202.5	0.78	0.58	11.67	244.7	0.78	0.33	11.67	264.6	0.78
9	2.25	12.5	202.5	0.14	0.73	11.67	245.7	0.14	0.41	11.67	266.8	0.14
10	0.75	9	207.5	3.85	0.41	8.514	245.4	3.85	0.26	8.514	263.7	3.85
11	1.25	9.5	207.5	30.55	0.53	9.456	243.7	30.55	0.31	9.456	260.8	30.55
12	1.75	10.5	207.5	11.49	0.67	10.5	244.5	11.49	0.39	10.5	263.3	11.49
13	2.25	11.5	207.5	1.51	0.83	11.67	246.2	1.51	0.48	11.67	266.7	1.51
14	2.75	12	207.5	0.1	1	11.67	247	0.1	0.59	11.67	267.9	0.1
15	0.75	8.5	212.5	16.08	0.44	8.514	244.5	16.08	0.27	8.514	261.2	16.08
16	1.25	9.5	212.5	77.97	0.57	9.456	244.451	77.97	0.34	9.456	261.7	77.97
17	1.75	10.5	212.5	25	0.76	9.456	245.7	25	0.45	10.5	264.6	25
18	2.25	11.5	212.5	3.58	0.95	10.5	247.6	3.58	0.57	11.67	268.9	3.58
19	2.75	12.5	212.5	0.35	1.15	11.67	249.1194	0.35	0.69	11.67	272.1	0.35
20	3.25	13.5	212.5	0.04	1.32	12.96	251	0.04	0.81	12.96	275.2	0.04
21	0.75	8.5	217.5	17.33	0.48	8.514	245.4194	17.33	0.3	8.514	262.0	17.33
22	1.25	9.5	217.5	72.38	0.62	9.456	245.4	72.38	0.38	9.456	263.2	72.38
23	1.75	11	217.5	23.32	0.84	10.5	247.2	23.32	0.51	10.5	267.7	23.32
24	2.25	12	217.5	4.26	1.06	11.67	249.2	4.26	0.65	11.67	271.5	4.26
25	2.75	13	217.5	0.37	1.26	12.96	251.1	0.37	0.78	12.96	275.0	0.37
26	3.25	14.5	217.5	0.03	1.49	14.39	253.6194	0.03	0.97	14.39	279.6	0.03
27	0.75	8.5	222.5	8.37	0.52	8.514	246.5	8.37	0.33	8.514	263.6	8.37
28	1.25	9.5	222.5	30.94	0.68	9.456	246.7	30.94	0.42	9.456	265.4	30.94
29	1.75	11	222.5	9.47	0.92	10.5	248.9194	9.47	0.57	10.5	270.6	9.47
30	2.25	12.5	222.5	1.71	1.18	11.67	251.8	1.71	0.75	11.67	275.6	1.71
31	2.75	13.5	222.5	0.16	1.38	11.67	252.2194	0.16	0.89	12.96	276.1	0.16
32	0.75	8.5	227.5	2.95	0.55	8.514	247.2	2.95	0.36	8.514	264.3	2.95
33	1.25	9.5	227.5	8.61	0.73	9.456	247.8	8.61	0.46	9.456	266.8	8.61
34	1.75	11.5	227.5	2.5	1	11.67	251.2194	2.5	0.64	11.67	273.7	2.5
35	2.25	13	227.5	0.32	1.27	12.96	253.3	0.32	0.83	12.96	277.4	0.32
36	0.75	8.5	235	2.11	0.6	8.514	248.1	2.11	0.39	8.514	265.5	2.11
37	1.25	9.5	235	3.37	0.77	9.456	248.6194	3.37	0.49	9.456	267.7	3.37
38	1.75	11	235	0.39	1.13	11.67	252.8	0.39	0.74	11.67	275.4	0.39
39	2.25	11.5	235	0.01	1.28	10.5	252.8194	0.01	0.84	10.5	275.0	0.01
40	0.75	9	250	0.62	0.68	8.514	249.9	0.62	0.45	8.514	267.4	0.62
41	1.25	9.5	250	0.68	0.89	9.456	251.9	0.68	0.59	9.456	271.8	0.68
42	1.75	11	250	0.16	1.25	11.67	254.8	0.16	0.85	11.67	276.9	0.16
				365				365				365

Table 5-3 – Wave climate at Lobito. Left: Original wave climate (~100km from coast), center: offshore wave climate at the spit, (~3.5km from coast) at the boundary of the wave model used to calculate the nearshore wave climates for the UNIBEST model. Right: nearshore derived wave climate (~200m from coastline). The yellow marked wave condition (no. 28) indicates the selected representative wave condition used for the ShorelineS model cases.

5.2 Results

In this section the results and observations for the simulated cases are presented and analysed. First the performance of the wave transformation module is discussed in section 5.2.1. In section 5.2.2 the performance of the different individual LST-formulae is analysed. All the 'raw' data sheets per case, including the resulting S, φ-curves for the different LST-formulae, can be found in Appendix C.

5.2.1 Wave transformation

In Figure 5-9 the calculated breaking wave height ($H_{s,br}$) and corresponding wave angle ($\varphi_{loc,br}$) for different coastal orientations for both cases (DB on and off) are shown compared to the values as calculated by the UNIBEST-LT model, it can be observed that both the wave height and wave angle better match up with the values from the UNIBEST-LT model when de dynamic boundary is activated.

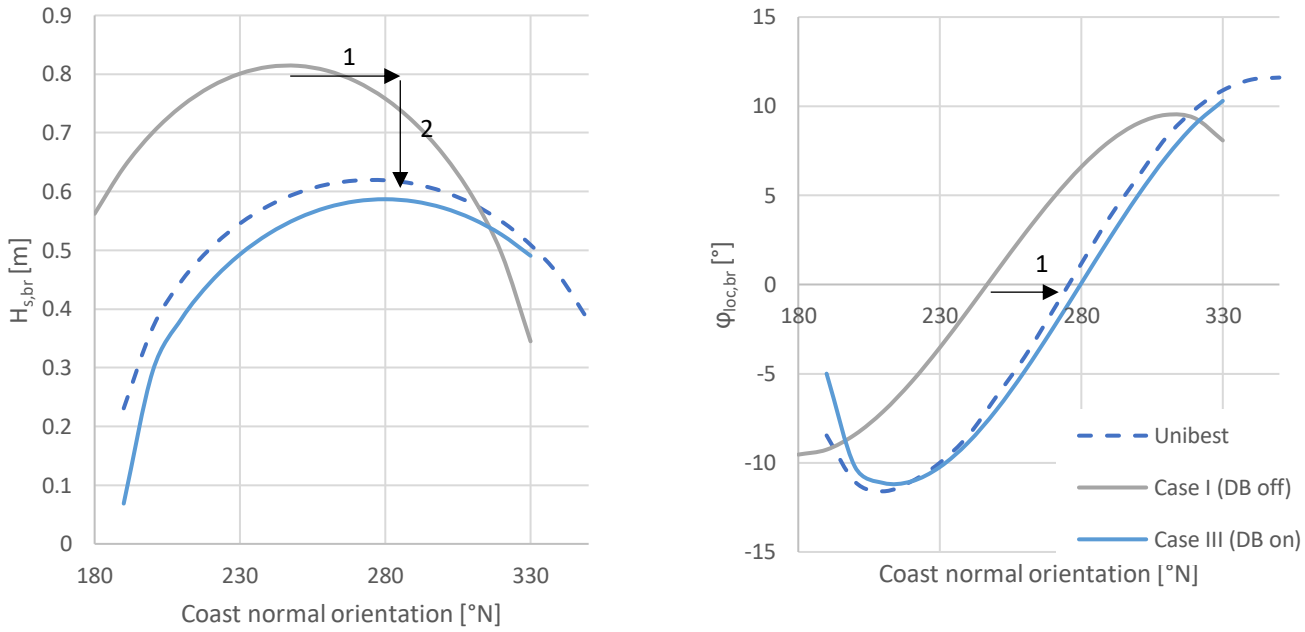

Figure 5-9 - Observed changes in breaking wave conditions (left: $H_{s,br}$ right: $\varphi_{loc,br}$) when the concept of a dynamic boundary is used (case III) versus the traditional modelling approach (case I) , both using offshore wave conditions as input, compared to the conditions calculated by UNIBEST.

Two main observations can be made:

1. A phase shift in the coastal orientation φ_c for which the of the local relative angle $\varphi_{loc,br} = 0$, thus $Q_s = 0$
2. A change (in this case reduction) of the overall breaking wave height $H_{s,br}$

The first observation can be related to the equilibrium coastline angle ($\varphi_{c,eq}$) for which $Q_s = 0$. 'Offshore' perpendicular directed waves with respect to the coastline over only coastline parallel depth contours do not refract, therefore the local or relative angle remains $\varphi_{loc,0} = \varphi_{loc,br} = 0°$. Hereby, normal incoming waves will not generate a longshore generated wave current through the 'longshore wave power' ($P \propto \sin 2\varphi_{loc,br}$, $P = 0\ for\ \varphi_{loc,br} = 0°$) as implemented in various LST-formulations. When the dynamic boundary is not activated the equilibrium orientation therefore equals the incoming wave angle by definition:

$$\varphi_{c,eq} = \varphi_{w,0} \qquad 5.11$$

This does not hold when the dynamic boundary is activated, which fixes the deep-water depth contours. The longshore wave power will still be zero for $\varphi_{loc,br} = 0°$. For coastline parallel uniform depth contours in the dynamic part, as assumed in the model, this implies that if $\varphi_{loc,br} = 0°$, $\varphi_{loc,db,B} = 0°$ too (i.e., equals zero when the offshore wave refracted towards a coast normal orientation). Applying this to eq. 5.11 the equilibrium coastline orientation $\varphi_{c,eq}$,when using a dynamic boundary, can be formulated as:

$$\varphi_{c,eq} = \varphi_f - \varphi_{loc,db,A} \qquad 5.12$$

In contrast to when no dynamic boundary is applied, eq. 5.11, $\varphi_{c,eq}$ is now not only related to the offshore wave direction but also depends on the refraction over deep water depth contours towards the dynamic boundary , thus $\varphi_{c,eq} = f(\varphi_{loc,db,A}) = f(\varphi_{w,0}, \varphi_f, T_p, h_{deep}, h_{nearshore})$.

Eq. 5.11 and 5.12 give insight into the observed phase shift of the calculated equilibrium coastline orientation $\varphi_{c,eq}$ due to the implementation of the dynamic boundary.

The second observation is the change in wave height due to the activation of the dynamic boundary. The wave height at an arbitrary point in the cross-shore profile can be calculated using eq. 5.1. Based on the assumptions made in Section 5.1.2. Wave shoaling (K_s) only depends on the change in the water depth, since the dynamic boundary only influences the orientation of the depth contours, and not the actual depth, K_s will not be influenced by the dynamic boundary.

For a uniform profile sloping upwards towards the coastline the K_r will, according to eq. 5.5, always be equal or smaller than 1. The wave height at shallow water will be maximum, in the case without a dynamic boundary, when the incoming wave is oriented perpendicular to the coastline for which $K_r = 1$ over the entire cross-shore profile (Figure 5-10 (left)).

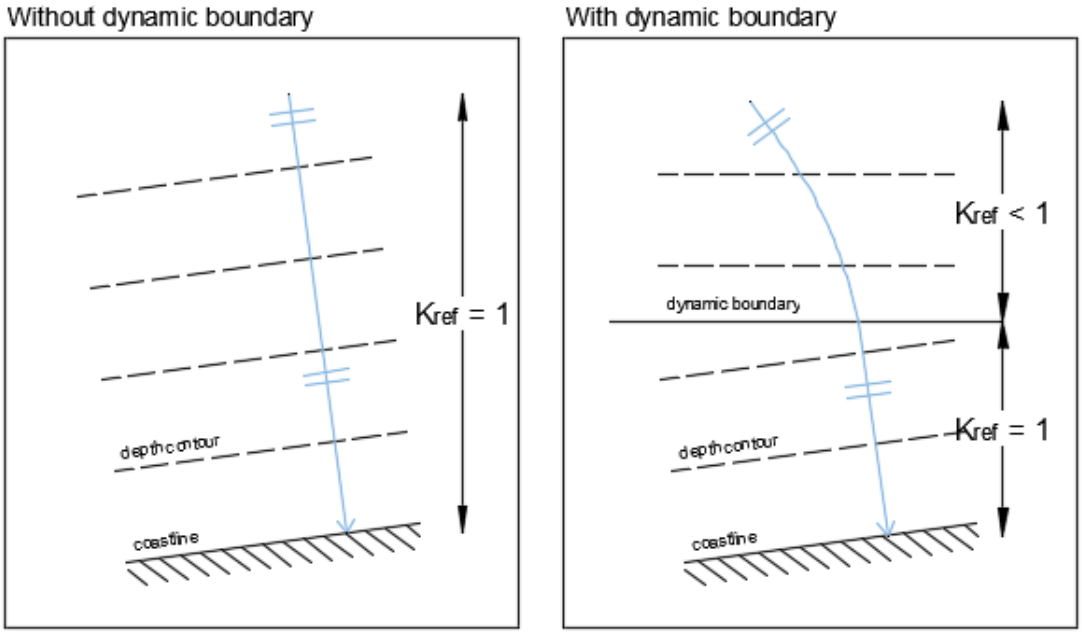

Figure 5-10 – Effect of dynamic boundary on refraction coefficient K_r for normal incident wave (at coastline)

When the dynamic boundary is activated K_r will always be smaller than 1 over the entire cross-shore profile due to the change in orientation at the boundary. This this shown in Figure 5-10 (right), in the shown example the waves are perpendicular orientated towards the coast over the dynamic part ($K_r = 1$) but still refract over the offshore depth contours ($K_r < 1$) leading to an overall coefficient of $K_r < 1$.

The phase shift and change in wave height can also be observed when comparing case II and case IV, for which the nearshore wave conditions were used (Figure 5-11). The phase shift is less pronounced compared case I and II, this is due to the fact that the used wave condition is derived from the SWAN model relatively close to the defined location of the dynamic boundary. Part of the wave transformation, up to the location of the nearshore wave climate, is therefore already implicitly included in the wave condition use for both case II and IV through the SWAN wave model. Note that this wave condition results in an almost identical representation of the breaking wave conditions in ShorelineS for case IV (using dynamic boundary) compared to the UNIBEST-LT model (Figure 5-11).

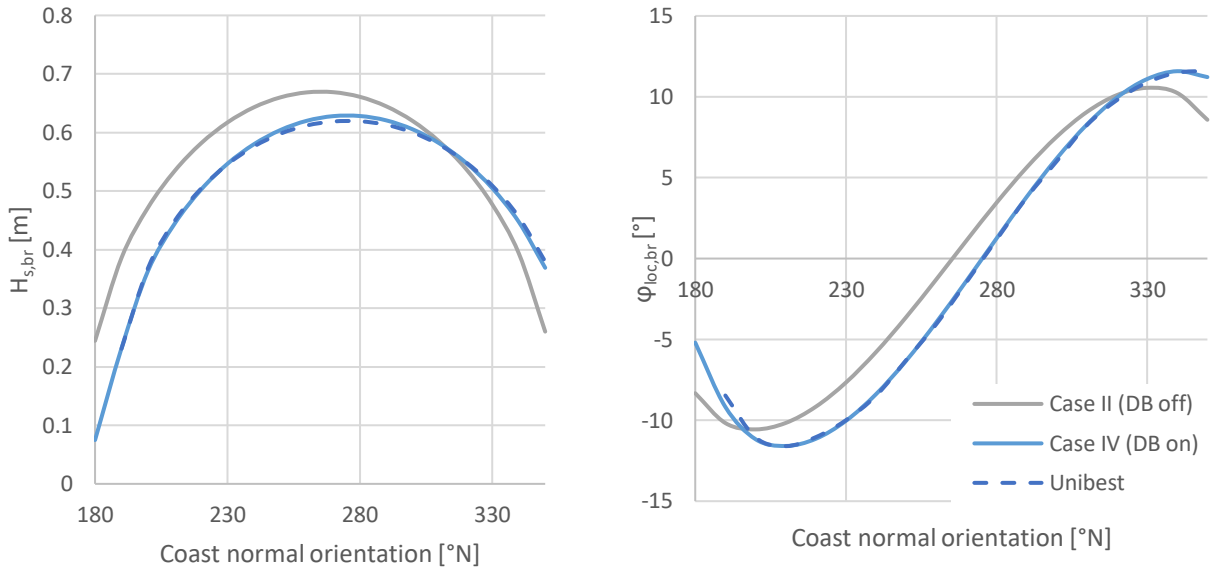

Figure 5-11 - Observed changes in breaking wave conditions (left: $H_{s,br}$ right: $\varphi_{loc,br}$) when the concept of a dynamic boundary is used (case IV) versus the traditional modelling approach (case II),both using nearshore wave conditions as input, compared to the conditions calculated by UNIBEST.

The calculated breaking wave conditions by ShorelineS are with the dynamic boundary more consistent for different cases. This means that the location where the wave climate is specified (e.g., $20m$ or $56m$) does not affect the wave transformation, which aligns with the expectations.

5.2.2 Performance of LST-formulae

The effect of the wave transformation due to the dynamic boundary on the resulting LST (S, φ-curves) is demonstrated by the generated transport curves by ShorelineS using the CERC3 formulation. Figure 5-12 shows the S, φ-curves for case I (offshore wave condition) and case II (nearshore wave condition), both cases use the traditional approach. This plot also includes the calibrated result 'UB Calibrated' and the rerun in UNIBEST using the uncalibrated CERC formula.

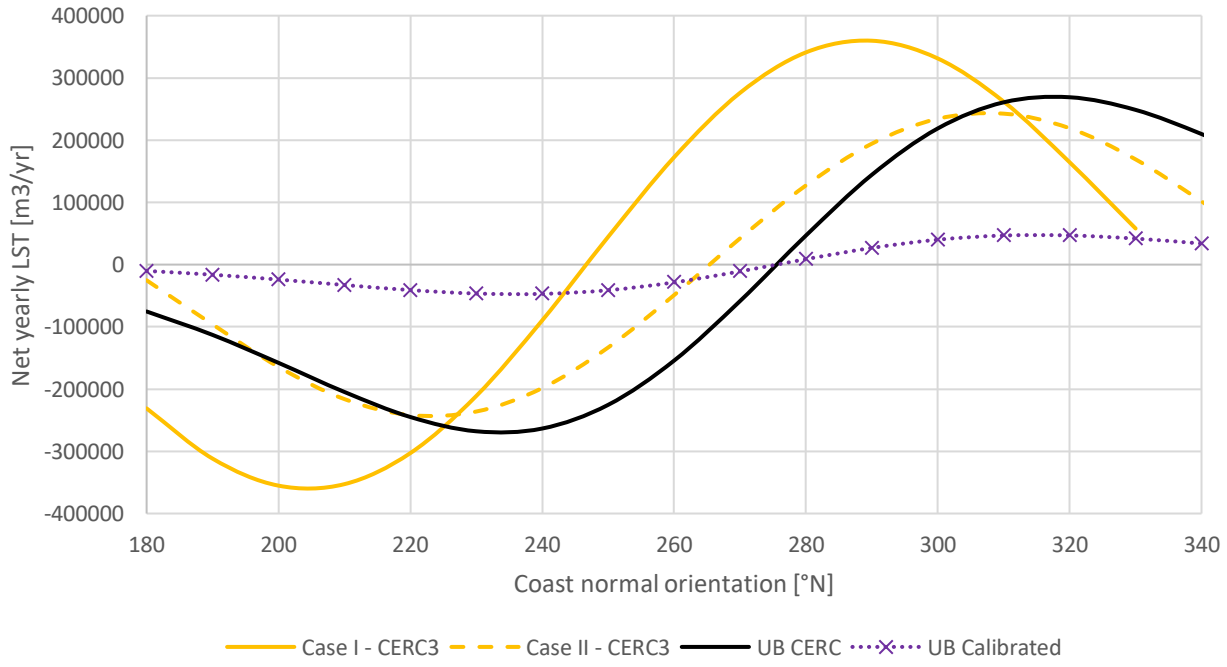

Figure 5-12 – S, φ-curves computed by ShorelineS for model case I and II (traditional approach) using CERC3 formula. Results of calibrated and CERC run in UNIBEST are included as well.

The first observation is the large deviation in order of magnitudes (or amplitude error ΔA) of the LST for the different cases with respect to the calibrated UNIBEST result. Where the maximum UB calibrated LST-quantity is in the order of $50.000\ m^3/yr$, the computed maximum transport in ShorelineS is for case I in the order of $360.000\ m^3/yr$ resulting in $\Delta A_{case\ I} = 7.6$ and $242.000\, m^3/yr$, $\Delta A_{case\ II} = 5.2$ for case II. Compared to the rerun of the UNIBEST-LT model using the standard CERC formula (black line, Figure 5-12) better matching amplitude factors were found (i.e., closer to 1) $\Delta A_{case\ I} = 1.3$ and $\Delta A_{case\ II} = 0.9$.

The second observation is the varying phase shift ($\Delta\varphi_{eq}$) for the different cases, similar as found in the wave transformation. For both the calibrated and CERC Unibest run the equilibrium coast angle was computed at $\varphi_{eq} = 275°$. ShorelineS computed the φ_{eq} for case I at $\varphi_{eq} = 245°$ ($\Delta\varphi_{eq,case\ I} = 28.9°$) and $\varphi = 265°$ ($\Delta\varphi_{eq,case\ II} = 10{,}2°$).

Although the overall shape and magnitude of the CERC cases (case I versus case II versus UB CERC) are comparable it should be noted that especially this phase shift can have a large impact when computing the actual LST for a specific coastal orientation. This is shown for an arbitrary coastal angle $\varphi_c = 270°$ (Table 5-4), the observations as described might have a large influence on the direction and magnitude of the LST along an actual (reorienting) coastline.

	$Q_s\ [m^3/yr]$ at $\varphi_c = 270°$
Case I	$276 \cdot 10^3$
Case II	$42 \cdot 10^3$
UB – CERC	$-59 \cdot 10^3$
UB – Calibrated	$-11 \cdot 10^3$

Table 5-4 – Observed variations in LST (Q_s) for $\varphi_c = 270°$ case I vs case II vs UNIBEST

For the simulation of case III and IV the dynamic boundary was activated, besides no other changes were made compared to the traditional approach case I and II (Figure 5-13).

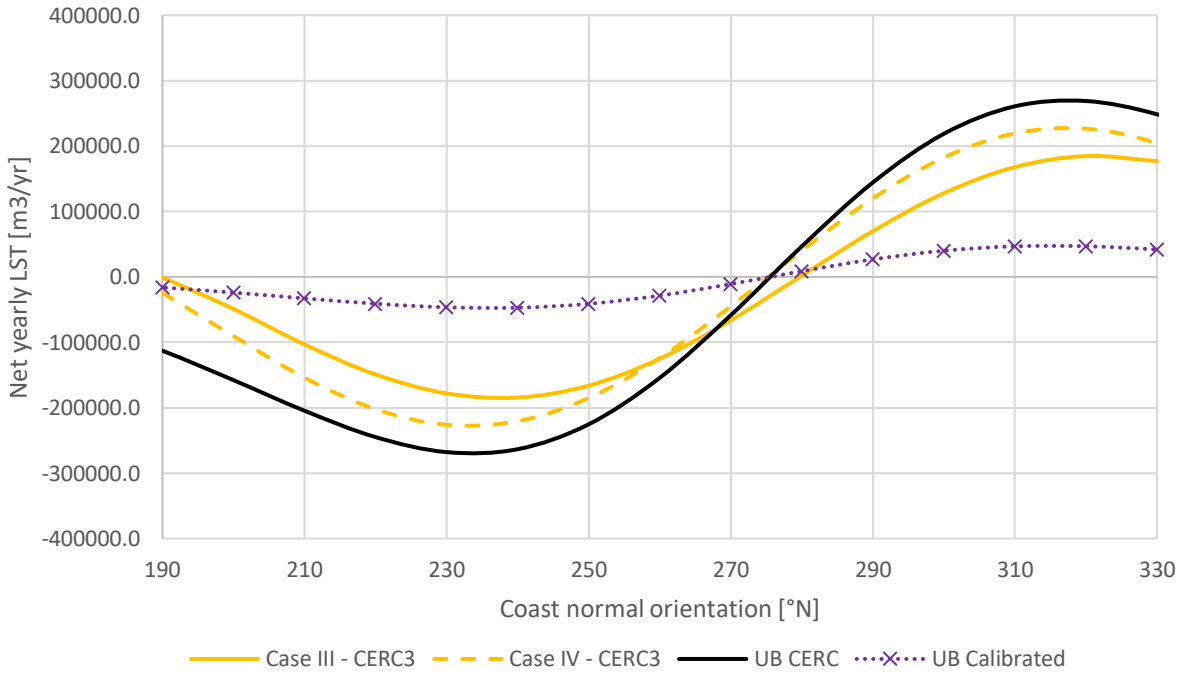

Figure 5-13 - S,φ-curves computed by ShorelineS for model case III and IV (dynamic boundary activated) using CERC3 formula. Results of calibrated and CERC run in UNIBEST are included as well.

It can be observed that the different cases are more in agreement with each other compared to the simulations without the dynamic boundary activated, especially the equilibrium angle φ_{eq} lines up better; $\Delta\varphi_{eq,case\ III} = 5°$ and $\Delta\varphi_{eq,case\ IV} = 0°$. The order of magnitude of the LST for the cases using the offshore wave climate (case I versus case III) has significantly reduced from $Q_{s,\max case\ I} = 360.00\ m^3/yr$ to $Q_{s,\max case\ III} = 185.000\, m^3/yr$. Or, compared to the UB CERC, from $\Delta A_{case\ I} = 1.3$ to $\Delta A_{case\ IV} = 0.7$.Apart from the change in the equilibrium coastline orientation φ_{eq} the shape and magnitude of case IV remained similar compared to the case II with $\Delta A_{case\ IV} = 0.84$.

The consequence of the better matching φ_{eq} and overall shape becomes clear when comparing the results at an arbitrary angle ($\varphi_c = 270°$) for the traditional (Table 5-4) and the cases for which the dynamic boundary was applied (Table 5-5): the direction of the transport and order of magnitude are in better agreement.

	Q_s $[m^3/yr]$ at $\varphi_c = 270°$
Case III	$-66 \cdot 10^3$
Case IV	$-45 \cdot 10^3$
UB – CERC	$-59 \cdot 10^3$
UB – Calibrated	$-11 \cdot 10^3$

Table 5-5 - Observed variations in LST (Q_s) for $\varphi_c = 270°$ case III vs case IV vs UNIBEST

The general performance, in terms of magnitude, for the different LST-formula with respect to the UB calibrated data is quantified with the amplitude factor ΔA (Table 5-6).

		CERC1	CERC2	CERC3	KAMP	MILH	VR14
Case I	*DB off, offshore WC*	24.2	14.8	7.6	7.9	2.4	2.9
Case II	*DB off, nearshore WC*	7.3	4.7	5.2	5.7	1.5	1.8
Case III	*DB on, offshore WC*	24.2	14.8	3.9	4.5	1.1	1.3
Case IV	*DB on, nearshore WC*	7.3	4.7	4.8	5.3	1.3	1.6

Table 5-6 – Amplitude factors ΔA compared to UNIBEST calibrated data for different LST-formulae and ShorelineS cases

The following observations can be made:

- The magnitude of CERC 1 & 2 are not influenced by the dynamic boundary (case I & II versus case III & IV) as they compute the LST using offshore wave data H_0 and $\varphi_{loc,0}$ only, thus $\Delta A_{case\ I} = \Delta A_{case\ III}$ and $\Delta A_{case\ II} = \Delta A_{case\ IV}$.
- The LST-formulae which are influenced by the dynamic boundary, using actual breaking wave parameters to compute the LST, (CERC3, KAMP, MILH and VR14) show better matching amplitude factors (i.e., closer to 1) when the dynamic boundary is applied. Especially compared to when a more offshore wave condition is applied (case I versus case III).
- The Mil-Homens- and Van Rijn 2014- formulae resulted in the best matching amplitude factors (i.e., closer to 1). The amplitude factors for the other formulae (CERC1-3 and KAMP) are quite high with an overestimation of the magnitude of at least 3.9 up to a factor 24.

To get better insight into the performance of each LST-formulae the results are further analysed per formulae. The observations as stated above are all based on the comparison with the calibrated UNIBEST. In the previous section (Figure 5-12) it was already observed that the calibrated UNIBEST data significantly deviates from the same UNIBEST model run using the same LST-formulations as used in ShorelineS (CERC, Kamp etc.). In addition to the amplitude factors related to the calibrated data (Table 5-6) therefore also the amplitude factor related to the UNIBEST rerun using the same LST-formula as used in ShorelineS is considered, which provide valuable information of the actual performance of the formula itself.

CERC

In ShorelineS three variances of the CERC formulae are implemented (Section 2.4):

- CERC 3 (Eq. 2.4) - Classical, most commonly used, CERC formulation, uses breaking wave conditions $H_{s,br}$ and $\varphi_{loc,br}$.
- CERC 2 (Eq. 2.5) - CERC (3) reformulated by Ashton et al., 2006a for the purpose of coastal modelling, uses offshore wave conditions H_0 and $\varphi_{loc,0}$ as input but accounts for shoaling and refraction over shoreline parallel contours.
- CERC 1 - Simplified formulation based on CERC3 but using offshore wave conditions input H_0 and $\varphi_{loc,0}$ instead of breaking wave conditions.

The CERC formula as defined in UNIBEST is similar but not equal to the formulations as used in ShorelineS. The formulation in UNIBEST uses offshore wave parameters $H_{s,0}$ and φ_0 as well the wave angle at breaker depth φ_b (Deltares, 2011):

$$S_c = A\, H_{s,0}^2\, 2\, c_{g,0}\, \sin\varphi_b \cos\varphi_0 \qquad 5.13$$

The results of the original CERC formula (CERC3) were already discussed (Figure 5-12 and Figure 5-13), which showed the best agreement with the result from UNIBEST using the CERC formulation (Table 5-7).

In contrast to original CERC3 formula, CERC1 and 2 uses offshore wave conditions as input. CERC2 includes a factor which accounts for wave shoaling and refraction over coastline parallel depth contours, which can be considered as a 'built-in' wave transformation. The 'relative' effectiveness is best shown by comparing the amplitude factors ΔA for the different cases (Table 5-7): for all cases the CERC2 formula resulted in a better matching amplitude factor (i.e., closer to 1) compared to the CERC1 without this build-in wave transformation term. However, this term does not account for effects dynamic boundary. This has two consequences (Figure 5-14): 1) the phase difference is still present when the dynamic boundary is activated, leading to a shift ($\Delta\varphi_{eq}$) of the entire S,φ-curve and 2) the wave height change (in this case reduction) due to the refraction over the static part of the profile is not included, leading to an overestimation of the LST-magnitude when the offshore wave climate was used (Case I and III).

	CERC1	CERC2	CERC3
Case I	4.2	2.6	1.3
Case II	1.3	0.8	0.9
Case III	4.2	2.6	0.7
Case IV	1.3	0.8	0.8

Table 5-7 – Amplitude factors of the different CERC formulae in ShorelineS with respect to UNIBEST CERC result

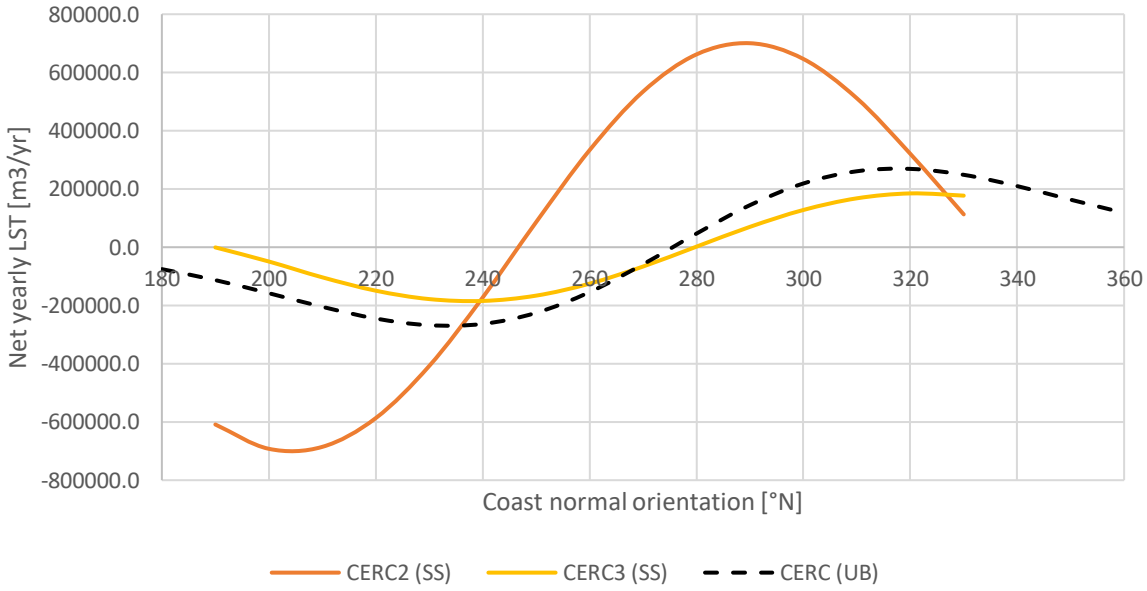

Figure 5-14 – S,φ-curves for Case III using CERC2 (by Ashton et al. (2001)) and CERC3 (original CERC formula using breaking wave conditions)

Kamphuis / Mil-Homens

The Kamphuis (eq. 2.6) and Mil-Homens (eq. 2.7) LST equations share the same structure and parameters, the Mil-Homens formula is in fact a re-evaluated version of the Kamphuis formula. The coefficients and exponents of the Kamphuis formula are adjusted in the Mil-Homens formula based on recalibration (Section 2.2).

Both formulae show good agreement with the runs using the same formula in UNIBEST (Table 5-8). Compared to the calibrated UNIBEST data Mil-Homens has a good matching amplitude with an ΔA of 1.1 (case III) up to 2.4 (case I). Larger deviations with the calibrated data can be seen for Kamphuis (Figure 5-15 and Table 5-8).

	KAMP	MILH
Case I	1.2	1.4
Case II	0.9	0.9
Case III	0.7	0.6
Case IV	0.8	0.8

Table 5-8 - Amplitude factors of the Kamphuis and Mil-Homens formulae in ShorelineS with respect to UNIBEST results using the same formulations

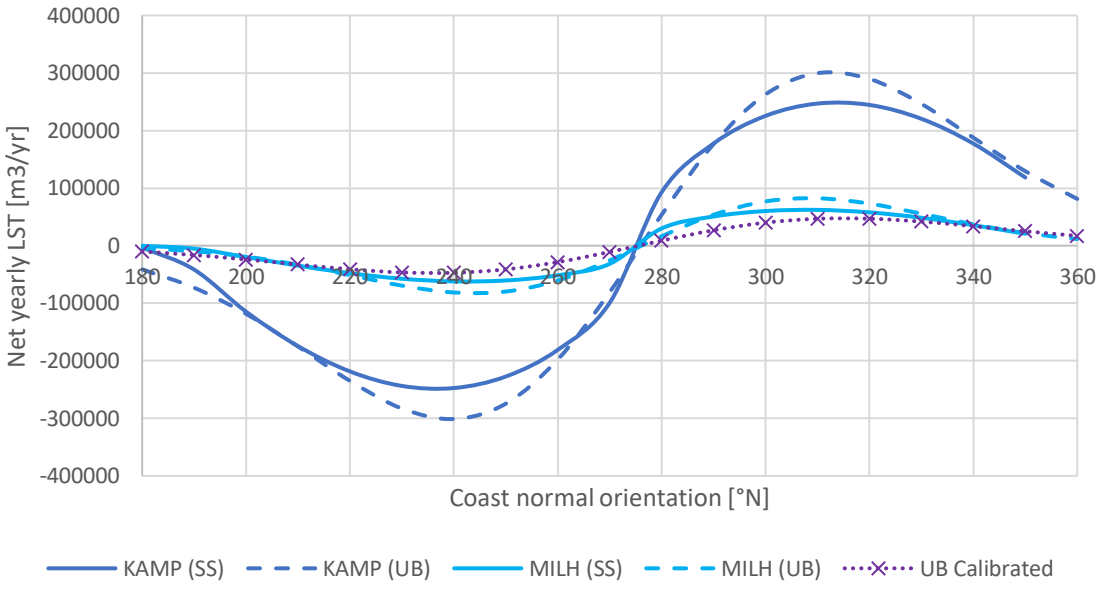

Figure 5-15 – S,φ-curves for Case IV using Kamphuis and Mil-Homens formulae

Van Rijn 2014

The Van Rijn 2014 formula, along with the Mil-Homens formula, resulted in the best matching results compared to the calibrated UNIBEST data of the considered LST-formulae (Figure 5-16 and Table 5-9).

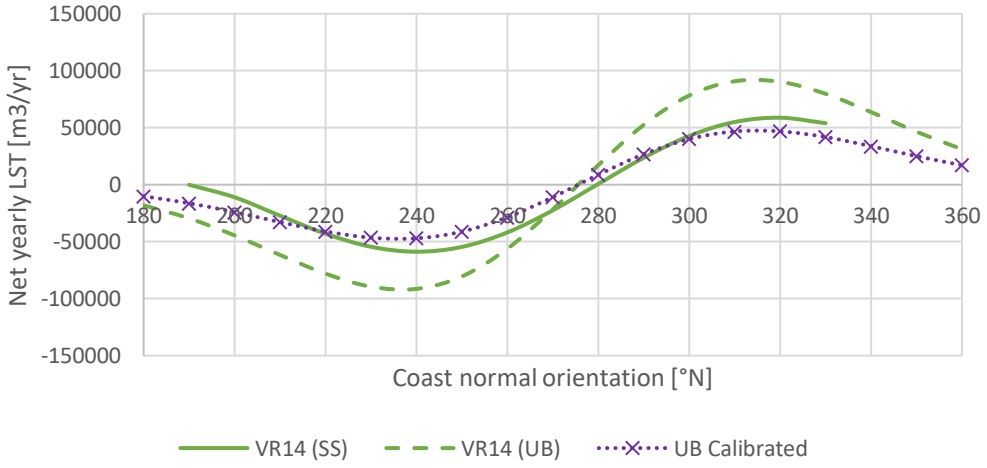

Figure 5-16 – S,φ-curves for Case III using Van Rijn 20114

	VR14
Case I	1.5
Case II	0.9
Case III	0.6
Case IV	0.8

Table 5-9 - Amplitude factors Van Rijn 2014 in ShorelineS with respect to UNIBEST using Van Rijn 2014

5.2.3 Sensitivity of different LST-formulae

Deviations of the maximum calculated LST quantity resulting in an amplitude factor ΔA up to a factor 24 were observed when comparing the results of different LST-formulae uncalibrated as calculated by ShorelineS to the results of the calibrated Lobito data. This raises the question whether certain formulae are applicable at all to derive LST-magnitude in the right order of magnitude using the uncalibrated formulae. To get some insight into the sensitivity and applicability of the different LST bulk formulae in general a number of sensitivity tests were done for varying wave conditions using UNIBEST-LT based on the following approach:

- An UNIBEST-LT test case was setup based on the cross-shore profile of the Lobito case.
- The S, φ-curves were calculated for a varying range of wave heights ($H_{s,0} = 0.5, 1, 1.5$ and $2m$) for varying wave period expressed as a ratio of the wave height: $T_p/H_{s,0} = 6, 12, 20$ leading to 10 different scenarios
- Each scenario was run using four LST bulk-formulae CERC, Kamphuis, van Rijn 2014 and Mil-Homens) and two semi processed based formulae; Van Rijn 2004 and Bijker.

In Table 5-10 the results of the test runs are shown. A larger, more detailed, version of this table can be found in Appendix D. Notice the increasing y-scale for increasing $H_{s,0.}$

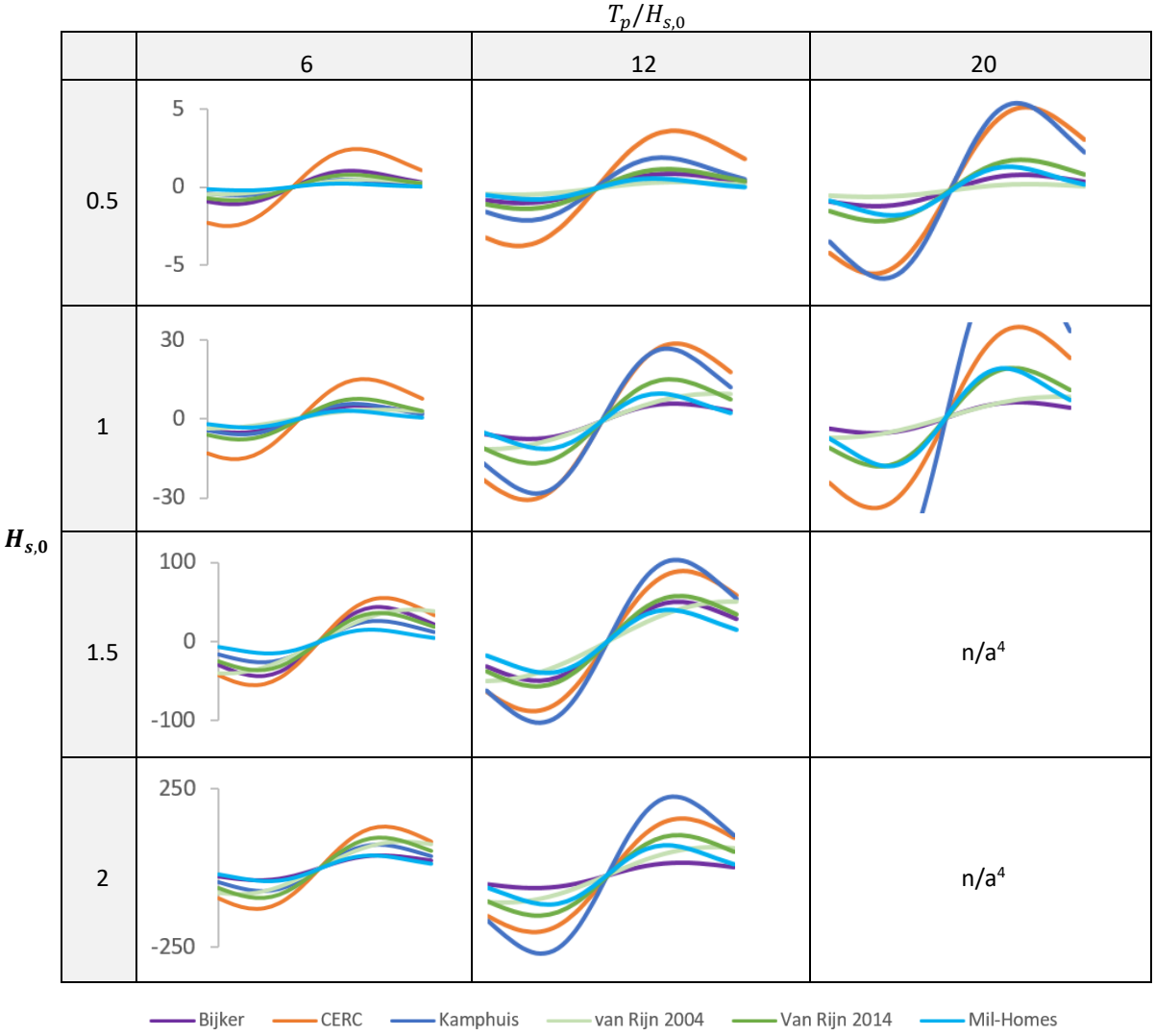

Table 5-10 – S, φ-scales for different LST-formulae (both bulk and processed based) in UNIBEST for different combinations of wave conditions (H_s and T_p) .Y-axis Q_s in $m^3/yr \cdot 10^5$

[4] Wave period in UNIBEST is limited to 25s, cases not analysed.

The two more advanced semi-process based formulations (Bijker and van Rijn 2004) resulted in consistent resulting LST-quantities. The average variation in predicted LST quantities ($Q_{s,Bijker}/Q_{s,VR2004}$) equals 1.3 with a maximum of 3, Figure 5-17. The variations are considered acceptable and are used as baseline prediction to compare the sensitivity of the bulk LST-formulae with.

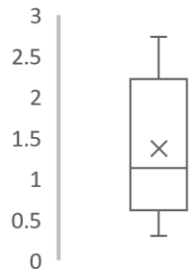

Figure 5-17 – Boxplot of variations in Q_s Bijker versus VR2004

Figure 5-18 shows the results of the sensitivity analysis, for this the amplitude factors (ΔA) are plotted against the different T_p/H_s-ratios for the different formulas. The amplitude factor is computed as the amplitude of the bulk formula over the average amplitude of baseline prediction of the Bijker and Van Rijn 2004 formula: $\Delta A = A_{bulk}/(0.5(A_{Bijker} + A_{VR04}))$.

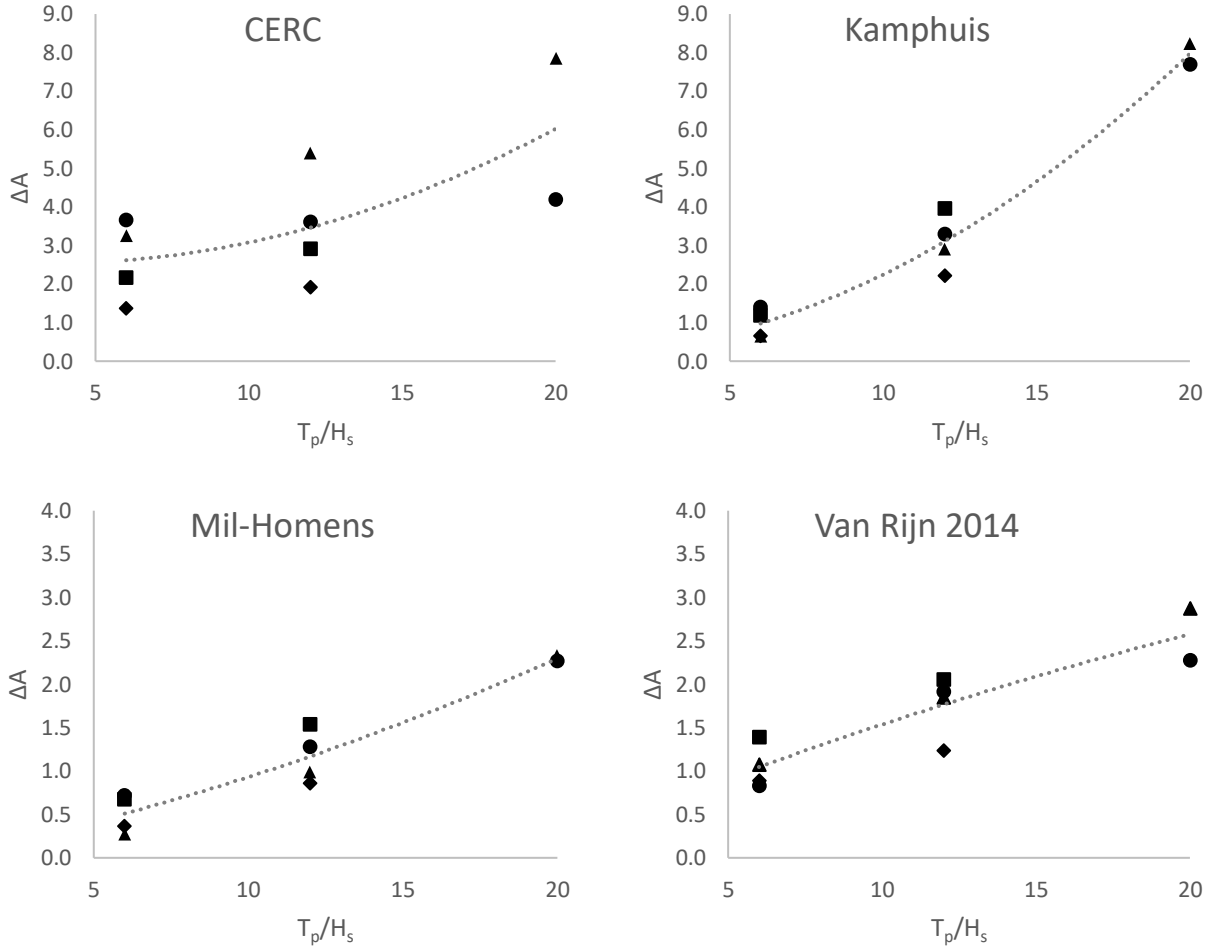

Figure 5-18 – Amplitude factors with respect to baseline prediction for four LST-bulk formulae for different T_p/H_s-ratios. The markers indicate the different considered wave height (▲=0.5m, ●=1m, ◆=1.5m, ■=2m)

Regarding to the sensitivity of the different uncalibrated bulk formulas the following observations can be made:

- For almost all scenarios the bulk transport formulas overestimates the LST with respect to the baseline prediction (i.e., $\Delta A > 1$).
- In general, the bulk formulae resulted in the best matching predictions for low T_p/H_s ratios in the order of 5.
- Increasing T_p/H_s-ratios (swell), as the case in the Lobito case study where $T_p/H_s \approx 14 - 22$, lead to larger deviations of the bulk formulae with respect to the more advanced predictions. The CERC and Kamphuis formula resulted in the largest overestimation of the transport rates up with an ΔA of 8.
- Mil-Homens and Van Rijn 2014 are most consistent in predicting the LST-quantities for all scenarios.

5.3 Validation case: Sandmotor

All observations in previous sections of this chapter are made using case models based on the Lobito spit using the results of the UNIBEST-LT model and local wave climate. To validate the general applicability of those observations the model was applied on a different case: the Sandmotor. The goal of the validation case is twofold: 1) Check the wave transformation module of ShorelineS and 2) Asses the effect of the dynamic boundary on LST. The data used for this ase study (wave climate, bathymetry, transport quantities) originates, unless stated differently, from Tonnon et al. (2018).

5.3.1 Wave transformation

For the first goal the wave conditions H_s and φ_w at different locations (depth) along the Sandmotor were extracted from a wave model and compared to the wave transformation of ShorelineS.

The input of the ShorelineS model is the offshore wave climate, consisting of 391 weighted wave conditions, located approximately 6km from the coastline at the 19m depth contour. The transformation was compared at two locations; nearshore at the 8m depth contour and at a point in between at the 13m depth contour. Both locations are located along a transect of the Sandmotor for which the depth contours are approximately all coastline parallel, thus no influence of the dynamic boundary (Figure 5-19).

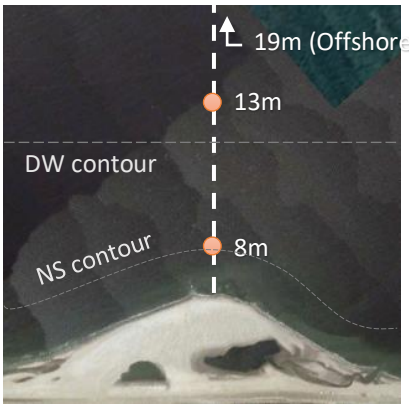

Figure 5-19 – Transect at top Sandmotor with location of 8m and 13m depth contours

In Figure 5-20 a comparison is made between the wave heights and wave angle computed by the ShorelineS transformation module (y-axis) versus the results the values from the Delft3D wave model (x-axis) at the location of the 8m depth contour. For a perfect match (i.e., $H_{s,Delft3D} = H_{s,ShorelineS}$) all values would line up on the 1:1 diagonal (indicated with the solid black line). The values of the non-transformed wave conditions (offshore waves at the 19m depth contour) are also indicated in the figure (red). The following observations can be made:

- For waves up to a wave height (left plot) of $1{,}5m$ a wave height reduction is clearly visible leading to better matching wave heights with respect to the Delft3D wave computations compared to the original offshore waves, for higher waves ($H_s = 1{,}5 - 3m$) this effect is less pronounced although an overall reduction can still be observed leading to better matching results.
- For even higher waves (in this case $H_s > 3m$) the H_s computed by ShorelineS are overestimated.
- The effect of refraction on the wave angle (Figure 5-20, right plot). The wave transformation by ShorelineS resulted in good matching wave angles with respect to the Delft3D results. For waves with an angle with a large deviation with respect to the coastline orientation ($\varphi_c = 314°$), i.e., high angle waves, the effects of refraction on the wave angle is best shown: a large difference transformed versus non-transformed waves.

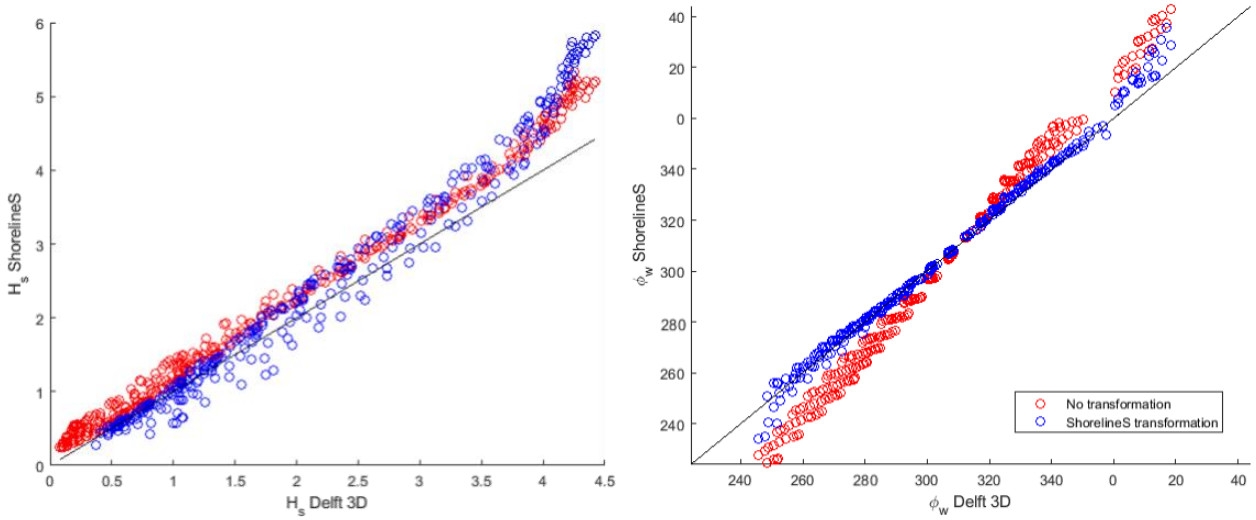

Figure 5-20 – Comparison of wave height- (left plot) and wave angle (right plot) transformation of Delft 3D versus Shoreline wave modules at the 8m depth contour. Blue markers indicate wave height computed by ShorelineS. Red values are non-transformed values (input) at d=19m.

At the intermediate water depth contour (13m) the observed transformation matches good with the Delft3D results, although the overall transformation compared to the original wave conditions is at this location less significant (Figure 5-21). The overestimation of the high waves ($H_s > 3m$) as observed at the 8m depth contour is not yet present at this depth, which implies that the overestimation arises between the 13m and 8m depth contour.

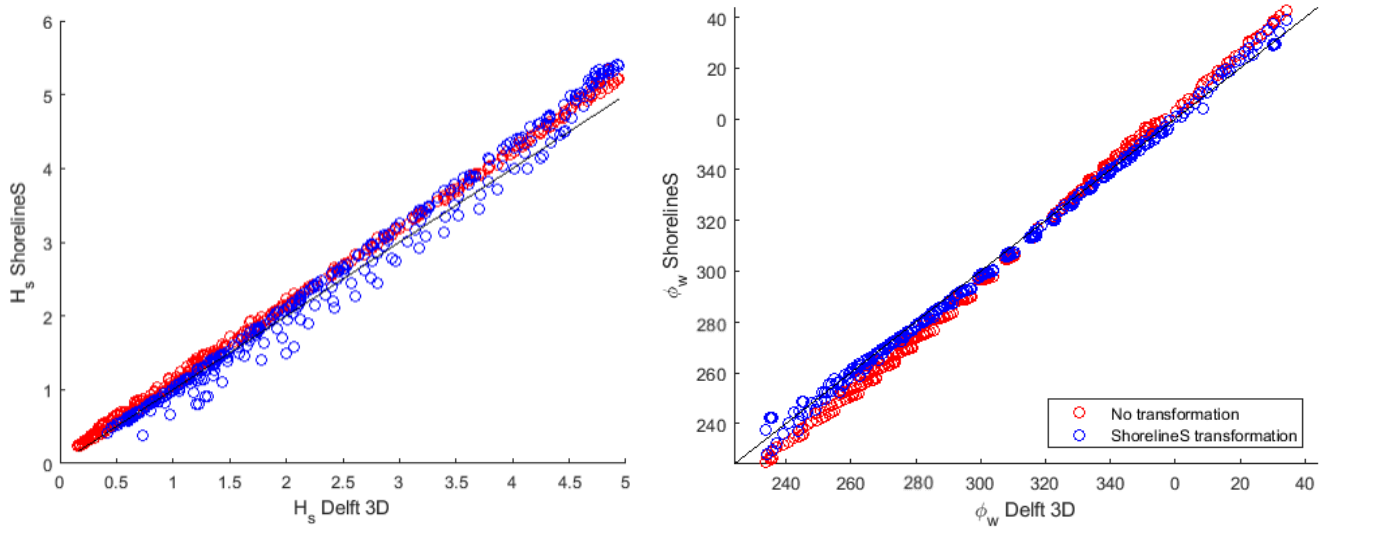

Figure 5-21 - Comparison of wave height- (left plot) and wave angle (right plot) transformation of Delft 3D versus ShorelineS at the 13m depth contour. Blue markers indicate wave height computed by ShorelineS. Red values are non-transformed values (input) at d=19m

The calculated wave conditions at the intermediate water depths at the $13m$ and $8m$ depth provide valuable insight into the performance of the wave transformation module, however for the calculation of the LST the (estimation) of the breaking parameters are used. For this, the breaker conditions computed by ShorelineS are compared when the deep-water wave climate (y-axis) or the nearshore wave climate (x-axis) was used as input (Figure 5-22).

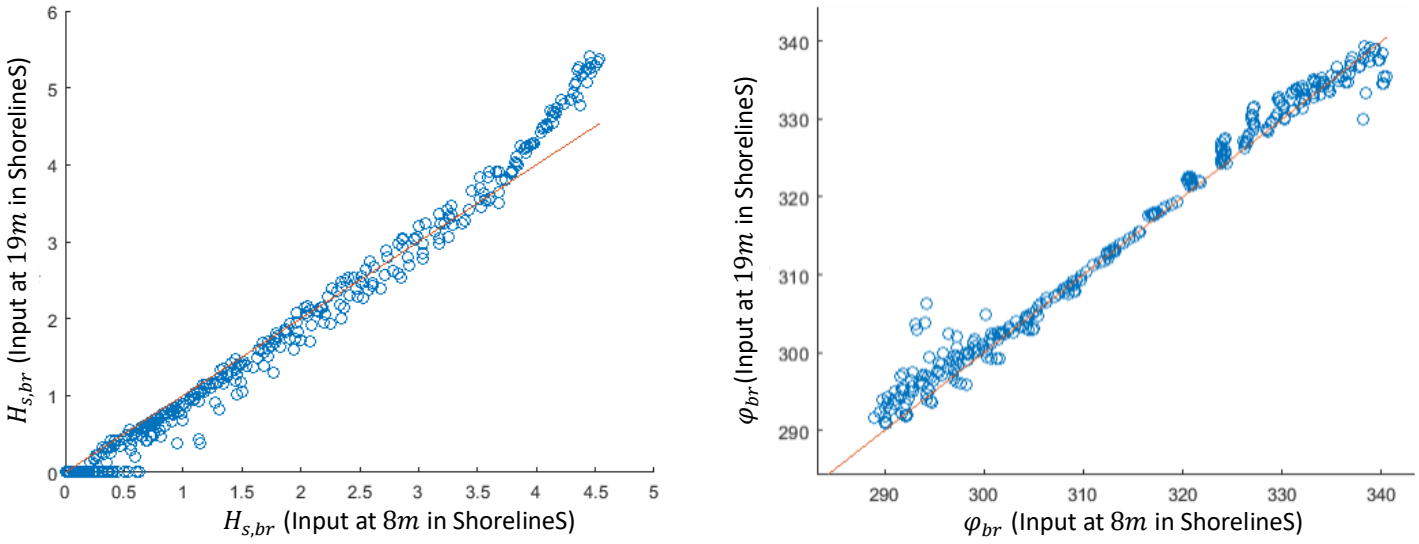

Figure 5-22 - Comparison of wave height- (left plot) and wave angle (right plot) at breaking point as calculated by ShorelineS using input at 8m depth contour (x-axis) versus input at 13m depth contour (y-axis and plotted values)

The estimated wave conditions match up to large extend, all waves refracted towards the coastline normal ($\varphi_c = 314°$ were φ_{br} are refracted to values within the interval $(290° - 340°)$). Larger waves ($H_s > 3.5m$) are overestimated when using the wave climate at the $19m$ depth contour with respect to the results when using the wave climate at the $8m$ depth contour as input.

The previous tests were applied on a transect for which the depth contours are all shoreline parallel up to the location where the offshore wave climate is imposed (Figure 5-19). In addition, a second transect has been considered at the flank of the Sandmotor for which the orientation of the coastline ($\varphi_c = 269°$) and nearshore depth contours rotate over the depth (Figure 5-23).

The wave transformation from deep water ($19m$) towards the $5m$ depth contour is computed in ShorelineS and compared to the results of Delft3D (Figure 5-24). Since over this transect the orientation of the depth contours changes, transformations with and without the dynamic boundary were performed. The dynamic boundary was fixed at a depth of 6.3m with an orientation equal to the offshore deep water contour orientation ($\varphi_f = 314°$) (Adopted from Tonnon et al. (2018)).

Figure 5-23 - Transect at left flank of Sandmotor with location of 8m and 13m depth contours indicated.

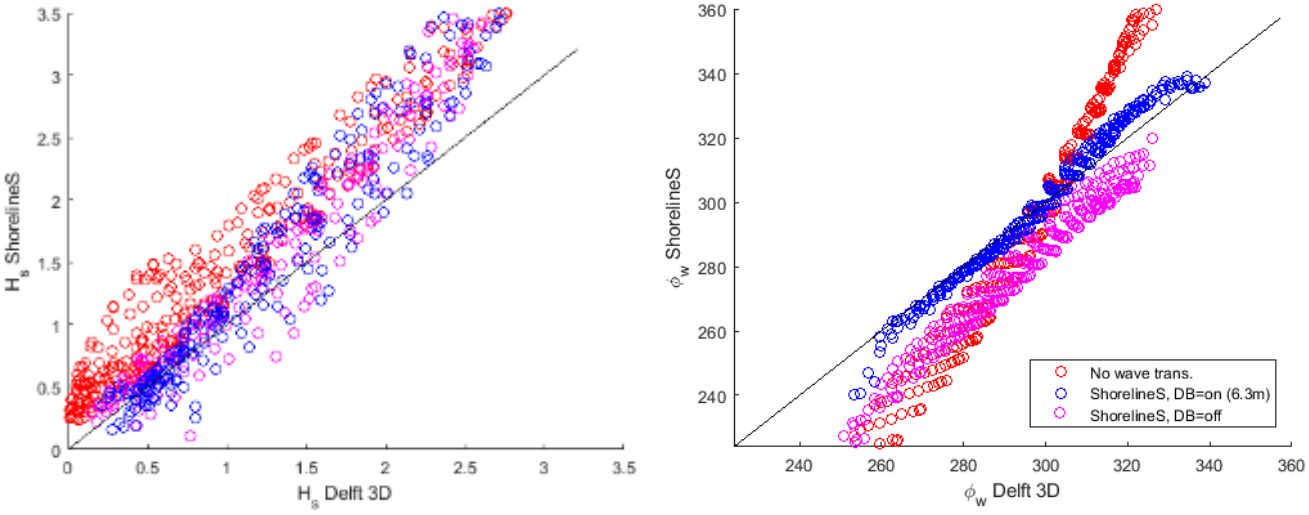

Figure 5-24 – Comparison of wave height- (left plot) and wave angle (right plot) transformation of Delft 3D versus ShorelineS at the 5m depth contour using ShorelineS wave transformation with dynamic boundary (blue) without dynamic boundary (magenta) and without transformation (reference, red)

Regarding the wave height, it can be observed that for both the wave transformations with and without the dynamic boundary deviations with respect to the Delft3D results arise for this location, however both results are still improved (i.e., closer to the values of Delft3D) with respect to the non-transformed waves.

The effect of the dynamic boundary is more clearly visible when looking at the calculated wave angle φ_w at this location (Figure 5-24, right plot). The calculated values for φ_w when the dynamic boundary is applied resulted in the best agreement with the Delft3D results. For the transformation where no dynamic boundary was applied an overall shift can be observed as described earlier (Section 5.2.1) resulting in a consistently underestimating the wave angle. It should be noted that for this location the nearshore wave refraction is up to $35° - 40°$ (indicated in red, right plot Figure 5-24).

5.3.2 Longshore sediment transport

The second goal of the validation case is to assess the effect of the dynamic boundary on the actual sediment transport quantities for the Sandmotor case. The model was set up using the data and parameters for the Sandmotor as described in Tonnon et al. (2018) (Not repeated here): Using a reduced wave climate consisting of 10 wave conditions located at the $19m$ depth contour, a dynamic boundary at the depth of 6.3m and depth contours fixed at $\varphi_f = 314°$ based on the orientation of the offshore depth contours. The schematized shape of the Sandmotor is derived from the Augustus 2011 bathymetry dataset. To calculate the initial LST the van Rijn (2014) bulk formula (eq. 2.8) was used. No calibration was applied. The LST quantities were computed for the case with and without the dynamic boundary activated.

The uncalibrated results (Figure 5-25, left) for a straight coastline (i.e., prior to the construction/updrift from the of the Sandmotor) are in the order of $200.000\, m^3/yr$ which is in the same other of the actual net alongshore transport for the central part of the Dutch coastline (Tonnon et al., 2018; van Rijn, 1997).

The magnitude and overall distribution of the wave climate averaged alongshore sediment for the simulating when the dynamic boundary activated, order of $Q_S = (800\ to\ 900) \cdot 10^3\ m^3/yr$, is in the same order of magnitude as found with advanced Delft3D modelling by Tonnon et al. (2018). Whereas, when no dynamic boundary was applied the local transport rates along the flank are underestimated $Q_{s,DB=off} = (300\ to\ 400) \cdot 10^3\ m^3/yr$ (Figure 5-25, left). It should be noted that those quantities should not be directly compared 1 to 1 to the values indicated by Tonnon et al. (2018) since the results of ShorelineS are based on the initial coastline ($T = 0yr$ at 08-2011) and the quantities as presented in Tonnon et al. (2018) are extracted at $T = 1yr$, thus including morphological change over one year.

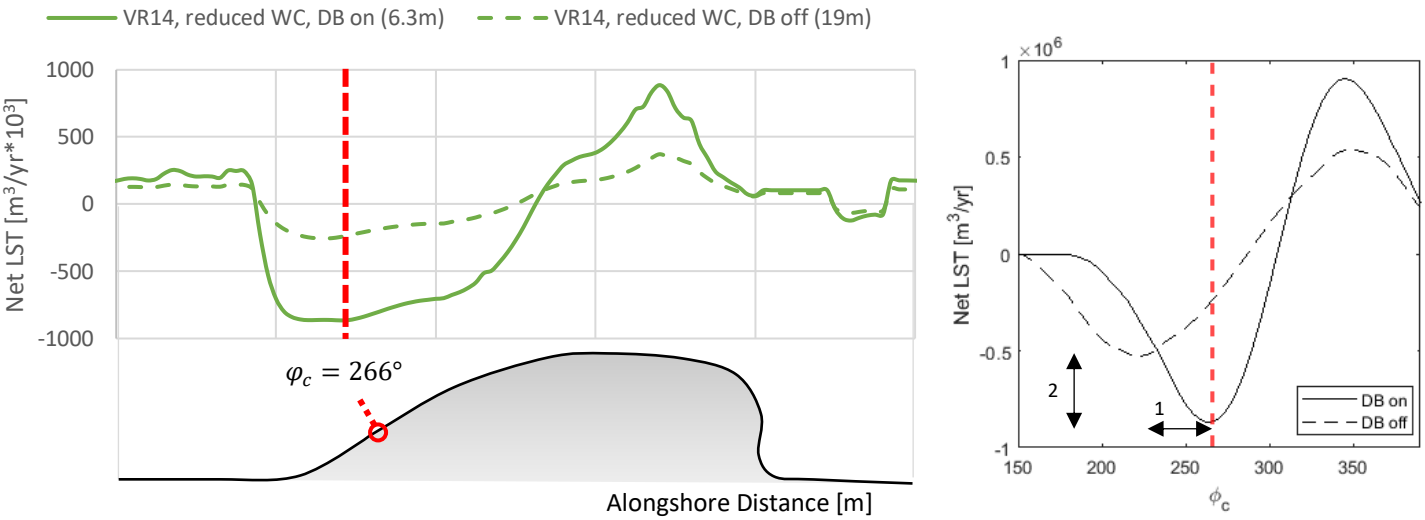

Figure 5-25 – Left: Computed LST at T=0 over Sandmotor initial coastline with ShorelineS with and without dynamic boundary using Van Rijn 2014 transport formula. Right: Net-S,φ-curves for case without and with the dynamic boundary enables. Values at the flanks orientation are highlighted by the red dashed line.

To get better insight into observed the differences in transport magnitude and the effect of the dynamic boundary on the LST a transect at the flank of the Sandmotor, with a local coastline orientation of $\varphi_c = 266°$, is evaluated (indicated with the red line in Figure 5-25). At this transect the maximum values for the LST along the Sandmotor's initial coastline are found for both the case with and without the dynamic boundary activated. The magnitude of the computed LST by ShorelineS when the dynamic boundary is used, is in the order of magnitude as the initial measured transport quantities as well more detailed Delft 3D simulations (Tonnon et al., 2018). For the case without the dynamic boundary the transport is a factor 3.7 less at this transect. This factor is best be explained using the S,φ-curve. Two major observations can be made, resulting in the factor 3.7 difference: (Figure 5-25, right)

1. **The phase shift of the S,φ-curve as discussed in section 5.2.1**
   Over the flank the coastline angles variate between $314°$ (coastline) and $260°$. Due to the phase shift the transport is maximum ($Q_s = Q_{s,max}$) for the case which uses the dynamic boundary, while for the case without the dynamic boundary it is still well below its maximum value, located within the linear part of the curve. In fact: the maximum value is not reached for the case without the dynamic boundary over the entire left flank of the Sandmotor for $\varphi_c = [260°, 314°]$.
2. **The difference in order of magnitude of LST**
   The overall magnitude of the S,φ-curve for the case without the dynamic boundary is much smaller compared the curve for the case with the dynamic boundary enabled. This effect was explained in Section 5.2.1 (Figure 5-10) based on the difference in refraction from offshore location where the wave climate was defined up to the point of breaking. For example: one of the 10 waves within the reduced wave climate with a duration of 16% of the time has a height of $H_s = 0.90cm$ and has an offshore orientation (at $d = 19m$) of $\varphi_w = 268°$. For the case without the dynamic boundary this wave is almost orientated coast normal orientation with respect to the flank/depth contours ($\varphi_c = 266$, $\Delta\varphi = -2°$), thus close to the equilibrium orientation for which $Q_s = 0$ thereby resulting in very limited LST (Eq. 5.11). While, for the case with the dynamic boundary enabled it has, up to the dynamic boundary ($\varphi_f = 314°$), a relative angle of $46°$. Resulting for this case in, even after refraction, a larger and even opposite directed LST.

Since the net-S,φ-curve (Figure 5-25, right) is a sum of the individual transport curves per wave condition, it can be understood why both S,φ-curves using the same wave climate, coastline and transport formulation can result in significantly different transport rates due to the implication of the dynamic boundary.

A comparison of the outcome of the different available bulk LST-formulae in ShorelineS on this case was made (Figure 5-26). For all those results the dynamic boundary was applied at a depth of 6.3m.

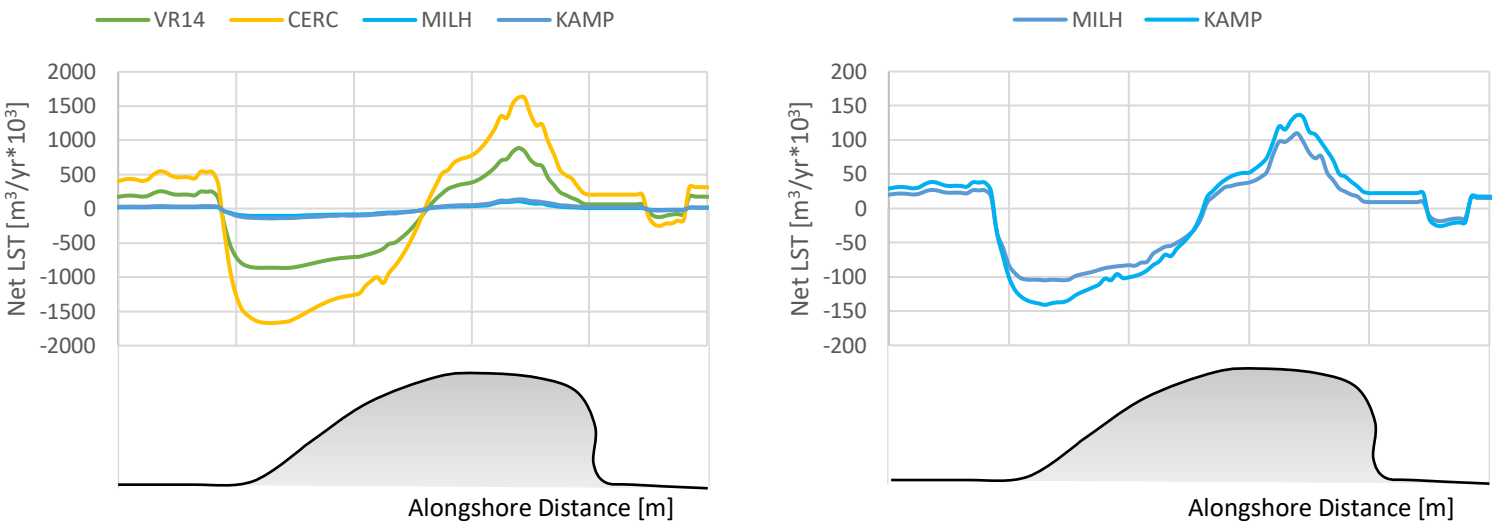

Figure 5-26 - Computed LST at T=0 with ShorelineS using a dynamic boundary for different LST formulae. Right plot only shows MILH and KAMP transport formula.

According to application of the different LST-formulae the following two main observations can be made:

1. The result of the CERC transport overestimated the overall LST by a factor 2, a factor similar as found in Section 5.2.3 for the ratio $T_p/H_s \sim 3-7$.
2. The quantities calculated using the Mil-Homens- and Kamphuis formulae largely underestimated the overall LST. This while the two results themselves are in the same order of magnitude (Figure 5-26, right). The latter can be related to the fact that the wave periods are for this case relatively short (compared to the Lobito case), whereas the influence of the wave period (power of the T_p term) on the LST is one of the most significant changes when comparing the Kamphuis formula to the recalibrated Mil-Homens formula (Eq. 2.6 and 2.7) which explains why for this case both formulae resulted in similar results.

For all tests a reduced wave climate was applied consisting of 10 wave conditions, when applying the full wave climate, consisting of 391 wave conditions, the LST quantities both for the cases (DB on and DB off) are overestimated up to a factor 2 using the van Rijn (2014) transport formula (Figure 5-27, left). This can probably be related to the overestimation of LST for high waves in combination with the wave climate schematisation:

1. The maximum wave height in the reduced wave climate equals $H_s = 2.64m$ while the full wave climate includes waves up to $5m$.
2. Wave transformation for larger wave heights are overestimated by ShorelineS (Figure 5-20).
3. The LST quantity resulting from the van Rijn (2014) transport formula is highly depending on the wave height $H_s$by a power 3. $Q_s \propto H_s^3$.

The influence of the larger waves on the resulting net LST is supported by a rerun of the model using the full wave climate but now limited to a wave height of $H_s = 3m$. While the duration of this portion of the wave climate is limited to 0.9% of the full duration (~ 3 days), it has a large influence on the net yearly transport calculated using the van Rijn (2014) transport formula. The rerun using $H_{s,0} < 3m$ resulted in the similar order of magnitude of the net transport compared to the run for which the reduced climate was used (Figure 5-27, right).

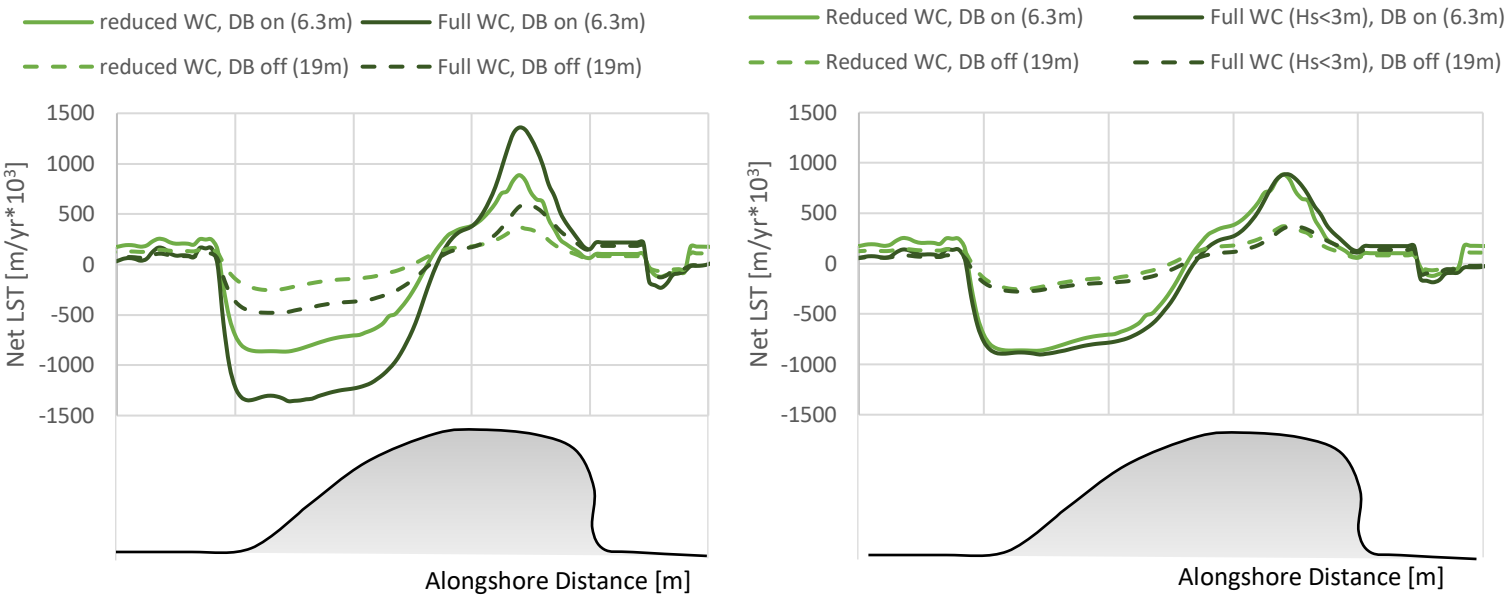

Figure 5-27 – Computed LST at T=0 with ShorelineS using Van Rijn 2014 sediment transport formula. Left plot: Comparison of result of full wave climate (391 conditions) and reduced climate (10 waves). Right plot: comparison of results of full wave climate and result of full wave climate but without the conditions with $H_s > 3m$.

5.4 Discussion and conclusions

Prior to the conclusions (Section 5.4.2) some points of discussions are addressed regarding 1) the wave transformation, 2) the used UNIBEST model which is used as baseline prediction and 3) the used LST-formulae.

5.4.1 Discussion

Wave transformation

To improve the wave transformation, the concept of a dynamic boundary was implemented in ShorelineS (Section 5.1.2) based on a number of assumptions which will be discussed here:

The wave transformation in ShorelineS accounts for wave shoaling and wave refraction over parallel depth contours, other mechanisms which may influences the wave transformation such as energy loss due to friction, wave focussing, effects of wave groups etc. are not included in this simplified model. This was shown in the validation case of the Sandmotor (Section 5.3.1) for which the higher waves ($H_s > 3m$) were overestimated compared to Delft3D results.

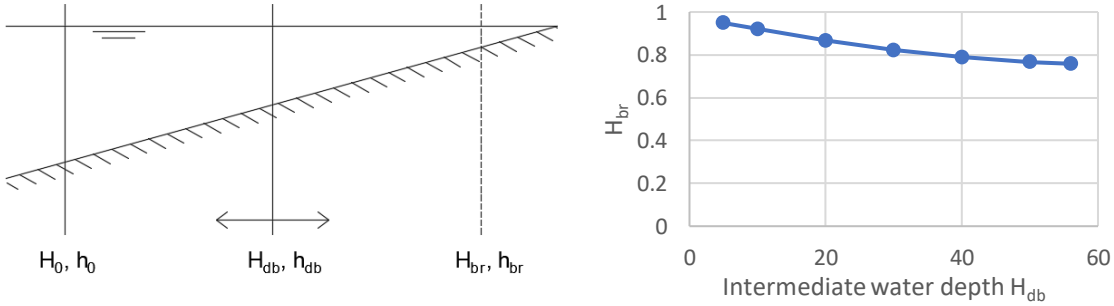

Figure 5-28 – Variation of intermediate water depth (left) leading to variation in breaking wave height (right)

The assumption of breaking wave speed $c_{br} \approx \sqrt{h_{br}\, g}$ and the use of the breaking parameter γ are used to rewrite eq. 5.8 as an explicit formulation. A consequence of those assumptions is that the breaking wave speed, and breaking water depth, is therefore implicitly depending on the location/depth of the offshore or intermediate wave condition (or H_{db} in case of a dynamic boundary), which should not be the case assuming no energy loss (Figure 5-28).

This is only of relevance when no dynamic boundary is used in the model, and the user is 'free' to choose an intermediate water depth which is used to estimate the breaker parameters. Small variations in the estimated breaking wave height H_{br} may arise for a different choice of the intermediate water depth as shown for a test case in Figure 5-28. When a dynamic boundary is applied the intermediate waterdepth is fixed at the dynamic boundary. For the cases where no dynamic boundary was activated (case I and II) no intermediate depth is used (i.e., set at same value of the offshore depth). In general, it can be argued that choosing an intermediate water depth closer to the 'real' breaking depth results in a better estimation of the breaker depth, however since the breaker depth is not known at forehand and since the formulation still depends on other assumptions as described above, setting the intermediate water depth equal to the offshore water depth when the dynamic boundary is not used, can be considered a save choice.

The goal of the wave transformation module is to provide a realistic estimation of the breaking wave parameters in a computational efficient matter. To achieve this, assumptions as discussed above are unavoidable. The implementation of the dynamic boundary provides a more realistic wave transformation for a reorienting coastline compared to the traditional wave transformation, however for a better representation of the actual wave transformation it is advised to use a more advanced wave computation model.

In the original wave climate for Lobito (located approx. 100km from the coast) 38 of the 42 waves conditions are directed off-coast for a coastline orientation of $\varphi_c = 325°$ (i.e., $\varphi_w < 235°$ for 38 wave conditions) (Table 5-3). The SWAN wave transformation showed that all wave conditions at the locations of the offshore wave climate (located 2.5km from the coastline) and nearshore wave climate (located 200m from the coastline) reoriented towards the coast (i.e., $\varphi_w > 235°$ for all wave conditions). This wave transformation cannot be reconstructed with the simplified wave transformation as implemented in ShorelineS as more complex offshore wave transformation mechanisms, as discussed earlier, are not included in this model. It is therefore important that the 'offshore' wave condition used as input in the ShorelineS model is located relatively close to the coast (i.e., close to the coast but outside the area which is morphologically affected during the simulation) at a location where preferably coast parallel depth contours can be distinguished. If a climate is not available at this location a more advanced wave transformation model can be used as intermediate step to derive a wave climate at this location as was done for the Lobito case.

UNIBEST model

For the model setup of the ShorelineS Lobito-model the data from the UNIBEST reference model was used as reference as actual (measured) data is limited. Since the model was already calibrated and validated it was decided to not change or adjust the original UNIBET model. Variations of the used schematisation and model parameters might influence the final derived transport quantifies. However, for the purpose of this study using the chosen method, namely; a model-to-model comparison the absolute transport quantifies are of less relevance. Therefore, in model-to-model comparison relative quantities (ΔA and $\Delta\varphi_{eq}$) were used to rate the ShorelineS model performance. For the hindcasting of the actual Lobito spit case the model-set up as used here, such as the use of a single representative wave condition and the schematization of the dynamic boundary, should be reconsidered.

LST-formulae

The shape of the Kamphuis and Mil-Homens S,φ-curves slightly deviates from the S,φ-curves as computed by UNIBEST, especially for the slope around the equilibrium angle (φ_{eq}) which can be observed in Figure 5-15. This is due to the fact that UNIBEST uses a fitted shape function to represent the sinusoidal S,φ-curve, Eq. 2.10. In the Kamphuis formulation the longshore wave power is set proportional to the power 0.6; $Q_{s,KAMP} \propto \sin\left(2\varphi_{loc,br}\right)^{0.6}$. The shape function used in UNIBEST cannot correctly be fitted for this function.

This can be shown by using the LTR-interactive mode of UNIBEST-LT to calculate the actual fit points used for the fitted shape function, those fit points better represent the actual LST which are in better agreement with the S,φ-curve resulting from ShorelineS.

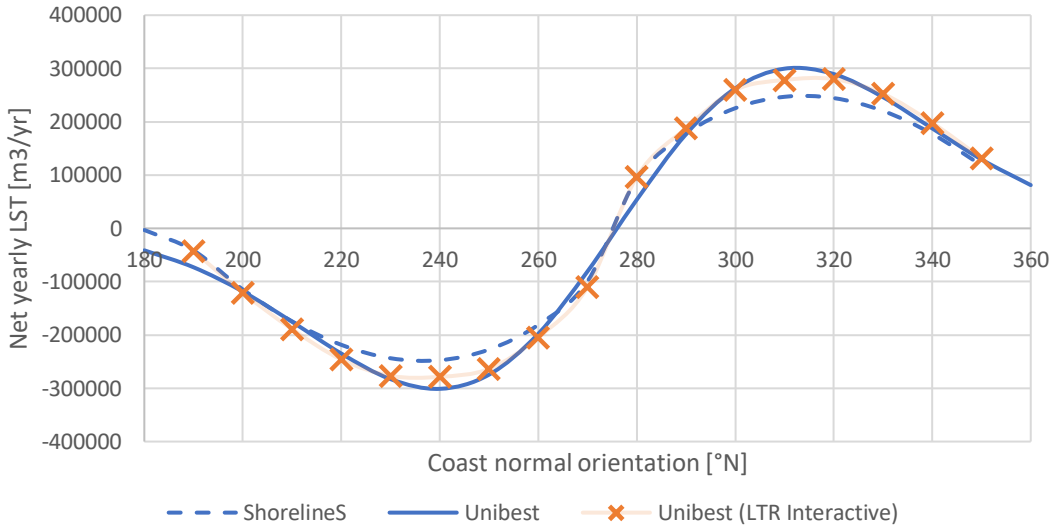

Figure 5-29 - S,φ-curves for ShorelineS (Case IV) using Kamphuis-formula, compared to fitted UNIBEST result and the actual values using the UNIBEST LTR interactive mode.

5.4.2 Conclusions

In this chapter the performance of the LST-module of ShorelineS was assessed with a focus on two main topics of interest: 1) the performance of the wave transformation-module and 2) the performance of the different LST-formulae itself. To do this the results of a number of ShorelineS case runs (Table 5-6) were compared to the calibrated data originating from the Lobito spit case UNIBEST model.

The fundamental basis of the ShorelineS model, namely the principle that the wave transformation and transport computation is done for every timestep for every individual coastal 'grid-cell', requires the use of simplified wave- and transport computations (using LST bulk formulae) to preserve the long-term model efficiency.

Regarding the wave transformation a new approach, including the concept of the dynamic boundary, was implemented in the wave transformation module in ShorelineS. It is shown that this new approach better represents the effect of a change of the coastline on the bathymetry. Two main effects of the dynamic boundary can be distinguished with respect to the traditional approach:

- A phase shift in the equilibrium orientation $\varphi_{c,eq}$ and the S,φ-curve as a whole
- A change in wave height at the breaker line.

When no dynamic boundary is applied $\varphi_{c,eq}$ only depends on the angle of the offshore wave $\varphi_{c,eq} = \varphi_{w,0}$, which implies that the shape of the S,φ-curve and LST quantities at the coastline largely depends on where (i.e., at what depth) the user decides to define the wave climate. When the dynamic boundary is activated this will change due to refraction over the deep water depth contours. The equilibrium coastline orientation will be influenced by the characteristics of the dynamic boundary thus $\varphi_{c,eq} = f(\varphi_{w,0}, \varphi_f, T_p, h_{deep}, h_{nearshore})$ leading to a more robust estimation of breaking wave conditions independent of the user defined location of the wave climate which is considered an important property for a robust coastline model. The change in wave height due to the dynamic boundary is related to the refraction over deep water depth contours as the split in the static and active part changes the overall refraction coefficient K_r.

Regarding the six available LST-bulk formulae in ShorelineS it was found that they are all implemented correctly. The model to model comparison using the same LST-bulk (uncalibrated) formulae in UNIBEST showed that the amplitude error (ΔA) (Figure 5-5), is consistent and in the order of 0.8, which is close to 1 (i.e., a perfect match). The phase of the S,φ-curve matched good ($\Delta\varphi_{eq} = 0°$). This means that the performance of the sediment transport module in ShorelineS is similar to the performance of the UNIBEST-LT module using LST-bulk formulae.

LST formulae which uses the offshore wave conditions to determine the LST (CERC1 and CERC2) are sensitive to the user defined boundary conditions as they do not include effects of the nearshore wave transformation and the dynamic boundary (if used). Such formula thereby implicitly assumes a constant wavefield along the entire coastline. Especially for an undulating coastline the wave height and wave angle can vary over the coastline due varying wave -shoaling and -refraction for different coastline orientations. The LST formula by Ashton et al. (2006a) (i.e., CERC2 in ShorelineS) is a CERC-type formulae which uses the offshore wave conditions but includes a term which accounts this nearshore wave transformation. It is shown that this 'built-in' wave transformation term is indeed able to better estimate the LST compared to the CERC1 formula (using only offshore wave conditions), however it does not include effects of the dynamic boundary.

Large deviations in the magnitude of the LST for the CERC and Kamphuis formulations (at least an amplitude error $\Delta A \geq 4$ up to a factor 24 for CERC1 or 8 for CERC3) were observed with respect to the calibrated result, expected at the coastline of Lobito. This does, however, not directly imply that such formulae are incorrect and should not be used. The sensitivity of the currently implemented LST-formulae for different wave conditions (H_s and T_p) was tested using UNIBEST-LT. This showed that for the local (swell) wave conditions at Lobito (T_P/H_s ratio in the order of $14-22$) large deviations with respect to more advanced processed based formulae indeed arise. For lower T_p/H_s-ratios (order $T_P/H_s \sim 5$) resulted in better matching results for all bulk formulae. Calibration of LST-bulk formulae using field data or more advanced processed based models is therefore still required. Even after calibration LST-bulk formulae will still be less applicable for modelling scenario's with wave climates which consists of a large range of different wave conditions (in terms of T_p/H_s-ratios). This was also shown in the validation case of the Sandmotor for which a small portion on the wave climate could have large/dominating effects on the total net transport.

The best performance was found for the van Rijn (2014) (Short: VR14) transport formula in ShorelineS. This formula showed the best matching results (ΔA in range 1.3-1.6) for the Lobito case, it showed a good consistency with processes-based formulas in the sensitivity analysis and resulted in a realistic initial transport pattern in the validation case for the sand engine. The Mil-Homens (2016) performed well for the Lobito case but resulted in large deviations in the sensitivity analysis as well in the sand engine validation case. For the other transport formulae (CERC & Kamphuis) overpredictions in the order of ΔA = 3.9-5.3 were found.

6 Spit formation in ShorelineS

Spit formation in general can be described by the three characteristic aspects of a spit (Figure 1-3) the spit migration direction, the width (and shape) of the spit and the migration rate. In this chapter the modelling performance of ShorelineS on the spit migration direction and the spit width and shape aspect have been assessed.

Section 6.1 focusses on the correct modelling on the spit migration direction. In this section the link is made between the theory on spit direction and the 'upwind-correction' routine in ShorelineS, which controls the spit direction in the model. An improvement was suggested and implemented based on the results of Chapter 5. The performance on modelling the spit direction has been validated by means of hindcasting the Lobito spit formation. In Section 6.2 it was analysed how the spit shape / width is currently controlled in ShorelineS and how the knowledge gained from the Chapter 4 (Spit formation processes) can be used to improve the model routine to better/more correctly represent the spit width. The chapter ends with a conclusion and discussion in Section 6.3 on the presented results and analysis.

6.1 Spit migration direction

6.1.1 Methods

The direction of the spit can, according to Ashton et al. (2006a), be related to the relative angle between the incoming wave and the coastal orientation for which the transport maximises defined as the critical angle (Section 2.1.2).

In ShorelineS the spit's orientation is controlled based on this principle by the upwind correction routine (Section 2.4.1). In the current version of ShorelineS the critical angle is set to a fixed for each LST-formula (Table 6-1), the values used as threshold in ShorelineS were derived by Elghandour (2018) similarly as which has been done by Ashton et al. (2006b). All values for the critical angle are fixed values related to the offshore wave angle ($\varphi_{w,0}$). The values are close to the theoretical value of $45°$ by CERC (using offshore conditions $H_{s,0}$ and $\varphi_{w,0}$ only) but slightly deviate due to wave-refraction.

Transport formula	Critical angle $\varphi_{loc,crit}$
CERC	$45°$
CERC2	$42.39°$
Kamphuis	$38.05°$
CERC3	$41.42°$
VR14	$39.9°$

Table 6-1 –Theoretical values for the critical angles (Elghandour, 2018)

The values presented by Elghandour (2018) and Ashton et al. (2006b) are all derived based on the assumption of coastline parallel depth contours. Relaxation of this assumption by using a dynamic boundary, which results in a better representation of the bathymetry for reoriented coastlines, demonstrated the effect of this assumption on LST and the shape of the resulting S, φ-curve (Chapter 5): an overall change in magnitude and a (phase) shift of the S, φ-curve as a whole. Especially the latter is of importance since a shift of the S, φ-curve also implies a shift of the critical angle for which the LST maximises. It was therefore hypothesized that the critical angle should not be a fixed value but should be variable depending on the model conditions (i.e., wave condition and bathymetry/dynamic boundary).

Determination of the (variable) critical angle

In Section 5.2.1 it was shown that the phase shift of the equilibrium angle $\Delta\varphi_{eq}$ can be determined explicitly (Eq. 5.12) as it is solitary depends on the effects of refraction on the wave direction due to the dynamic boundary. The determination of the critical angle $\varphi_{loc,crit}$ is not that straightforward since it is both depending on the wave height- and the wave direction transformation through the non-linear LST-bulk formula. This is shown in Figure 6-1 for the Lobito case using a single (reduced) offshore wave condition and a dynamic boundary.

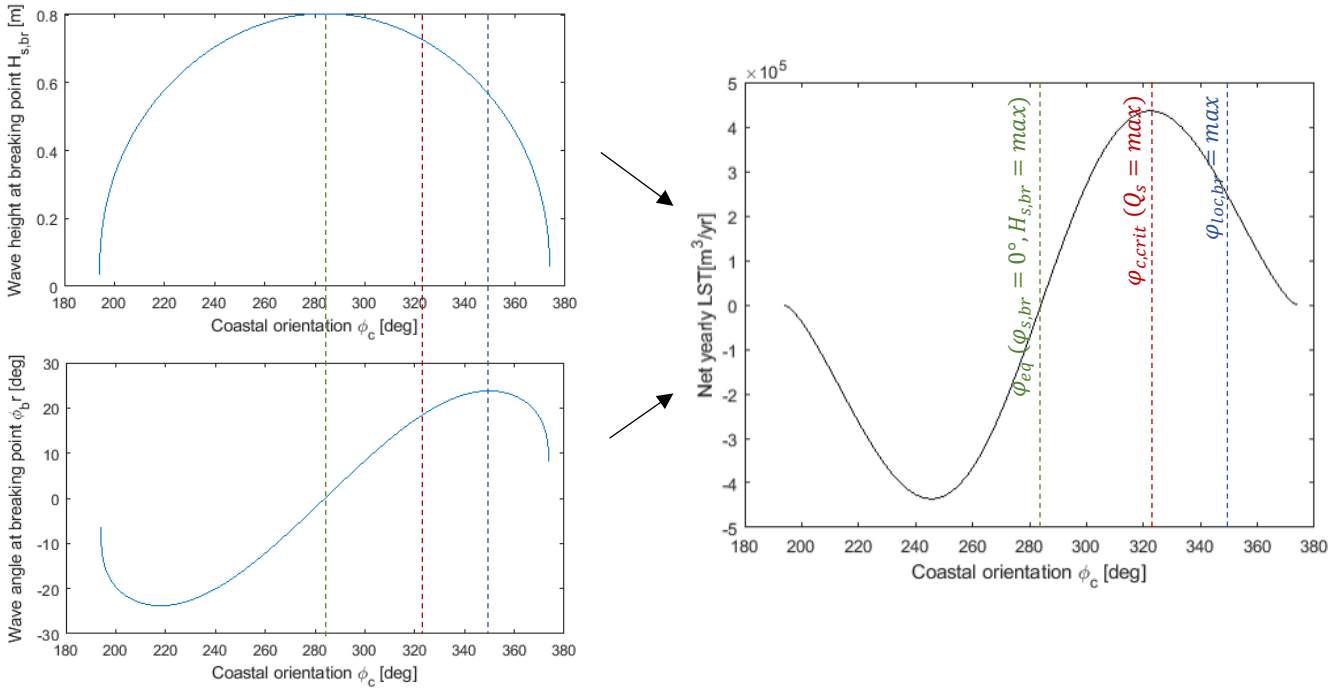

Figure 6-1 –Breakdown of non-linear terms leading in LST-formula to determine critical angle. Top left: breaking wave height ($H_{s,br}$) Bottom left: wave angle at breaking point ($\varphi_{s,br}$) Right: resulting S,φ-curve using. Vertical lines indicate the equilibrium orientation (green), critical orientation (red) and orientation for which the breaking angle is maximum (blue)

The equilibrium orientation (φ_{eq}) follows from Eq. 5.12, indicated with the green dashed line in Figure 6-1 ($\varphi_c = 284°$). For this orientation the wave is orientated shore normal in the nearshore (Figure 5-10), the wave height at breaking is therefore maximum compared to other coastline orientations since no wave energy is spread due to refraction. For coastline orientation which deviates from φ_{eq}, the wave height reduces as energy is spread due to wave refraction, resulting in a decrease in wave height (Eq. 5.5). The wave angle at breaking point ($\varphi_{w,br}$) is for orientations other than the equilibrium orientation implicitly depending on the breaking wave height (Section 5.1.2), the maximum breaking wave angle for this case is indicated by the blue dashed line ($\varphi_c = 350°$). The actual critical coastline orientation ($\varphi_{loc,crit}$, indicated by the red dashed line) results from the contribution of both non-linear terms through the (non-linear) LST-formula in the general form $Q_s \sim H_{s,br}^p \sin(2\,\varphi_{loc,br})$ (Section 2.2). The critical angle is for this case equal to $\varphi_{c,crit} = 322.4°$ or a relative angle with respect to the offshore wave angle ($\varphi_{w,0} = 246.7°$) of $\varphi_{loc,crit} = 75.7°$ which differs significantly from the fixed values for $\varphi_{loc,crit} \approx 45°$ (Table 6-1).

Since no explicit formulation exists to calculate the critical angle including effects of the dynamic boundary, a new routine has been implemented in ShorelineS to find/derive the critical angle. For this each timestep the following extra calculation routines are added to step 2 and 4 of the morphological loop of ShorelineS (Table 2-2): Each timestep a S,φ-curve, including nearshore wave transformation using the dynamic boundary, is generated for all $360°$ possible coastline orientations based on the wave condition of the considered time step. Using this S,φ-curve the critical orientations corresponding to the maximum and minimum LST are derived and translated back into a relative angle with the offshore wave angle $\varphi_{w,0}$. This angle is then used as critical angle in the upwind correction instead of the fixed (hardcoded) values.

An additional benefit of this procedure is that the coastal angles for which the wave is directed off coast (morphological loop (Table 2-2), step 9) can now also be determined easily using the S,φ-curve at which $Q_s = 0$.

Test case setup

To evaluate & show the effect of the dynamic boundary (Chapter 5) and the implementation of the variable critical angle three testcase were performed:

- **Case I: 'Traditional approach'**
  The first case can be considered as the traditional approach. For this the CERC1 formulation (Table 2-1) was used which uses offshore wave conditions without nearshore wave transformation (thus no effect of the dynamic boundary and thereby using a fixed value for φ_{crit} Table 6-1).
- **Case II: 'Dynamic boundary + fixed critical angle'**
  The second case uses the Van Rijn 2014 sediment formulation, which performed the best for the Lobito case. The Van Rijn 2014 LST-formula requires breaking wave parameters. For the wave transformation the dynamic boundary was activated, for the critical angle the fixed value was used (Table 6-1).
- **Case III: 'Dynamic boundary + variable critical angle'**
  The third case is similar to the second case (Van Rijn 2014 LST formulation, dynamic boundary activated) however for this case the critical angle is not fixed but variable computed using the new routine.

All tests were performed using the full (i.e., 42 wave conditions) 'offshore' weighted wave climate derived at the 56m depth contour (Table 5-3). The initial ($T = 0$) coastline is based on the Lobito coastline with the seaward extended sand delta (Section 3.2) but without the spit (Figure 6-2, white dashed line). A revetment (i.e., nonerodable coastline section) was applied along the upstream section of the coastline since this part of the coast consists of rock material (Figure 6-2, white/red dashed line).

Figure 6-2 – Initial coastline used for modelling cases ShorelineS (White dashed line). White/red dashed line indicates revetment

Dynamic boundary for Lobito

In the UNIBEST-CL+ model used by Deltares (2015), which was used to evaluate the LST performance, the dynamic boundary was set at an orientation of $\varphi_f = 325°$ at the 16m depth contour. For the model-to-model comparison, as performed in Chapter 5, those values were directly adopted in the ShorelineS model runs to make them as similar to each other as possible.

For the purpose of actually hindcasting the spit formation the model setup and the choice for the dynamic boundary was reconsidered. The orientation of the offshore depth contours (φ_f) used for the test cases was fixed at an orientation of $305°$ which is consistent with the local orientation of the depth contours at the location of the offshore wave climate at the 56m depth contour (Figure 6-3). The depth of the 'dynamic boundary', which defines the border between active part (inside longshore transport zone, depth contours coastline parallel) and the static part (outside longshore transport zone, depth contours related to offshore orientation) is set at the 4m depth contour. At this depth the depth contours are fully rotated to the spits orientation, as well a significant change in the average cross-shore bed slope can be observed (e.g., transects 1-5 Figure 6-3 and Table 6-2). From a depth of approximately of 4m and on the cross-shore profile changes to a slope up to 1:4 which is very steep for a sandy profile. Such steep cross shore profiles are typically formed by cross shore processes (e.g., avalanching of sediment from the dynamic part) instead of longshore sediment. transport.

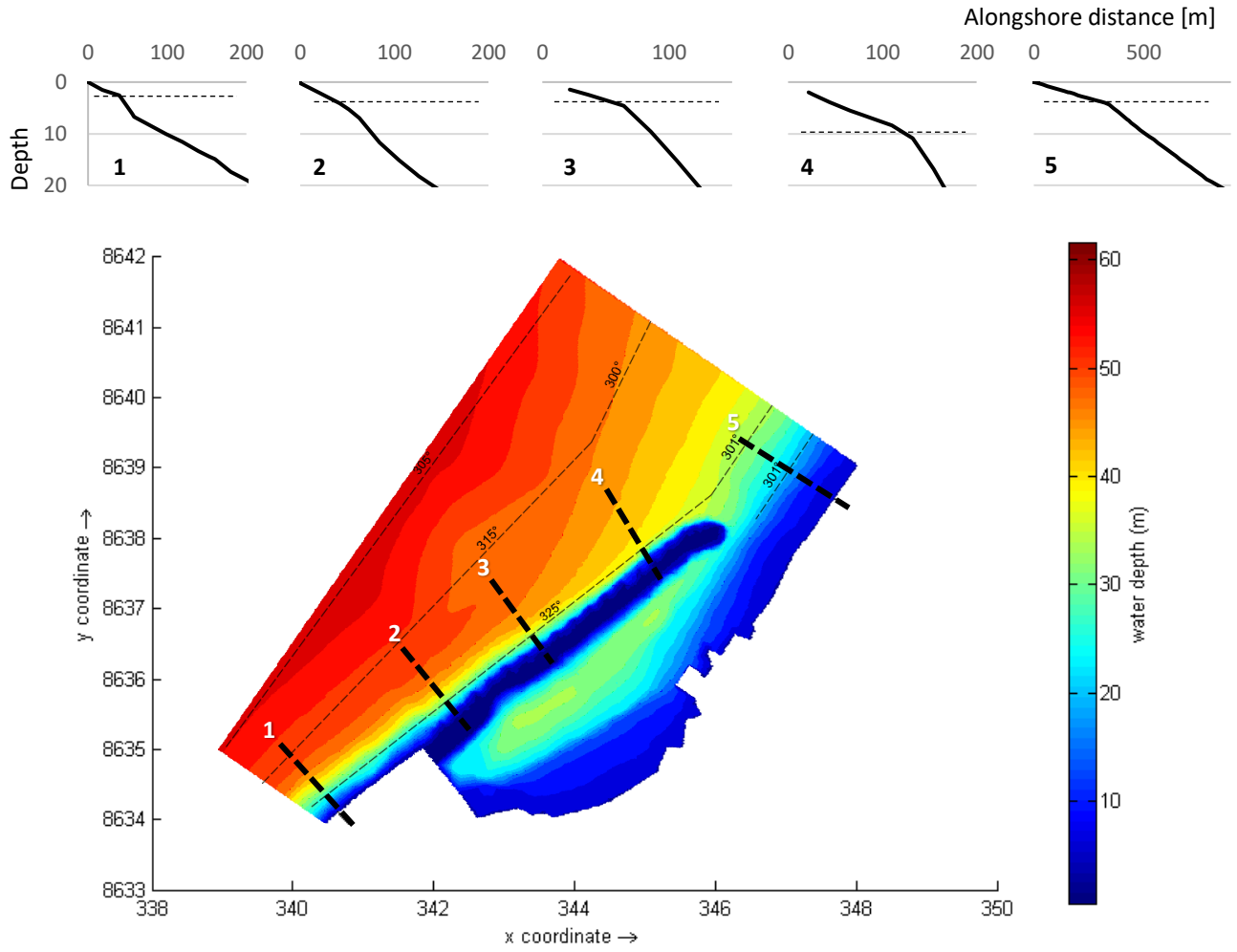

Figure 6-3 – Bathymetry of Lobito with cross shore profile for 5 locations (transects) along the coastline/spit

Transect	**1**	**2**	**3**	**4**	**5**
Nearshore slope	1:25	1:12	1:15	1:17	1:80
h_{change} **[m]**	3	5	4	10	4
Offshore slope	1:10	1:5	1:4	1:4	1:32

Table 6-2 – Nearshore and offshore slope characteristics and depth of change in slope for 5 transects

6.1.2 Results

For all three cases the model run for 15 years of simulation, in this section the resulting coastlines per case at the end ($T = 15$ year) and halfway through ($T = 7$ years) the simulation are presented an further analysed.

Case I

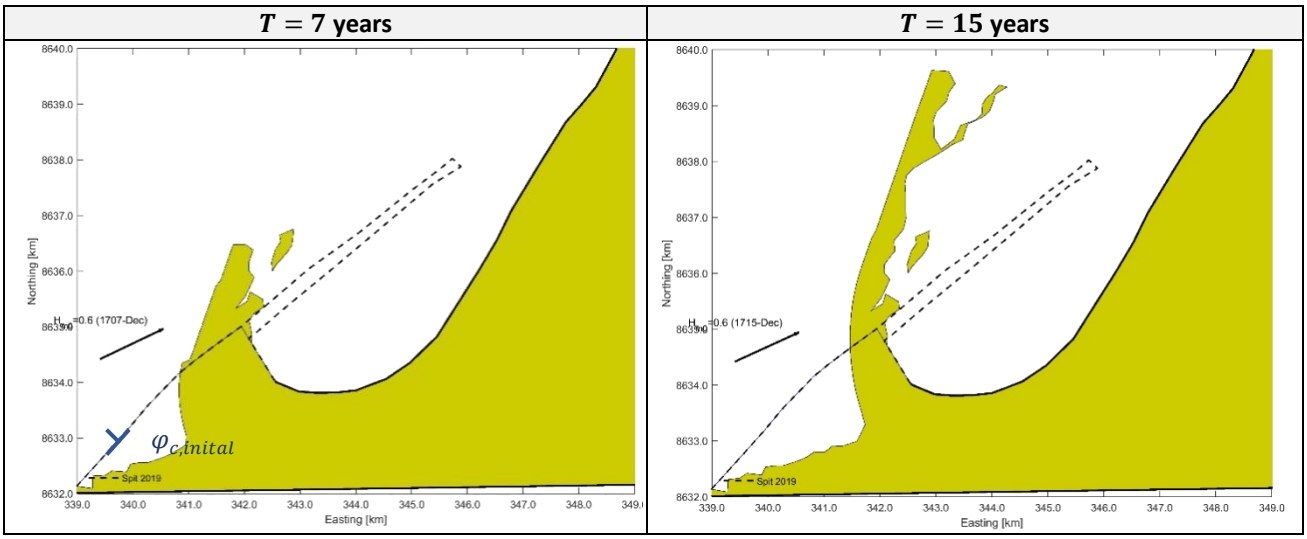

Table 6-3 – Resulting coastline changes at T=7yr and T=15yr for case I.

At the end of the first case simulation a spit has formed with an orientation of $\varphi_c \approx 287°$, which largely deviate from the observed spit at Lobito (indicated with the black dashed line Table 6-3). With respect to the average incoming offshore wave angel ($\varphi_w \approx 244°$) this results in a relative angle of $\varphi_{w,loc} \approx 43°$ which is close to the fixed critical angle of $\varphi_{crit,loc} = 45°$ as used in the upwind correction (Table 6-1).

In addition to the spit formation, a large coastline erosion can be observed updrift from the spit. The wave climate averaged S, φ-curve for this case (Figure 6-4) provides better insight into the observed coastline change and spit formation. In the S, φ-curve both the critical angle (φ_{crit} , red dashed) and the initial orientation ($\varphi_{c,initial} = 312°$, blue dashed) of the coastline are indicated. The initial coastline orientation is based on the sandy coastline section updrift from the spit (indicated in Table 6-3). It should be noticed that the initial coastline orientation is, according to the S, φ-curve for this case, unstable (i.e., $\varphi_c > \varphi_{crit}$). As result the sediment transport (Q_s) significantly increases between the initial orientation and the orientation of the spit, resulting in the updrift erosion which has not been observed in reality.

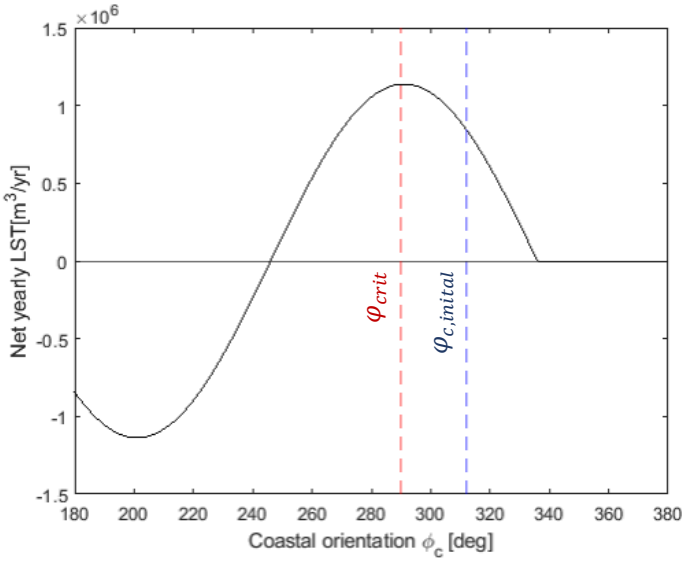

Figure 6-4 – Wave climate averaged S, φ-curve for case I. Orientation of initial coastline ($\varphi_{c,initial}$) and critical orientation as used by ShorelineS (φ_{crit}) are indicated.

Case II

$T = 7$ years	$T = 15$ years
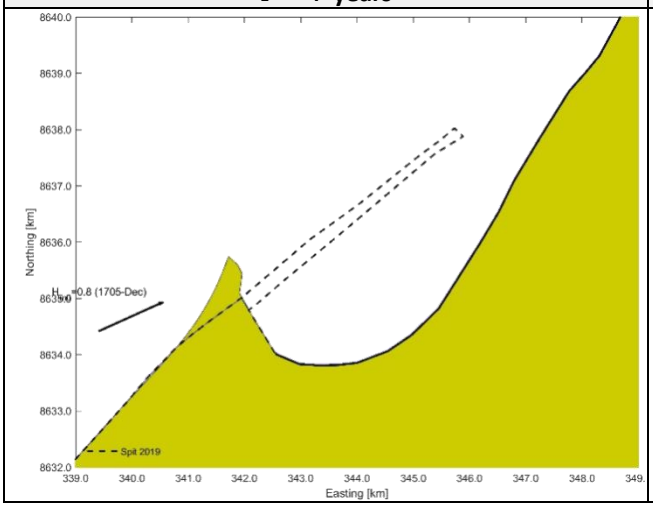	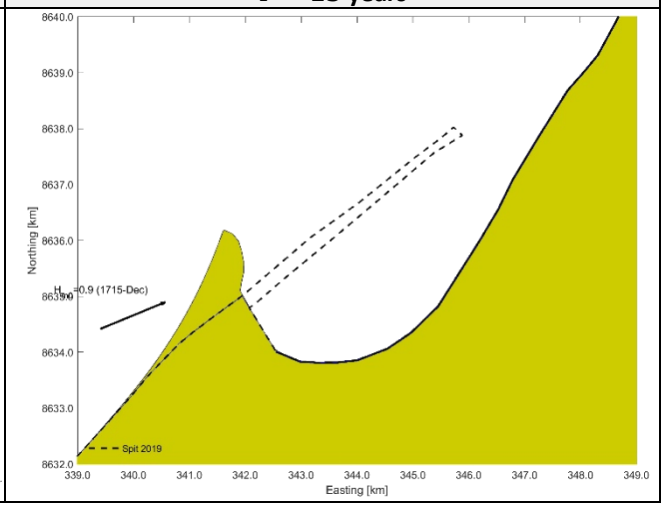

Table 6-4 - Resulting coastline changes at T=7yr and T=15yr for case II.

For the second case the sandy coastline section upstream from the spit for this case remains at a stable orientation compared to the first case, the large erosion over this part is not present in this model run. A spit forms with an orientation similar to the orientation of case I, which is still more seaward orientated compared to the actual observed spit of Lobito (Table 6-4).

The S, φ-curve for this case (Figure 6-5) has shifted with respect to the S, φ-curve of the first case due to the inclusion of the dynamic boundary and wave transformation towards the coast (described in Chapter 5). As result of this shift the initial coastline orientation corresponds now with the a 'stable' orientation close to the orientation for which $Q_s = max$. However, for this simulation the critical angle in ShorelineS uses the fixed value for Van Rijn 2014 LST-formula $\varphi_{loc,crit} = 39.9°$ ($\varphi_{crit} \approx 290°$). From the S, φ-curve it can be observed that this angle does not correspond correctly with the angle for which $Q_s = max$, the fixed angle for φ_{crit} for this case is actually located close to the equilibrium orientation for which $Q_s = 0$. The spit's orientation will be 'forced' by the model to develop with a fixed orientation of $\varphi_{c,spit} \approx 290°$ by the upwind correction.

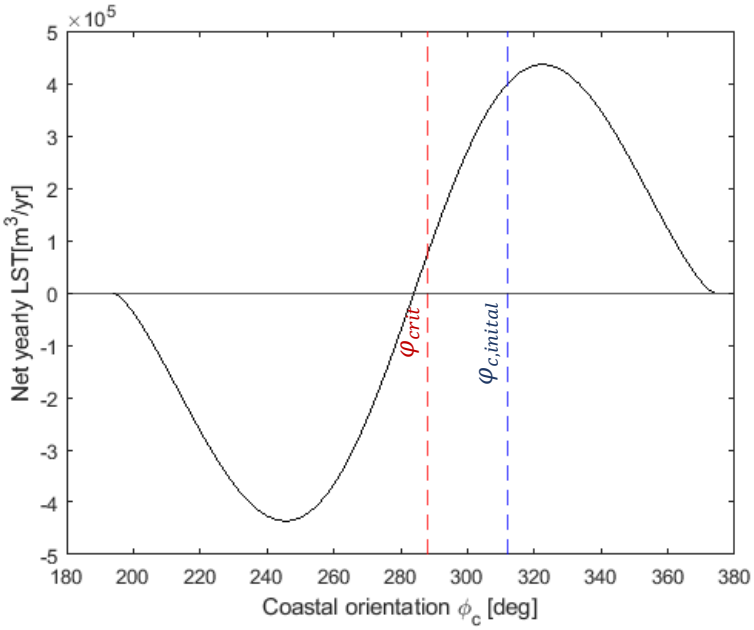

Figure 6-5 - Wave climate averaged S, φ-curve for case II. Orientation of initial coastline ($\varphi_{c,initial}$) and critical orientation as used by ShorelineS (φ_{crit}) are indicated. φ_{crit} mismatches the actual peak of the S, φ-curve for this case.

As the spit develops the entire front side of the spit is located in the stable part of the S, φ-curve. This implies that, in contrast to case I, there is now a significant decrease in LST resulting in sedimentation. This means that the spit will not extend as a straight landform but act more as a sandy groyne where at the front side sediment builds up. This can also be observed in the coastline development of simulation of case 2: coastline gradually fills up the front side of the spit.

The difference in length of the resulting spit for Case I and II at $T = 15yr$ can be related to the fact that: 1) the LST-magnitude as enforced by the upwind correction is derived from a coastal orientation near φ_{eq} thus not corresponds the maximum magnitude (as stated before) and 2) the overall magnitude of the S, φ-curve is significantly smaller due to the used LST-formula. It was shown (Section 5.2.2, Table 5-6) that for the CERC1 formula, as use for Case I, the overprediction of the overall magnitude was the largest.

Case III

$T = 7$ years	$T = 15$ years
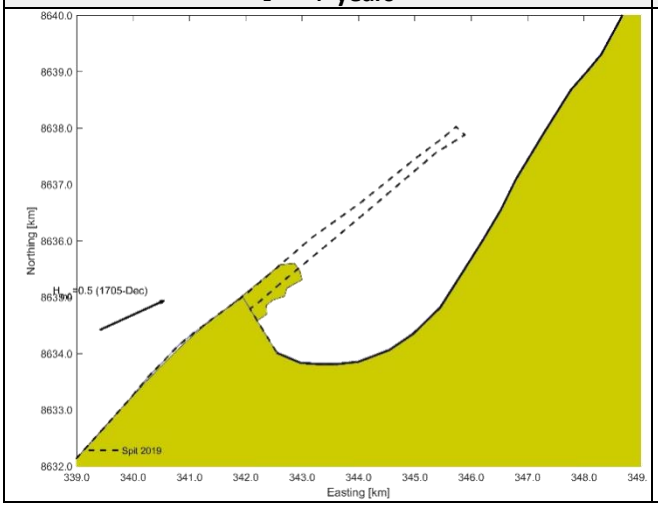	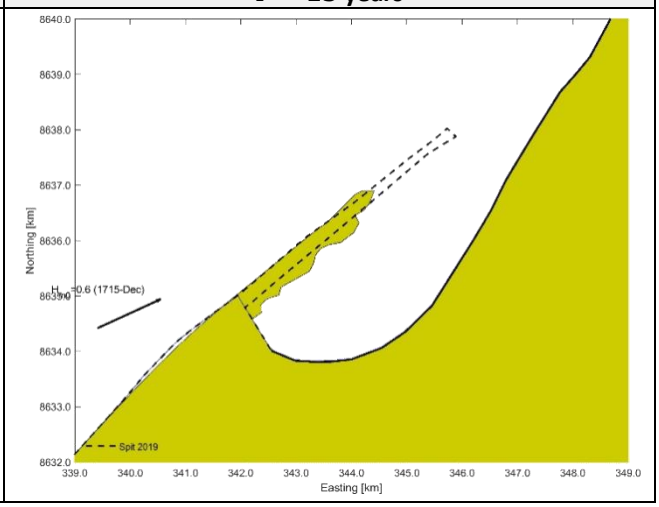

Table 6-5 - Resulting coastline changes at T=7yr and T=15yr for case III.

For the third case, which uses the dynamic boundary and a variable value of the critical angle, the resulting spit direction significantly adjusted into an orientation which is in good agreement with the observed spit orientation (Table 6-5).

The S, φ-curve for this case (Figure 6-6) is identical to the one of case II, however for this simulation the critical angle is determined using the new procedure (Section 6.1.1) and thus corresponds with the orientation for $Q_s = max$. The initial orientation is for this case is now close to the critical angle, in contrast to case I and II no severe erosion or sedimentation on the updrift side of the spit is present in this model run, which is in better agreement with the stable coastline as observed in reality. The latter is an indicator that the LST quantities are well represented.

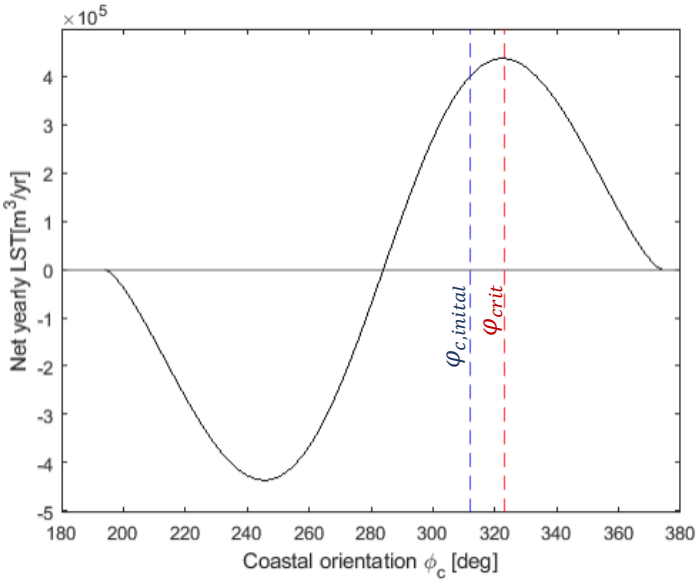

Figure 6-6 - Wave climate averaged S, φ-curve for case III. Orientation of initial coastline ($\varphi_{c,initial}$) and critical orientation as used by ShorelineS (φ_{crit}) are indicated.

6.2 Spit width and shape

It was found (Chapter 4) that the distribution and decay of the longshore sediment transport over the head of the spit is closely related to the width and shape of the spit formation.

In ShorelineS the upwind correction-routine was implemented to ensure the smooth development of spit formation and control the spit migration as discussed in the previous section. Besides controlling the spit migration direction, this routine also directly influences the width of the spit formation. The basic routine functions as follows (Figure 6-7) when over a part of the coastline the local angle with respect to the incoming wave direction exceeds the critical defined angle, the transport is set at the maximum transport. This controls the spit migration direction as discussed in Section 6.1. The sediment transport over the next two grid cells is manually controlled decreasing from $Q_{S,max}$ to $Q_s = 0$.

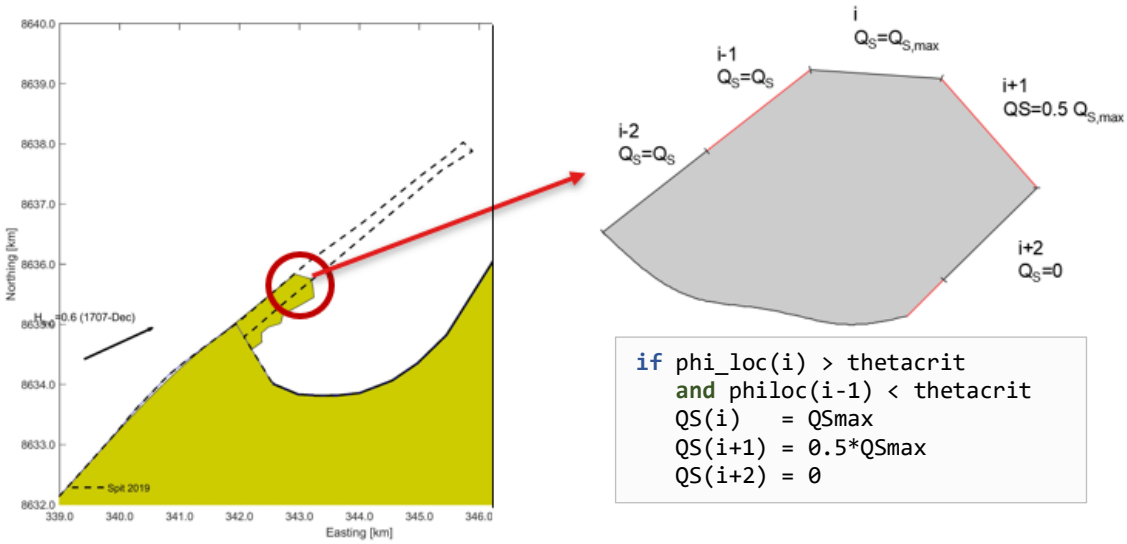

Figure 6-7 – Visual representation of current upwind correction routine

Without this routine the sediment will build up at the cell just before where the 'curvature' of the head begins `(i-1)`. The manually forced sediment transport quantities in the adjacent cells `(i+1)` and `(i+2)` is necessary since 1) the current wave shielding routine (Section 2.4) would prevent transport in those cells, as based on simple wave shielding the landmass of the spit itself in combination with the high angle wave would shadow the adjacent cells and 2) all wave transformation is based on the assumption of quasi-uniform wave refraction(Section 5.2.1) , which is not the case around the head of the spit where the curvature is large.

An implication of this current routine is that the width of the formed spit is directly depending on the user defined grid cell resolution, as the grid resolution gets (de)refined the resulting width of the spit changes accordingly (e.g., see model run results for the identical Lobito model run but with changing grid resolution, Figure 6-8). The used disbrubition in the original model has therby no phisical meaning.

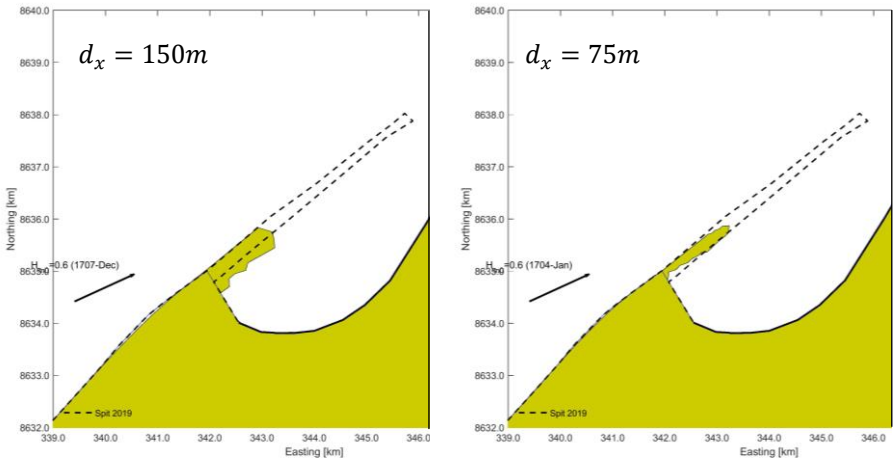

Figure 6-8 – Influence on grid resolution in ShorelineS on spit formation

6.2.1 Improved upwind correction

The influence on physical processes by non-physical model (schematization) parameters in computational models, in this case the grid resolution dependency for the spit width, is something which is generally unwanted as they influence the outcome of a model. Users who are unaware of those (hidden) dependencies of a certain model might draw physical unjustified conclusions based on the model results.

Due to the current limitation of the (simplified) wave transformation as implemented in ShorelineS, the model itself is currently not capable of determining the local wave field along the curved head of the spit (e.g., Figure 4-11 from the XBeach analysis) and resulting sediment distribution along the head of the spit. Therefore, an improved version of the upwind correction was suggested and implemented based on the concept of the current upwind correction and the gained knowledge on the transport distribution along the head of a spit from the more advanced XBeach-model study.

The routine of this proof-of-concept as implemented in ShorelineS works as follows (Figure 6-9):

1. **The user provides the expected spit width as input parameter**
   This can be based on historical and/or existing spit data around the project location, model results from more advance models (e.g., using the analyses for different hypothetical spit formation using the same framework as discussed in Section 4.3.1 using XBeach model runs)
2. **The upwind correction check for exceedance of the critical angle**
   Similar to the current workaround the upwind correction checks whether for a certain part of the coast the critical angle is exceeded. If so, the upwind correction routine is activated, which overrule the sediment transport over the next cell(s).
3. **Based on the user specified spit width the alongshore distance is determined**
   In ShorelineS the 'grid' is defined as an alongshore polyline with grid points (Section 2.4) therefore, the alongshore transport must also be defined along this alongshore grid. The users specified spit width is transformed into an alongshore distance based on a hypothetical shape of the head of the spit. For this proof-of-concept a symmetrical circular shape was used ($dist = (2W_{spit})/\pi$). Other hypothetical shapes such as the asymmetrical half elongated (elliptical) shape with ratio r, as used in in Section 4.2.2, can easily be implemented (e.g., $dist = 0.5\pi\sqrt{((rW_{spit})^2 + W_{spit}^2)/2}$).
4. **Linear decay over the spit at each cell center is determined and feed back to the model**
   The transport over alongshore distance is based on the linear decay (assuming equilibrium shape/width of the head of the spit). Although the cell resolution input parameter is a fixed parameter, ShorelineS allows for stretching (or shrinking) up to two times the given resolution of each cell before it gets split (or merged) with the adjacent cells. To prevent instabilities the actual cell width of each cell gets extracted each timestep and used to determine the linear interpolated transport at the center of each individual cell.

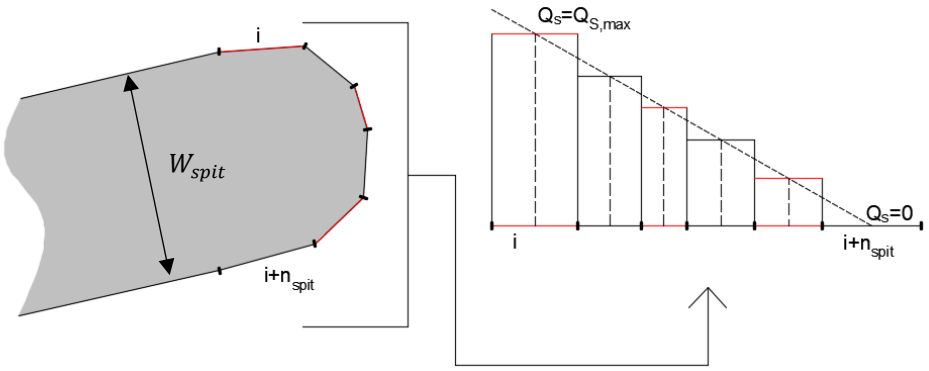

Figure 6-9 – Updated upwind correction based on W_{spit}

After this the model calculation proceeds as usual (see morphological loop, Table 2-2). As the transport decays linearly over the spit, the head of the spit migrates uniformly (Eq. 2.11).

The effect of this updated routine is shown using a series of test runs using ShorelineS with this new updated upwind correction routine versus the old routine (Table 6-6). In those series the upwind correction is triggered by the initial change in the coastline in combination with a high incident angle wave, similarly as the extended delta shape as observed in

Lobito. The grid resolution was changed over the test runs from $d_x = 150$ to $d_x = 200$ and eventually $d_x = 300$. For the runs with the updated upwind correction the input parameter of the width was set at $W_{spit} = 600m$.

From the spits formed in the runs which uses the current routine the grid cell-dependency can be clearly be observed. For those runs the resulting width of the spit variates from $400m$ ($d_x = 150m$) up to $900m$ ($d_x = 300m$). Those model runs also show a second implication of the current routine; as the migration rate (v) is proportional to the width, depth and transport at the tip ($v \propto Q_s / (W_{spit} \cdot d)$) the length of the resulting spit is also indirectly depending on the grid size. The resulting width and length of the spit resulting from the updated routine are more consistent.

	$d_x = 150m$	$d_x = 200m$	$d_x = 300m$
Current routine	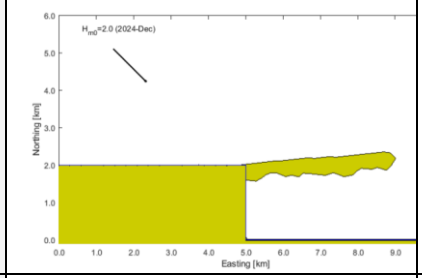	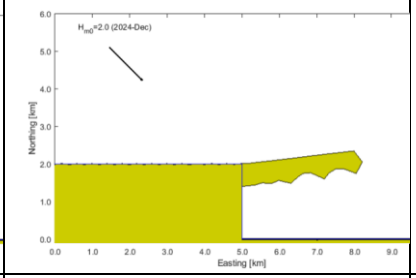	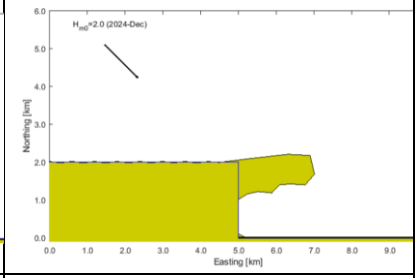
Updated routine	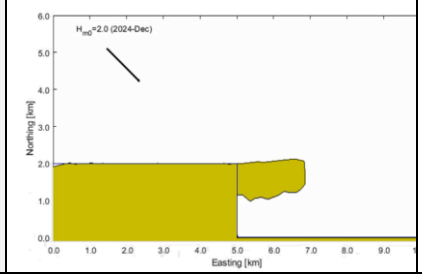	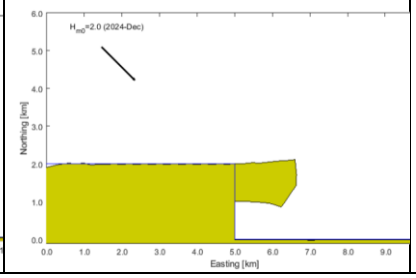	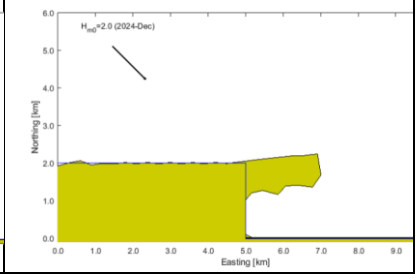

Table 6-6 -Results of series of test runs with current and updated upwind routine for different grid resolutions ($d_x = 150, 200, 300m$)

6.3 Discussion and conclusions

Prior to the conclusions (Section 6.3.2) some points of discussions are addressed regarding 1) the determination of the dynamic boundary, 2) the limitations of the updated upwind correction and 3) the modelling of spit processes and types in ShorelineS.

6.3.1 Discussion

Determination of dynamic boundary

The concept of a dynamic boundary has been implemented in ShorelineS to better schematize the bathymetry in the coastline model. Without the dynamic boundary it was assumed that all depth contours are parallel to the coastline, also for reoriented coastlines. Whereas in reality coastal changes will not influence (reorient) the depth contours over all depth. This thereby influences the wave refraction, it was shown that this schematization of the bathymetry was important for both the (consistent) calculation of the longshore sediment transport (Chapter 5) and the determination of the critical angle used to describe the orientation of spit formation (this chapter).

Although the concept of the dynamic boundary and required modelling parameters are in essence non-physical model schematization parameters, they can be related to physical processes. The determination of parameters used for the dynamic boundary in the model can be approached in two ways

1. **From a visual perspective**
   Using information of the local bathymetry. If within or close to the area of interest already a perturbation along the (original) coastline is present, the effect of this feature can be used to get insight into the zone and depth over which the depth contours are affected. This approach was for example used by Tonnon et al. (2018) to define the dynamic boundary for the Sand engine as used as validation case (Section 5.3).

2. From a physical perspective

The depth of closure (DoC) is commonly used concept in coastal engineering which is, according to the definition of Kraus et al. (1198): the depth/boundary of which seawards no significant net sediment exchange exists between the nearshore and offshore and therefore no significant change in the bottom elevation is expected. Empirical formulations, such as the Hallermeier (1981) or Birkemeier (1985) -equation, can be used to calculate the DoC. Such formulations are based on the breaker zone as wave induced sediment transport is limited to the area near the coast. As there is no sediment exchange and bed level change (thus change in depth contours) seaward from the DoC, this distinction between the active (dynamic) and static zone, is similar to the definition to the dynamic boundary.

There is no generic method to determine the 'correct' parameters of the dynamic boundary. Besides, the dynamic boundary is schematized as a single point (depth) resulting in an abrupt change in the offshore and nearshore orientation of the depth contours. In reality the change in the orientation of the depth contours is more gradual and takes place over an intermediate area (Figure 6-10). However, the implementation of the dynamic boundary has led to a better schematization of the actual bathymetry and thereby improving the wave transformation in a computational efficient matter as shown for the Lobito case study (this chapter) and the sand engine validation case (Section 5.3).

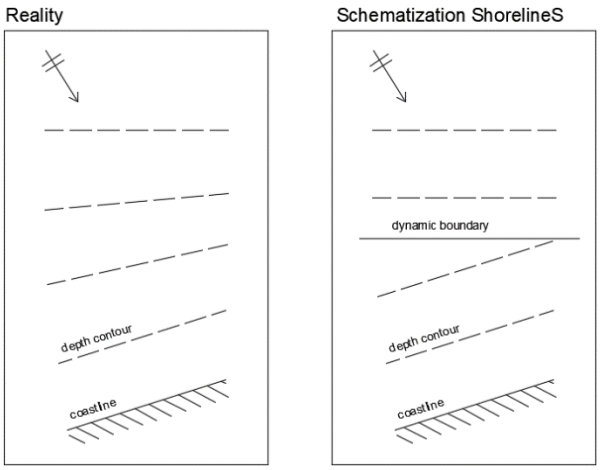

Figure 6-10 - Left: Real gradual reorientation of depth contours Right: schematization in ShorelineS

Figure 6-11 gives insight into the sensitivity of the critical angle with respect to the offshore wave angle (φ_{crit}) for variations in the parameters describing the of the dynamic boundary: the x-axis shows the difference between the incoming wave (φ_w) and the offshore fixed depth contours (φ_f): $\Delta\varphi_f = \varphi_f - \varphi_w$. The plotted lines are related to variations of the depth from which on it is presumed that the depth contours are parallel to the coastline resulting in a shift of the theoretical (fixed) value for the critical angle (y-axis, φ_{crit}). The graph is based on the Lobito case parameters (singe representative wave (Table 5-3) $H_s = 0.68m$, $\varphi_w = 246.7°$, $T_p = 9.456s$) for which the Van Rijn 2014 transport formula was used with a theoretical/fixed critical angle of $\varphi_{crit} = 39.9°$ (Table 6-1).

When no dynamic boundary is applied ($d_{db} = 56m$, i.e., equal to depth at which the wave climate is imposed) the model responds as a classical coastline model where all depth contours are assumed to be coastline parallel. The value for the critical angle is in this case independent of the orientation of the offshore depth contour and therefore equal to the theoretical value of $\varphi_{crit} = 39.9°$ for all values of $\Delta\varphi_f$. When waves approach the coast at a low angle ($\Delta\varphi_f$ close to 0°) refraction on fixed depth contours up to $d = d_{db}$ is limited and thereby the shift in φ_{crit} as well. In fact, in the theoretical case of perfectly depth-contour normal incoming waves ($\Delta\varphi_f = 0$) there will be no refraction of the wave on the fixed depth contours, the φ_{crit} is therefore equal to the theoretical value of $39.9°$ independent of d_{db}.

For high angle waves, which approach with larger $\Delta\varphi_f$ values, the shift and non-linearity increases and becomes more significant. The latter emphasizes the importance of the shift for especially high angle waves compared to low angle waves as discussed before, but more importantly, supports the conclusion that the phase shift can lead to significant changes in the S, φ-curve which influences the spit direction.

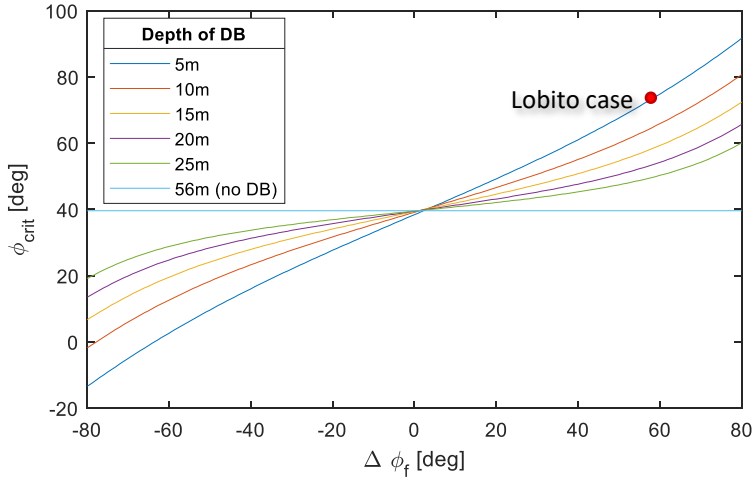

Figure 6-11 – Difference in critical angle depending on depth of dynamic boundary for Lobito case

This result might imply that traditional coastline models (such as GENESIS or LONGMOR) which assume coastline parallel depth contours result in an incorrect representation of the LST (S, φ-curve) and thereby coastal evolution. For low angle wave (diffusive) environments, however, the coastal orientations are located in the 'linear' part of the S, φ-curve close to the equilibrium coastal orientation ($\varphi_{c,eq}$). A shift in the S, φ-curve, as a result of the reorientation of the nearshore bed contours, will not affect the gradient in LST (ΔQ_s) in this part which drives the coastal change in one-line models. It might influence the overall quantity of the LST, however this is usually considered a calibration parameter and is therefore generally manually adjusted to match up with field data for a certain orientation.

It should be noticed that the conclusions regarding the spit direction presented as result of this chapter are based on the interaction of the wave transformation over a schematized representation of the bathymetry in relation with the critical angle. Which is observed to be the driving mechanism for the spit formation in Lobito and spits in general. Other mechanisms (Section 2.1) such as a (strong) tidal flow, geological features (non-uniform bathymetry) can in the current release of ShorelineS not be modelled but might influence the spit formation (direction) for certain model scenarios.

Limitations updated upwind correction in ShorelineS

The new updated routine should be considered as a proof-of-concept and a first important step into the development a more robust implementation of the upwind correction and better representation of physical processed in general in the ShorelineS model. It has resulted in in a more consistent width (and thereby length) of the formed spit, however should be noted that limitations exist. The first, and main, limitation of this proof of concept is the fact that the width and the resulting decay in the transport distribution are still enforced in the model routine. An implication of this method is that there is currently no feedback mechanism between the model/wave environment, the spit/coastal geometry and the resulting transport distribution. The effect of this could be observed in the performed model tests with this updated upwind correction (Table 6-6):

The width the resulting spits in ShorelineS ($W_{spit} \approx 950m$) for the test cases with the updated routine does not match the prescribed spit width as used as input parameter for those runs ($W_{spit} = 600m$). This is due to the fact that the model assumes a half circular shape to estimate the alongshore distance ($dist = (2W_{spit})/\pi = 942m$). As the initial coastline is a straight line and the transport is applied linearly decreasing, this would result in a uniform migration of this initial shape; the circular shape will not arise.

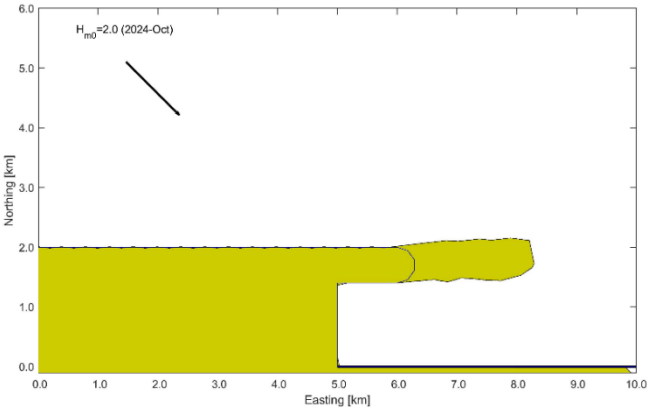

Figure 6-12 – Model run with brute forced initial spit shape and width

It is theoretically possible to 'brute force' a shape to the spit and force a spit with a width and shape which corresponds to the predefined parameters (Figure 6-12), however this requires the initial coastline to match the grid, shape and width of the expected spit, which is not a workable solution for real life modelling studies. Besides; the circular shape as assumed and forced in this model does not match the equilibrium shape for which the geometry agrees with the natural forcing (in this case a single wave condition from one high angle wave direction). Even if the

It can be questioned if for the purpose of this coastline model (namely the assessment of the long-term coastal evolution) the ability of the correct modelling of the 'local' shape of the spits head is of relevance. Using this newly proof-of-concept the average width and thereby overall long-term formation is better reproduced. However, the further research into a better predictor of the spit width depending on the local environmental conditions, and thereby introducing a first step for a feedback mechanism, is still of relevance. Especially for model scenarios with a variable wave climate (next point of discussion).

Modelling spit processes and types in ShorelineS

In this chapter the Lobito spit case study was used as a reference case to assess the performance of modelling spit formation in ShorelineS. This spit was classified as a type-A spit in the conceptual model (Section 4.1), from the detailed modelling study in XBeach (Section 4.2) it was found that the Lobito spit formation is mainly formed under the influence of the uni-directed wave climate. In the modelling study and literature study (Section 2.1.3) other mechanisms were

mentioned. Here the different mechanisms related to spit formation are recapped, it is discussed how (and if) those different processes have been addressed in this chapter and how they are currently represented in ShorelineS.

1) **Wave climate variabilities**
   It was shown that two effects due to the variability in wave climate can be distinguished: 1) the variability in the high angle wave portion of the wave climate resulting in the average spit direction and 2) the effects of the wave climate resulting in the redistribution/reshaping of the head of the spit (Figure 4-15).
   The first effect is well captured in ShorelineS as the critical angle, which results in the migration direction, is variable for each wave condition. The resulting (average) spit orientation is therefore the result of the combination and duration of the different high angle wave components. The second effect is partly captured in ShorelineS; i.e., waves from an opposite direction will expose the head of the spit resulting in a redistribution (split in sediment direction) over the head in ShorelineS, similarly as found in XBeach (Section 4.2.4), however the decay to the $Q_s = 0$ point over the head of the spit is depending on the refraction over the head, which can be less good modelled in ShorelineS (See next point).
2) **Wave refraction**
   The local wave refraction at the head of a spit is, as stated before, not well represented in ShorelineS. This has been solved by the introduction of the 'spit-width' parameter. This parameter forces the transport decay, it therefore implicitly accounts for the local wave refraction over the head. However, this is a static parameter and there is in this proof-of-concept no feedback mechanism with the actual imposed wave condition (discussed in previous point of discussion). The spit width is based on the average expected spit width, an implication of this method is, is that the 'refraction' or the width due to the for the secondary wave component (previous point) is the same as for the primary wave component. Variations in this 'spit width' parameter for different wave conditions might be required in the upwind routine to represent the decay of sediment transport for different (e.g., opposite) wave conditions.
3) **Flow/sediment inertia**
   In the derivation from the hydrodynamics to the sediment distribution along the spit no significant 'lag' was observed between the alongshore current- and transport distribution (i.e., there was no noticeable sediment transport past the point where the flow velocity was reduced significantly). The potential transport capacity of the sediment settling lag around the head of the spit was therefore not further considered for the Lobito spit case.
   It should be noted that this effect is not included in the LST-bulk formulae, as used in ShorelineS, which determine the instantaneous transport capacity based on the local wave conditions only. For cases where this effect is of relevance it could be implicitly included in the 'spit-width'-parameters used to describe the transport distribution over the head of the spit.
4) **Overwash / Aeolian transport**
   The effects of overwash and aeolian transport are generally considered longer term/extreme processes (re)shaping the neck of a spit (i.e., landward migration or breaching). The combined effect of overwash and aeolian transport on spit migration is included in ShorelineS by the formulation by Leatherman (1979) (Section 2.4.1). This is a simplified schematization which results basically in a threshold for the minimum spit/neck width and thereby resulting overall landward migration of the neck of a spit. More complex features, such as overwash fans at the backside of a neck due to breaching events, or actual aeolian transport over the spit can, currently, not be modelled in ShorelineS.
5) **Tidal Current**
   The effect of the tidal current on the sediment transport for the Lobito case was considered neglectable (Figure 6-18) and was not further analysed in this chapter.
   The driver for sediment transport in ShorelineS is the wave induced, effects on transport due to tide induced currents are currently not included in the model. In the van Rijn (2014) bulk-formula (Eq. 2.8) the V_{total}-term can used to represent the net effect due to asymmetry of tide (or wind) induced alongshore currents, however only as factor over the wave indicated transport, thus no transport for areas where no waves are present (i.e., the semi enclosed basin behind a spit). Besides, this requires the input or calculation of the spatial and temporal changing alongshore tidal current based on the coastal geometry and tidal characteristics (e.g., Figure 4-17) which is currently not possible with the model.

For the different defined spit types in the conceptual model (Section 4.1), different processes are of relevance leading to the final characteristic shape of the spit. As stated earlier: the Lobito spit is considered a Type A spit, which is mainly controlled by the uni-directed wave climate. It was shown by the hindcasting of this case study and the improvement of the upwind correction that for this spit-type the ShorelineS model works well.

For the type B spit the (reshaping) effects due to secondary wave condition(s) is of relevance, which might require further development of the upwind routine to account for the variability of the, now statically defined 'spit-width'-parameter for changing wave conditions. The potential smoothing of the coastline due to the tide, relevant for this spit type, might also

be implemented to be able to recreate the typical smooth spit formations. The latter is, however, considered quite complex as it requires actual interaction of the tide with the local coastal geometry, a first step can be to implement/apply a tide-derived smoothing (diffusion) on the coastline to schematically simulate the smoothing effect of the tide. The latter requires further research.

For the type C spit the effects due to and modelling of the secondary wave conditions are also of relevance (as described above). This type of spit is characterised by the presence of the 'shoots' and a lack of the tide, thus no smoothing. The shoots can be both the result of a (seasonal) variability in the wave climate (which can be modelled in ShorelineS) or extreme overwash / breaching events. The latter, modelling of the actual overwash fans, is currently not possible in ShorelineS. As with the simplified overwash formulation (Leatherman, 1979) the basic effects of overwash are included, it raises the question whether the actual modelling of those smaller scale, more complex, features using a coastline model is of relevance to assess the overall formation and migration of this spit type for which this type of model is generally used.

6.3.2 Conclusions

In this chapter the modelling of the spit migration direction and spit width/shape in ShorelineS were investigated. The direction in which a spit develops in the ShorelineS model is controlled by the upwind correction using the critical angle for which the LST maximises. In the current version of ShorelineS the critical angle was set to an fixed value based on the studies by Ashton et al. (2006b) and Elghandour (2018). The derivation of the critical angle was based on the assumption of shoreline parallel depth contours. In Chapter 5 the performance of ShorelineS on predicting LST was investigated. It was shown that the LST, and in particular the phase of the S,φ-curve, is influenced by the bathymetry. For reoriented coastlines, which is often the case for spits, the assumption of coast parallel depth contours might not be valid as coastal changes with respect to the original coastline do not influence the deeper located depth contours, this principle was implemented in ShorelineS with the concept of the dynamic boundary. Continuing on those results it can also be concluded that as result of the phase shift the critical angle is not be a fixed value, but is variable influenced by the wave condition, the nearshore wave transformation and bathymetry (i.e., taking into account the reorientation of the nearshore depth contours by means of the dynamic boundary). The variability of the critical angle was implemented in ShorelineS with a new routine which determines the critical angle for each timestep by finding the $Q_s = max$ in the local S,φ-cure for each timestep.

Three test cases were performed to assess the effect of the dynamic boundary (Chapter 5) and variable critical angle (this chapter) on the spit formation for the Lobito case study. Only the case in which both the dynamic boundary and variable critical angle were applied (case III) resulted in a spit formation for which the direction was in agreement with the observed spit formation at Lobito. The other cases both resulted in spit formation which deviated (i.e., oriented more seaward up to 37°) from the actual observed spit. In addition, severe erosion (case I) or sedimentation (case II) of the updrift, in reality stable, coastline was observed in those model runs. This also indicates that the model performance was not correct for those cases. From this it can be concluded that both the dynamic boundary and variable critical angle are required in the model in order to correctly represent the wave transformation and transport curve to correctly predict and simulate the spit formation (orientation).

The inclusion of the dynamic boundary resulting in the phase shift of the S,φ-curve and the change in critical angle is especially of importance when modelling (unstable) spit development due to high incident angle waves. For this situation the coastal orientations with respect to the incoming waves are located near the non-linear part of the S,φ-curve (i.e., the top of the curve where $Q_s = max$). In contrast to orientations on the linear part of the S,φ-curve, a phase shift of the S,φ-curve for orientations located in the non-linear part can have a large influence on the overall behaviour of the coastal system: transport gradients (ΔQ_s) can increase or decrease, the critical angle changes and coastal sections can change from the stable to the unstable part of the transport curve and vice. This effect was also observed in case I and II of the performed test cases.

Regarding the modelling of the spit width/shape in ShorelineS it was found that in the current release of ShorelineS the width of the spit is controlled by the upwind correction, this routine activates when the critical angle gets exceeded. A drawback of the current implementation of this routine is that the width, and thereby migration rate, of the spit is directly depending on the grid size resolution. An improved version of the upwind correction has been suggested and implemented as a proof-of-concept which linearly decreases the transport over the head of the spit once the critical angle is exceeded based on a predefined spit width input parameter. The spit width can be based on historical and/or existing spit data around the project location or model results from more advance models, for the latter the modelling of the of the spit of Lobito using XBeach can be used as framework (Section 4.3.1) for certain analysis.

7 Conclusions and recommendations

7.1 Key findings

For this thesis the following main research question was formulated (Section 1.2):

What are the capabilities of the ShorelineS coastline model, applied on the Lobito Spit case to accurately model/predict the longshore sediment transport and spit formation? And how can this be improved?

Related to this main research question three objectives were defined, namely 1) gain insight into the physical processes related to spit formation, 2) validate Longshore Sediment Transport (LST) rates in ShorelineS and 3) validate migration and shape of spit formation in ShorelineS. In this section the key finding(s) per research objective are summarised.

Spit formation processes

Insight into the spit formation processes was gained by means of a literature study (Chapter 2), an inventory and analysis of existing natural spits and a modelling study using XBeach on the sediment transport distribution along the head of a spit (Chapter 4). The analysis of existing natural spits was used to classify the spits into three typical shapes (Section 4.1). This resulted in the following key finding:

1. The (presence of) bimodality in the wave climate is an important factor controlling the resulting spit shape.

In coastal environments where a strongly unidirectional wave climate with a high angle is present the shape of the spit tends to be relatively straight with a limited curvature. Whereas, for environments with a bimodal wave climate (i.e., where apart from a predominance average high angle wave orientation a wave component originating from a secondary, opposite, direction is present) the spit tends to have a wider, rounded off or recurved head, sometimes accompanied by long, narrow 'shoots'.

In unidirectional wave climates the shape (and width) of the spit is determined by the reach of the LST over the head of the spit. This reach is depending on the combined effect of wave refraction and wave height reduction over the head. In a bimodal wave climate, the waves from the secondary orientation tend to redistribute the sediment over the head of the spit. This leads to a sediment supply for parts of the spit (i.e., over the tip) which cannot be reached by the LST due to the predominant high angle wave, resulting in a wider, recurved tip.

For the Lobito case the wave climate is characterised by a very unidirectional wave climate (93% of the waves in the local wave climate originates from the small band of $\varphi_w = 244°$ to $248°$), which resulted in a straight spit of relatively uniform width and more asymmetric (blunt)-shaped spit head.

Longshore sediment transport in ShorelineS

The assessment of the longshore sediment transport in ShorelineS was based on a model-to-model comparison of ShorelineS and UNIBEST (Chapter 5). For this the LST along the (straight) Lobito coastline was used as reference case. This resulted in the following key finding:

2. A distinction between static offshore depth contours with a fixed orientation and dynamic nearshore depth contours of which the orientation dynamically updates with the coastline orientation is crucial to obtain accurate nearshore wave transformation and, hence, longshore sediment transport rates in ShorelineS.

By taking into account the distinction between the static and active zone in the wave transformation calculation in ShorelineS the wave transformation module, and thereby longshore transport calculation, was made more accurate and robust. In the original ShorelineS model all depth contours were assumed coastline parallel. It was found that the magnitude of the calculated longshore sediment transport for different coastal orientations deviated considerably from the UNIBEST benchmark depending on the location (depth) at which the wave climate was imposed.

For the Lobito case study by average 45% difference in longshore sediment transport magnitude (ΔA) was found with the original schematization. In addition to this also a shift in the by the model determined coastline equilibrium orientation ($\Delta\varphi_{eq}$) was found. The equilibrium orientation is an important parameter describing the overall alongshore sediment transport for a coastal system (i.e., the phase of the 'S, φ-curve'). For Lobito this angle deviated $10°$ up to $29°$ with respect to the actual, calibrated φ_{eq} for Lobito). Including the distinction between offshore and nearshore depth contours reduced the differences in transport magnitude to contours reduced the differences in transport magnitude to 15% and

in equilibrium coastline angle to 5° to 0° compared to the UNIBEST benchmark, thus less depending on the location of the imposed wave climate and better matching prediction of the actual calibrated alongshore sediment transport for Lobito.

The distinction between the static and active part of the bathymetry in ShorelineS was implemented using the concept of the 'dynamic boundary'. In this schematization of the bathymetry the orientation of the offshore depth contours are fixed up to the depth of the, user defined, depth of the dynamic boundary. In the zone between this depth and the coastline the depth contours are parallel to the coastline orientation, thus rotate accordingly for a changing coastline orientation.

Spit formation in ShorelineS

The modelling of the migration-direction and width/shape of a spit in ShorelineS was analysed in Chapter 6 using the insights from the first and second research objective and by hindcasting the evolution of the spit of Lobito with ShorelineS. This resulted in the following key finding:

3A. The angle of maximum transport should be calculated dynamically based on the local longshore sediment transport curve to simulate the spit migration direction correctly.

The direction in which a spit develops is related to the coastline angle for which the sediment transport is at its maximum (i.e., the 'critical angle'). In ShorelineS the orientation of the spit was based on a fixed critical angle of approximately $45°$ (i.e., the relative angle between the shore-normal and the incoming wave direction). In the so called 'upwind-correction' model routine the longshore transport is set to the maximum ($Q_{s,max}$) when the critical angle is locally exceeded, which prevents coastline instabilities and fixes the spit's orientation to the critical angle.

It was, however, found that due to the nearshore wave transformation and the effect of reorienting depth contours on the wave refraction (key finding 2) the critical angle deviates from this fixed angle and should therefore be based on the local calculated transport rates. Using model scenarios, it was shown that both the dynamic boundary condition and the use of a variable critical angle were required to be able to correctly hindcast/predict the spit orientation for the Lobito case study using ShorelineS. The improvement for the upwind correction, as suggested and implemented in ShorelineS, determines the critical angle based on the actual local maximum transport (trough the S,φ-curve) for each timestep and grid point depending on the actual wave- condition and transformation.

With the original ShorelineS model routine, using the fixed value for the critical angle as suggested by Ashton et al. (2001), the resulting spit was oriented $37°$ more seaward with respect to the actual observed spit orientation in Lobito. With the updated model routine ShorelineS correctly predicted (hindcasted) the Lobito spits orientation. The implementation of the updated upwind correction was therefore essential to be able to correctly derive the migration direction.

3B. By implementing a user defined spit width with linear decay of sediment transport over the spit head, the simulation of the spit shape and migration in ShorelineS is made more robust and independent of the of the grid resolution.

With the simplified quasi-uniform wave model and shielding routine in ShorelineS is not possible to correctly model the decay of the longshore sediment distribution over the head. The distribution of LST over the head is therfore manually controlled as part of the so called 'upwind-routine' in ShorelineS once the coastline reaches the critical angle (previous key finding).

An improved version of the upwind correction has been suggested and implemented as a proof-of-concept. In this proof-of-concept the longshore sediment transport over the head of the spit decreases linearly once the critical angle is exceeded. This forces the sediment distribution over the head of the spit corresponding to the 'equilibrium spit shape' as described by Petersen et al. (2008) and as found in the XBeach modelling study based. For this a new user defined spit width parameter is required, over which the sediment decays.

In the original ShorelineS model, and original model routine, the used sediment decay was defined rather arbitrary without a physical meaning. In fact; the width and shape, and thereby migration rate, were directly influenced by the user defined grid resolution. It should be noticed that updated routine implicitly assumes an equilibrium spit head independent of the actual forcing and/or shape as is no feedback mechanism in the model between the forcing and the shape. However, with the updated model routine, a first step is made in incorporating the physical representation of spit (shape and width) formation processes in the ShorelineS coastline model.

7.2 Recommendations

The following recommendations form opportunities for future development of the ShorelineS are defined based on the key findings, point of discussion and limitations of this research.

1. **Influence of bathymetry on spit formation rate**
   The third defined aspect of spit formation, (Figure 1-3), is the migration rate (or grow rate) of the spit. The migration rate can be described by the simple mass balance (Eq. 2.2) depending on the sediment supply at the tip, the width of the spit and depth. The first to aspects (sediment supply at the tip and the width) have been treated extensively in this thesis. It was shown that with the improved upwind correction (Section 6.2) also the migration rate was more consistent. However, as a spit moves seawards the depth will increase, the increase in depth will decrease the migration rate of the spit. For the calculation of the coastline displacement in the current release of ShorelineS a fixed active height (depth) is used (Eq. 2.11). To be able to better represent the effect of the increasing depth on the spit formation further research is required on 1) how the depth influences the spit formation and 2) how to incorporate this in ShorelineS (i.e., by relating the active height to an initial bathymetry).
2. **Predictor for spit width**
   With the updated upwind routine (proof-of-concept) the user is required to manually provide the expected spit width, this is considered a suitable approach for existing spits for which the width is known. It would be better if this parameter is predicted by ShorelineS itself, based on the local environmental conditions and coastal geometry (i.e., feedback mechanism). Currently no (empirical) formulations exist to quickly derive an indication of the spit width (and shape) based on the local conditions.
   Another way to find an indication of the spit with is by further developing and possibly automating the suggested framework (Section 4.3.1). This framework is basically a trial-and-error procedure which involves the modelling of the transport distribution over the head of as spit using a more advanced coastal area model. This way an indication for the equilibrium shape and width (characterised by a linear decay in LST) can be found iteratively.
3. **Modelling of different spit types**
   In this thesis the Lobito case study was treated extensively. The Lobito spit is, based on the conceptual model as suggested in Section 4.1, classified as a type A spit. For this spit the uni-directed wave climate was considered the main driver for the final spit shape, for the other spit type (B and C) processes such as overwash (resulting in overwash fans) and the variation in wave climate are important mechanisms influencing the final shape of a spit. The potential use of ShorelineS on those other spit was discussed (Section 6.3.1) but further research is required to explore the modelling of certain spits.
4. **Further improvement of alongshore sediment transport calculation**
   Currently the alongshore sediment transport is calculated using empirical bulk transport relations. Although it was shown that those transport formulations were implemented correctly in ShorelineS, still a large deviation could be observed in the calculated (uncalibrated) transport rates. One possible way to further improve the LST-prediction is by considering the coupling of the UNIBEST-LT module and ShorelineS. In the UNIBEST-LT module S, φ-curves can be calculated by more advanced semi process-based sediment relations such as Bijker (1971) and Van Rijn 2004 using the actual cross-shore profile and a more advanced wave transformation module. The resulting transport curves for different wave conditions can be used as (offline) look-up tables in ShorelineS as alternative for the LST-bulk transport calculations. This way the power of the UNIBEST-LT module and the flexibility of the ShorelineS model can be combined in an efficient way. An additional benefit of this coupling could be the allowance of spatially varying environmental conditions (wave climates) and /or coastal sections (cross shore profiles) in ShorelineS.

   Challenges regrading this recommendation are the technical coupling of the models and how to deal with changes in (local) wave formation due to, for example, wave shielding or diffraction during the model simulation.
5. **Interaction spit formation with human interventions**
   In this thesis the focus is on natural forming spits due the interaction with the (wave) environment. In the spit inventory (Appendix A) and the analysis of the Lobito spit (Chapter 3) it was shown that coastal engineering issues regarding (existing) spits are usually related to or caused by human interactions. For example: the Lobito spit along which groynes where constructed to fix its position and halt further migration, in the spit inventory cases were described where updrift changes (i.e., change in sediment supply due to constructions, dredging activities etc.) led to erosion, and in the end breaching, off the spit. For long-term engineering issues regarding spit it is therefore valuable to investigate how (and if) those aspects can be represented in ShorelineS.

Other topics such as the effects of climate change (e.g., sea level rise) or human interventions and the ability to efficiently model those aspects on a long-term basis with the ShorelineS mode, are outside the scope of this thesis but might be of interest for the further development of ShorelineS.

Overall the work regarding this relatively new ShorelineS coastline model is far from done. The scope of this thesis has focussed mainly on the longshore transport rates and spit formation due to (high incident) wave exposure. This research and the suggested improvements hope to contribute to the overall understanding of the capabilities of ShorelineS and provide a basis for the further development of ShorelineS

References

Ashton, A. D., & Murray, A. B. (2006). High-angle wave instability and emergent shoreline shapes: 2. Wave climate analysis and comparisons to nature. *Journal of Geophysical Research: Earth Surface*, *111*(4).

Ashton, A. D., Nienhuis, J., & Ells, K. (2016). On a neck, on a spit: controls on the shape of free spits. *Earth Surface Dynamics*, *4*(1), 193–210.

Ashton, A., Murray, A. B., & Arnault, O. (2001). Formation of coastline features by large-scale instabilities induced by high-angle waves. *Nature*, *414*(6861), 296–300.

Battjes, J. A., & Stive, M. J. F. (1985). Calibration and verification of a dissipation model for random breaking waves. *Journal of Geophysical Research*, *90*(C5), 9159.

Bijker, E. W. (1967). *Some considerations about scales for coastal models with movable bed*. Delft.

Bijker, E. W. (1971). Longshore Transport Computations. *Journal of the Waterways, Harbors and Coastal Engineering Division*, *97*(4), 687–701.

Birkemeier, W. A. (1985). Field Data on Seaward Limit of Profile Change. *Journal of Waterway, Port, Coastal, and Ocean Engineering*, *111*(3), 598–602.

Booij, N., Ris, R. C., & Holthuijsen, L. H. (1999). A third-generation wave model for coastal regions 1. Model description and validation. *Journal of Geophysical Research: Oceans*, *104*(C4), 7649–7666.

Bosman, D. ., & Joubert, J. R. (2008). Wave, Wind and Water level conditions at Walvis Bay, (April), 1–92.

Campbell, S. K., Sterling, S. L., & Lewarch, D. E. (2019). Building a landscape history and occupational chronology at Číxwicən, a coastal village on the Strait of Juan de Fuca, Washington State, U.S.A. *Journal of Archaeological Science: Reports*, *23*(August 2018), 1104–1130.

Castanho, J. (1973). *Transporte litoral com ondas regulares e irregulares. Importância dos factores secundários no transporte litoral.* Lisbon.

Castanho, J., Gomes, A., Reis de Carvalho, J., Vera-Cruz, D., Arjaújo, O., Teixera, A., & Weinholtz, M. (1973). Means of controlling littoral drift to protect beaches, dunes, estuaries and harbour entrances. Establishment of artificial beaches. (p. 26). Lisbon.

Ciavola, P. (1997). Coastal dynamics and impact of coastal protection works on the Spurn Head spit (UK). *CATENA*, *30*(4), 369–389.

Cooper, J. A. G., & Pilkey, O. H. (2007). Field measurement and quantification of longshore sediment transport: an unattainable goal? *Geological Society, London, Special Publications*, *274*(1), 37–43.

Cowell, P. J., Thom, B. G., & van de Plassche, O. (1995). Morphodynamics of coastal evolution. In R. W. G. Carter & C. D. Woodroffe (Eds.), *Coastal Evolution* (pp. 33–86). Cambridge: Cambridge University Press.

Dan, S. (2013). *Coastal Dynamics of the Danube Delta*. TU Delft. https://doi.org/https://doi.org/10.4233/uuid:9c19651e-e744-43c3-aa85-7ea7abd14a2

Davidson-Arnott, R. (2009). *An Introduction to Coastal Processes and Geomorphology*. Cambridge: Cambridge University Press.

Davidson-Arnott, R. G. D., & Reid, H. E. C. (1994). Sedimentary processes and the evolution of the distal bayside of Long Point, Lake Erie. *Canadian Journal of Earth Sciences*, *31*(9), 1461–1473.

Davidson-Arnott, R. G. D., & Van Heyningen, A. G. (2003). Migration and sedimentology of longshore sandwaves, Long Point, Lake Erie, Canada. *Sedimentology*, *50*(6), 1123–1137.

Delta Programme. (2013). *Compass for the Coast*. The Hague.

Deltares. (2011). UNIBEST-CL+ Manual, 147.

Deltares. (2015). *Rehabilitation of groyne scheme at Lobito*. Delft.

Dinis, P. A., Huvi, J., & Callapez, P. M. (2018). The Catumbela delta (SW Angola). Processes determining a history of changing asymmetry. *Journal of African Earth Sciences*, *145*, 68–79.

Dinis, P. A., Huvi, J., Cascalho, J., Garzanti, E., Vermeesch, P., & Callapez, P. (2016). Sand-spits systems from Benguela region (SW Angola). An analysis of sediment sources and dispersal from textural and compositional data. *Journal of African Earth Sciences*, *117*, 171–182.

Elfrink, Berry Prestedge Gordon, R. X. J. J. (2003). *Shoreline Evolution Due To Highly Oblique Incident Waves At Walvis Bay, Namibia*.

Elghandour, A. M. (2018). *Efficient Modelling of coastal evolution Development , verification and validation of ShorelineS model*. IHE-Delft.

Furmanczyk, K., & Kawińska, M. (1995). Coast changes of the Hel Spit over the last 40 years. *Journal of Coastal Research*, (22), 193–196.

Google LLC. (2019). Google Earth Pro.

Guo, J. (2002). Simple and explicit solution of wave dispersion equation. *Coastal Engineering*, *45*(2), 71–74.

Hallermeier, R. J. (1980). A profile zonation for seasonal sand beaches from wave climate. *Coastal Engineering*, *4*, 253–277.

Hanley, M. E., Hoggart, S. P. G., Simmonds, D. J., Bichot, A., Colangelo, M. A., Bozzeda, F., … Thompson, R. C. (2014). Shifting sands? Coastal protection by sand banks, beaches and dunes. *Coastal Engineering*, *87*, 136–146.

Hanson, H. (n.d.). *EUROSION Case Study Falsterbo Peninsula*.

Hayashi, K., Hayashimoto, K., Yagisawa, K., & Kobayashi, N. (2011). Beach Morphologies At Notsukezaki Sand Spit, Japan. *Coastal Engineering Proceedings*, *1*(32), 48.

Holthuijsen, L. H. (2010). *Waves in Oceanic and Coastal Waters*. *Cambridge University Press*. Cambridge University Press.

Huisman, B. J. A. (2012). *Webinar Large-scale long-term coastline modelling, using UNIBEST and Delft3D*. Delft.

Huisman, B. J. A. (2014). *Modelling Coastline Evolution*. Delft.

Hurst, M. D., Barkwith, A., Ellis, M. A., Thomas, C. W., & Murray, A. B. (2015). Exploring the sensitivities of crenulate bay shorelines to wave climates using a new vector-based one-line model. *Journal of Geophysical Research: Earth Surface*, *120*(12), 2586–2608.

Jiménez, J. A., & Sánchez-Arcilla, A. (2004). A long-term (decadal scale) evolution model for microtidal barrier systems. *Coastal Engineering*, *51*(8–9), 749–764.

Kamphuis, J. W. (1991). Alongshore Sediment Transport Rate. *Journal of Waterway, Port, Coastal, and Ocean Engineering*, *117*(6), 624–640.

Kosyan, R. D., & Krylenko, M. V. (2019). Modern state and dynamics of the Sea of Azov coasts. *Estuarine, Coastal and Shelf Science*, *224*(February), 314–323.

Kraus, N. C., Larson, M., & Wise, R. A. (1198). Depth of closure in beach-fill design. *Coastal Engineering (Technical Note CETN II-40, 3/98)*.

Kristensen, S., Dronen, N., Deigaard, R., & Elfrink, B. (2017). Bypass in groyne fields: Case study along the Lobito spit. In *Coastal dynamics 2017*.

Leatherman, S. P. (1979). Migration of Assateague Island, Maryland, by inlet and overwash processes. *Geology*, *7*(2), 104.

Lindhorst, S., Fürstenau, J., Christian Hass, H., & Betzler, C. (2010). Anatomy and sedimentary model of a hooked spit (Sylt, southern North Sea). *Sedimentology*, *57*(4), 935–955.

Longuet-Higgins, M. S. (1970). Longshore currents generated by obliquely incident sea waves: 2. *Journal of Geophysical Research*, *75*(33), 6790–6801.

Losada, M. A., Medina, R., Vidal, C., & Roldán, A. (1991). Historical evolution and morphological analysis of "El Puntal'' Spit, Santander (Spain)." *Journal of Coastal Research*, *7*(3), 711–722.

Medellín, G., Medina, R., Falqués, A., & González, M. (2008). Coastline sand waves on a low-energy beach at "El Puntal" spit, Spain. *Marine Geology*, *250*(3–4), 143–156.

Meteo365.com Ltd. (2019). Tide Times And Tide Charts Worldwide. Retrieved from https://www.tide-forecast.com/

Mil-Homens, J. (2016). *Longshore Sediment Transport*.

Mil-Homens, J., Ranasinghe, R., van Thiel de Vries, J. S. M., & Stive, M. J. F. (2013). Re-evaluation and improvement of three commonly used bulk longshore sediment transport formulas. *Coastal Engineering*, *75*, 29–39.

Petersen, D., Deigaard, R., & Fredsøe, J. (2008). Modelling the morphology of sandy spits. *Coastal Engineering*, *55*(7–8), 671–684.

Rangel-Buitrago, N., Williams, A. T., & Anfuso, G. (2018). Hard protection structures as a principal coastal erosion management strategy along the Caribbean coast of Colombia. A chronicle of pitfalls. *Ocean and Coastal Management*, *156*(April), 58–75.

Ribeiro, M., Barrio-Parra, F., Taborda, R., Cascalho, J., Bosnic, I., Rodríguez-Santalla, I., & Sánchez García, M. J. (2012). Longshore drift: experimental and empirical predictors. The example of the Ebro Delta. *Actas Das 2as Jornadas de Engenharia Hidrográfica*, (3), 271–274. Retrieved from http://www.hidrografico.pt/jornadas2012.php

Rodríguez-Santalla, I. (2004). *EUROSION Case Study Ebro Delta (Spain)*. EUROSION. Retrieved from http://link.springer.com/10.1007/978-94-007-6173-5_145-1

Roelvink, D., Huisman, B., & Elghandour, A. (2018). Efficient modelling of complex coastal evolution at monthly to century time scales - ShorelineS. In *Sixth International Conference on Estuaries and Coasts (ICEC-2018)*.

Roelvink, D., & Reniers, A. (2011). *A Guide to Modeling Coastal Morphology* (Vol. 12). WORLD SCIENTIFIC.

Różyński, G. (2010). Wave Climate in the Gulf of Gdańsk vs. Open Baltic Sea near Lubiatowo, Poland. *Archives of Hydroengineering and Environmental Mechanics*, *57*(2), 167–176.

Rusu, L., Raileanu, A., & Onea, F. (2018). A Comparative Analysis of the Wind and Wave Climate in the Black Sea Along the Shipping Routes. *Water*, *10*(7), 924.

Schwartz, M. L., Fabbri, P., & Wallace, R. S. (1987). Geomorphology of Dungeness Spit, Washington, USA. *Journal of Coastal Research*, *3*(4), 451–455.

Serizawa, M., Uda, T., & Miyahara, S. (2019). Prediction of Formation of Recurved Sand Spit Using Bg Model. *Coastal Engineering Proceedings*, *1*(36), 24.

Stewart, C. J., & Davidson-Arnott, R. G. D. (1988). Morphology, formation and migration of longshore sandwaves; Long Point, Lake Erie, Canada. *Marine Geology*, *81*(1–4), 63–77.

Szmytkiewicz, M., Biegowski, J., Kaczmarek, L. M., Okrój, T., Ostrowski, R., Pruszak, Z., … Skaja, M. (2000). Coastline changes nearby harbour structures: comparative analysis of one-line models versus field data. *Coastal Engineering*, *40*(2), 119–139.

Szmytkiewicz, M., Zeidler, R. B., Rózyński, G., & Skaja, M. (1999). Modelling Large-Scale Dynamics of Hel Peninsula, PL. In *Coastal Engineering 1998* (pp. 2837–2850). Reston, VA: American Society of Civil Engineers.

The UK hydrographic office Admiralty EasyTide. (2019). ADMIRALTY EasyTide. Retrieved from http://www.ukho.gov.uk/easytide/EasyTide/index.aspx

Tonnon, P. K., Huisman, B. J. A., Stam, G. N., & van Rijn, L. C. (2018). Numerical modelling of erosion rates, life span and maintenance volumes of mega nourishments. *Coastal Engineering*, *131*(November 2017), 51–69.

Uda, T., Serizawa, M., & Miyahar, S. (2014). Development of Sand Spits and Cuspate Forelands with Rhythmic Shapes and Their Deformation by Effects of Construction of Coastal Structures. In *Computational and Numerical Simulations* (pp. 419–450). InTech.

USACE. (1984a). *SHORE PROTECTION MANUAL US Army Corps of Engineers* (Vol. II). US Army Corps of Engineers.

USACE. (1984b). *SHORE PROTECTION MANUAL US Army Corps of Engineers* (Vol. I). US Army Corps of Engineers.

van Rijn, L. C. (1997). Sediment transport and budget of the central coastal zone of Holland. *Coastal Engineering*, *32*(1), 61–90.

van Rijn, L. C. (1998). *Principles of coastal morphology*. Amsterdam: Aqua Publications.

van Rijn, L. C. (2011). *Principles of Fluid Flow and Surface Waves in Rivers, Estuaries, Seas and Oceans*. Aqua Publications.

van Rijn, L. C. (2014). A simple general expression for longshore transport of sand, gravel and shingle. *Coastal Engineering*, *90*, 23–39.

van Rijn, L. C., Walstra, D. J. ., Grasmeijer, B., Sutherland, J., Pan, S., & Sierra, J. . (2003). The predictability of cross-shore bed evolution of sandy beaches at the time scale of storms and seasons using process-based Profile models. *Coastal Engineering*, *47*(3), 295–327.

Vespremeanu-Stroe, A., & Preoteasa, L. (2015). Morphology and the Cyclic Evolution of Danube Delta Spits. In G. Randazzo, D. W. T. Jackson, & J. A. G. Cooper (Eds.) (Vol. 12, pp. 327–339). Cham: Springer International Publishing.

Wegmann, K. W., Bohnenstiehl, D. R., Bowman, J. D., Homburg, J. A., Windingstad, J. D., & Beery, D. (2012). Assessing Coastal Landscape Change for Archaeological Purposes: Integrating Shallow Geophysics, Historical Archives and Geomorphology at Port Angeles, Washington, USA. *Archaeological Prospection*, *19*(4), 229–252.

Winter, C. (2011). *Observation- and Modelling of Morphodynamics in Sandy Coastal Environments*. Universität Bremen.

Zijlema, M. (2015). *Computational Modelling of Flow and Transport January 2015*. Delft University of Technology.

Appendices

Appendix A

Existing spit inventory

Appendix A- Existing spit inventory

In this appendix provides a brief analysis of in total 14 spits spread over 11 locations around the world (Figure A: 1-1). The analysis are based on site specific (geological) studies and open data sources such as tidal charts (Meteo365.com Ltd., 2019) and (historical) Google Earth satellite imagery. The locations and consulted studies are stated in Table A: 1-1.

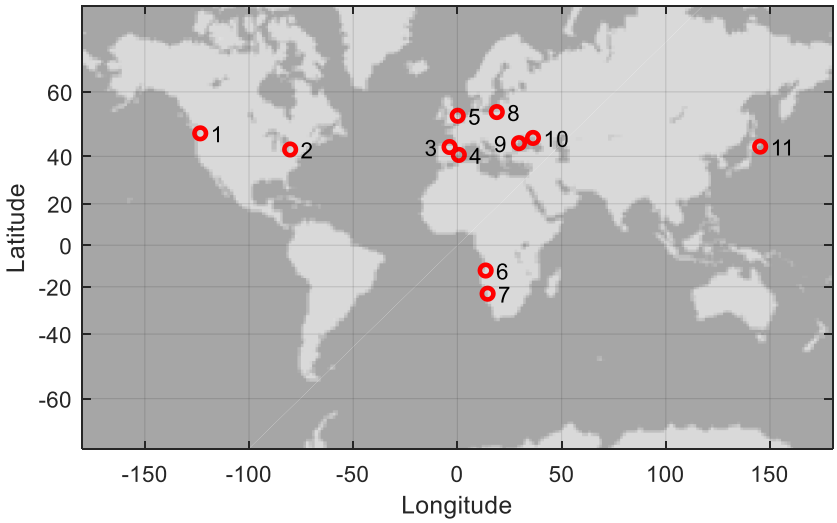

Figure A: 1-1 - World map showing locations of the analyzed spits

Location	Consulted literature
1) Ediz Hook	(Campbell et al., 2019; Schwartz et al., 1980; Wegmann et al., 2012)
2) Long point	(Davidson-Arnott et al., 1994, 2003; Stewart et al., 1988)
3) El Puntal	(Losada et al., 1991; Medellín et al., 2008)
4) Punta de la Banya	(Ibáñez et al., 2016; Jiménez et al., 2004; Ribeiro et al., 2012)
5) Spurn Head	(Ciavola, 1997)
6) Lobito	n/a[1]

Location	Consulted literature
7) Walvisbaai	(Bosman et al., 2008; Elfrink, Berry Prestedge Gordon, 2003; Serizawa et al., 2019)
8) Hel Penninsula	(Furmanczyk, 1994; Hanson, n.d.; Mechanics, 2010; Szmytkiewicz et al., 1998)
9) Danube Delta	(Dan, 2013; Vespremeanu-Stroe et al., 2015)
10) Azov	(Kosyan et al., 2019; Rusu et al., 2018; Uda et al., 2014)
11) Notsukezaki spit	(Hayashi et al., 2010)

Table A: 1-1 - Names associates with the locations of the spit and the consulted literature. [1]The spit of Lobito is treated ex treated extensively in the main thesis report (chapter 3).

The analysis on each spit is focusing on the following points of interest:

- **General description of the shape**
  Length, width
- **Description of environmental conditions**
  Tide/ wave information
- **Historical development / sediment budget**
  Literature about historical formation of spit, for some locations geological studies are found which describes the relevant hydrodynamical/morphological processes around the spit

1 Ediz Hook – Washington (USA)

1.1 General description

Figure A: 1-1 - Ediz hook spit, USA

The Ediz Hook spit is located in the U.S. state of Washington at the coast of the city of Port Angeles and the Salish Sea. The Salish Sea is in open connection with the North Pacific Ocean. The spit has a total length of 5.5km. The narrow neck has a width of 40m at narrowest part at the neck, towards the tip the width gradually widens up to a maximum width of 250m at the head of the spit. Nowadays the seaside and the head are protected by a rock revetment to protect the roadway connection on the neck and the coast guard air station which is located at the tip of the spit.

1.2 Environmental conditions

The spit is exposed to ocean swell-driven waves entering the Salish sea via the Strait of Juan Fuca. Those waves approach the spit from the west under a high angle. In addition to the predominance swell-driven high angle waves, the spit is also exposed from wind waves from two main fetch orientations: again, coming from the west over the Strait of Juan de Fuca and a second component originating from the east. The maximum tidal range at Ediz hook equals 3.3m

1.3 Historical development and sediment budget

Over the last millennia the spit evaluated towards its current position, whereas the orientation and the global shape of the spit remains unchanged. The evolution can be coupled to the local sea level rise over this period (Figure A: 1-2). The formation of the 'modern' spit at its current position started about 5000 years ago as since then the sea level reached a level similar to the sea level today.

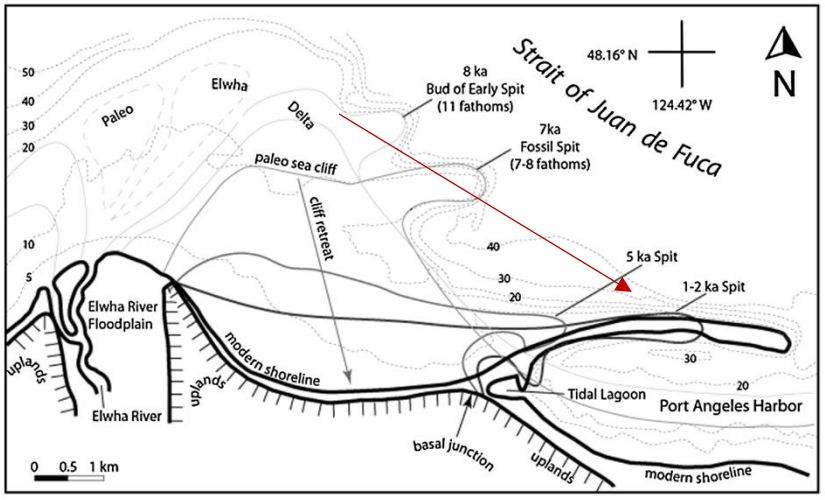

Figure A: 1-2 - Evolution of the Ediz spit over the last 8000 years, arrow indicates overal trend towards current position. (Wegmann et al., 2012)

The main source of sediment originates from the Elwha river and the erosion of the adjacent cliff (Figure A: 1-3, left) which is transported towards the spit by the high angle waves. As the spit is currently protected by a rock revetment further migration over the period of 1984-2019 cannot be observed.

The tidal filling and draining of the Strait of Juan de Fuca and especially the waterbody behind the Ediz hook resulted in a current circulation in the lee side of the Ediz hook spit, this circulation pattern has led to the formation of another spit "Číxwicən" (Figure A: 1-3 ,right).

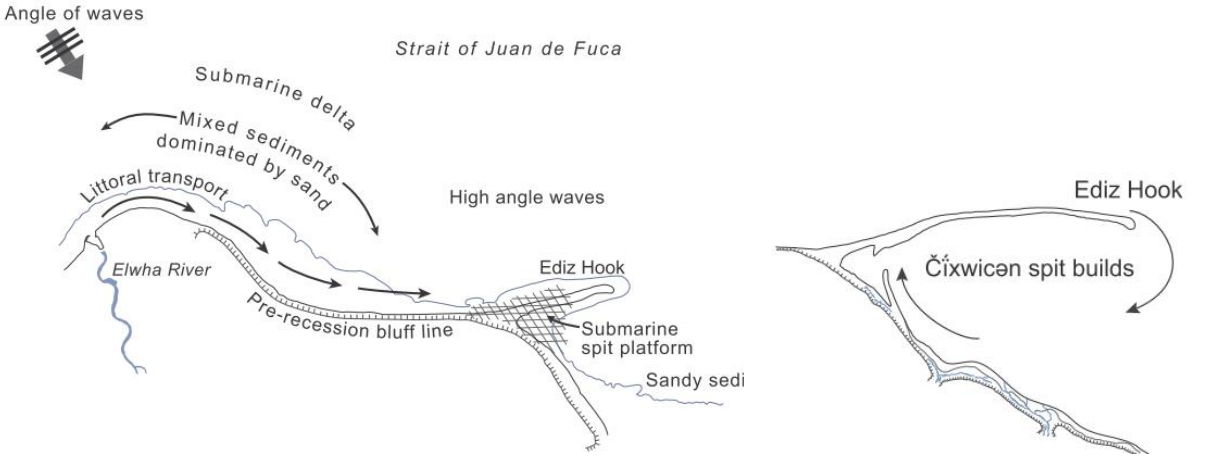

Figure A: 1-3 - Left: Alongshore sediment transport feeding the spit of Ediz hook Right: Circulation pattern in the semi enclosed water basin (Campbell et al., 2019)

2 Long point – Canada

2.1 General description

Figure A: 2-1 - Long point spit, Canada

The Long Point spit is located in Lake Erie which is part of the Greak Lake Basin in the province of Ontario in Canada. The spit has a length of approximately $37km$, the narrowest width ($\sim 500m$) is located near the base of the spit near the town of Old Cut. The spit is characterised by a series of dune ridges and ponds at the backside of the spit. The width of the neck and head of the spit is in the order of 1 to $1.5km$ (including the dune ridges). The head of the spit has a pointed shape and spit is slightly recurved. At the backside of the Long point spit, near the head a spit-like extension can be found.

2.2 Environmental conditions

As the spit is located in a lake, the generation of the (wind) waves are limited by prevailing wind direction and the available fetch. The dominance prevailing direction is west and southwest this in combination of the relative long fetch ($\sim 250km$ Figure A: 2-2, left) results in a predominance waves from W to SW at the Long point spit. Those high incident waves typically have a height of $H_s = 1 - 2m$ with a period of $T_p = 4 - 6s$.

In the wave climate a secondary wave component can be found which originates from N-E direction. Those waves are of less magnitude due to the shorter available fetch ($\sim 100km$). Waves from east to south directions are limited because of the short fetch ($50km$) and the much lower frequency waves from this direction.

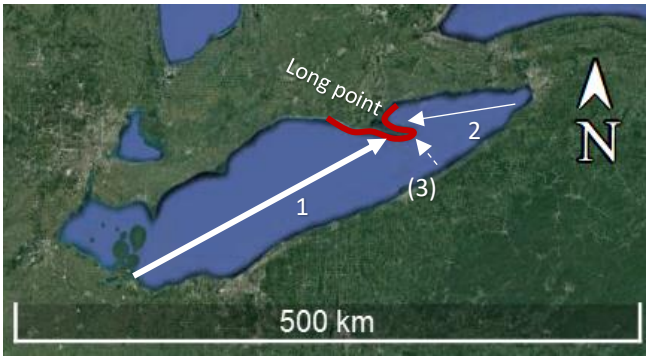

Figure A: 2-2 - Wave/Wind (fetch) directions for differen orientations with respect to the Long point spit

While there is no tidal water level variation in Lake Erie, long-term- and annual-scale mean water level fluctuations can be found associated to the varying water input and output (evaporation) of the lake and the Great Leak basin system resulting in variations of 0.3-0.6m (annual) up to 1.9m (long term).

2.3 Historical development and sediment budget

The spit formation started 4000 years ago when the water levels in Lake Erie stabilized, the average migration speed of the spit is 4-7m/yr. It is likely that the formation of the spit started of relatively fast. Nowadays, as the head of the spit has reached greater depths (>40m), the spit migration is limited to $\sim 1m/yr$.

The annual sediment supply to the lake side of the spit is in the order of $1 \cdot 10^6 m^3/yr$ and originates from the erosion of the upstream ($95km$) cosatal bluffs. Due to the large water depths at the end of the spit, the refraction of the dominant wave (Figure A: 2-3, (a) and (b)) around the head of the spit is limited. The transport along the head of the spit is therfore also limited and a large part of the sediment is diverted offshore. The waves from the secondary diretion (N-E) cannot transprot the sediment along the head but rather push the sediment from the head, this had lead to the formation of the spit-like coastline extention(s) at the backside of the spit. The combination of those two effects has resulted in the formation of the relativley narrow head.

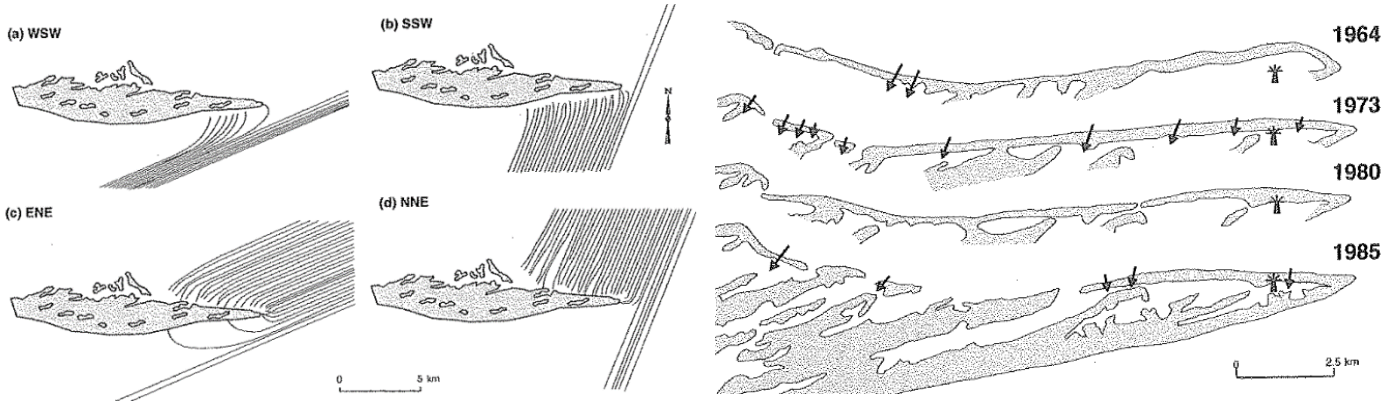

Figure A: 2-3 - Left: Wave refracting patterns for different wave directions (a-d) at the head of the spit. Right: Overwash events and resulting beaches along the spit (Davidson-Arnott et al., 1994)

Along the head the spit is subject to frequent overwash events. During the high-water periods the overwash results in breaching of the spit. During low water periods the overwash has a healing effect, closing off the earlier breached areas. This cycle of breaching and healing resulted in the, for this spit characteristic, dune ridges at the backside of the spit along the entire neck.

3 El Puntal – Spain

3.1 General description

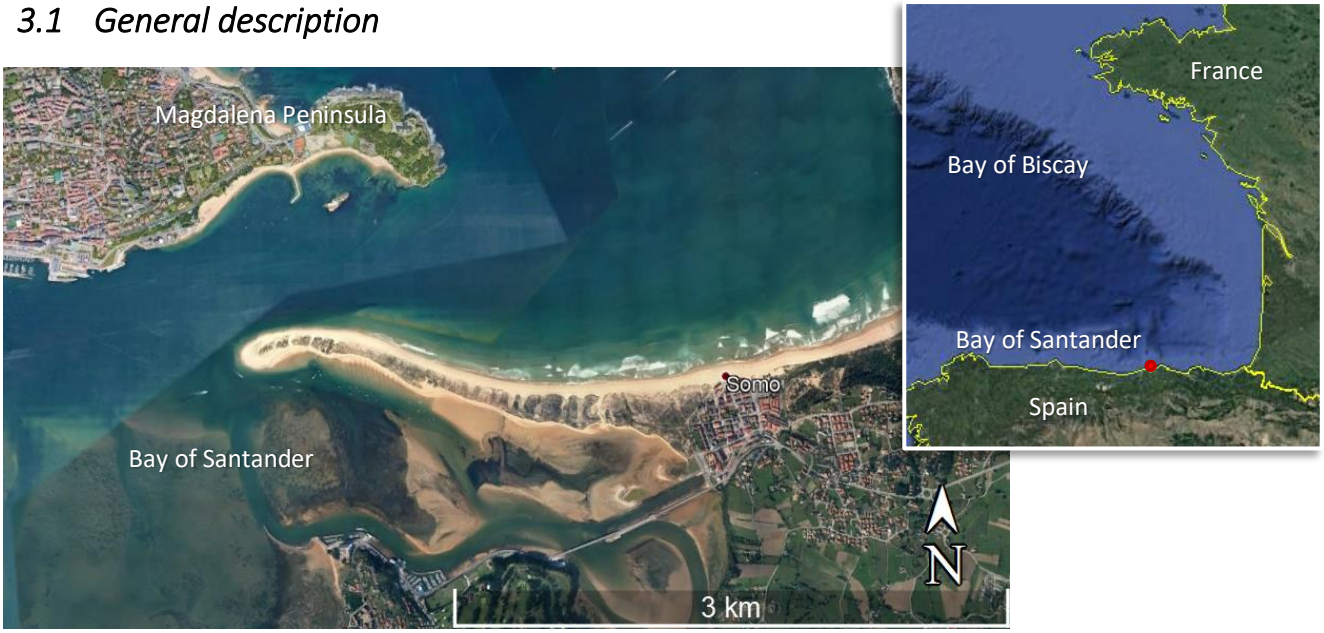

Figure A: 3-1 - El Puntal spit, Spain

The El Puntal spit is located on the North-coast of Spain in the Bay of Biscay (Figure A: 3-1, right). This part of the coast is divided in a series of beach pockets with inlets which are enclosed by rocky headlands at both sides. The El Puntal spit party encloses the Bay of Santander (Figure A: 3-1, left).

The spit has a length of approximately 2.7km, along the spit the spit gradually decreases in width from $300m$ at the base of the spit to $160m$ towards the head of the spit. Near the head of the spit the spit slightly recurves towards the Bay of Santander. There is no distinctive distinction between the head and the neck of the spit.

3.2 Environmental conditions

As the bay is sheltered by the landmass of France (Figure A: 3-1, right) waves approach the Bay of Santander from a north to north west direction with a typical wave height of $H_S \approx 1m$ up to $5m$ during winter storm events. The mean tidal range equals $3m$ and a spring tidal range of $5m$.

Due to the coastal geometry and in particularly the presence of the landmass of Magdalena Peninsula a part of the coast (and the spit) is sheltered from the direct wave attach from NW direction. Waves diffract and refract around Magdalena Peninsula resulting in a very uni-directed local high incident wave along the spit, this in contrast to the unsheltered part of the coastline more upstream (east from the spit) where the coast is subject to low indecent waves (Figure A: 3-2).

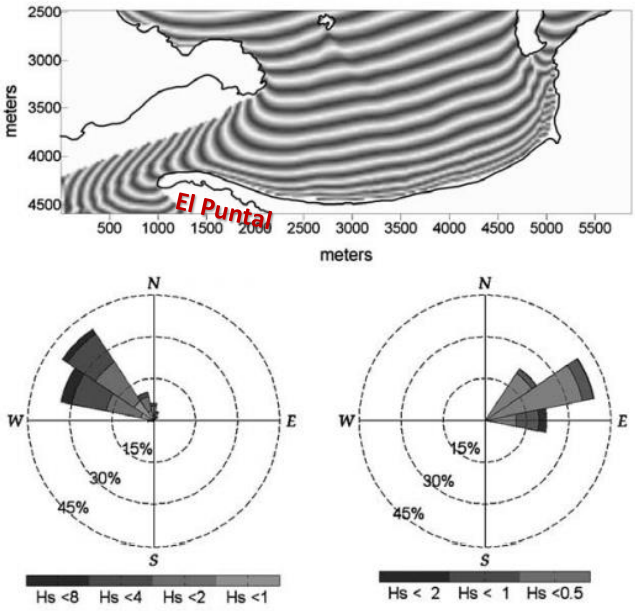

Figure A: 3-2 - Top: Wave propagation near El Puntal spit. Bottom left Wave rose offshore. Bottom right: wave rose near head of the spi (Medellín et al., 2008)

3.3 Historical development

The spit as it is positioned nowadays has formed during the 19th and first half of the 20th century. During this period land reclamations were carried for the extension of the harbour and a part of the city of Santander. This reduced the tidal prism of the bay of Santander with approximately 40%. Prior to the land reclamations a shoal 'Las Querants' was located in front of the coast (Figure A: 3-3) on which the waves were breaking. Once the land reclamation was construction, this shoal disappeared (i.e. it advanced towards the beach). From this moment on the spit was exposed by the waves (Figure A: 3-2) and started to migrate under the influence of the alongshore transport.

Nowadays the position of the spit is maintained by the harbour authority to keep the entrance channel of the harbour accessible for navigation. This requires frequent maintenance dredging around the head of the spit.

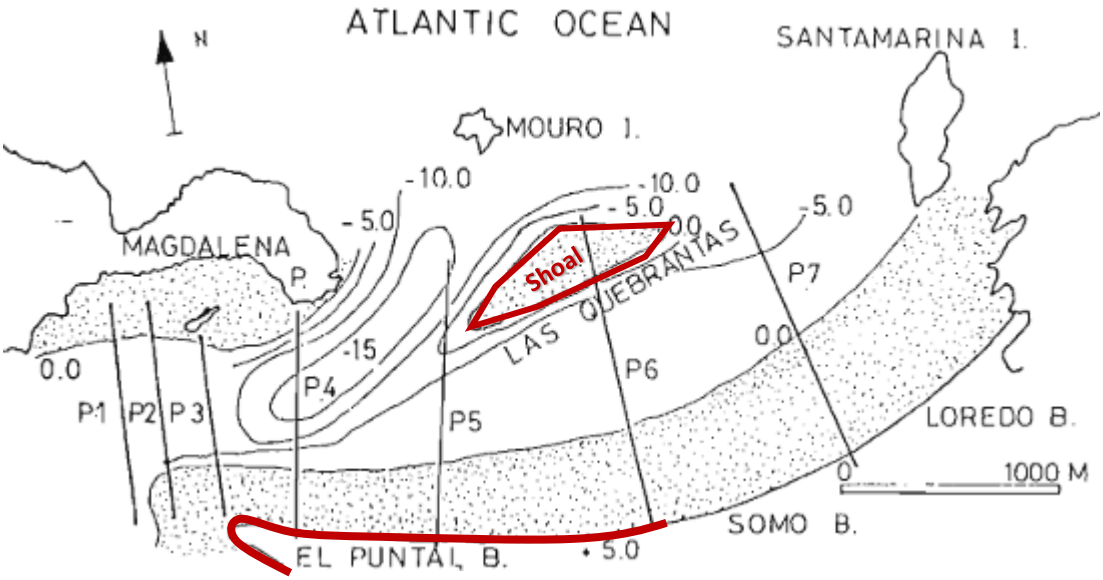

Figure A: 3-3 - Bay of Santander entrance prior to the land reclamations (ca. 1730) (Losada et al., 1991)

4 Punta de Banya – Spain

4.1 General description

Figure A: 4-1 - Punta de Banya spit, Spain

The Punta the Banya is a sand spit is located at Spanish Mediterranean coast and extends form the Ebro Delta. The spit has a straight uniformly orientated narrow neck which has a width of 110m at its narrowest point. At the tip a strongly recurved head is present which has a width of 1-2km. The head of the Punta de Banya spit is a lowlying marsh area with spots with vegetation and narrow branched channels.

4.2 Environmental conditions

The Balearic sea has a microtide with a maximum tidal range of 21cm, waves are generated by waves and come from three main directions: E, S and NW. Due to the coastal orientation and the wave sheltering by the Ebro spit is exposed to predominantly high angle eastern waves and, in lesser extent, waves from the west (Figure A: 4-2).

4.3 Historical development

The formation of the modern spit stared around 1580 A.D. at the tip of a former south branch in the Ebro delta near Els Muntells (Figure A: 4-1), this branch is now inactive as the river mouth shifted northwards. The neck of the spit is subject to a constant landward migration due to overwash and breaching with an average rate of 10m/year. The head still extends in south-westward direction and has grown approximately 260 meters over the last three decades (Figure A: 4-2).

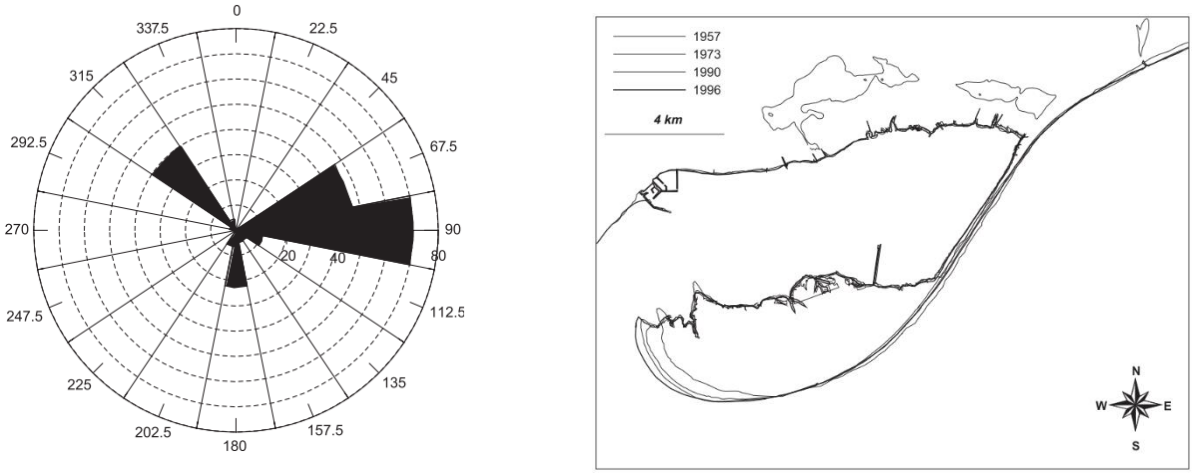

Figure A: 4-2 - Right: Deepwater Distribution of yearly integrated deep-water flux ($H^2\,T_p$ $in\ m^2s$) Left: Coastline changes 1957-199((Jiménez et al., 2004)

5 Spurn Head – United Kingdom

5.1 General description

Figure A: 5-1 - Spurn Head spit, United Kingdom

The Spurn head spit is located as an extension of the Holderness coast in England in the mouth of the Humber estuary. The spit has a length of 5.5km. The 'neck' of the spit is over the fist 2.5km highly curved and narrow, the narrowest part has a width of 75m. Towards the end of the spit it becomes wider, at the end of the spit the head builds out land towards the estuary to a to a maximum width of 380m.

5.2 Environmental conditions

Altrough the wind is predominating originated from Soutern to Western orientations (Figure A: 5-2) the mean wave condition orientates from the north east with a mean wav e height of $0.85m$. The mean wave direction relates to the orienation for which a considerable fetch exsists, in contrast to the predominance wind directions for which the fetch is limited.

The tide is significant with an maximum tidal range of $6.4m$ leading to tidal flow velocities in the Humber estuary up to $1.8m/s$.

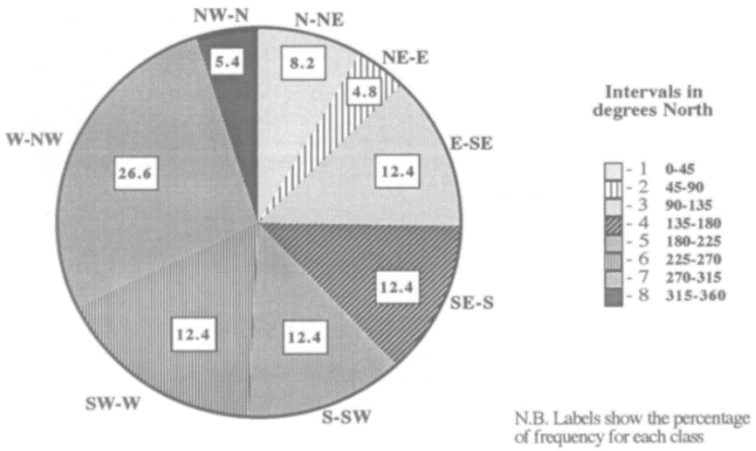

Figure A: 5-2 - Offshore wave distribution (Ciavola, 1997)

5.3 Historical development and sediment budget

Over the centuries during extreme conditions breaches occur resulting in smaller disconnected island, they however re-joined in the years after. During WWI and WWII hard sea defences were constructed which prevented overwash and new breaches.

The sediment budget and morphological processes were analysed and described by (Figure A: 5-3):

- N-E waves result in a LST along the spit's neck up to the tip. Those waves cannot transport the sediment along the tip.
- At the tip sediment is deposited which forms a sediment buffer in the form of shallow sand banks called 'The Binks'
- Smaller waves (limited fetch) from S-SE direction can reach (refract on) the tip and carry the sediment around the tip.

Over the last three decades (period 1984-2017) the following changes can be observed (Figure A: 5-4): a continuation of the spit migration (1) (approx. 65m) and the side sedimentation (2).

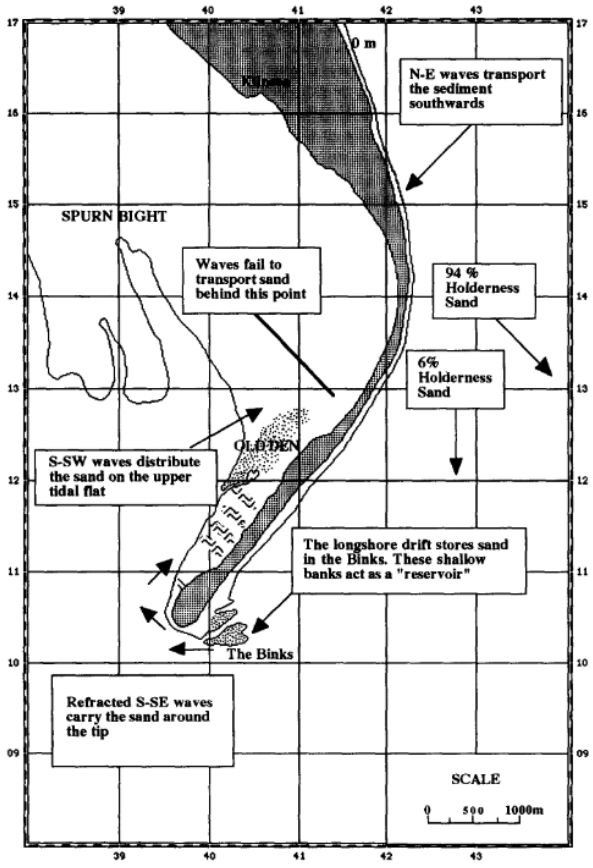

Figure A: 5-3 - Sediment pattern around the spit (Ciavola, 1997)

Figure A: 5-4 - Spit development 1984-2017

6 Lobito – Angola

The Lobito spit in Angola is treated extensively in the main thesis report (chapter 3).

7 Walvisbaai- Namibia

7.1 General description

Figure A: 7-1 - Walvisbaai spits, Nambia

At the coastline of West Africa and the Atlantic a number of spits can be found among which two spits close to each other located near the town of Walvis Bay in Namibia (here denoted as Spit A and B, Figure A: 7-1). In Figure A: 7-1 the main dimensions of the spits are stated. Both spits have similar shape and orientation with a wide recurved head and narrower neck. The area behind both spits consist of low water level bays and sand dunes. At the tip of spit B a narrow extension with a length of 6km can be observed, here denoted as the 'upper part'.

	A	**B**
Width of the head	1.5 - 2km	Ca 2.6km (upper part: 1km)
Overall Length	22km	Total: 51km (upper part: 6.1km)
Narrowest width of the neck	800m	Ca 300-500m (upper part 380m)

Table A: 7-1 - Main dimensions of the Walvisbay Spits

7.2 Environmental conditions

The prevailing tide has a maximum range of 1.9m. The wave climate is dominated by high obliquely incident swell driven waves (S-SW). Aside from the predominance S-SW waves a secondary wave component can be found in the wave climate with waves with a relatively high magnitude coming from northern directions (Figure A: 7-2).

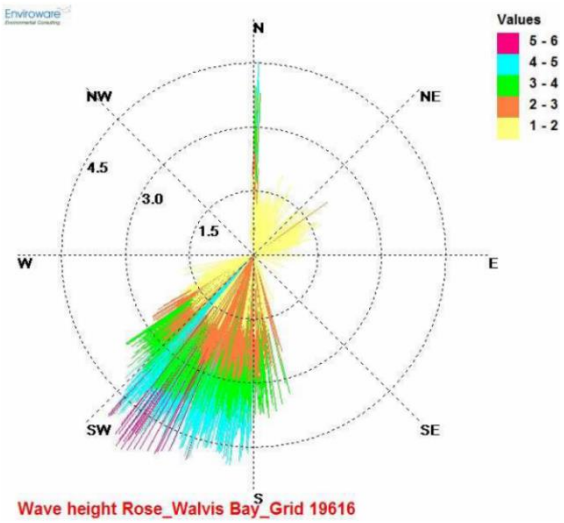

Figure A: 7-2 - Wave rose at Walbisbaai (Bosman et al., 2008)

7.3 Historical development

A large part of the coastline of Namibia, as well as the two spits considered here, is part of the Nambib coastal desert, providing a great sandy source for the spits. The initial spits have probably been formed many millennia ago. The necks of the spits are now more or less in a 'stable'/fixed position as no change in orientation can be observed over the last three decades. The spits still extend, the tip of spit A has grown almost 650m over the last 34 years (Figure A: 7-3, left). The same holds for spit B which has two extending fronts (the 'main' spit and the 'upper part' extension at the tip) which have both extended over distance in the order of 600-650m, although the front of the upper part is extending less fast. As the front of the 'main spit' of spit B became steeper, the width of the upper part reduced. From this it can be argued that the main spit is currently slowly overtaking the narrow extension at the main spits' tip (Figure A: 7-3, right).

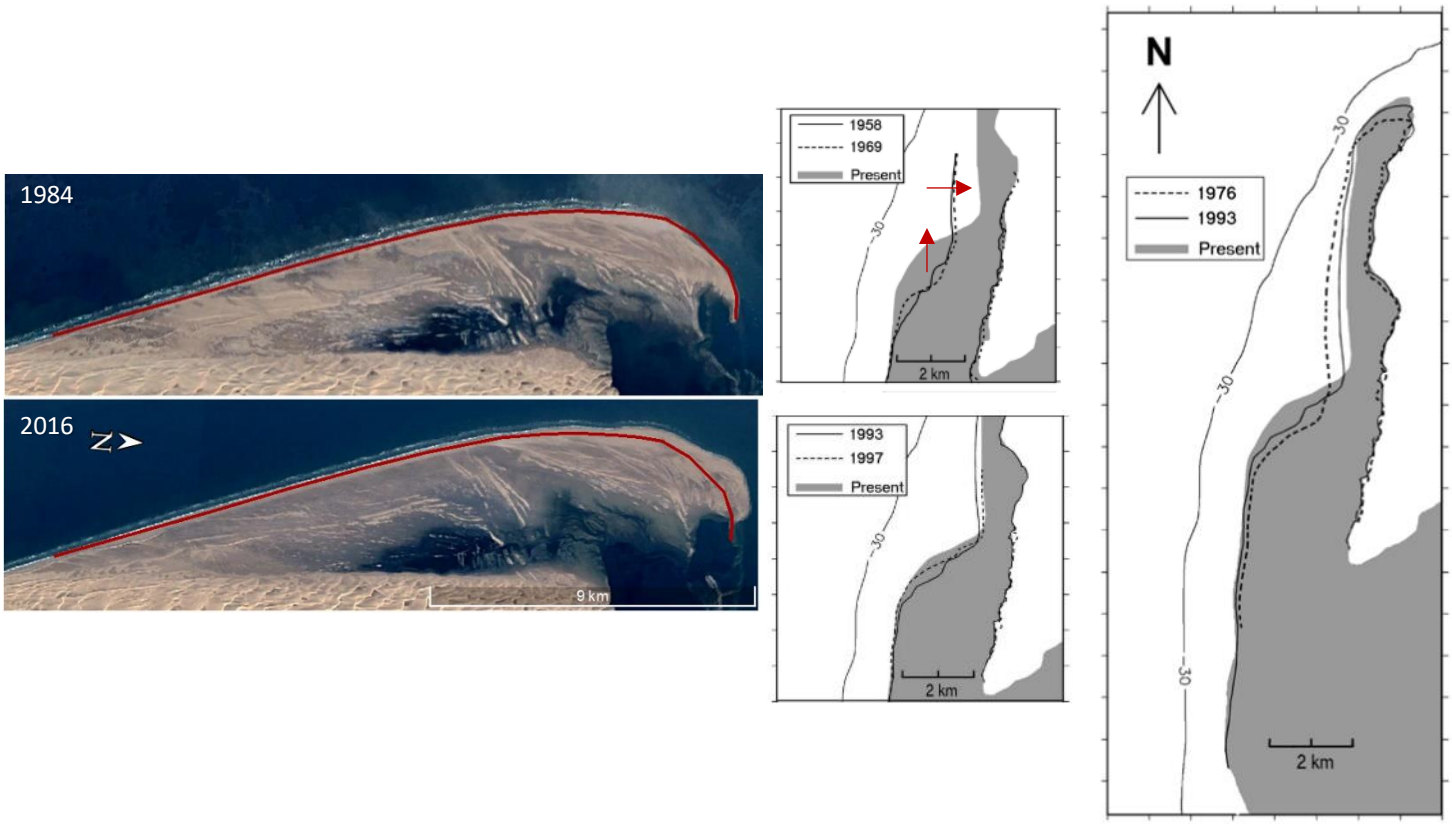

Figure A: 7-3 - Left: Coastline changes 1984-2016 (Spit A) Right: coastline changes spit (B)

8 Hel Peninsula – Poland

8.1 General description

Figure A: 8-1 - Hel Peninsula spit, Poland

The Hel Peninsula spit is located at the north coast of Poland and the Baltic sea in the Gdansk Bay. The spit has a length of 34km. Along the spit a number of small villages are established as well the required infrastructure (railway and high way connection).

The 'neck' of the spit is long and narrow, the narrowest part has a width of 190m. At the end of the spit the head builds out land inward to a to a maximum width of 2.7km.

8.2 Environmental conditions

As the Baltic sea is relatively small waterbody the tide is limited to maximum 3cm. The wave climate is dominated by wind waves. For the Baltic sea and Southern Baltic the wind is predominance from S and SW directions. However, due to the geometry and location of the Gdansk Bay the fetch is limited, and the spit sheltered from waves originating from S/SW directions. At the spit two main wind/wave conditions can be distinguished which have influenced the shape of the spit: a dominance N-NW wind orientation leading to very obliquely incident waves at the spit in combination with less dominance E-SE wind direction which lead to waves at the normally sheltered part of the spit's head.

8.3 Historical development and sediment budget

In the period of 1957 to 1991 erosion along the neck and sedimentation at the spit head was observed (Figure A: 8-2) which agrees with the description of spit morphology by Ashton et al., (2016). The net longshore sediment transport rate is, according to UNIBEST and SAN94 calculations, in the order of $3 - 5 \cdot 10^4\ m^3/yr$. To protect the rail- and highway connection at the neck various hard and soft coastal protection measures were carried out which effectively halted the spit formation and migration. Over the last 35 years (1984-2019) the change in coastline position was minimal, only at the head itself small coastline accretion can be observed (Figure A: 8-2, right)

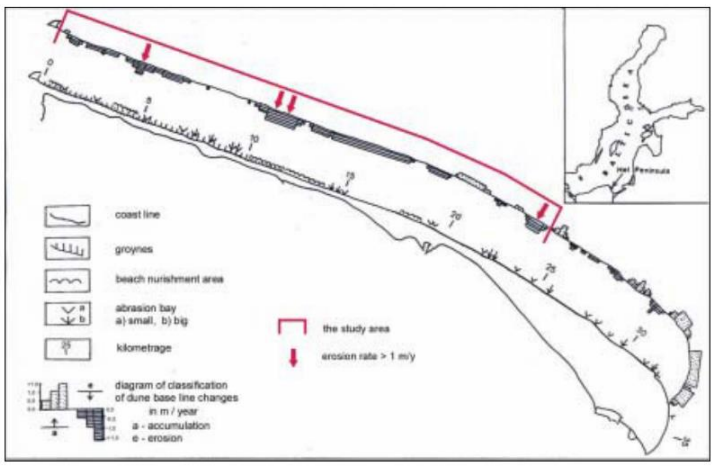

Figure A: 8-2 - Sediment budget along the spit (Furmanczyk, 1994)

9 Danube Delta – Romania

9.1 General description

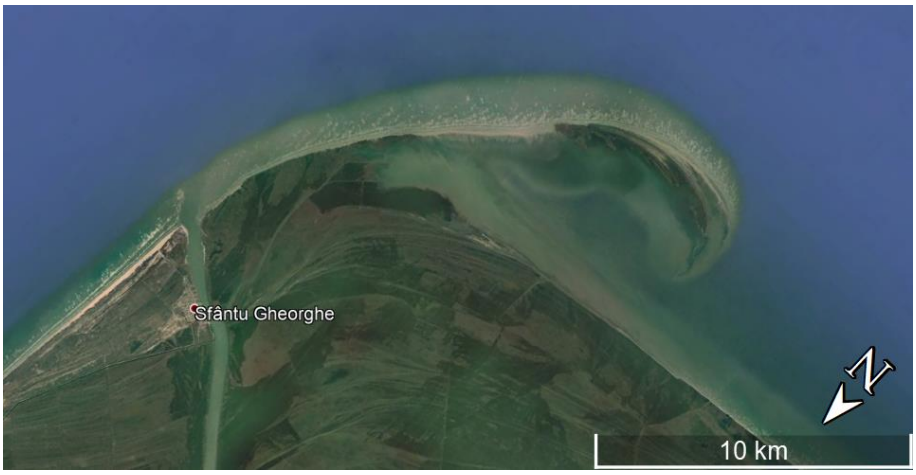

Figure A: 9-1 - Danube Delta spit, Romania

The Sahalin spit extends southwards from the mouth of the Danube Delta at the coast of Romania and the Black Sea. The spit is very dynamic and. The current length of the spit is 18km, the spit has a slight curvature along the long narrow (approx. 200m at the narrowest transect). The head of the spit is more recurved and consists of different ridges end islands alternated by channels, it is thereby wider than the neck with a width of 600-800m.

9.2 Environmental conditions

This spit is located in the Black Sea in which the maximum tide is limited to a couple of centimetres. The spit is exposed wind generated waves originating from two major directions: a dominant wave direction coming form the NE and a secondary S-orientated wave (Figure A: 9-2). The depth contours follow the strongly recurved shape of the delta the NE wave energy reduces therefore over the length of the spit due to refraction and wave sheltering by the delta/spit itself.

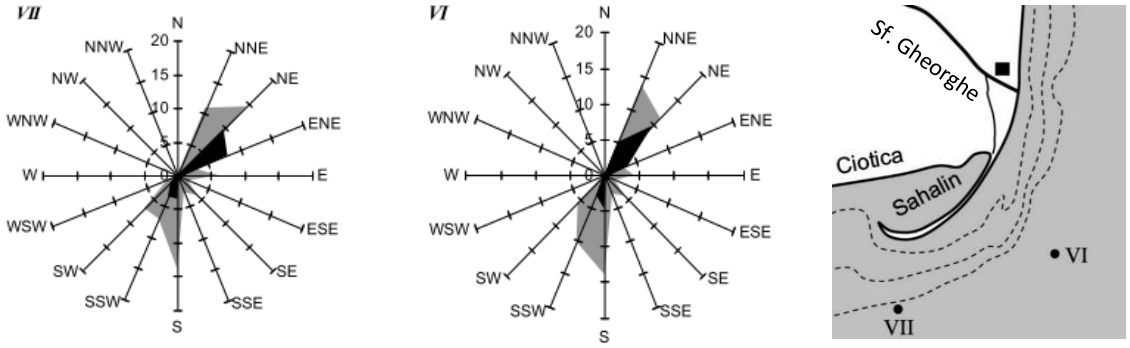

Figure A: 9-2 - Wave roses along the spit. Black indicates waves with a wave height $H_s > 1m$,gray indicates a wave heigh $H_s < 1m$ (Dan et al., 2011)

9.3 Historical development and sediment budget

The main source of sediment originates from the different rivers which end up in the black sea including the Sfântu Gheorghe branch mouth at the Danube spit which is located directly north at the base of the Sahalin spit. It was first formed around 1897 and has since then been very dynamic as it constantly extended southwards and migrated towards the mainland.

The alongshore sediment transport capacity along the spit was computed and has a maximum of approximately $1.6 \cdot 10^6\ m^3/year$ at the neck of the spit and gradually decreases to 0 at the tip of the spit resulting in deposition thus extension of the spit. The landward migration is the result of overwash when waves are orientated almost perpendicular to the spit as well as breaching (and afterwards restoration) of the neck during storm events. Over the last three decades (1984-2019) the spit has migrated up to 800m land inwards, the tip of the spit extended over almost 4.5km (Figure A: 9-3, right). Over the period of 2010 till 2019 a large breach and restoration can be observed (Figure A: 9-3, left) which locally pushed the spit up to 500m land inward.

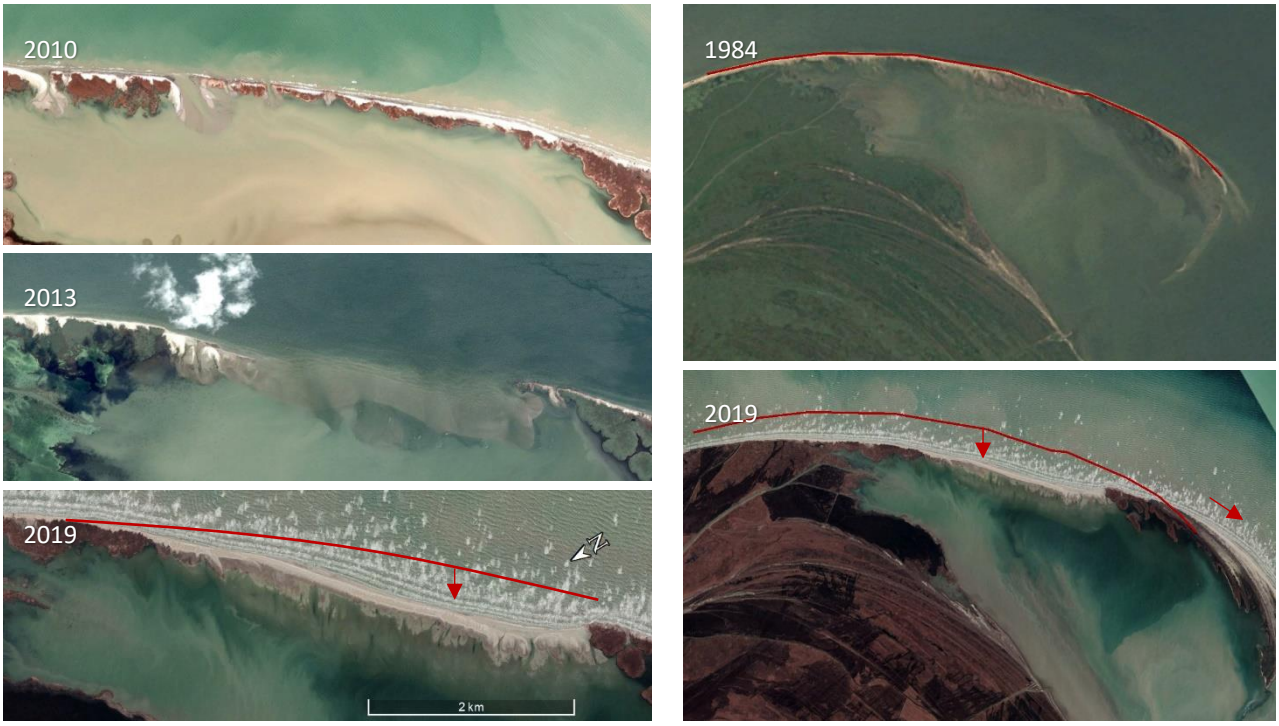

Figure A: 9-3 - Left: Overwash and breaching events resulting in landward migration of the neck of the spit (2010-2019) Right Coastline changes of the spit (1984-2019)

10 Sea of Avoz – Ukraine

10.1 General description

Figure A: 10-1 - Spits of Avoz (Labelled), Ukraine

The Sea of Azov is one of the smallest seas of the world with a water surface of $39000km^2$ and an average depth of 7.4m. It has an open connection to the Black sea by the Strait of Kerch to the. Along the coastline of the Sea of Azov many unstable coast formations can be found, especially at the SE coast of Ukraine. Here three spits (labelled A,B,C Figure A: 10-1) are considered with a varying length of 28km (spit A,B) up to 44km (spit C). The main dimensions (length, narrowest width and width of the head) can be found in Table A: 10-1.

All three spits share a similar shape: a long narrow neck with a wide head. The heads of the spits consist of recurved 'shoots' of land alternated by (enclosed) water bodies.

	Spit A	**Spit B**	**Spit C**
Width of the head	1.8km	1-2km	3-5km
Overall Length	28km	27km	44km
Narrowest width of the neck	80m	60m	160m

Table A: 10-1 - Main dimensions of spits of Avoz

10.2 Environmental conditions

Due to the limited size of the Sea of Azov's waterbody the tidal range is limited to a maximum of 2cm. The main driver for longshore transport are the wind-generated waves. There is a clear seasonal distinction in wind direction (thus wave direction): The wind is predominantly orientated in NE direction leading to a yearly average a high incident wave along the spits at the west coast of Ukraine, during the spring the average SE wind orientation (Figure A: 10-2).

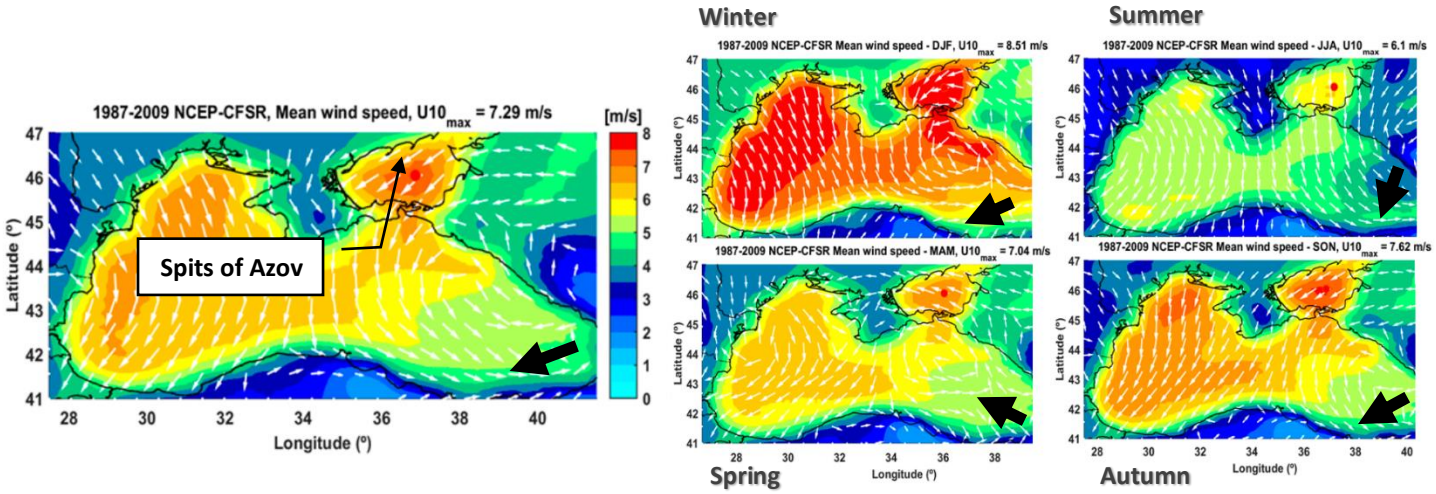

Figure A: 10-2 - Windspeed and directions over (generating waves) over the Black sea and the Sea of Avoz. Left: Mean direction. Right Seasonal variability of the wind (Rusu et al., 2018)

10.3 Historical development and sediment budget

The increasing size of the spits (A →C, Figure A: 10-1)can be related to the increasing fetch. As the high incident wave is a result of the NE-wind the fetch is the longest, thus wave energy strongest, at spit C. This also holds for the second wave component during the spring, the fetch (thus wave energy) is the largest for spit C and more limited at spit A and B. This explains why spit C is the largest and has the most flatted head of all three spits.

Especially spit A and B are characterised by the triangular base, this is a result of the wave shielding from the predominance wave energy originating from NE waves by the neck. Secondary waves from other SE-W directions can still reach the lee side of the spit ensuring an onset movement of sediment towards the base of the spit resulting in the triangular shape.

Nowadays the spits are still extending, over the last three decades (1984-2018) approximately 615m of coastline was added at the head of spit C (Figure A: 10-3).

Figure A: 10-3 - Coastline changes at the head o spit C (1984-2018)

11 Notsukezaki spit – Japan

11.1 General description

Figure A: 11-1 - Left: Location of Notsukezaki spit and surrounding area. Right: zoom on the spit itself (Google LLC., 2019)

The Notsukezaki spit is a hook shaped sand spit located at the eastern side of Hokkaido, which is the upmost northern island of Japan. The northside of the spit faces the Nemuro strait, which is located in between the main land of Hokkaiko and the Kunashiri island, the strait of Nemuro is connected to the sea of Okhotsk. The south part, curved head, of the spit faces towards the Pacific Ocean. The spit has an overall alongshore length of 22km (including the curved head). The neck of the spit is fairly narrow with a width of $75m$ at the narrowest part. The backside of the spit is characterized by the presence of the different (overwash)fans. At the head of the spit the consist of a marshy area with channels and vegetation, the width of the spit increases up to 1km.

11.2 Environmental conditions

The maximum tidal range equals 1.3m. The wave climate along the spit is very variable along the coastline of the spit due to the presence of the landmass of the Kunashiri Island and the difference in wave origin along the spit. Along the neck the waves are predominance NW-directed, 80% of the local wave climate originates from NW, NNW and Northern directions (originating from the Nemuro strait) with a significant wave height of 2.9m (Figure A: 11-2, location St.1). Offshore waves from other (eastern) directions are shielded by the Kunashiri island.

In contrast to the neck, the curved head of the spit is exposed from waves from different directions. In fact, 40% of the waves in the local wave climate are originating from an eastern direction (originating from the Pacific Ocean) with a smaller significant wave height of 0.9m.

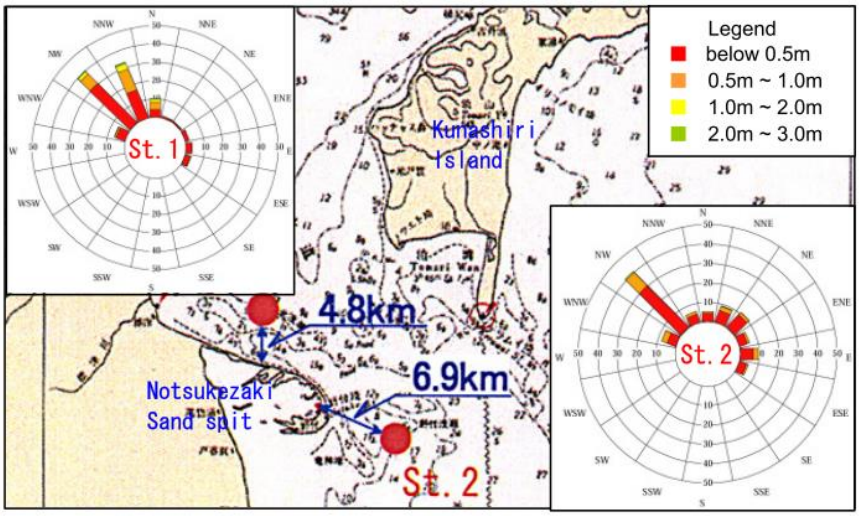

Figure A: 11-2 - Wave climate at two points along the spit: St.1 at the neck of the spit ST. 2 at the head of the spit (Hayashi et al., 2010)

11.3 Historical development and sediment budget

The sediment is supplied by updrift rivers (Churui- and Shibetsu- river, Figure A: 11-1) and the updrift cliff erosion. The construction of the Minehama fishing port near the Shibetsu river outlet has (partly) blocked the alongshore transport and thereby reduced the sediment supply at the spit. This has resulted in recent erosion, breaching and subsequent construction of al types of coastal protection works to prevent further erosion (i.e. groyne schemes, offshore breakwaters and revetments can be found along the neck and head of the spit). The construction of those coastal protection measures has halted the further spit migration.

Interestingly at the absolute end of the curved inwards head of the spit new dynamic spit formation can be found. This part of the spit is probably fully shielded from wave exposure other than south-east direction. This currently 'unprotected' part of the spit is very dynamic as it has grown/accreted 110m of land at the tip of this spit over 4 years (Figure A: 11-3).

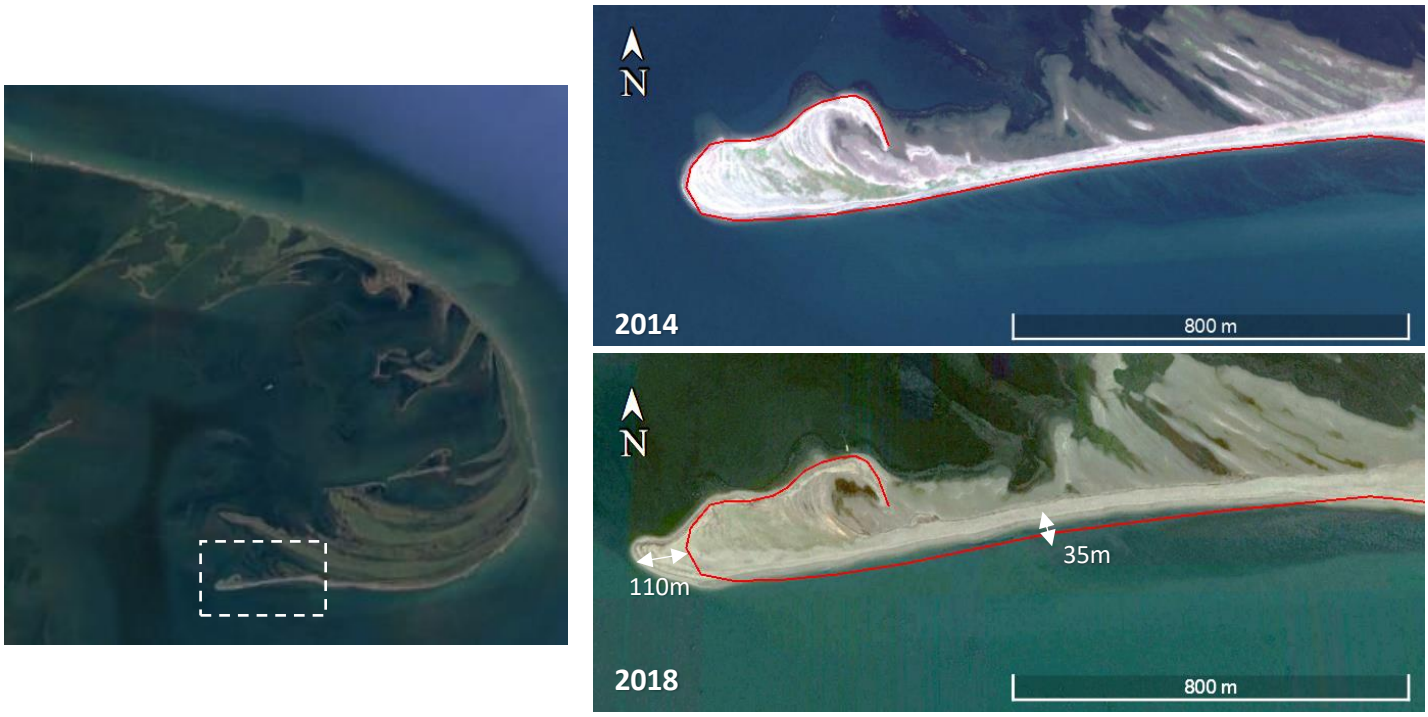

Figure A: 11-3 - Evolution of recently formed spit formation during 2014 until 2018 (Google LLC., 2019)

Appendix B

XBeach modelling results for different spit geometries

In this appendix the alongshore transport distribution for the different spit shapes and width are displayed. In total 5 different shapes are considered; the shape of the current spit and four hypothetical shapes:

- **Case 5** - Current shape
- **Case 6** - Round shape
- **Case 7** - Elongated shape with ratio 1:2
- **Case 8** - Elongated shape with ratio 1:3
- **Case 9** - Blunt shape

For each shape the width was variated with respect to the base case, this results in four subcases per shape case: Case x**(a-b)** (Table B: 1).

	Spit width (W) [m]			
Shape	$a)\ 0.75W_{base}$	$b)\ W_{base}$	$c)\ 1.25W_{base}$	$d)\ 1.5W_{base}$
Current	240	180	300	360
Shape var.	160	120	160	240

Table B: 1 - Base width and width variations for the different considered cases.

In section 1 a visual representation of each shape and the width variations are given. The values indicate the alongshore distance ($d = 600m$ is used as scaling point). In section 2 the resulting alongshore sediment transport plots are provided both as function of the alongshore distance as over the width of the spit.

1 Shapes

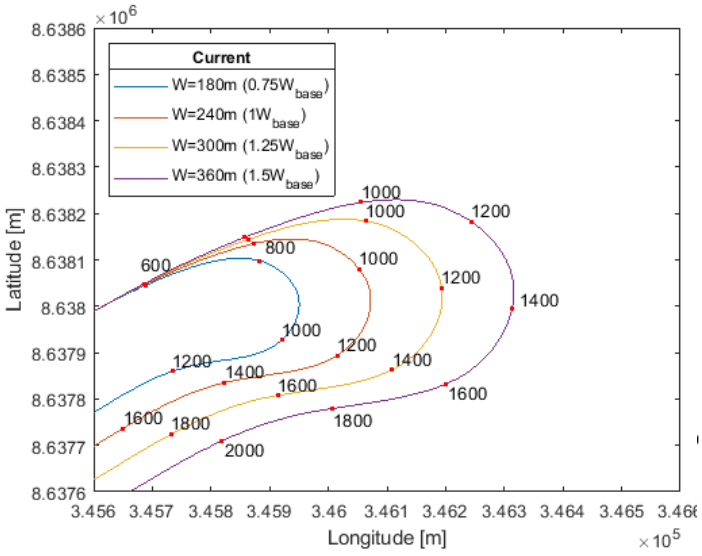

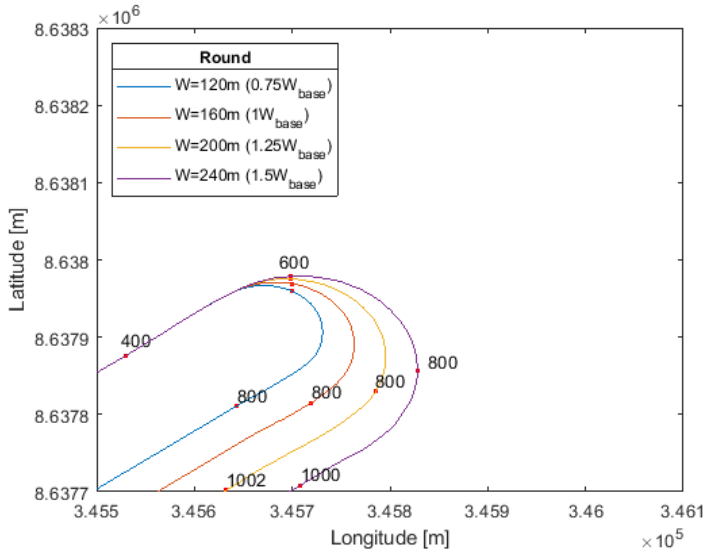

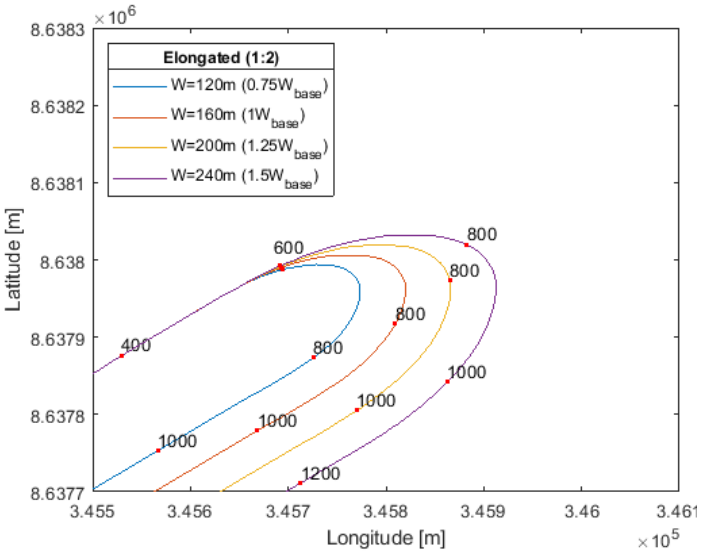

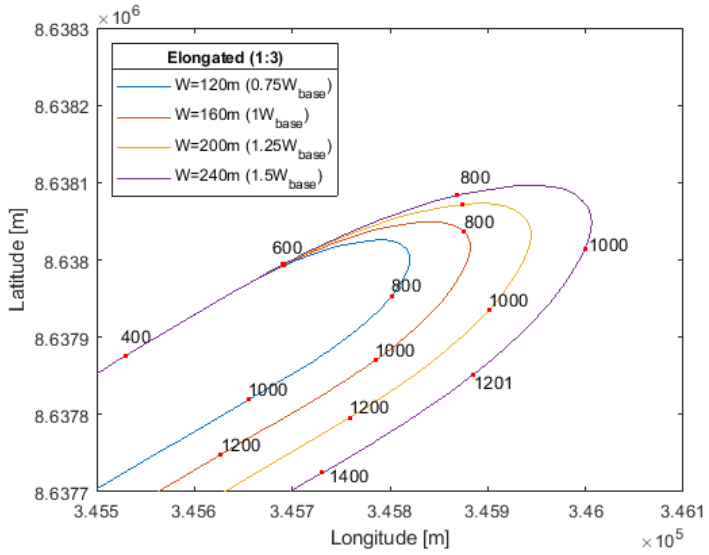

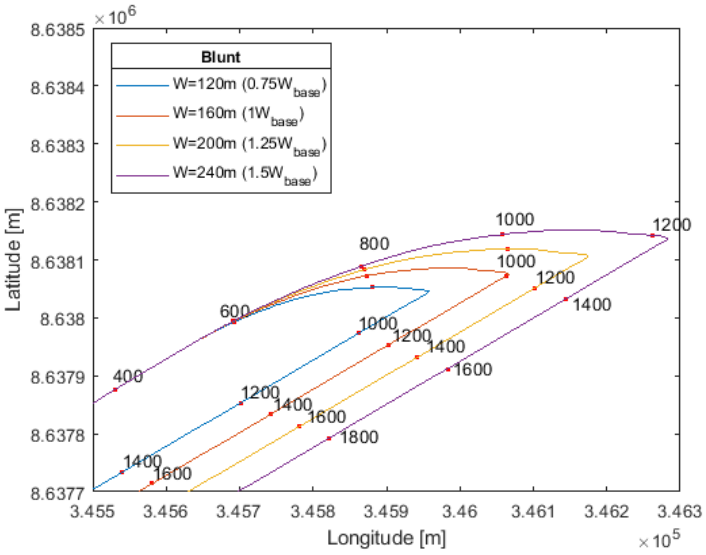

2 Results: Alongshore sediment transport distributions

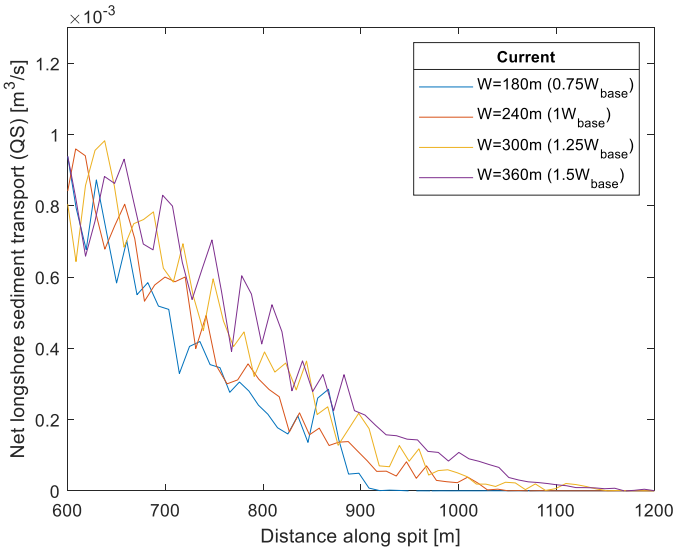

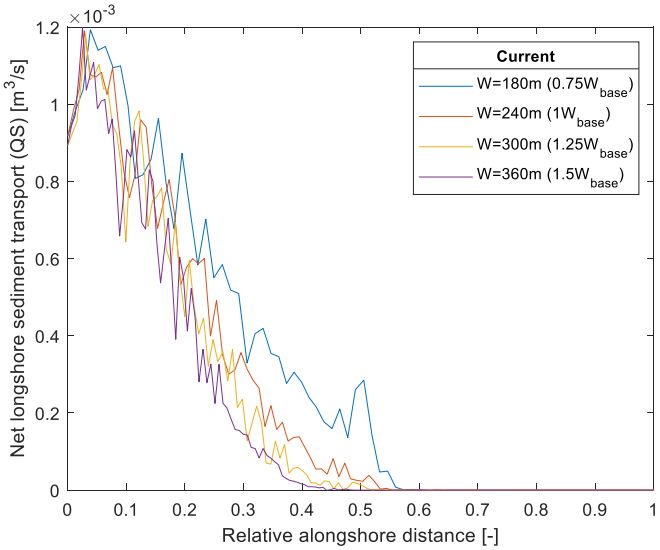

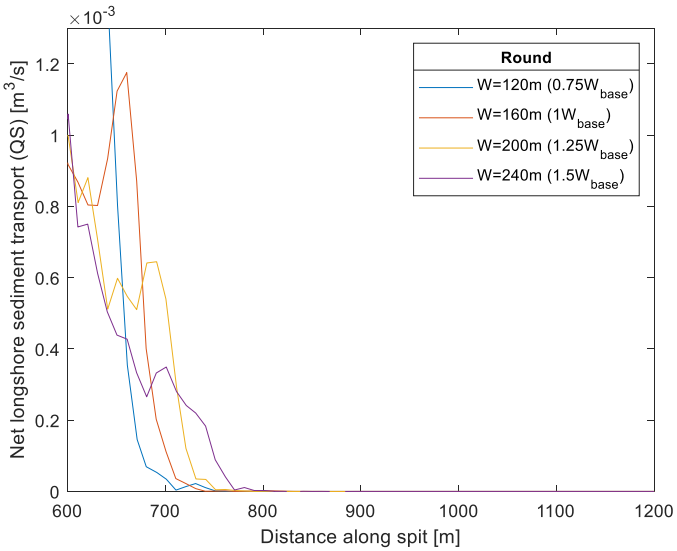

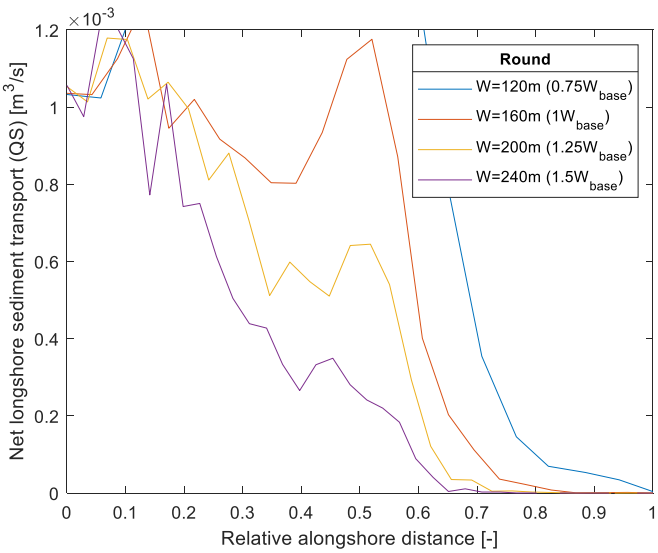

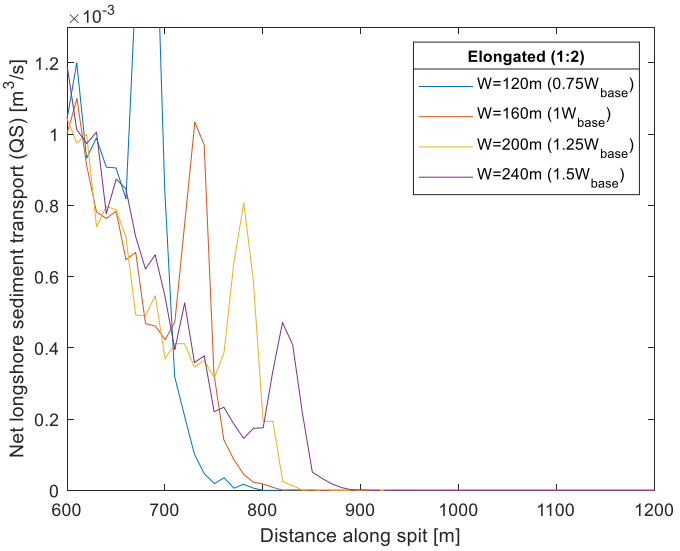
×10-3
Net longshore sediment transport (QS) [m3/s]
Distance along spit [m]
Elongated (1:2)
W=120m (0.75Wbase)
W=160m (1Wbase)
W=200m (1.25Wbase)
W=240m (1.5Wbase)

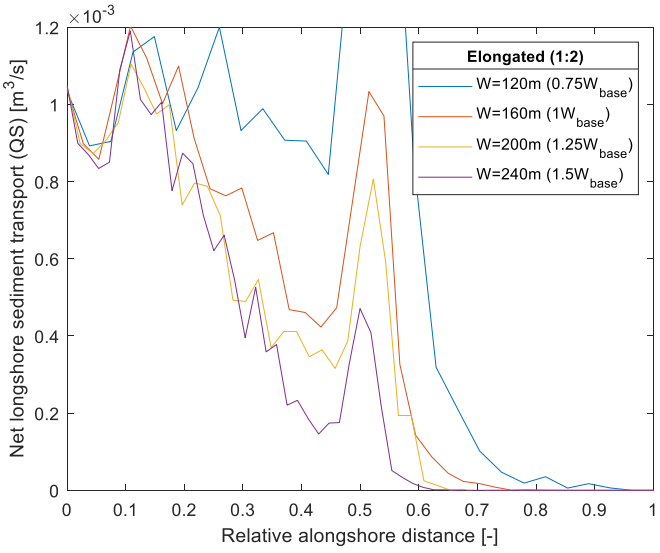
×10-3
Net longshore sediment transport (QS) [m3/s]
Relative alongshore distance [-]
Elongated (1:2)
W=120m (0.75Wbase)
W=160m (1Wbase)
W=200m (1.25Wbase)
W=240m (1.5Wbase)

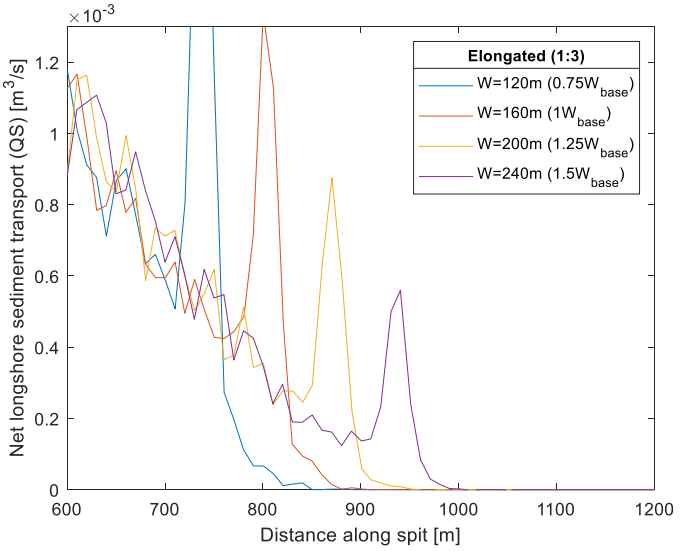
×10-3
Net longshore sediment transport (QS) [m3/s]
Distance along spit [m]
Elongated (1:3)
W=120m (0.75Wbase)
W=160m (1Wbase)
W=200m (1.25Wbase)
W=240m (1.5Wbase)

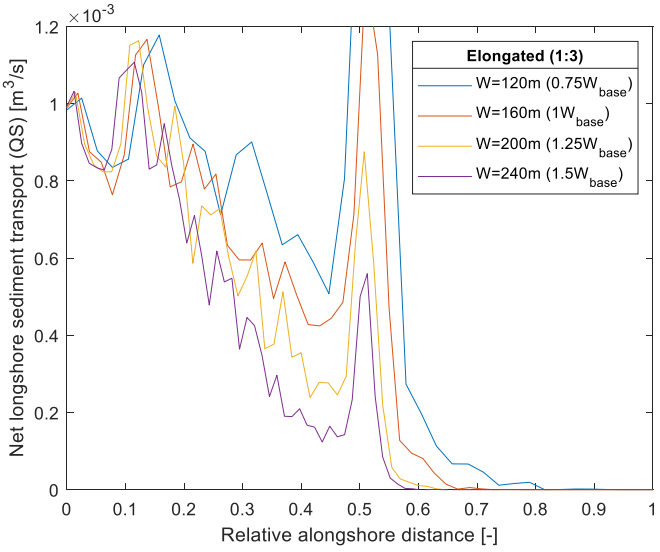
×10-3
Net longshore sediment transport (QS) [m3/s]
Relative alongshore distance [-]
Elongated (1:3)
W=120m (0.75Wbase)
W=160m (1Wbase)
W=200m (1.25Wbase)
W=240m (1.5Wbase)

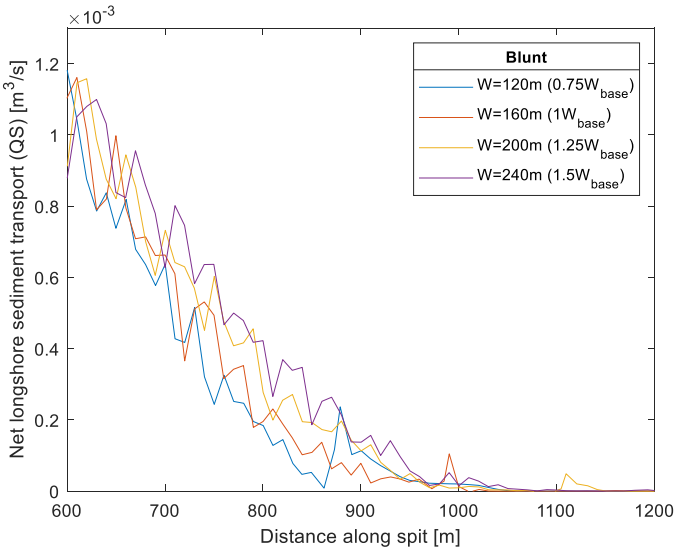
×10-3
Net longshore sediment transport (QS) [m3/s]
Distance along spit [m]
Blunt
W=120m (0.75Wbase)
W=160m (1Wbase)
W=200m (1.25Wbase)
W=240m (1.5Wbase)

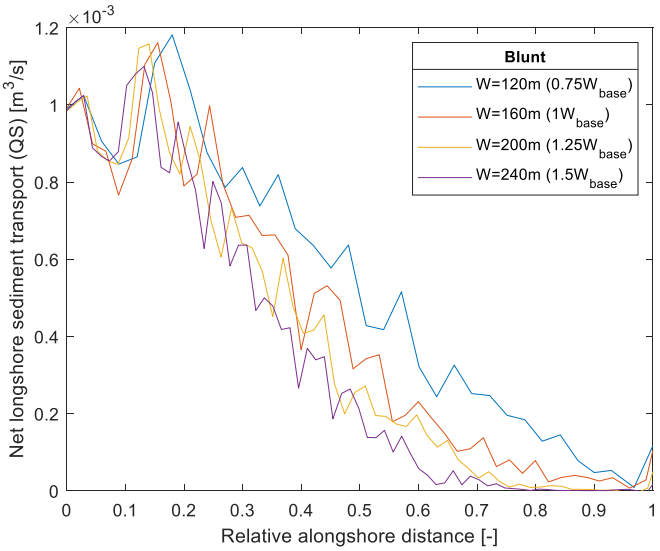
×10-3
Net longshore sediment transport (QS) [m3/s]
Relative alongshore distance [-]
Blunt
W=120m (0.75Wbase)
W=160m (1Wbase)
W=200m (1.25Wbase)
W=240m (1.5Wbase)

Appendix C

Data sheets LST-comparison ShorelineS versus UNIBEST-LT

Case I

Input

Wave Climate	Offshore	phi_w	246.7
Dynamic boundary active	no (56m)		

Results

DATA

Coastline orientation (°N)	LST-Formlea						Wave transf			
	CERC1	CERC2	KAMP	CERC3	MILH	VR14	H_s,br	h_br	phi_w,br	Phi_loc_off
180	-826512.6	-451287	-250355	-231057	-60593.7	-76438.2	0.56	0.70	-9.54	-66.7
190	-1043989	-608664	-319945	-311735	-85683.5	-111571	0.64	0.80	-9.26	-56.7
200	-1135544	-692165	-361740	-355179	-104520	-134092	0.70	0.88	-8.42	-46.7
210	-1090137	-685575	-371709	-352786	-114403	-138276	0.75	0.93	-7.13	-36.7
220	-913242.3	-586889	-346639	-302906	-113116	-121848	0.78	0.97	-5.47	-26.7
230	-626197.5	-408067	-283065	-211141	-98470.7	-86366.3	0.80	1.00	-3.54	-16.7
240	-263624	-173043	-170562	-89671	-65582.9	-37000	0.81	1.02	-1.45	-6.7
250	130746.37	85911.06	112184	44529.51	46359.79	18396.67	0.81	1.02	0.72	3.3
260	509346.84	332978.2	251447	172399.7	89832.55	70789.17	0.81	1.01	2.84	13.3
270	826512.57	534101.5	329583.6	275918.7	109767.3	111732.2	0.79	0.98	4.84	23.3
280	1043988.7	662034.5	367263.1	341022.6	115320.2	135005.9	0.76	0.95	6.60	33.3
290	1135544.4	700433.4	368875.6	359741.9	109004.1	137763.5	0.72	0.90	8.03	43.3
300	1090136.6	646443.1	337494.6	331251.7	92936.5	120994.4	0.66	0.83	9.03	53.3
310	913242.32	511517.6	276850.4	261866.6	69634.25	89321.81	0.59	0.74	9.52	63.3
320	626197.51	320745.3	191463.2	164382.7	42192.4	50366.62	0.49	0.62	9.33	73.3
330	263624.05	112756.3	85599.02	58029.71	14596.62	14321.4	0.34	0.43	8.08	83.3
340	N/a - Wave sheltered by coastline									93.3
350										103.3
AMP	1135544.4	696299.1	370292.3	357460.6	114861.5	138019.9				

Graphs

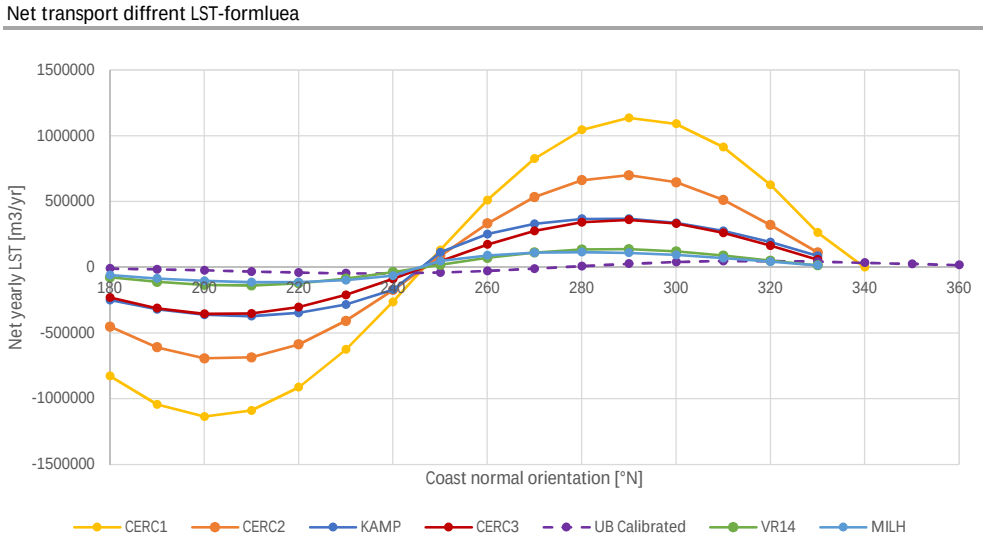

Case I

Graphs

Performance of Kamphuis (ShorlineS vs UNIBEST)

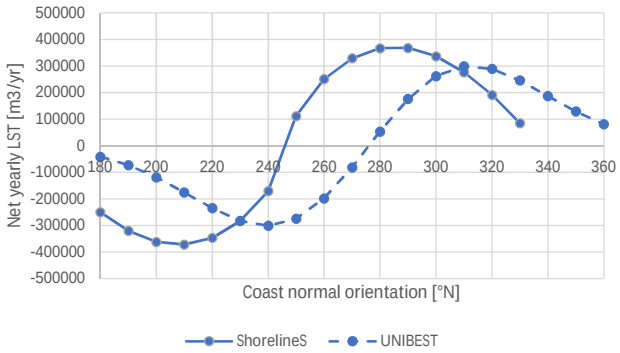

Performance of CERC (ShorlineS vs UNIBEST)

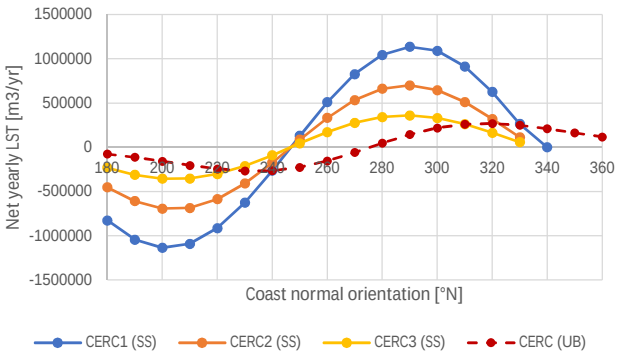

Performance of Mil-Homens (ShorlineS vs UNIBEST)

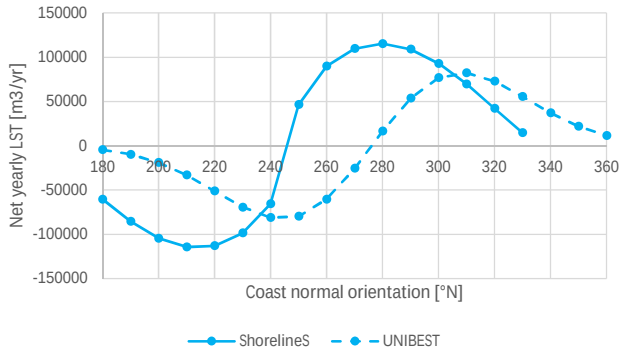

Performance of Van Rijn 2014 (ShorlineS vs UNIBEST)

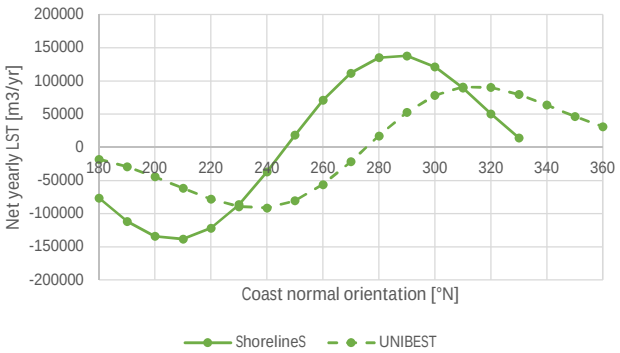

Calculated wave angle at breaking point (ShorelineS vs UNIBEST)

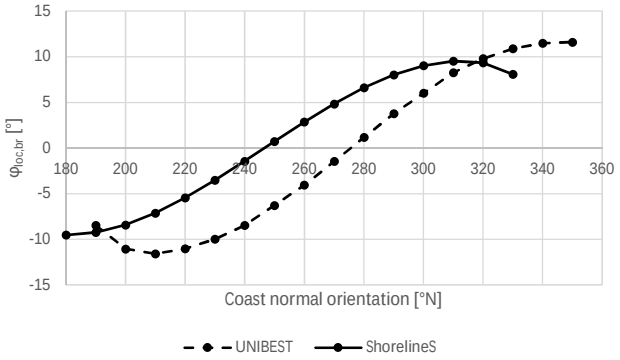

Calculated wave height at breaking point (ShorelineS vs UNIBEST)

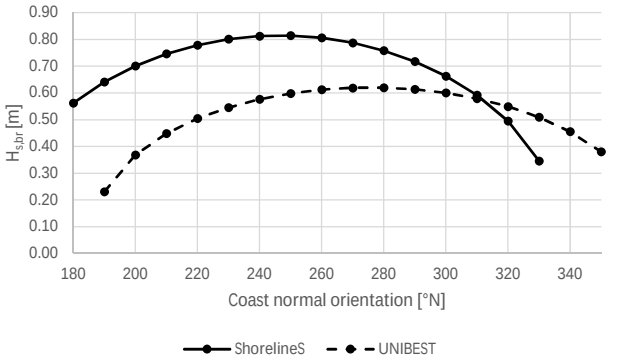

Case II

Input

Wave Climate	Nearshore	phi_w	265.3887
Dynamic boundary active	no (20m)		

Results

DATA

Coastline orientation (°N)	LST-Formlea						Wave transf			
	CERC1	CERC2	KAMP	CERC3	MILH	VR14	H_s,br	h_br	phi_w,br	Phi_loc_off
180	-54657.0	-22770.7	-43700.6	-25225.7	-5736.6	-5061.76	0.24	0.31	-8.33	-85.3887
190	-166499.6	-87190.8	-122494.5	-96016.9	-22227.4	-25351.2	0.39	0.48	-10.17	-75.3887
200	-258260.0	-149506.6	-186950.3	-164356.7	-39286.8	-48943.2	0.47	0.59	-10.56	-65.3887
210	-318870.3	-196414.5	-234437.1	-216119.5	-54271.0	-69334.1	0.53	0.67	-10.17	-55.3887
220	-341020.2	-219165.9	-261651.5	-241805.7	-65201.0	-81628	0.58	0.73	-9.16	-45.3887
230	-322038.0	-213232.7	-265751.0	-236118.5	-70460.8	-82612.8	0.62	0.77	-7.67	-35.3887
240	-264213.3	-178575.5	-244424.6	-198477.8	-68706.9	-71176.1	0.64	0.80	-5.79	-25.3887
250	-174520.6	-119499.1	-194941.3	-133216.7	-58529.7	-48524.6	0.66	0.83	-3.62	-15.3887
260	-63778.1	-43951.7	-107770.3	-49080.2	-36216.8	-18015.8	0.67	0.84	-1.29	-5.3887
270	54657.0	37675.1	98280.2	42073.9	33556.2	15448.41	0.67	0.84	1.10	4.6113
280	166499.6	114090.0	189756.9	127210.1	57320.0	46377.15	0.66	0.83	3.45	14.6113
290	258260.0	174773.0	241633.0	194303.6	68239.4	69785.13	0.64	0.81	5.63	24.6113
300	318870.3	211537.1	265031.8	234310.6	70592.1	82167.51	0.62	0.77	7.53	34.6113
310	341020.2	219761.9	262832.1	242526.6	65832.3	82138.62	0.58	0.73	9.06	44.6113
320	322038.0	199136.6	237322.0	219148.9	55289.7	70633.94	0.54	0.67	10.11	54.6113
330	264213.3	153846.4	191297.2	169125.4	40555.1	50716.53	0.48	0.60	10.56	64.6113
340	174520.6	92322.4	128042.8	101642.2	23575.5	27164.88	0.39	0.49	10.24	74.6113
350	63778.1	27410.1	50364.4	30343.0	6907.0	6320.131	0.26	0.33	8.58	84.6113
AMP	341020.21	219463.9	265391.4	242166.1	70526.42	82390.14				

Graphs

Net transport diffrent LST-formluea

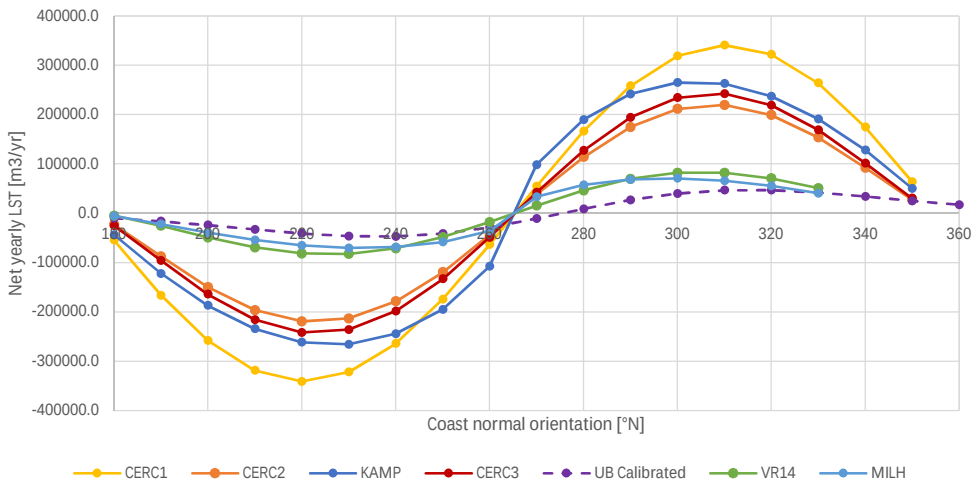

Case II

Graphs

Performance of Kamphuis (ShorlineS vs UNIBEST)

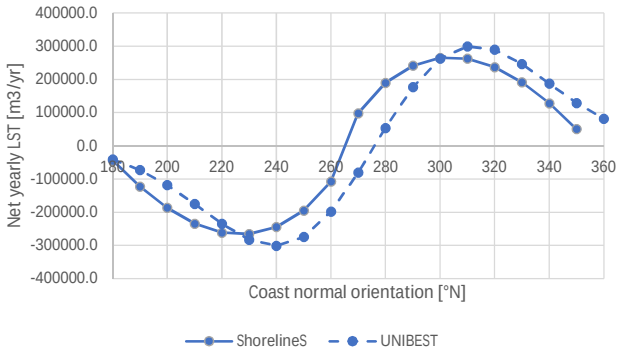

Performance of CERC (ShorlineS vs UNIBEST)

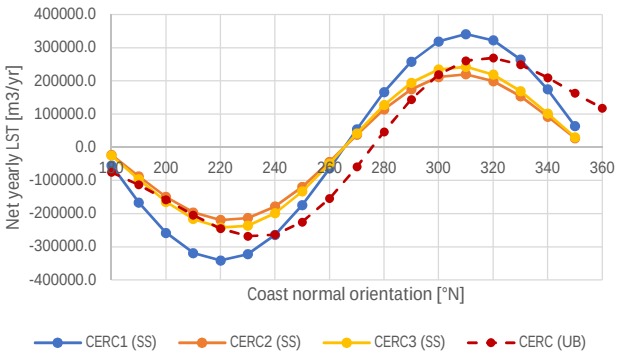

Performance of Mil-Homens (ShorlineS vs UNIBEST)

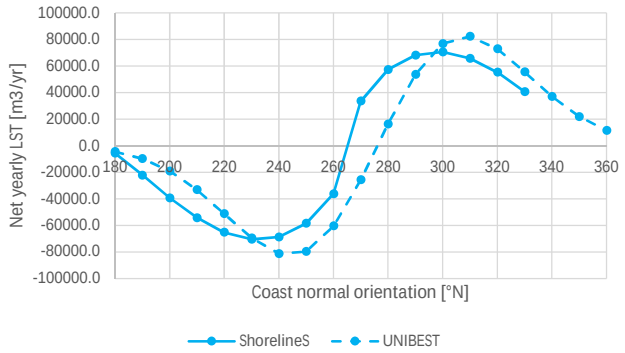

Performance of Van Rijn 2014 (ShorlineS vs UNIBEST)

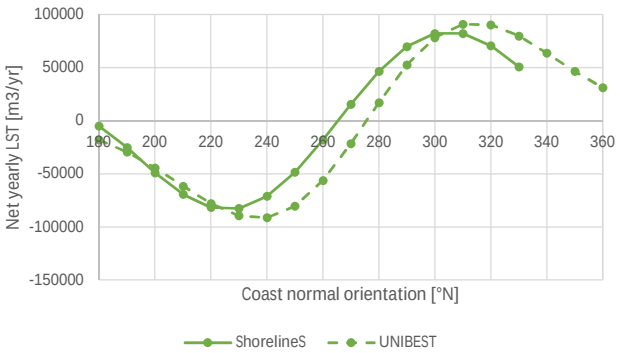

Calculated wave angle at breaking point (ShorelineS vs UNIBEST)

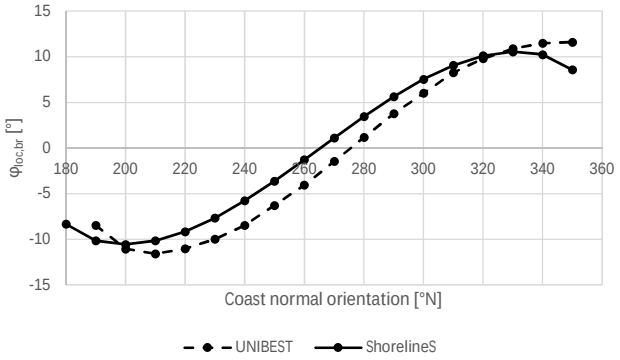

Calculated wave height at breaking point (ShorelineS vs UNIBEST)

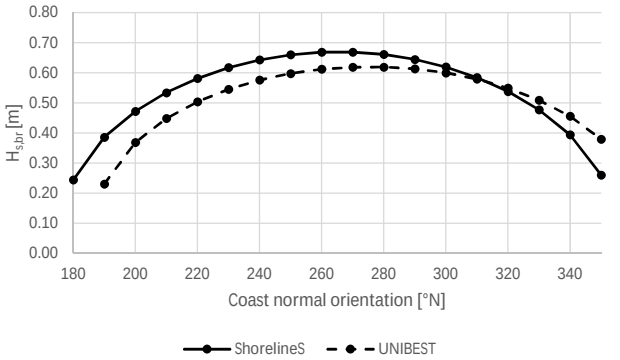

Case III

Input

Wave Climate	Offshore	phi_w	246.7
Dynamic boundary active	yes (14m)		

Results

DATA

	LST-Formlea						Wave transf			
Coastline orientation (°N)	CERC1	CERC2	KAMP	CERC3	MILH	VR14	H_s,br	h_br	phi_w,br	Phi_loc_off
180										-66.7
190	-1043989	-608663.8	-2556.4	-640.3	-136.203	-59.9974	0.07	0.09	-5.00	-56.7
200	-1135544	-692164.8	-71450.5	-48998.8	-10577.1	-10996.6	0.29	0.37	-10.22	-46.7
210	-1090137	-685575.2	-127678.2	-103320.8	-22882.2	-27196.5	0.38	0.48	-11.13	-36.7
220	-913242.3	-586889.1	-171560.7	-149187.2	-34434.5	-42968.2	0.45	0.56	-11.04	-26.7
230	-626197.5	-408067.4	-200498.9	-178054.6	-43672.5	-54436.5	0.49	0.62	-10.24	-16.7
240	-263624	-173042.7	-212030.9	-184448.1	-49334.7	-58792.9	0.53	0.66	-8.87	-6.7
250	130746.37	85911.1	-204138.7	-166278.4	-50382.6	-54568.9	0.55	0.69	-7.04	3.3
260	509346.84	332978.2	-174962.7	-125178.2	-45881.8	-41883.5	0.57	0.72	-4.86	13.3
270	826512.57	534101.5	-120710.6	-66405.0	-34353.2	-22465.3	0.58	0.73	-2.45	23.3
280	1043988.7	662034.5	14234.5	1874.0	5821.337	636.1863	0.59	0.73	0.07	33.3
290	1135544.4	700433.4	124424.6	69883.5	35206.56	23632.69	0.58	0.73	2.59	43.3
300	1090136.6	646443.1	177109.9	127894.3	46282.13	42757.33	0.57	0.72	4.99	53.3
310	913242.32	511517.6	205084.6	167866.9	50458.71	55018.76	0.55	0.69	7.15	63.3
320	626197.51	320745.3	211889.1	184726.0	49139.53	58770.45	0.53	0.66	8.95	73.3
330	263624.05	112756.3	199367.7	177041.0	43257.32	53981.77	0.49	0.61	10.30	83.3
340	N/a - Wave sheltered by coastline									93.3
350										103.3
AMP	1135544.4	696299.1	211960	184587	50420.67	58781.65				

Graphs

Net transport diffrent LST-formluea

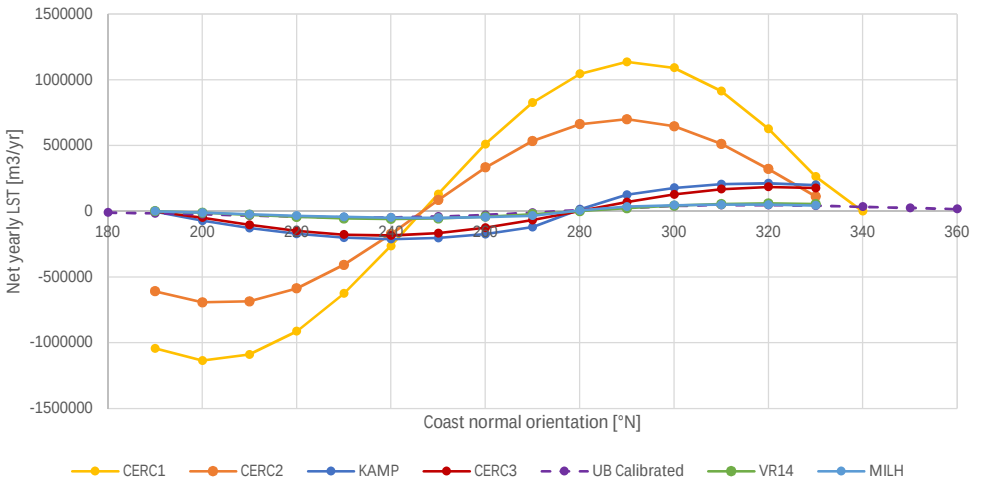

Case III

Graphs

Performance of Kamphuis (ShorlineS vs UNIBEST)

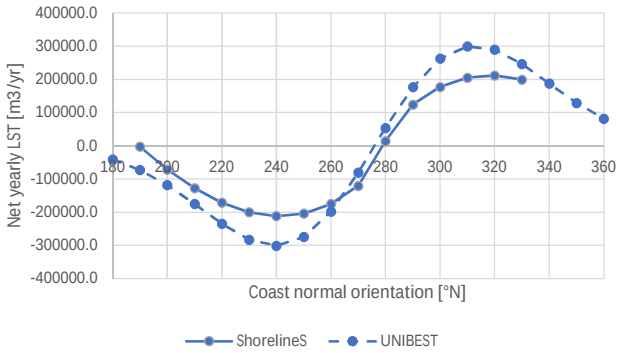

Performance of CERC (ShorlineS vs UNIBEST)

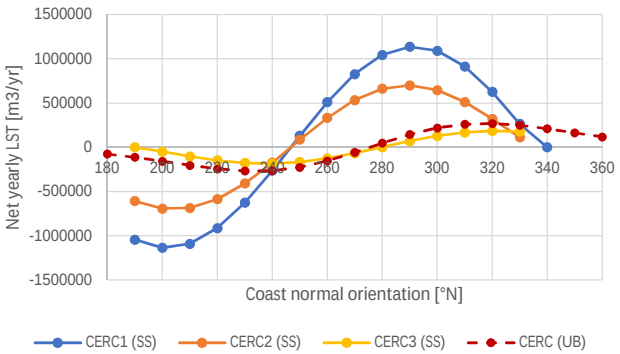

Performance of Mil-Homens (ShorlineS vs UNIBEST)

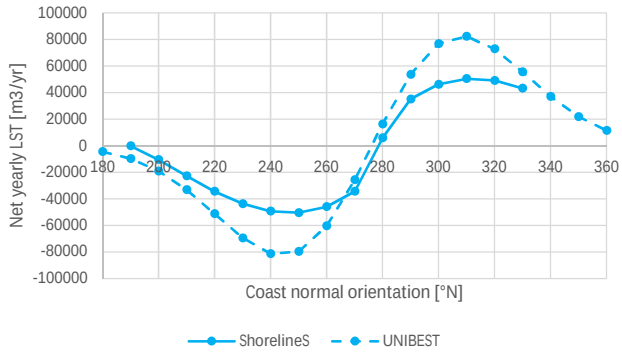

Performance of Van Rijn 2014 (ShorlineS vs UNIBEST)

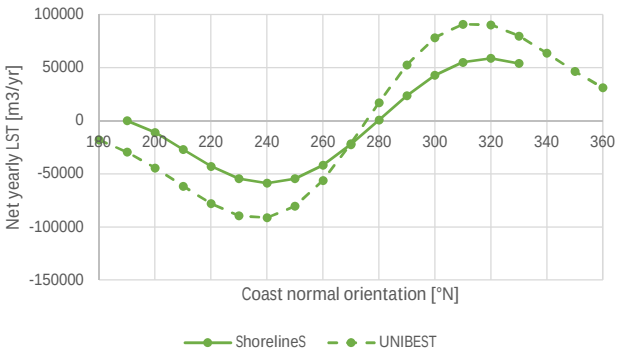

Calculated wave angle at breaking point (ShorelineS vs UNIBEST)

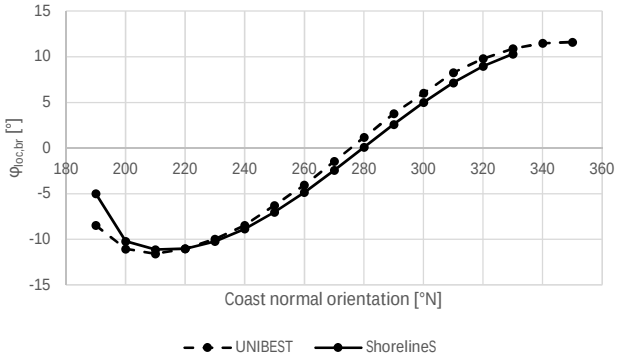

Calculated wave height at breaking point (ShorelineS vs UNIBEST)

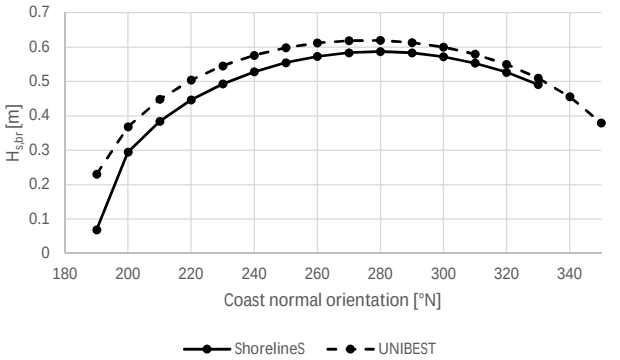

Case IV

Input

Wave Climate	Nearshore	phi_w	265.3887
Dynamic boundary active	yes (14m)		

Results

DATA

Coastline orientation (°N)	LST-Formlea						Wave transf			
	CERC1	CERC2	KAMP	CERC3	MILH	VR14	H_s,br	h_br	phi_w,br	Phi_loc_off
180	-54657.01	-22770.7	-3104.51	-824.105	-175.71	-81.2956	0.07	0.09	-5.20	-85.3887
190	-166499.6	-87190.8	-41601.4	-24284.2	-5199.92	-4720.86	0.23	0.29	-9.17	-75.3887
200	-258260	-149507	-114717	-90454.2	-19729.50	-23043.8	0.36	0.45	-11.17	-65.3887
210	-318870.3	-196415	-174488	-154132	-34723.60	-44251.6	0.44	0.55	-11.59	-55.3887
220	-341020.2	-219166	-218494	-202288	-47879.37	-62546	0.50	0.63	-11.14	-45.3887
230	-322038	-213233	-243671	-226108	-57463.66	-73548.4	0.55	0.68	-10.03	-35.3887
240	-264213.3	-178576	-247346	-220622	-62052.94	-74368.3	0.58	0.73	-8.39	-25.3887
250	-174520.6	-119499	-227314	-185233	-60455.50	-63990.1	0.60	0.76	-6.32	-15.3887
260	-63778.07	-43951.7	-180960	-123961	-51412.43	-43493.1	0.62	0.78	-3.94	-5.3887
270	54657.009	37675.05	-99178.1	-45021.1	-31579.01	-15916.8	0.63	0.79	-1.38	4.6113
280	166499.64	114090	92954.92	40400.72	29929.73	14286.2	0.63	0.79	1.24	14.6113
290	258259.96	174773	177562.8	120004.4	50663.03	42130.68	0.62	0.78	3.81	24.6113
300	318870.32	211537.1	225489	182489.8	60166.89	63109.99	0.61	0.76	6.20	34.6113
310	341020.21	219761.9	246881.3	219441.6	62135.73	74089.37	0.58	0.73	8.28	44.6113
320	322038.03	199136.6	244450.4	226591.2	57855.89	73875.03	0.55	0.69	9.96	54.6113
330	264213.31	153846.4	220386.5	204285.2	48510.79	63370.79	0.51	0.63	11.10	64.6113
340	174520.57	92322.35	177333.8	157267	35508.90	45374.22	0.45	0.56	11.58	74.6113
350	63778.067	27410.06	118347.3	94149.25	20563.88	24191.33	0.37	0.46	11.22	84.6113
AMP	341020.21	219463.9	247113.5	226349.4	62094.34	74228.82				

Graphs

Net transport diffrent LST-formluea

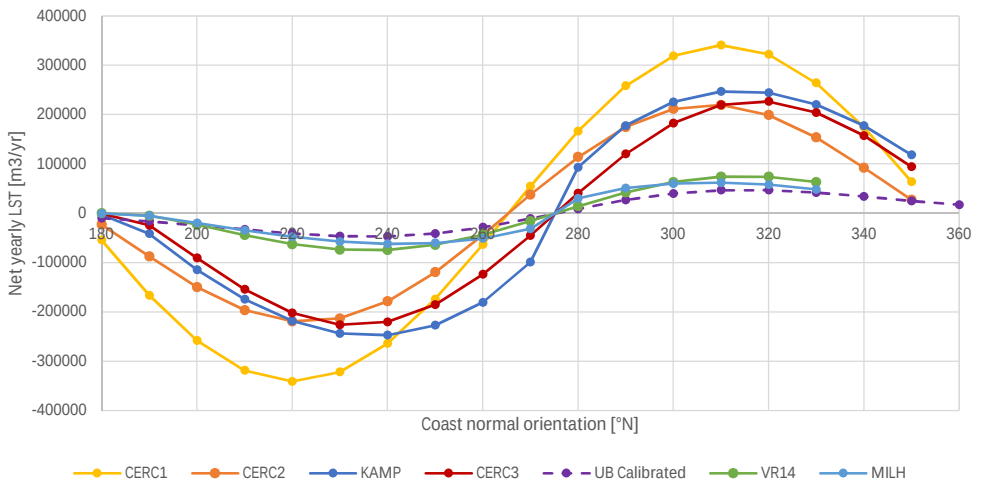

Case IV

Graphs

Performance of Kamphuis (ShorlineS vs UNIBEST)

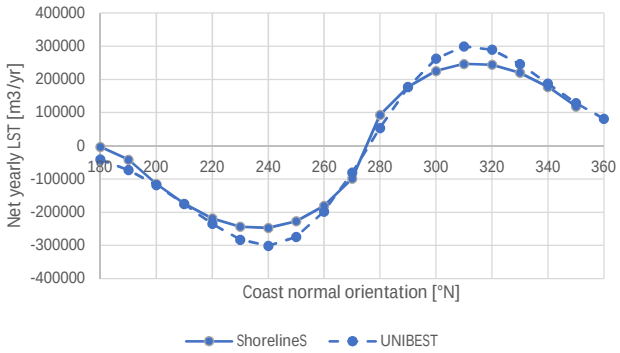

Performance of CERC (ShorlineS vs UNIBEST)

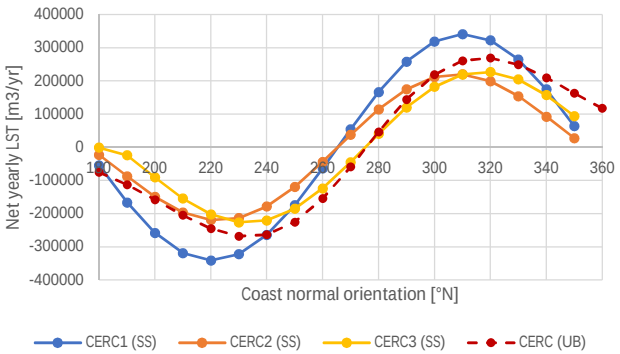

Performance of Mil-Homens (ShorlineS vs UNIBEST)

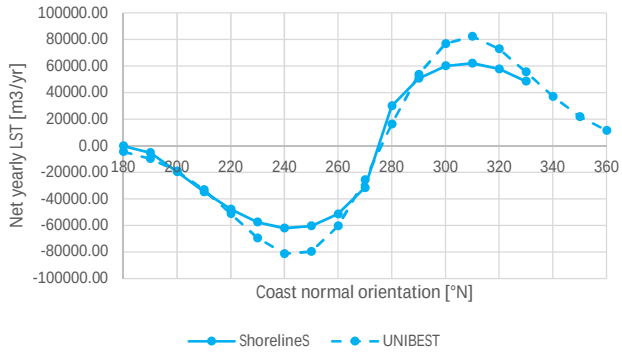

Performance of Van Rijn 2014 (ShorlineS vs UNIBEST)

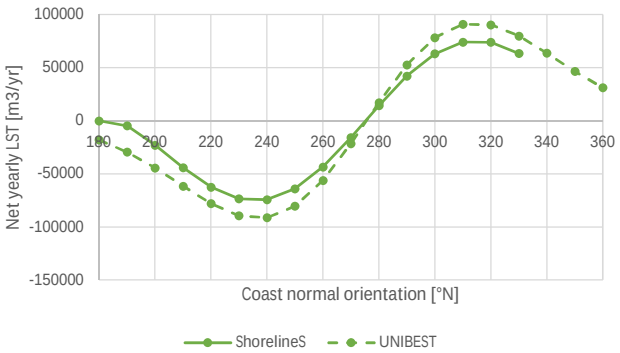

Calculated wave angle at breaking point (ShorelineS vs UNIBEST)

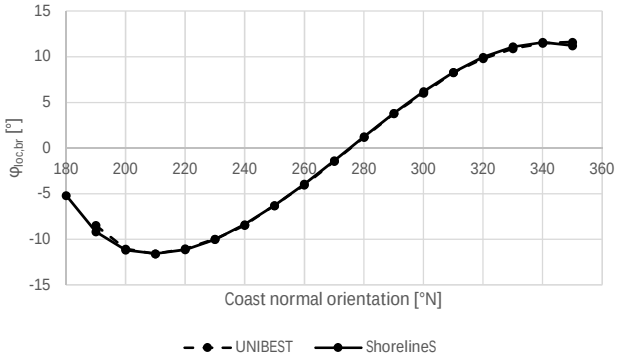

Calculated wave height at breaking point (ShorelineS vs UNIBEST)

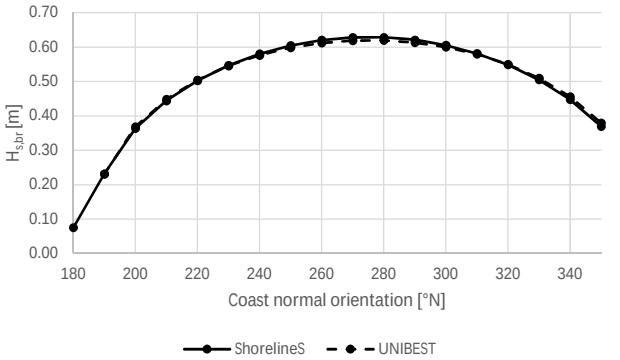

Appendix D

Sensitivity analysis LST-formulae (UNIBEST)

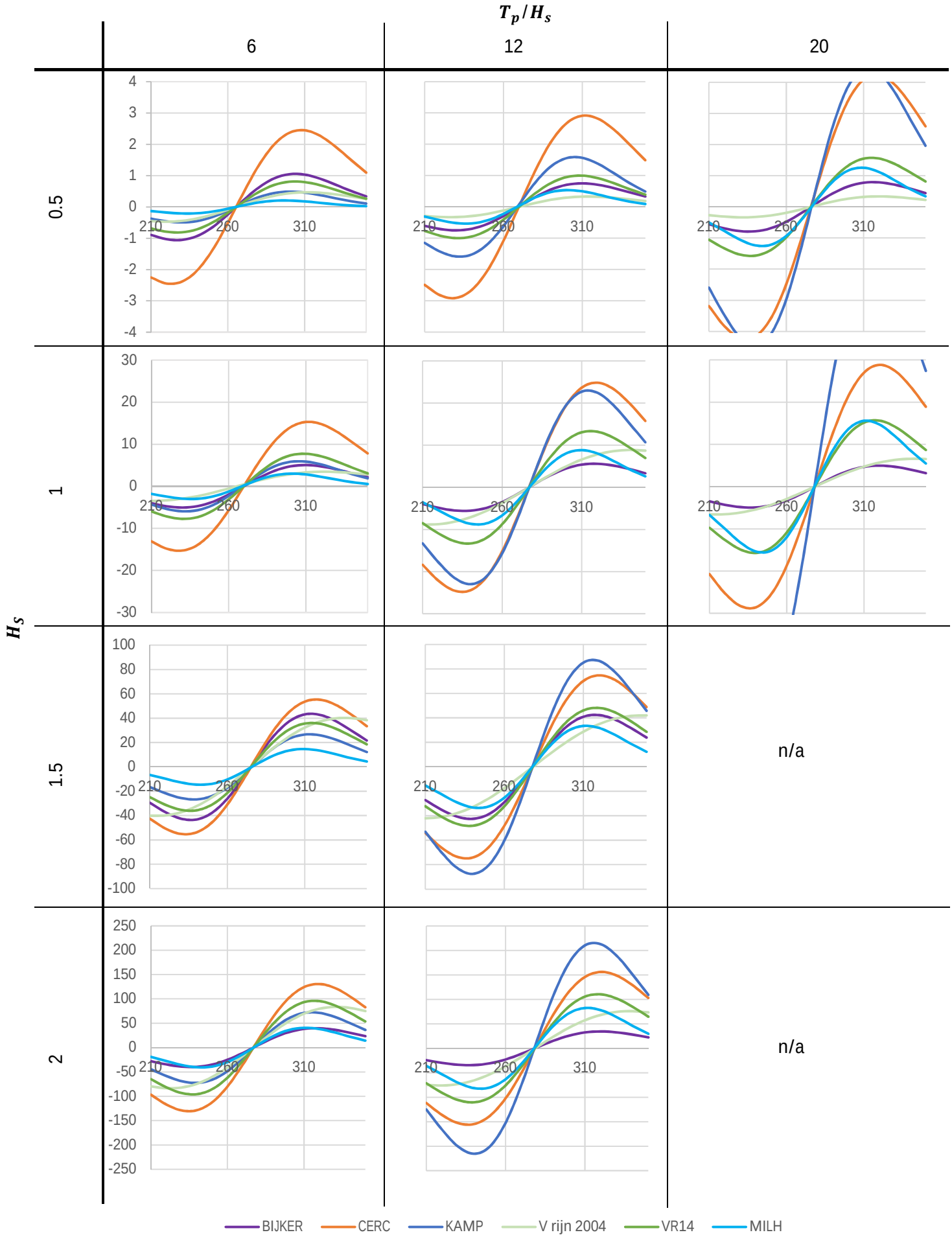
T_p / H_s
6
12
20
H_s
0.5
1
1.5
2
n/a
n/a
BIJKER
CERC
KAMP
V rijn 2004
VR14
MILH